Tesis doctoral

Autophagy-related proteins:

in vitro studies of protein-lipid interactions modulating autophagosome elongation

Unidad de Biofísica (CSIC, UPV/EHU)

Departamento de Bioquímica y Biología Molecular

Facultad de Ciencia y Tecnología

Universidad del País Vasco (UPV/EHU)

Memoria presentada por D. Javier Hervás Hidalgo para optar al grado de Doctor por la Universidad del País Vasco (UPV/EHU)

Directoras: Prof. Alicia Alonso Izquierdo y Dra. Lidia Ruth Montes Burgos

Doctoral Thesis

Autophagy-related proteins:

in vitro studies of protein-lipid interactions modulating autophagosome elongation

Candidate: Javier Hervás Hidalgo

Supervisors: Prof. Alicia Alonso Izquierdo

Dr. Lidia Ruth Montes Burgos

A Aita, Ama y Marta

Contents

Chapter 2: Experimental Techniques

Abbreviations

AC: Alternating Current

AcMNPV: *Autographa californica nucleopolyhedrovirus*

AD: Adenylation Domain

Akt: RAC-alpha serine/threonine-protein kinase

ALPS: Amphipathic Lipid Packing Sensor

Amp: Ampicillin

ANTS: 8-aminonapthalene-1,3,6 trisulfonic acid

AP: Autophagosome

ArfGAP1: ADP-ribosylation factor GTPase-activating protein 1

ATG: AuTophaGy-related

ATP: Adenosine Triphosphate

BAR: Bin–Amphiphysin–Rvs domain

Barkor: Beclin 1-associated autophagy-related key regulator

BCA: Bicinchoninic acid assay

Beclin-1: Coiled-coil myosin-like BCL2-interacting protein

BEVS: Baculovirus Expression Vector System

bI-PI: bovine-liver PhosphatidylInositol

BmNPV: *Bombyx mori nucleopolyhedrovirus*

BSA: Bovine Serum Albumin

BV: Baculovirus

CBB: Coomassie Brilliant blue

CD: Circular Dichroism

Cer: Ceramide

Chol: Cholesterol

CL: Cardiolipin

Cryo-EM: Cryo-Electron Microscopy

CTD: C-terminal Domain

DAG: Diacylglycerol

DAPI: 4',6-diamidino-2-phenylindole

Deptor: DEP domain containing MTOR-interacting protein

DFCP1: Double FYVE-containing protein 1

DLS: Dynamic Light Scattering

DOPE: 1,2-dioleoyl-sn-glycero-3-phosphoethanolamine

DPPC: 1,2-dipalmitoyl-sn-glycero-3-phosphocholine

DPX: p-xylene-bis-pyridinium bromide

DTT: DL-Dithiothreitol

ECTD: Extreme C-terminal domain

EDTA: Ethylenediaminetetraacetic acid

ER: Endoplasmic Reticulum

FCS: Fetal Calf serum

FIP200: FAK family kinase-interacting protein of 200 kDa

FR: Flexible Region

FRET: Förster Resonance Energy Transfer

FT: Flow-Through

GABARAP: GABA(A) Receptor-Associated Protein

GATE-16: Golgi-associated ATPase enhancer of 16 kDa

GPI: Glycosylphosphatidyl-Inositol

GSL: Glycolsphingolipid

GST: Glutathione S-Transferase

GβL: G protein beta subunit-like

HEK293: Human Embryonic Kidney 293 cells

HEPES: 2-[4-(2-hydroxyethyl)piperazin-1-yl]ethanesulfonic acid

HOPS: Homotypic Fusion and Protein Sorting

hpi: hours post-infection

HR: Handle Region

HRP: Horse-Radish Peroxidase

H5: High Five cells

IPTG: Isopropil-β-D-1-tiogalactopiranósido

LAMP2: Lysosomal Associated Membrane Protein-2

LB: Luria Broth

LC3B: Microtubule associated protein 1 light chain 3 B

LPC: Lysophosphatidylcholine

LUV: Large unilamellar vesicle

L_o: Liquid-ordered lamellar lipid phase

L_α: Fluid, Liquid-disordered or Liquid-crystalline lamellar lipid phase

L_β: Gel or Solid-ordered lamellar lipid phase

$L_{\beta'}$: Oblique lamellar lipid phase

$L_{\beta I}$: Interdigitated lamellar lipid phase

MCF7: Michigan Cancer Foundation-7 cells

MLV: Multilamellar vesicle

MOI: Multiplicity of Infection

mTORC1: mammalian target of rapamycin complex 1

NBD: 7-nitrobenz-2-oxa-1,3-diazol-4-yl

NTD: N-terminal Domain

OD: Optical Density

OG: n-octyl-β-D-glucopyranoside

OV: Occluded Virus

PA: Phosphatidic Acid

PAS: Preautophagosomal Structure

PBS: Phosphate Buffered Saline

PC: PhosphatidylCholine

PDI: Polydispersity Index

PE: Phosphatidylethanolamine

PEmal: 1,2-dioleoyl-sn-glycero-3-phosphatidylethanolamine-p-maleimidomethyl-cyclohexanecarboxamide

PG: Phosphatidylglycerol

PI3P: Phosphatidylinositol 3-phosphate

PIK3C1: class I phosphatidylinositol-3-kinase

PITPα: Phosphatidylinositol Transfer Protein alpha

PLC: Phospholipase C

PLD1: Phospholipase D1

polh: Polyhedrin

PRAS40: Proline-rich AKT substrate 40 kDa

PS: Phosphatidylserine

PTEN: Phosphatidylinositol 3,4,5-trisphosphate 3-phosphatase and dual-specificity protein phosphatase

Pβ´: Rippled lamellar gel phase

QELS: quasi-elastic light scattering

Rab: Ras-related GTP-binding protein

Raptor: regulatory associated protein of mTOR

rBV: recombinant Baculovirus

Rho: Rhodamine

Rho-PE: 1,2-dioleoyl-sn-glycero-3-phosphatidylethanolamine-N-(lissamine rhodamine B sulfonyl)

ROS: Reactive Oxigen Species

SDS-PAGE: Sodium dodecyl sulfate polyacrylamide gel electrophoresis

SM: Sphingomyelin

SUV: Small unilamellar vesicle

TCEP: tris(2-carboxyethyl) phosphine

TEV: Tobacco Etch Virus nuclear-inclusion-a endopeptidase

Tm: Melting temperature

TSC1-2: Tuberous sclerosis 1-2 protein

UBL: Ubiquitin-Like

ULK1-ULK2: Uncoordinated-51 (unc-51)-like kinase 1 or 2

UVRAG: UV-radiation resistance associated gene

WIPI1-2: WD repeat domain phosphoinositide interacting 1 and 2

Π_c: Critical surface pressure

Index of Experimental Protocols

1. Introduction and Aims

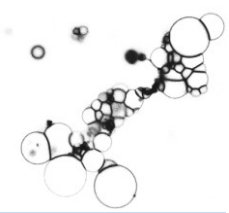

CHAPTER 1:

Introduction and Aims

1.1 Cell Membranes

1.1.1 Common Properties and Functions

Living cells need to be connected with and protected from the outer environment. Membranes confer the main protection against the different environmental conditions for survival. Plasma membrane surrounds the cytoplasm of living cells and physically separates the intracellular components from the extracellular ones. Membranes constitute a selective barrier that regulates the exchange of molecules between defined compartments. Unlike prokaryotes, eukaryotic cells have not only a plasma membrane but also intracellular membranes surrounding various organelles. All of these membranes are part of an extensive endomembrane system.

The plasma membrane is composed of a thin layer of lipid molecules with large amounts of embedded proteins (Singer & Nicolson, 1972; Goñi, 2014). Both lipids and proteins participate in anchoring the membrane to the cytoskeleton thus providing a shape to the cell, and interact with the extracellular matrix to maintain tissue organisation. Furthermore, many other processes such as cell signalling, cell adhesion, ion conductivity, nutrient uptake or disposal of unwanted material are regulated by membrane components and take place either within or in the membrane vicinity.

Cell membrane is selectively permeable and facilitates the transport of materials needed for survival. Due to this selective transport property membranes can maintain the cell potential. The movement of solutes across the membrane is controlled by some mechanisms that often involve proteins. Small molecules such as carbon dioxide and oxygen can move across the membrane by simple diffusion. In contrast, charged particles (ions) or larger nutrients (amino acids, sugars) need a more complex

mechanism of transport which entails the participation of proteins and an energy expense.

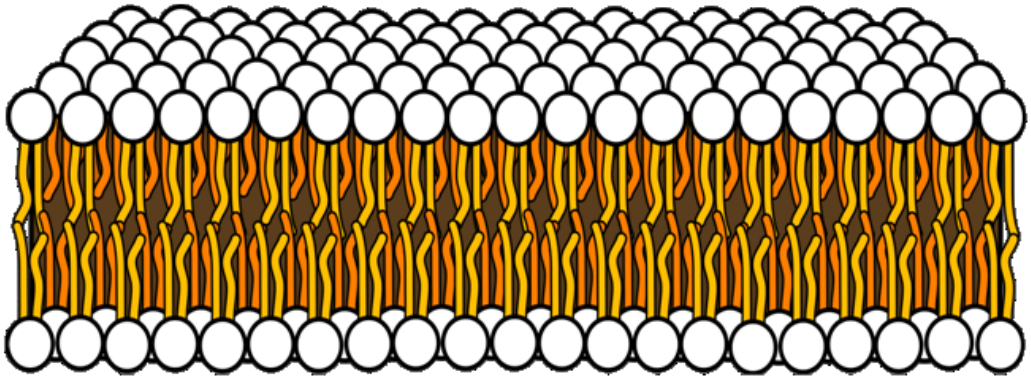

Figure 1.1. Schematic diagram of a lipid bilayer

Membrane lipids are amphipatic molecules containing a hydrophobic tail and a polar head group, and can self-assembly into lipid bilayers (**Figure 1.1**). When exposed to a water solvent, these lipids can be spontaneously arranged so that the hydrophilic head groups interact with the water molecules isolating the hydrophobic tails from the water environment (Israelachvili *et al.*, 1980). Thus, lipids in cell membranes characteristically adopt a bilayer structure with the hydrophobic tails facing each other and the polar heads interacting with the cytoplasm or extracellular medium. Proteins, the other main component, accommodate along the membrane extension up to 50% of the plasma membrane mass.

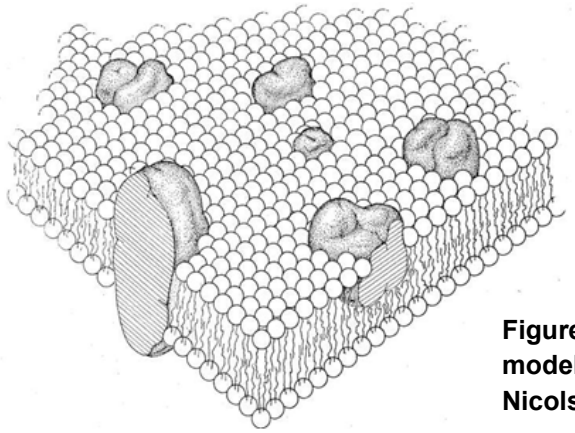

Figure 1.2. Lipid and protein "fluid mosaic" model of biomembrane structure by Singer-Nicolson [Taken from Singer and Nicolson (1972)]

In this context, Singer and Nicholson proposed the current view of cell membranes as a fluid mosaic model, in which lipids and proteins can rotate and diffuse easily along the plane of the membrane (**Figure 1.2**). Thus, the membrane would be asymmetric as a consequence of the restricted transbilayer movement. Membrane proteins are usually classified as peripheral or integral proteins. Integral (also called intrinsic) proteins have one or more segments embedded in the phospholipid bilayer. Most integral proteins contain hydrophobic residues that interact with the fatty acyl chains of phospholipids in order to anchor the protein to the membrane. However, the polypeptide chain does not always enter the phospholipid bilayer, as it is the case of proteins anchored by covalent binding to fatty acids. On the other hand, peripheral (also called extrinsic) proteins usually interact with the lipid polar head groups or intrinsic proteins.

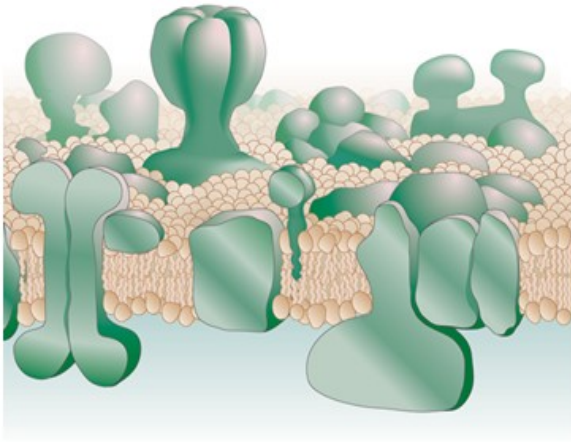

Figure 1.3. An amended and updated version of the Singer-Nicolson model. [Adapted from Engelman (2005)].

However, subsequent adjustments and evolutions of this model have emerged in the following decades (Jacobson *et al.*, 1995; Engelman, 2005; Goñi, 2014). Now, the intrinsic membrane proteins are considered to be very abundant, and distributed inhomogeneously along the membrane (**Figure 1.3**). Even some proteins are not always in contact with the membrane, existing part-time in the cytosol and part-time docked to a membrane. Moreover, biological membranes present lateral heterogeneity. It can be divided into subdomains composed of specific proteins or lipids, allowing spatial segregation of biological processes associated with membranes such as ion and metabolite transport, signalling, cell adhesion, and migration. Additionally, in practice the membrane bilayer is not flat. Local curvature of the membrane can be caused by the asymmetry and non-lamellar organization of lipids. Some non-bilayer lipid structures can transiently occur, with important biological functions, as is the case

of membrane fusion events or cell division. Lipid asymmetry in the membrane has been discovered to be controlled by flippase or scramblase proteins. Lipid flip-flop motion is of great importance for instance during the apoptotic response in a cell, in which an externalisation of phosphatidylserine (PS), a phospholipid present only in the cytosolic leaflet of plasma membranes, is promoted to potentiate macrophage cell recognition and death (Fadok *et al.*, 2000).

1.1.2 Membrane Lipids

Lipids include a heterogeneous group of molecules, with important biological functions. In the cell, they are involved in the formation of cellular membranes. But largest amounts of lipids are used for energy storage, principally as triacylglycerols and sterol esters, in lipid droplets. Also, lipids can act as first and second messengers in signal transduction and molecular recognition processes (Bartke & Hannun, 2009; van Meer, 2005; van Meer *et al.*, 2008).

In this thesis, lipids are considered mainly as related to membrane formation. Cellular membranes are formed by polar lipids, which consist of a hydrophobic and a hydrophilic area. The propensity of the hydrophobic moieties to self-associate, and the tendency of the hydrophilic moieties to interact with the aqueous environment are the physical basis of the spontaneous formation of membranes. Regarding the head group charge, all these lipids can be either neutral (zwitterionic) or electrically (usually negatively) charged. From the head group, generally one or two fatty acyl hydrophobic tails emerge. These can contain from 2 to 28 carbon atoms and also can be saturated or unsaturated with one or more *cis* or *trans* double bounds (Berg *et al.*, 2002).

1.1.2.1 Classification of Membrane Lipids

The predominant lipids in cell membranes are glycerolipids, sphingolipids and sterols.

A) Glycerolipids

Glycerolipids are the major structural lipids in eukaryotic membranes. There are two classes of glycerolipids, glycerophospholipids and glyceroglycolipids. Glycerophospholipid structure is based on a glycerol molecule to which two fatty acids

are bound via ester linkages to the carbons in *sn*-1 and *sn*-2 positions of glycerol. To the carbon in the glycerol *sn*-3 position a phosphate group is attached, and a polar residue is esterified to the phosphate group (**Figure 1.4**). Depending on the length and saturation of the acyl chains attached to the glycerol, and on the polar group bound to the phosphate, a large variety of glycerophospholipid species arises.

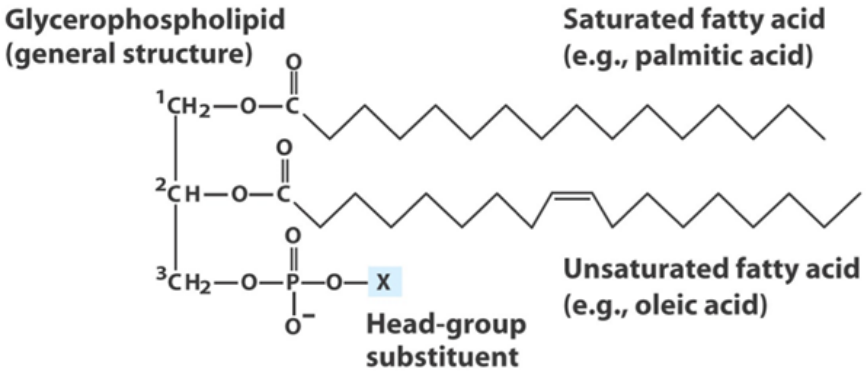

Figure 1.4. General structure of glycerophospholipids.

The other class of glycerolipids, glyceroglycolipids, are less abundant in animal cell membranes but are present in huge quantities in plant and some bacterial membranes. They lack a phosphate group, but contain a mono- or oligosaccharide group linked through a glycosyl linkage to carbon *sn*-3 of glycerol.

B) Sphingolipids

Sphingolipids can be sorted into phosphosphingolipids and glycosphingolipids. Their hydrophobic backbone is sphingosine, a long chain unsaturated amino octadecyl alcohol. N-hexadecanoyl-D-erythro-sphingosine, ceramide, an important sphingolipid in cell signalling, is originated by a fatty acyl chain attached through an amide linkage to sphingosine (**Figure 1.5**). Binding of a phosphorylcholine polar residue to ceramide originates sphingomyelin, an abundant phosphosphingolipid in the external leaflet of cell plasma membrane.

The binding of complex sugar structures gives rise to a class of sphingolipids named glycosphingolipids, which can be classified into cerebrosides and gangliosides, depending on the number of sugar residues and the presence of sialic acids.

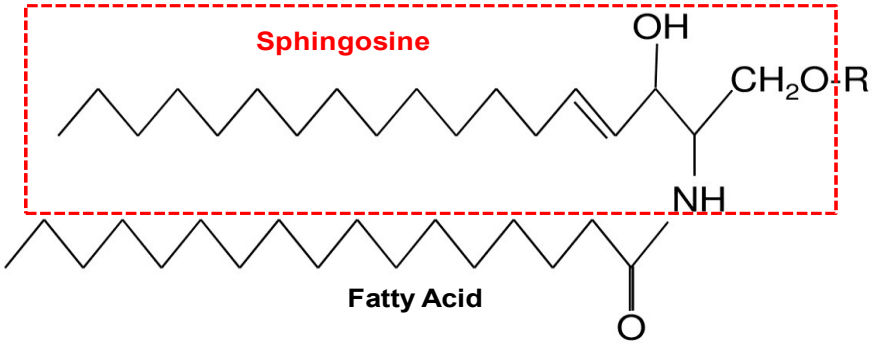

Figure 1.5. General structure of sphingolipids. Sphingosine in a red square, fatty acid in black, and R corresponds to the variable head group. [Taken from Fuller, (2010)]

C) Sterols

The third class of lipids that integrate cell membranes are sterols. These lipids are the major non-polar lipids in cell membranes. Sterols have a hydrophobic four-membered fused ring rigid structure, and a small polar head group. In general, sterols are synthesized via the mevalonate pathway of isoprenoid metabolism. The most abundant sterol in mammals is cholesterol (**Figure 1.6**), whereas ergosterol predominates in yeast.

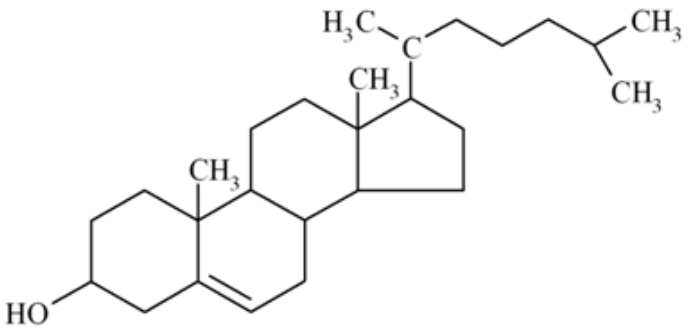

Figure 1.6. Structure of cholesterol.

1.1.2.2 Lipid Distribution and Asymmetry

Eukaryotic cells contain well over 1000 different lipid species in the membranes. Variation in headgroups and aliphatic chains of each kind of lipid generates this enormous lipid diversity. Interestingly phospholipids, sphingolipids and sterols are not

distributed homogeneously throughout the main organelles of mammals, conferring special characteristics to them (**Figure 1.7**). This segregation reflects the different physiological role, local lipid metabolism of each lipid in the cell and specific physicochemical membrane properties generated by differences in lipid composition. For example, sphingomyelin and cholesterol are principally found in the plasma membrane, while cardiolipin can be found almost exclusively in mitochondrial membranes.

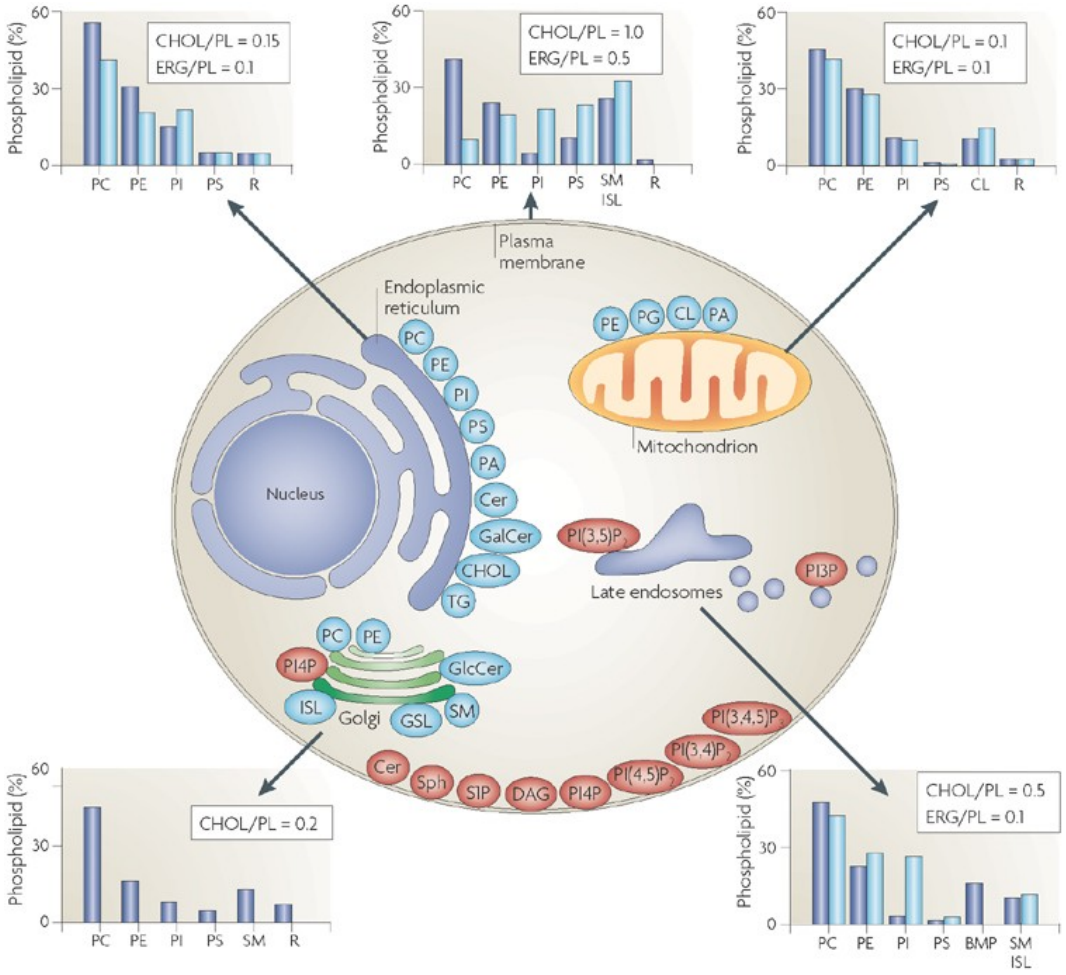

Figure 1.7. **Lipid compositions of different membranes within the cell.** [Taken from van Meer *et al.* (2008)].

Furthermore, lipid heterogeneity is not only present between different membranes in the cell, but also within single membranes. Lipids can be asymmetrically distributed between the two monolayers of a lipid bilayer. This characteristic is named lipid transversal asymmetry (**Figure 1.8**). The Golgi, plasma membrane and endosomal membranes display an asymmetric distribution with sphingomyelin (SM) and glycosphingolipids (GSLs) on the non-cytosolic side, as well as with phosphatidylserine

(PS) and phosphatidylethanolamine (PE) enriched in the cytosolic leaflet. The main reason of lipid composition differences between both monolayers is the asymmetric synthesis of certain lipids or the presence of transporters that allow unidirectional lipid translocation.

In model membranes the rate of spontaneous polar lipid movement between bilayer leaflets is slow [hours to days for Phosphatidylcholine (PC)] and is governed by the size, charge and polarity of the headgroup. The half time for translocation is days for complex GSLs but seconds for Ceramide (Cer), Diacylglycerol (DAG) and sterols. Hence, in cell membranes some proteins (flippases, floppases, scramblases), facilitate this movement, sometimes with energy cost under specific circumstances (Contreras *et al.*, 2010).

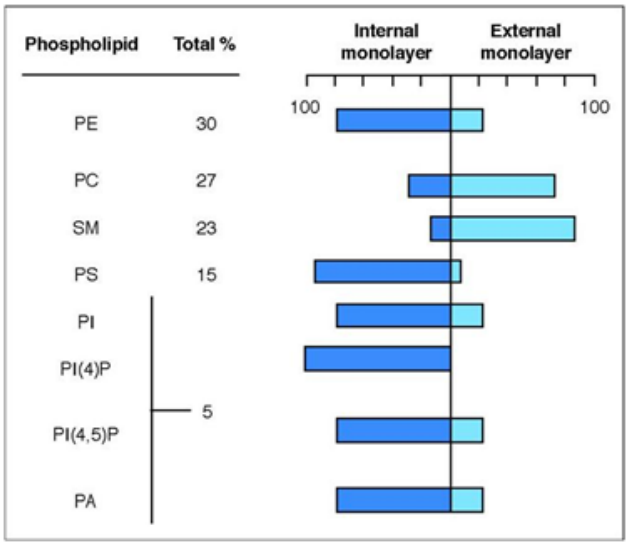

Figure 1.8. Asymmetric phospholipid distribution in erythrocyte plasma membrane.

In addition, lipids are not homogeneously located even along one leaflet of the membrane. Lipids display certain lateral asymmetry. Membrane fluidity is connected to the lipid motion, and regulates the capacity of free lateral movement. In this context, lipid domains and rafts are related to this lateral heterogeneity.

1.1.2.3 Lipid Polymorphism

Morphological plasticity of biological membranes is critical for cellular life, as cells need to quickly reorganise their membranes for a proper response to a given stimulus. Cell membranes are basically organised in a unidimensional lamellar structure. However, some crucial events are characterised by the formation of more

complex non-lamellar structures, such as the inverted hexagonal or cubic phases. From macromolecule transversal motion across the membrane to cell division, many processes require the generation of these unstable structures (Epand, 1998). Membrane fusion and fission processes, that include virus infection, vesicular transport from the Endoplasmic reticulum (ER) to the Golgi or endocytic and exocytic transport, are good examples of energetically unfavourable events that require the transient formation of non-lamellar structures (Basañez, 2002; Burger, 2000). However lipid polymorphism is not only associated to two-dimensional structural changes. For instance, the formation of laterally segregated structures within a membrane, where protein complexes can adopt a more stable conformation is dependent on unidimensional alterations of lipid order or rigidity.

A lipid phase is a thermodynamic concept corresponding to different structural patterns that a lipid or a lipid mixture adopt in aqueous solution. Biological membranes under equilibrium conditions are composed of a lipid bilayer in a lamellar configuration, where the most significant phases are: fluid or liquid-disordered or liquid-crystalline (L_α), gel or solid-ordered (L_β) and a phase with intermediate properties between fluid and gel denoted as liquid-ordered (L_o). In a L_α phase, lipids are free to diffuse laterally or rotationally, and display their acyl chains in a disordered state with high flexibility, and at least one of the acyl chains is normally unsaturated. Lipids in the L_β phase have highly ordered acyl chains and display high proportions of trans C-C conformers, being almost immobile and not allowing lateral or rotational motion (Marsh, 1980). The L_β to L_α phase transition is usually know as the main phase transition (**Figure 1.9**).

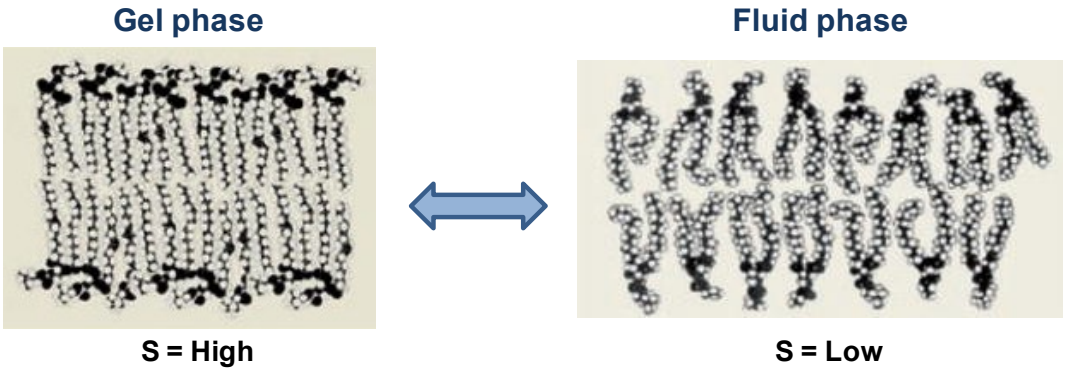

Figure 1.9. Lamellar gel-fluid phase transition and its associated height and chain order transformation. S represents de order parameter of the acyl chains. Redrawn from van Meer *et al.*, (2008).

Other lamellar phases include $L_{\beta'}$, in which acyl chains are tilted with respect to the plane of the membrane, the interdigitated $L_{\beta I}$ where acyl chains from the two membrane layers are interdigitated (typical from lipids with a short and a large acyl

chain), and the rippled $P_{\beta'}$ phase, which can be adopted by a few saturated phosphatidylcholines and phosphatidylglycerols, and characterised by the ripples seen by electron microscopy in freeze-fractured surfaces of lipid samples in this phase.

1.1.2.4 Lipid Geometry

The formation of some non-lamellar structures is strongly influenced by the lipid molecular geometry. Differences in the cross-sectional areas between the polar headgroup and the hydrophobic tail could determine the overall structure of the lipid aggregates (Israelachvili *et al.*, 1980). From this point of view, lipids are mainly classified into three groups: lipids with cone, cylindrical or inverted-cone shapes (**Figure 1.10**). These shapes could be summarized by the morphological parameter S:

$$S = V/A_oL_c$$

Equation 1. Morphological parameter S.

where:

V = is the volume of the lipid molecule,
A_o = is the area of the molecule in the lipid-water interface and
L_c = the length of the extended acyl chain.

Taking into account these parameters and the lipid cross-sectional area in the hydrophobic tail "A_H", which would reflect a volume of $V = A_HL_c$ for a lipid displaying cylindrical shape, we can review the different morphological geometries as:

- $A_0 = A_H$ (S = 1): The molecule presents a cylindrical shape
- $A_0 < A_H$ (S > 1): The molecule presents a cone shape
- $A_0 > A_H$ (S < 1): The molecule presents an inverted cone shape

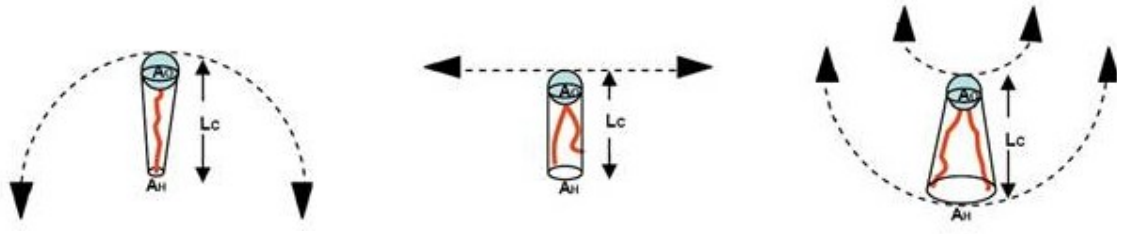

S < 1
Inverted cone shape

S = 1
Cylindrical shape

S < 1
Cone shape

Figure 1.10. Molecular shape of physiological lipids.

Pure lipids in aqueous solutions will self-aggregate into different structures depending on their molecular geometry. Cylindrical shapes displaying lipids as PC or SM will become organised in the form of lamellar bilayers. Cone shaped lipids as PE, DAG or sterols will tend to form “hexagonal” (tubular) arrangements, while inverted-cone-shaped lipids as is the case of lysophospholipids (LPC) will aggregate into micelles (**Figure 1.11**). However, these non-cylindrical lipids could be part of a lipid bilayer structure whenever lipids such as PC, SM or PS are present. For instance, a 20 to 50 mol % of cylindrical lipids are necessary when mixed with conical lipids in order to have an overall lamellar structure (Cullis *et al.*, 1986).

Thus, it could be summarised that lipid polymorphism reflects the lipid behaviour under specific physical conditions in which long-range ordered structures are generated by the lipids in a given phase.

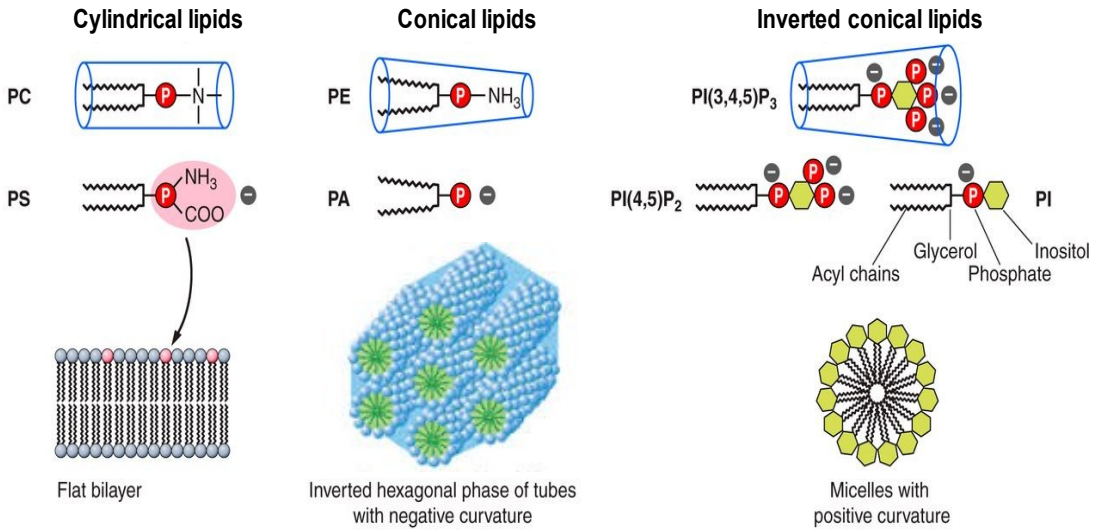

Figure 1.11. Molecular shape, curvature and overall structure adopted by some lipids from biological membranes. Redrawn from Suetsugu *et al.*, (2014)

1.1.3 Membrane Fusion

Fusion processes imply that the membrane bilayers of two vesicles merge and their aqueous contents connect. When it occurs, the lamellar structure is transiently altered in a regulated manner. These fusion events are observed in many biological processes such as fertilisation, cell division, phagocytosis, membrane recycling, viral

infection and exocytosis in higher organisms. All these processes are controlled by the protein machinery of the cell, but they are highly dependent on the lipid composition of membranes. Despite the important events that involve fusion, many mechanistic and molecular features are still unknown.

The first step in membrane fusion is to bring membranes together in close proximity, in order to remove the water in between the two membranes. Once this step has been accomplished, the membrane is destabilised, and undergoes changes leading to the mixing of aqueous contents within the resulting single vesicle (Siegel, 1986). Previous work has related the destabilisation of the membrane to lipid polymorphism (transition from lamellar to non-lamellar phase) (Gilbert, 2015). Moreover, the presence of a common intermediate for leakage and fusion has been suggested (Siegel *et al.*, 1994).

The stalk hypothesis is currently the most accepted fusion model. It involves the formation of a lipid intermediate with a semi-toroidal shape, termed stalk, that is formed from the two membranes that are about to fuse (Chernomordik & Kozlov, 2008; Chernomordik *et al.*, 1987; Kozlov & Chernomordik, 2015). The stalk enables mixing of the two outer monolayers, a process known as hemifusion. This intermediate is transient, and is rapidly converted into a more stable structure that connects the two membranes. It is proposed to be a non-lamellar structure with a high curvature. Model membranes have helped to study this process and it has been possible to explain certain stages of the stalk model (**Figure 1.12**).

I. Membranes are brought together into a close apposition, for this electrostatic forces need to be overcome.

II. Hemimembrane fusion of the outer monolayers, when the stalk structure is formed.

III. Formation of an aqueous fusion pore by hemimembrane fusion of the inner monolayers.

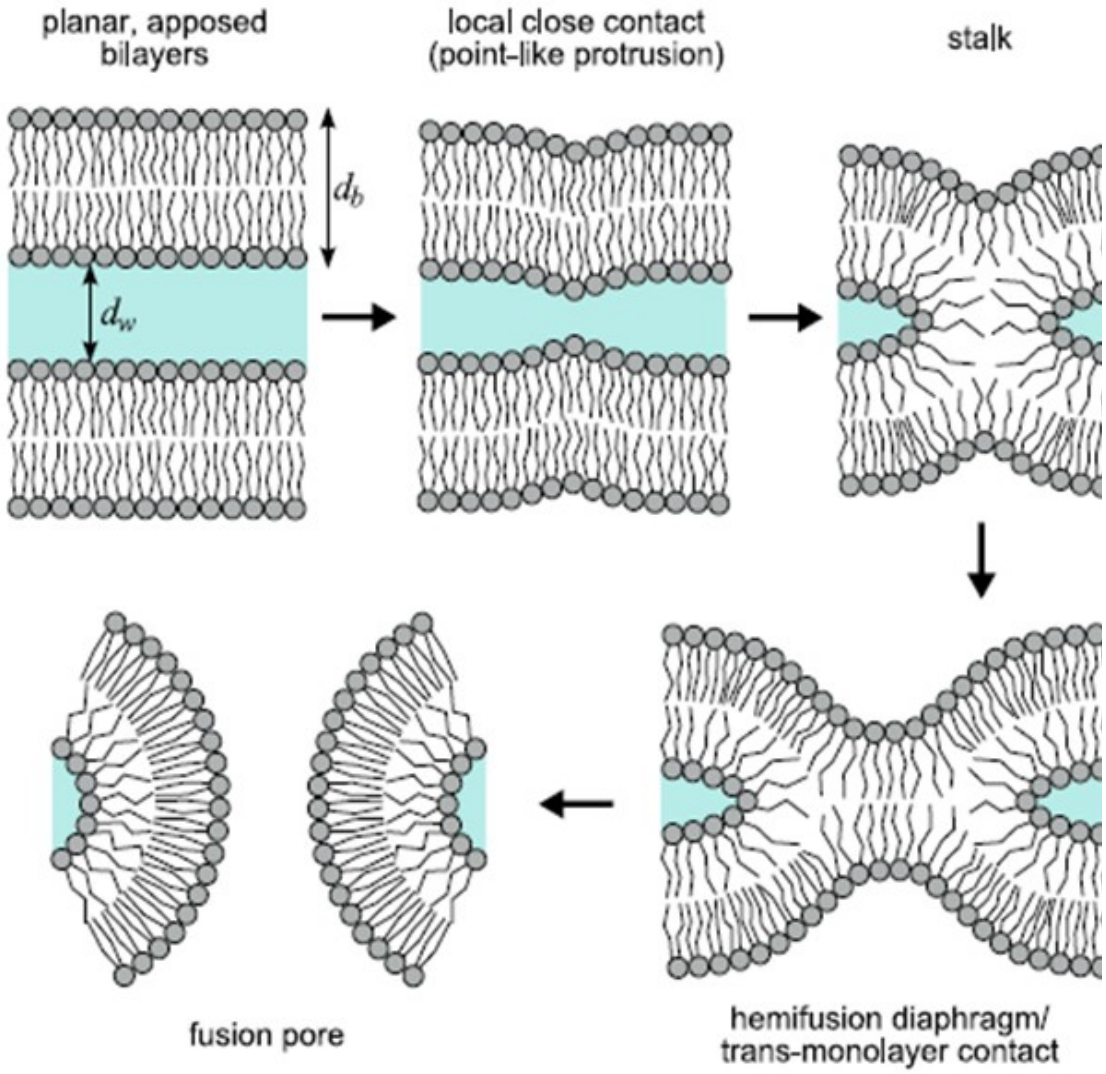

Figure 1.12. Schematic representation of the stalk fusion model.

The first step when the two membranes come in contact requires overcoming the highest energetic barrier, because both surfaces are hydrated and repel each other. This step is facilitated by lipids that induce localised negative curvature, such as cholesterol or DAG, the latter is mostly produced by phospholipase C (PLC) (Goñi *et al.*, 2012). These lipids are known to induce non-lamellar structures because of their cone shape, and diminish the energetic barrier of repulsion favouring the stalk formation (Khattari *et al.*, 2015), but no the stalk expansion (Risselada *et al.*, 2014). X-ray studies have revealed changes in the water layer thickness (d_w) in between apposed bilayers, depending on the lipid composition (Aeffner *et al.*, 2012). Moreover, it is known that lipids with an inverted cone shape, that induce positive curvature, inhibit fusion.

1.1.4 Protein-lipid Interactions

Membrane proteins are associated in different ways with membranes and enable them to carry out their distinctive activities. Each particular bilayer contains a specific pool of proteins that confers to it some particular properties.

As it was said in **section 1.1.1**, membrane proteins are commonly classified as peripheral or integral proteins. Integral (also called intrinsic) proteins contain one or more segments embedded in the phospholipid bilayer. Most integral proteins contain hydrophobic residues that interact with the fatty acyl chains of phospholipids in order to anchor the protein to the membrane. However, the polypeptide chain does not always enter the phospholipid bilayer, as is the case of proteins anchored by covalent binding to fatty acids. On the other hand, peripheral (also called extrinsic) proteins usually interact with the lipid polar head groups or intrinsic proteins.

Moreover, a large amount of membrane proteins do not spend their whole life attached to the membrane. Some of them contact the lipid bilayer only under certain conditions, thereby remaining membrane bound (either as integral or as peripheral proteins) or returning promptly to the aqueous medium (non-permanent membrane proteins).

In this regard, these non-permanent proteins can be classified according to the reversibility of the membrane contact or to the nature of the interaction. The first criterion assumes that there are some proteins that interact reversibly with the membrane and others with very long-lived (irreversible) contacts. The second one sorts the proteins into groups depending of the strength of the interaction, considering weak or strong associations, either in a transient or a permanent way, with the membrane (Goñi, 2002).

Protein-membrane association can also rely on specific protein domains that recognize some pecularities of the membrane (Hurley, 2006; Lemmon, 2008; Moravcevic *et al.*, 2010). At least ten different types of protein domains bind phospholipids at the membrane surface. These interactions can fall into two classes: highly specific, involving the recognition of a particular phospholipid in the membrane, or non-specific, implying a physical property of the membrane surface (Lemmon, 2008). For instance, C1, C2, PH, PX, FYVE or PROPPINs domains belong to the first type. In contrast, BAR domains, ALPS motifs or N-terminal amphiphatic α-helices recognize physical properties such as membrane curvature (Antonny, 2011). More about the latter will be discussed below regarding Atg3 interaction with membranes.

1.2 Autophagy

Autophagy (from the Greek auto-, "self" and phagein, "to eat") is a general biological process conserved among eukaryotes that allows the regulated degradation of unnecessary or dysfunctional cellular materials. This event occurs under normal conditions of cell development, but it can be highly active in the context of disease to promote survival, or in some cases cell death, or under starvation conditions when autophagy promotes the maintaining of cellular energy levels. However, autophagy does not only provide nutrients to maintain vital cellular functions under amino-acid limiting conditions, but also plays an important role in a wide range of physiological processes, such as development, differentiation or immunity. Not surprinsingly, impaired autophagy underlies a wide range of pathological conditions.

1.2.1 Origin

The process of autophagy was observed by Keith R. Porter and his postdoctoral student Thomas Ashford at the Rockefeller Institute, New York. In January 1962 they reported an increased number of lysosomes in the liver cells of rat after addition of glucagon, and that some displaced lysosomes towards the centre of the cell contained other cell organelles such as mitochondria. This was the first reported evidence in the English literature of intracellular digestion of cell organelles. In early 1963, the American Journal of Pathology published a detailed ultrastructural description of focal cytoplasmic degradation, which referenced a 1955 German study of injury-induced sequestration. Z. Hruban and colleagues recognised three continuous stages of maturation of the sequestered cytoplasm to lysosomes, and noted that the process was not limited to injury states, but also functioned under physiological conditions for reutilization of cellular materials (Hruban *et al.*, 1963). Inspired by this discovery, the term "autophagy" was invented by Christian de Duve (de Duve, 1963), the Nobel Prize-winning discoverer of lysosomes and peroxisomes. Unlike Porter and Ashford, de Duve conceived the term as a part of lysosomal function while describing the role of glucagon as a major inducer of cell degradation in the liver. With his postdoctoral student Russell L. Peter, he subsequently established that lysosomes are indeed responsible for glucagon-induced autophagy. This was the first time that lysosomes were established as the sites of intracellular autophagy.

1.2.2 Types of Autophagy

Three different types of autophagy have been described in mammalian cells (**Figure 1.13**) (Okamoto, 2014):

a) Macroautophagy is the main pathway, occurring mainly to eradicate damaged cell organelles or unused proteins. This involves the formation of a double membrane around cytoplasmic substrates resulting in the organelle known as autophagosome. The autophagosome travels through the cytoplasm of the cell to a lysosome, and the two organelles fuse; intersection with endosomal pathways also occurs. Within the lysosome, the contents of the autophagosome are degraded via acidic lysosomal hydrolases. This pathway is conserved from yeast to humans.

b) Microautophagy, on the other hand, involves the direct engulfment of cytoplasmic material by the lysosome. This occurs by invagination, meaning the inward folding of the lysosomal membrane, or cellular protrusion. It is also conserved from yeast to humans.

c) Chaperone-mediated autophagy refers to the chaperone-dependent selection of soluble cytosolic proteins that are then targeted to lysosomes and directly translocated across the lysosome membrane for degradation. It is found only in mammals (Bejarano & Cuervo, 2010).

Autophagy can also be classified into selective or non-selective autophagy, depending on whether there are signals to degrade a specific cellular component or else it is a bulk process. This is particularly important for the cell when only some specific organelles are damaged. In this context, the word organellophagy arises.

Different organelles could be specifically selected to be degraded using the macroautophagy or microautophagy pathways. In the last years almost every cell organelle has been suggested to be a candidate for this selective mode of autophagy. For instance, mitochondria (Mitophagy), peroxisome (Pexophagy), lipid droplets (Lipophagy), nucleus (Nucleophagy), lysosome (Lysophagy), ER (reticulophagy) or ribosomes (Ribophagy) (Okamoto, 2014).

In this thesis, we are interested in the biogenesis of the autophagosome, so in the context of this work, autophagy is to be understood as macroautophagy, the most widely studied and potentially the most powerful form of autophagy.

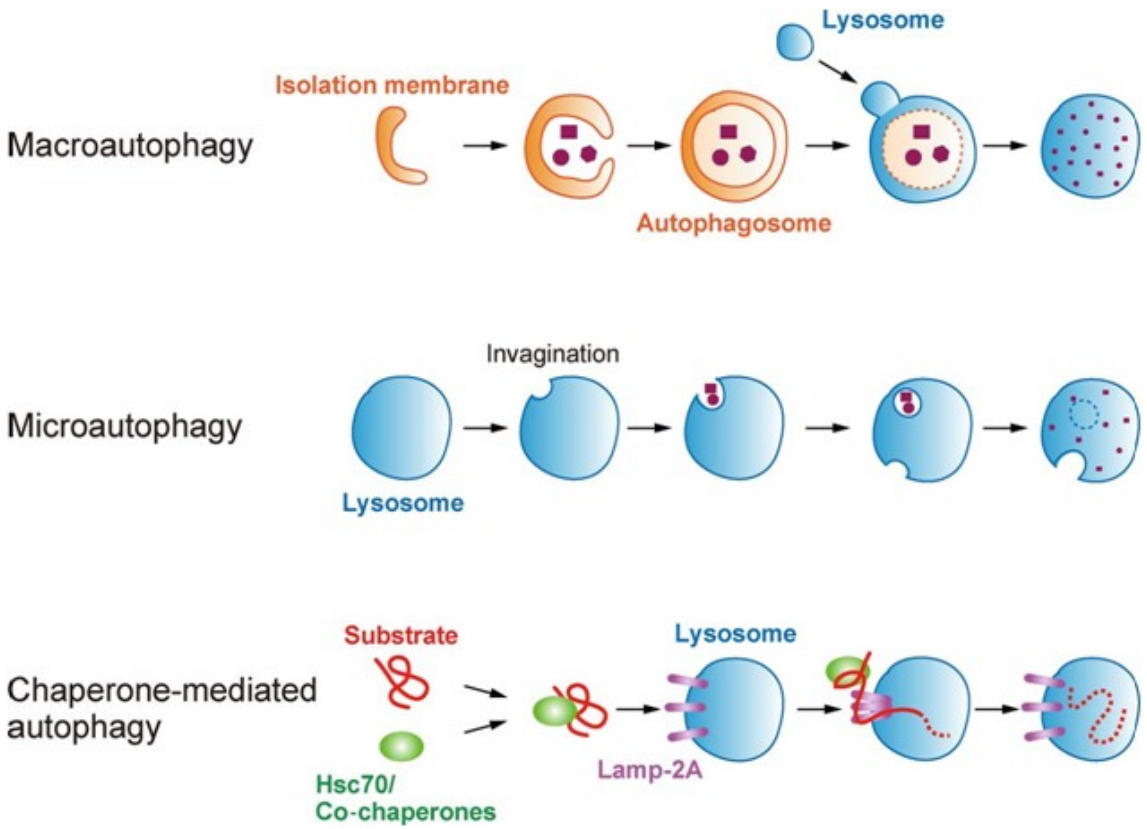

Figure 1.13. Scheme of the three types of autophagy in mammalian cells. Macroautophagy, Microautophagy and Chaperone-mediated autophagy. [Okamoto K. (2014)]

1.2.3 Molecular Machinery of Macroautophagy

The landmark event in autophagy is the formation of a double-membrane structure called autophagosome (AP) (Noda & Inagaki, 2015). The first step for this process is the generation of an isolation membrane. The origin of that initial membrane is not yet known, but some evidences suggest as possible sources the ER, plasma membrane or even mitochondria (Hamasaki *et al.*, 2013; Mari *et al.*, 2011; Mizushima *et al.*, 2011).

Hereafter, the adhesion and fusion of membrane structures is necessary for autophagosome elongation. While membrane material, in the form of vesicles, is reaching the pre-autophagosome, new selected or non-selected cellular contents start to come into this preformed structure. In a final step, the autophagosome closes and upon fusion with a lysosome, the inside contents are degraded by lysosomal hydrolases (**Figure 1.14**) (Tooze & Yoshimori, 2010). Regarding the last step in autophagosome formation, a new study suggest that the autophagosome closure would be based on membrane scission rather than on membrane fusion as most of the

publications in autophagy field sustain (Knorr *et al.*, 2015). Autophagosome sealing comprise the process in which one bilayer splits-up into two separate ones, generating two aqueous compartments, one of which is enclosed by the other. Thus, the correct terminology to name this process would be membrane scission.

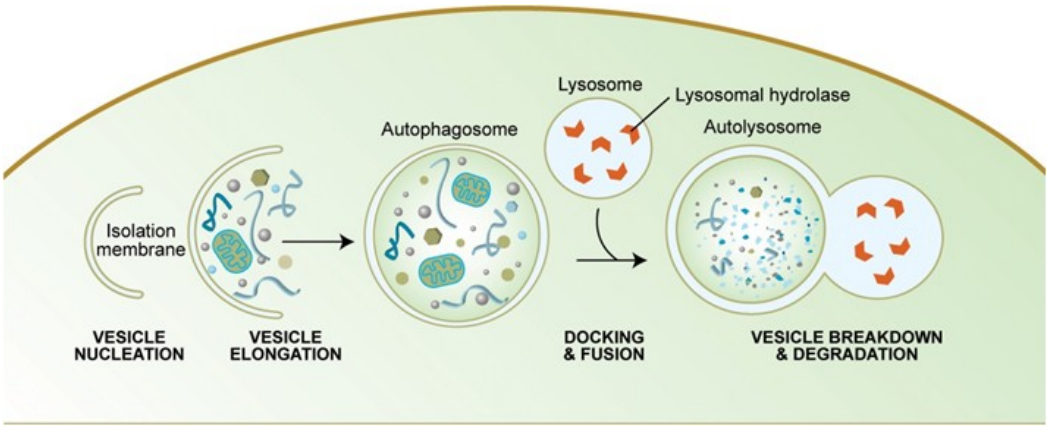

Figure 1.14. Scheme of the current working model of autophagosome formation. Four main steps are distinguished in the process: Membrane or vesicle nucleation, phagophore elongation and closure, autophagosome-lysosome fusion and a final degradation of the contents. [Taken from Meléndez A. et al (2009)]

To date at least 35 autophagy-related (ATG) genes (**Table 1.1**), divided into several groups depending on the timing of their participitacion during AP biogenesis, have been identified and related to the process (Lamb *et al.*, 2013). Among them, the Atg8 family of ubiquitin-like proteins, studied in this thesis, are late autophagosome-specific proteins that bind the AP, and are involved in phagophore expansion.

Table 1.1. Essential Atg proteins for autophagosome formation. [Taken from Lamb CA et al (2013)]

Protein	Position in autophagic pathway	Alternative name and function
ULK1 and ULK2	ULK complex	Atg1 orthologues; Ser/Thr kinases that mediate mTOR signalling and ATG9 cycling
ATG13	ULK complex	ULK1 and ULK2 substrate that also modulates the activity of the ULK complex
FIP200	ULK complex	Atg17 orthologue; ULK1 and ULK2 substrate that also modulates the activity of the ULK complex
ATG101	ULK complex	Interacts with ULK1 and ATG13
Beclin 1	PI3K complex	Atg6 orthologue; part of the PI3K complex and also has a role in autophagy during initiation, formation and maturation
VPS34	PI3K complex	Catalytically active subunit of the PI3K complex
p150	PI3K complex	Vps15 orthologue; recruits the PI3K complex to membranes
ATG14L	PI3K complex	Atg14 orthologue; directs the PI3K complex to the omegasome; also known as Barkor
WIPI1 and WIPI2	PtdIns(3)P-binding protein	Atg18 orthologues; bind to PtdIns(3)P on the autophagosome
ATG3	LC3-PE conjugation	Similar to the E2 ubiquitin conjugating enzyme; conjugates LC3 to phosphatidylethanolamine
ATG4	LC3–PE conjugation	Cys protease that cleaves carboxy-terminal Gly residues from LC3 homologues and is also required to recycle LC3 from the autophagosome outer membrane
ATG7	LC3–PE and ATG12 conjugation	Similar to E1 ubiquitin activating enzymes; activates ATG12 and LC3 homologues
LC3-A, LC3-B, LC3-C, GATE16, GABARAPL1, GABARAPL2 and GABARAPL3	LC3– PE conjugation	Atg8 homologues; ubiquitin-like proteins that recruit cargo to autophagosomes and may aid in membrane fusion
ATG5	ATG5–ATG12 conjugation	Conjugated to ATG12
ATG10	ATG5–ATG12 conjugation	Similar to E2 ubiquitin conjugating enzyme; links ATG12 to an internal Lys residue in ATG5
ATG12	ATG5–ATG12 conjugation	Ubiquitin-like protein conjugated to ATG5 that functions in the activation of ATG3
ATG16L1	ATG5–ATG12 complex	Binds to the ATG5–ATG12 conjugate and directs LC3 conjugation at the isolation membrane
ATG9A and ATG9B	Integral membrane proteins	Atg9 orthologues; required for autophagosome formation
ATG2A and ATG2B	Localize to omegasome	Atg2 orthologues; required for closure of isolation membranes to form autophagosomes

1.2.4 Autophagy Signalling Cascade

Autophagy induction is controlled by a complex regulatory mechanism involving different input signals that include nutrients, growth factors, hormones, ATP levels, and various others. Many signals converge at the level of the mammalian target of rapamycin complex 1 (mTORC1). mTORC1 consists of mTOR, regulatory associated protein of mTOR (raptor), DEP-domain-containing mTOR-interacting protein (Deptor), proline-rich AKT substrate 40 kDa (PRAS40) and G-protein β-subunit-like protein (GβL) (Wirawan *et al.*, 2012). When amino acids and growth factors are present, class I phosphatidylinositol-3-kinase (PIK3C1) activates mTORC1, which suppresses autophagic signalling. Active mTORC1 inhibits autophagy by binding and phosphorylating uncoordinated-51 (unc-51)-like kinase 1 or 2 (ULK1 or ULK2) and Atg13 within the ULK complex. This complex is composed of ULK1 or ULK2, atg13, focal adhesion kinase family interacting protein 200 kDa (FIP200) and Atg101 (Noda & Inagaki, 2015). Consequently, repression of mTORC1 by nutrient deprivation or rapamycin treatment is commonly used to activate autophagy. Thus, when mTORC1 is inactivated, it dissociates from the ULK complex, allowing ULK activity (**Figure 1.15**) (Noda & Fujioka, 2015). In yeast, Atg17, Atg29 and Atg31 are also components of the Atg1 complex and participate in the recruitment of Atg9 vesicles to the PAS, through an Atg1-dependent interaction of Atg17 with Atg9 (Ragusa *et al.*, 2012; Stanley *et al.*, 2014). This aspect represents an important difference between the yeast and mammalian pathway.

During starvation, ULK1 plays an important role in regulating mATG9 trafficking, the unique multispanning transmembrane protein, that cycles between the trans-Golgi network and the endosomal compartment in basal conditions. Upon autophagy induction, mATG9 is recruited to the growing autophagosome, where it might supply lipids needed for membrane elongation (Orsi *et al.*, 2012; Webber *et al.*, 2007).

After autophagy induction, several protein complexes participate in the isolation membrane elongation to build the mature autophagosome. This process can be divided into three stages: vesicle nucleation, elongation and maturation. In order to develop these actions, proteins take part each one in a specific step.

In the first step, a huge number of different proteins are recruited to the site of autophagosome formation, in a process called autophagosome nucleation. PIK3C3, p150, Ambra1 and Bcl-2-interacting protein (Beclin-1) form the core of the PIK3C3 complex, which can also bind the product of UV-radiation resistance associated gene (UVRAG) or Atg14L. Within the complex, Beclin-1 is the target to which some protein

regulators of PIK3C3 bind in order to modulate the generation of phosphatidylinositol-3-phosphate (PI3P). This phospholipid plays the role of recruiting more Atg proteins to the nucleation site. Among the PI3P interacting proteins, WD repeat domain phosphoinositide interacting 1 (WIPI1) and 2 (WIPI2) (Dooley *et al.*, 2014; Polson *et al.*, 2010), mAtg2 and double-FYVE containing protein-1 (DFCP1) are the most well known even if their exact role needs to be further studied.

Afterwards two ubiquitin-like (UBL) conjugation systems participate in autophagosome membrane elongation, shaping and closure. These two systems are interconnected and need to act together for a proper autophagosome growing *in vivo*. The first UBL system is composed of Atg5, Atg12, Atg10 and Atg16L1. Initially, Atg12 is activated by Atg7 (E1-like enzyme), transferred to Atg10 (E2-like enzyme) and finally covalently bound to Atg5. Atg12-Atg5 interacts also with Atg16L1 to create a complex that homodimerizes forming a multimeric complex (**Figure 1.15**). The final action of this complex is to interact with the outer autophagosomal membrane and to act as the E3 ligase enzyme of the second UBL conjugation system (Romanov *et al.*, 2012; Walczak & Martens, 2013).

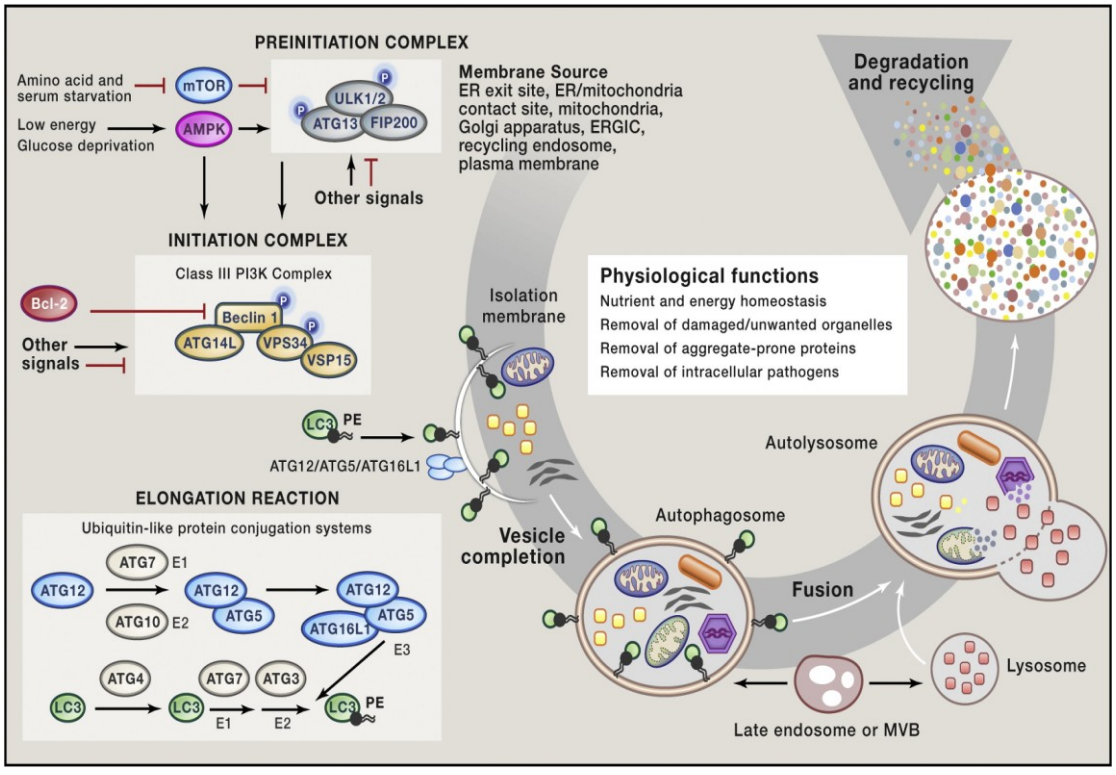

Figure 1.15. Macroautophagy signaling pathway. From top to bottom, different signals act as upstream inhibitors of mTOR. ULK and PI3KC3 complex participate and recruit more proteins for membrane nucleation. Both, Atg8 and Atg5 UBL systems work in collaboration in autophagosome elongation and closure. [Taken from Green & Levine, (2014)]

This second UBL system is constituted by ATG4, ATG7, ATG3 and LC3 (**Figure 1.15**). First of all, LC3 is cleaved in its C-terminal end by ATG4, exposing a glycine. Next, LC3 is associated with ATG7 and then transferred to ATG3 in an ATP dependent transthioesterification process. Once bound to ATG3, the latter directs LC3 to the autophagosomal membrane, and in collaboration with the E3-ligase complex catalyzes the conjugation of LC3 to phosphatidylethanolamine (PE) to produce LC3-PE (Nakatogawa *et al.*, 2007; Noda *et al.*, 2011; Tanida *et al.*, 2004).

The final product, LC3-PE, is considered as the main autophagy-specific marker in cells, and is also the best known effector in autophagosome elongation. Moreover LC3 in the preautophagosomal membrane recruits partner proteins, through its LC3-interacting motif (LIR), involved in autophagy regulation and autophasome growth (Hurley & Schulman, 2014; Noda *et al.*, 2010a). Once the autophagosome is formed and closed with the corresponding material to degrade, ATG4 participates again removing LC3-PE from the outer autophagosomal membrane in the recycling of LC3. Nevertheless, LC3 associated to the inner autophagosomal membrane will be degraded by the lysosomal enzymes. More about the Atg8 UBL system will be explained in **section 1.2.7**.

In the last step of autophagy and regarding the enclosured material degradation, autophagosome travels along the cytoplasm through microtubules and fuses with the lysosomes. The outer autophagosomal membrane fuses with the lysosomes so that the inner autophagosomal membrane and their contents come into contact with the lysosomal hydrolases and lipases. Many proteins take part in the autophagosome-lysosome fusion event such as LAMP2, Ras-related GTP-binding protein (Rab), homotypic fusion and protein sorting (HOPS), SNAREs, LC3, ESCRT, FYCO1 and UVRAG-C-Vps tethering complex (Wirawan *et al.*, 2012).

The result of the autophagy process is the generation of recycled amino acids, fatty acids and nucleosides that will come back to the cytosol for new anabolic reactions.

1.2.5 Autophagy is a Lipid-modulated Process

In the autophagy network, the main object of study in this thesis, there are several proteins that associate with different cell membranes. Those proteins may associate through a lipid moiety, a fatty acid or prenyl group, a glycosylphosphatidyl-

inositol (GPI) anchor, an amphipathic alpha helix, a domain such as FYVE (that binds PtdIns 3-phosphate), or a PH domain (that binds PtdIns 3,4-bisphosphate). Unusually, Atg8 and mammalian Atg8 protein family associate with autophagosomal membranes through PE that is covalently attached to the C-terminal glycine residue. This type of modification is so far unique to the Atg8 family. Peripheral membrane proteins known to be involved in autophagosome formation include for example ULK1 and ULK2, known to be present in a salt- and detergent-resistant membrane fraction, and DFCP1, that contains a FYVE domain (Tooze, 2010).

The initiation of the autophagic signalling under starvation conditions starts in the plasma membrane where phosphoinositides are recognized by proteins (Phosphatidylinositol-3-kinase or phosphoinositide phosphatases). In addition, from the beginning to the end of autophagosome formation a huge amount of membrane material is constantly moving through different cell localizations with many proteins transiently associated, such as Atg9, Atg5-12-16 complex, Atg3, Atg14 or WIPI proteins.

1.2.6 Autophagy in Health and Disease

Autophagy is activated as an adaptive catabolic process in response to different forms of metabolic stress, including nutrient deprivation, growth factor depletion and hypoxia. Generation of free amino acids and fatty acids as a result of autophagy are further used for *de novo* synthesis of cellular building blocks and energy production essential for stress adaptation.

The repertoire of housekeeping actions performed by autophagy covers the removal of defective proteins, organelles, abnormal protein aggregates and intracellular pathogens. These functions make autophagy a critical process involved in the protection against cancer, infection, neurodegenerative diseases and aging (Galluzzi *et al.*, 2016; Levine & Kroemer, 2008; Rubinsztein *et al.*, 2011).

Autophagy may have a multifactorial influence on the initiation and progression of cancer, as well as being a valuable target in its treatment (Choi *et al.*, 2013). The regulation mechanism of autophagy overlaps with signalling pathways of tumorigenesis, as is the case of the tumour suppressor genes upstream of TOR signalling such as PTEN, TSC1 and TSC2. However Akt, an oncogene product of this pathway, also crosstalks inhibiting autophagy (Levine & Kroemer, 2008). Inhibition of

autophagy may allow the continuous growth of precancerous cells, but conversely when tumours grow, cancer cells need autophagy to survive under nutrient-limiting conditions. A good example of the involvement of autophagy in cancer is beclin 1. This protein is monoallelically deleted in a high percentage of breast, ovarian and prostate cancers. Stable transfection of beclin 1 in MCF7 cells promotes autophagic activity and reduces tumorigenic capacity, which suggests a possible tumor suppressor role of the autophagic protein beclin 1 (Liang *et al.*, 1999; Shintani & Klionsky, 2004).

Furthermore, some reports show evidences of the involvement of autophagy in neurodegenerative diseases (Menzies *et al.*, 2015; Wong & Cuervo, 2010; Wong & Holzbaur, 2015). An accumulation of autophagosomes has been observed in many disorders such as Parkinson´s, Alzheimer´s and Huntington´s diseases. These illnesses share the accumulation of protein aggregates of α-synuclein, tau or polyglutamine-rich proteins, respectively (Lynch-Day *et al.*, 2012; Martinez-Vicente *et al.*, 2010; Nixon *et al.*, 2005). In order to fix the critical situation, cells highly increase their autophagic activity to eliminate these protein aggregates (aggrephagy), but nevertheless the presence of this kind of aggregates impairs autophagy. Thus, autophagy represents an important target in the treatment of these disorders.

Moreover, the homeostatic functions of autophagy in the long-lived protein turnover and removal of damaged organelles are thought to act as an anti-aging process. Analysis of autophagy related genes (BECN1, Atg7 or Atg5) showed an important down-regulation in old people compared to the younger ones, which is correlated with a reduction in autophagy rate (Lipinski *et al.*, 2010). This could explain why a caloric restriction might induce autophagic activity, representing a possible mechanism for life-span extension (Jia & Levine, 2007). In addition to the above discussed implications of autophagy, pathogen infection, muscular disorders, immunity, cardiovascular, pulmonary and metabolic diseases are partly regulated by the autophagic pathway (Jiang & Mizushima, 2014; Levine & Kroemer, 2008).

1.2.7 Atg8 Conjugation System

The autophagosome elongation and sealing process involves two UBL systems, Atg8 and Atg5. Both of them work together *in vivo*, although *in vitro* the presence of the second one is not strictly necessary for their main goal, Atg8 lipidation. Since the main work in this thesis is focused on the Atg8 UBL system, a detailed description of its action mode is shown below.

Atg8, a crucial protein in the autophagic process of autophagosome elongation in yeast, is the central player and also the final effector of the UBL system. At least eight Atg8 orthologs have been identified in mammals, divided into two subfamilies, LC3 and GABARAP. LC3A, LC3B, LC3B2 and LC3C constitute LC3 subfamily, whereas GABARAP, GABARAPL1, GABARAPL2/GATE-16 and GABARAPL3 comprise the GABARAP one (Weidberg *et al.*, 2010). In the context of this thesis, LC3B, GABARAP and GATE-16 will be studied. LC3B (MAP1LC3B; Microtubule associated protein 1 light chain 3 B) is the most extensively studied ortholog in mammals and it participates in autophagosome biogenesis as it does Atg8 in yeast. GATE-16 (Golgi-associated ATPase enhancer of 16 kDa) and GABARAP (γ-aminobutyric acid type A receptor associated protein) were identified as an intra-Golgi vesicular transport factor and a protein that facilitates clustering of GABAA receptors in combination with microtubules, respectively (Tanida *et al.*, 2004). Both of them are the most recently but less characterized orthologs in terms of their role in autophagosome formation.

LC3B, GABARAP and GATE-16, as well as the other Atg8 orthologs, share a strong structural similarity with ubiquitin, despite the lack of similarity in amino acid sequence (Shpilka *et al.*, 2011). The C-terminal ubiquitin core is mainly conserved, and the larger differences are located in the regions surrounding it (**Figure 1.16**).

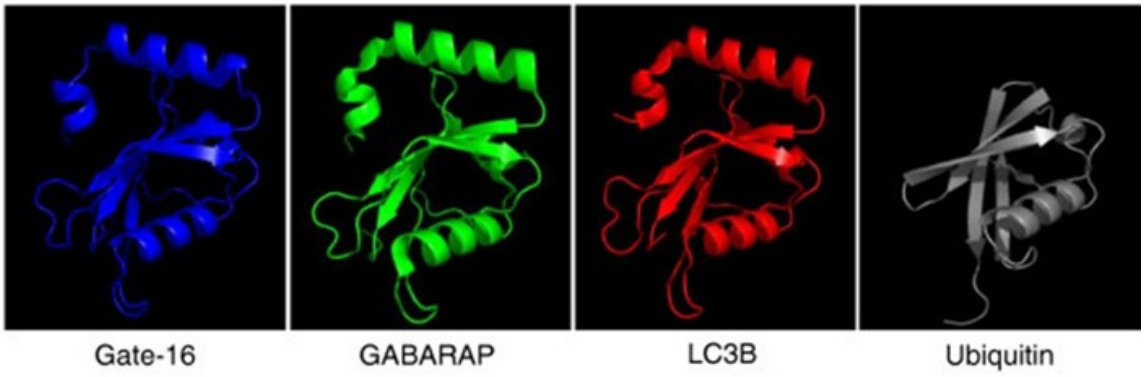

Figure 1.16. Crystal structures of 3 different mammalian orthologs of Atg8, and ubiquitin. [Taken from Shpilka et al. (2011)]

Atg8 UBL system contains three other proteins, ATG4, ATG7 (E1- like enzyme) and ATG3 (E2-like enzyme). ATG4 is a cysteine protease responsible for the post-translational cleavage of LC3 last five amino acids to expose a C-terminal glycine (G120) (Kirisako *et al.*, 2000). This glycine is essential for the final conjugation to PE.

After that cleavage, LC3 (125 aa, 14.6 kDa) interacts with the E1-like enzyme of the system, ATG7. ATG7 (703 aa, 77.9 kDa) is a symmetric homodimer with two catalytic cysteine residues that allow it to activate two different UBL proteins, LC3 and Atg12 (Hong *et al.*, 2011; Kaiser *et al.*, 2013). Each Atg7 monomer is comprised of two globular domains, the C-terminal domain (CTD) and the N-terminal domain (NTD), connected by a short linker (**Figure 1.17**). The CTD includes an Adenylation domain (AD), the cysteine-containing domain and a final homodimerization motif (ECTD), whereas the NTD just recognizes the E2-like enzyme Atg3 or Atg10 (Noda *et al.*, 2011). Among these domains, the ECTD is suggested to be responsible for Atg7 homodimerization and interaction with LC3, the cysteine-containing domain accommodates the catalytic cysteine (C572) which is critical for UBLs activation, and the AD binds the MgATP molecule necessary for the subsequent formation of thioester bonds between the proteins. In contrast, the NTD is unique in E2 enzymes, and it is responsible for the recognition of Atg3 by a highly basic patch (Ohashi & Otomo, 2015).

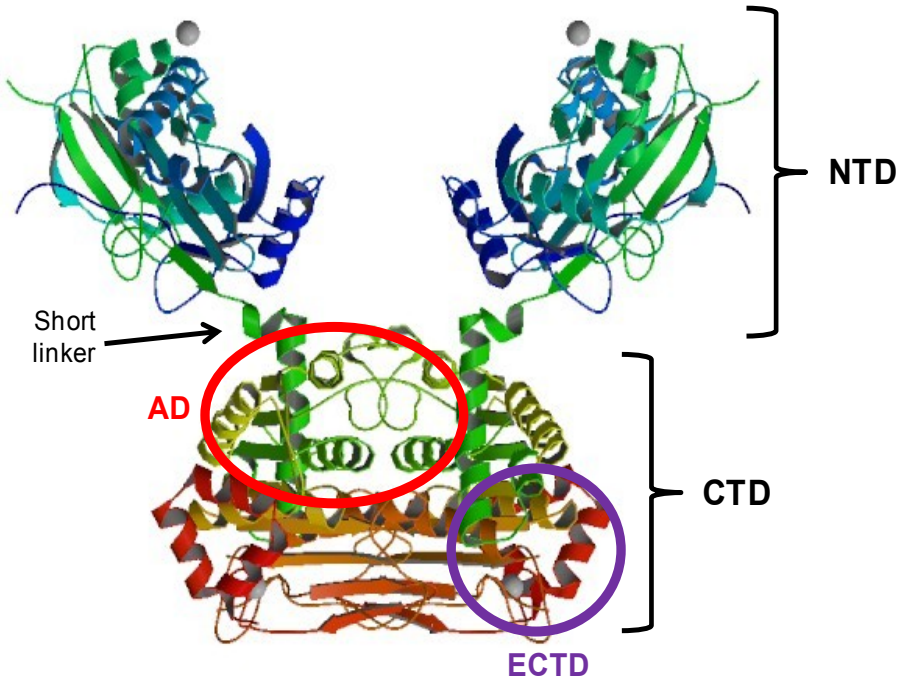

Figure 1.17. Yeast Atg7 crystal structure. AD in red, ECTD in violet and NTD and CTD indicated with brackets.

ATG3, the E2-like enzyme of this system, receives LC3 from ATG7 and is thought to be engaged in bringing LC3 to the membrane for its final lipidation. Atg3 has mainly two characteristic regions, a handle region (HR) for interaction with LC3 and a highly acidic flexible region (FR) through which it interacts with Atg7 (Yamada *et al.*,

2007). Additionally, a predicted N-terminal α-helix is suggested to recognize the autophagosomal membrane (Nath *et al.*, 2014).

Taking this into consideration, the operation of the Atg8 UBL system is as follows (**Figure 1.18**):

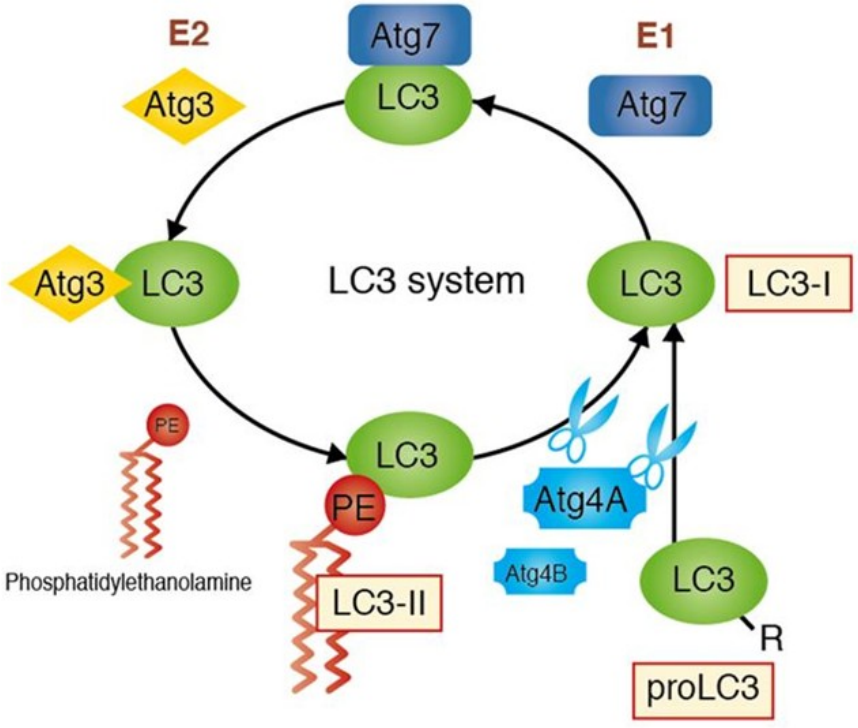

Figure 1.18. Schematic representation of Atg8 UBL system. [Taken from http://ruo.mbl.co.jp/g/product/protein/autophagy/autophagy.html]

I. First, ATG4 cleaves the last 5 amino acids of LC3, exposing a final Glycine (G120) to which PE can then be coupled during the following steps.

II. Next, ATG7 binds both MgATP in its AD and LC3 in the ECTD. After moving LC3 from ECTD to AD, ATG7 catalyzes the adenylation of LC3 in its C-terminal Glycine. Subsequently, ATG7 catalytic cysteine (C572) attacks the LC3-acyl adenylate intermediate to generate a thioster bond between ATG7-LC3 (Taherbhoy *et al.*, 2011).

III. Then, ATG3 associates with ATG7 NTD and a transthiolation reaction occurs whereby LC3 is transferred from ATG7 C572 to ATG3 C264 in a trans manner. A new thioester-linked ATG3-LC3 intermediate is generated.

IV. Finally, ATG3 redirects LC3 to the autophagosomal membrane where the latter one will be transferred from ATG3´s catalytic cysteine to the amine head group of PE via an amide bond. This final reaction is stimulated by the other UBL system participating in autophagy, Atg5-Atg12-Atg16 complex. This complex acts as the E3-ligase enzyme of this sophisticated reaction.

1.2.8 ATG3, the E2-like Enzyme in the Atg8 Conjugation System

LC3 lipidation requires the approach of this protein to a PE-enriched membrane. This approach would be catalyzed by ATG3, the E2-like enzyme of the UBL system. ATG3 and canonical E2 enzymes have similar structures, despite having little sequence homology. Human ATG3 (314 aa, 35.8 kDa) has a partially conserved core region with two unique and large insertions, the FR and HR regions (**Figure 1.19**). These two regions participate in the interaction of ATG3 with the E1-like (ATG7) and the UBL (LC3) enzymes of the system, respectively. HR domain consists of a long α-helix F and a loop, whereas the FR is a highly acidic, 80-100 residue long, very mobile domain situated between strands 2 and 3 (Yamada *et al.*, 2007). Aditionally, ATG3 interaction with membranes was proposed to be directed by the N-terminal region of the protein. In yeast, Atg3 first seven amino acids are essential to the recognition of PE-containing membranes and also to Atg8-PE formation (Hanada *et al.*, 2009; Oh-oka *et al.*, 2008).

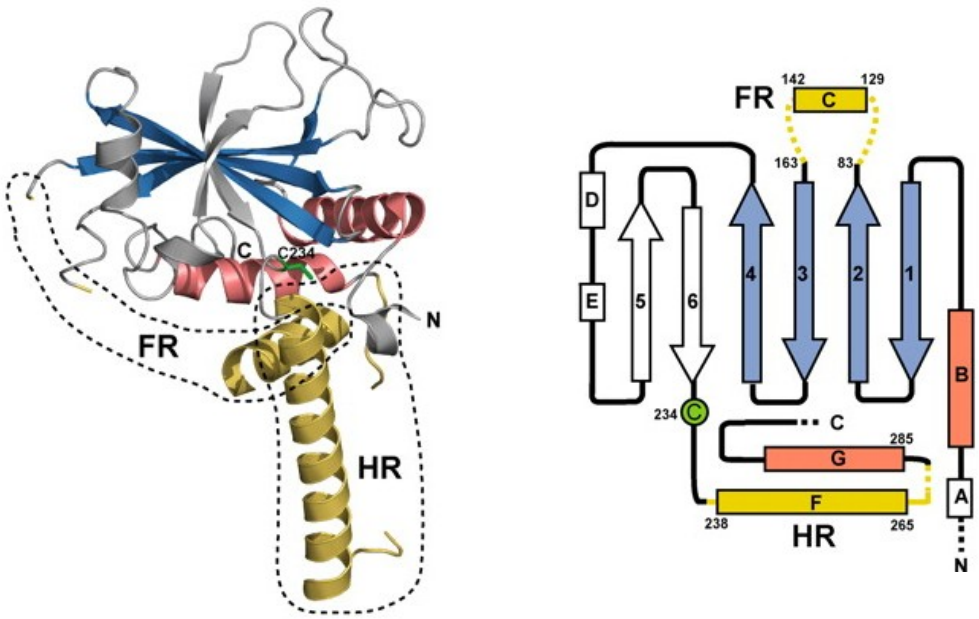

Figure 1.19. Yeast Atg3 crystal structure. FR and HR domains indicated with dotted lines (left). Conserved α-helices and β-strands are coloured red and cyan, respectively, and non-conserved α-helices, β-strands, and loop regions are coloured gray. The two unique inserted regions of Atg3, FR and HR, are coloured yellow (right). Regions lacking defined electron density are indicated with dotted lines (right).

In contrast, mouse ATG3, practically identical to human (97.5% identity), was suggested and demonstrated to insert into membranes through an N-terminal amphipathic helix comprising the first 26 amino acids of the protein (Nath *et al.*, 2014). This helix would present a large hydrophobic moment and an amphipathic distribution. There are two hydrophobic and polar faces clearly separated by two lysines, one in each border and probably defining the surface of the bilayer. The hydrophobic face is mainly composed of small hydrophobic residues such as valine and leucine, just as the polar face contains small polar and anionic residues. These characteristics suggest a weak interaction with stable bilayers. Recently it has been proposed ATG3 N-terminal helix as a membrane curvature sensor, more specifically sensing membrane defects created in highly PE-enriched membranes. They demonstrated that ATG3 interacts more strongly with very small liposomes and that the lipidation reaction is most efficient in these small-sized vesicles (Nath *et al.*, 2014).

Taking this into consideration and comparing with other examples of curvature sensors and amphipathic helices containing proteins such as ADP-ribosylation factor GTPase-activating protein 1 (ArfGAP1) and Beclin 1-associated autophagy-related key regulator (Barkor) (Fan *et al.*, 2011), or α-synuclein (Antonny, 2011; Bartels *et al.*, 2010; Jo *et al.*, 2000), Atg3 shares some characteristics of both groups. It contains two lysines important for the interaction with the polar groups of phospholipids, but also a mildly hydrophobic face. So ATG3 ability to bind to membranes would rely on both properties. In this context, human ATG3 interaction with model membranes has been studied in this thesis.

1.2.9 ATG9: the Only Transmembrane Atg Protein

In yeast there is just one transmembrane protein involved in autophagy up to date: Atg9. It possesses 6 transmembrane helices, in addition to both N-terminus and C-terminus ends oriented to the cytosol (**Figure 1.20**).

Atg9 has been well characterized in yeast, where it was demonstrated that in contrast to most of the Atg proteins, Atg9 does not localize to the preautophagosomal structure (PAS) (Mari & Reggiori, 2007). Atg9 seems to be located in some vesicles distributed around the cytosol. Its function is not yet known, but it was suggested to move cyclically to the PAS in order to deliver some membrane portions for autophagosome elongation. It is also thought that these vesicles are the membrane source for phagophore formation. Atg9 is not present as part of the mature

autophagosomes, so it is thought that it is previously removed from there by the Atg1-Atg13 complex, the PI3K complex, Atg2 and Atg18. Atg1 and PI3K complex would associate with the PAS and the Atg9 removal would start by recruiting at the same time Atg2 and Atg18 to the autophagosomal membrane (He *et al.*, 2006; Reggiori *et al.*, 2004). Despite the no incorporation to the mature autophagosome, Atg9 has been demonstrated to be transiently embedded in the autophagosomal outer membrane (Yamamoto *et al.*, 2012). Atg17-Atg29-Atg31 protein complex is suggested to bind to Atg9 vesicles through the interaction of Atg17 with Atg9. This complex would bind two Atg9 vesicles in order to carry out the tether and fusion of these vesicles and generate early isolation membranes (Ragusa *et al.*, 2012).

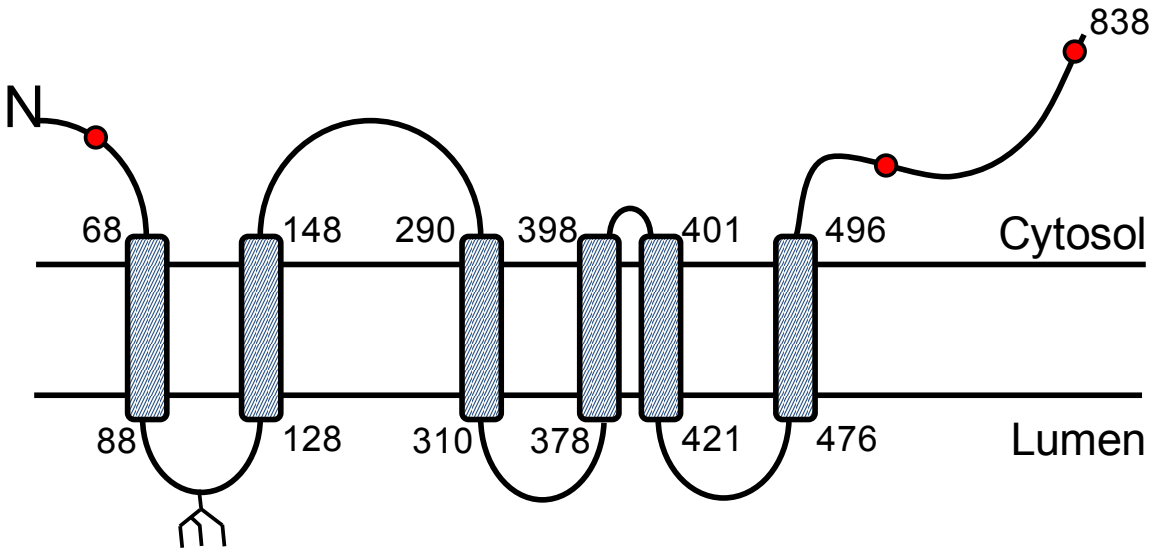

Figure 1.20. Schematic representation of Atg9. It consist of 6 transmembrane helices and two N- (68 aa) and C- terminal (342 aa) domains exposed to the cytosol. A glycosilation site is located in the first luminal loop.

From all the hypothesis about Atg9 trafficking, it could be extracted that if Atg9 trafficking is increased then the autophagosome would grow. Some Atg9 intermolecular interactions would facilitate fusion of small vesicles that deliver membrane material for PAS elongation.

In mammals, ATG9 (829 aa, 94.4 kDa) is also a multispanned protein with 6 transmembrane helices, and both N and C terminal domains are exposed to the cytosol. However, there are some characteristics in these domains that confer specific properties to the mammalian homologue. In HEK293 cells, mATG9 is localised to the trans-Golgi region and to peripheral endosomes when cells are grown in complete medium (Young *et al.*, 2006). Nevertheless, when amino acids are restricted,

autophagy is induced and mATG9 moves away from these regions, and colocalizes with Rab7 and GFP-LC3 (Longatti *et al.*, 2012; Orsi *et al.*, 2012). Comparing with the Atg9 behaviour in yeast, there is no evidence of proteins that interact with Atg9 in order to fuse Atg9 vesicles as in the case of Atg17-Atg29-Atg31 complex in yeast. Therefore further efforts must be done in this context to establish the basic molecular mechanism of autophagy initiation.

Taking this into account and considering that there is no data about hATG9 function in vitro, an important contribution in this area must be done. The continuous movement of the hATG9 vesicles in the cytoplasm might contribute to the regulation of autophagosome size. The delivery of these vesicles to the forming autophagosome might provide lipid material for its growth. Thus recombinant hATG9 purification has been tried in order to know the presence of lipids associated to the protein and to perform experiments with model membranes.

1.3 Aims

The present work is focused on a better understanding of how autophagosome elongates and of the proteins involved in the process. Atg8 lipidation is proposed to engage in vesicle-phagophore fusion events along the nascent autophagosome growth. The involvement of lipid-lipid and protein-lipid interactions in this process constitutes the basis of our interest in the autophagy pathway. Biophysical approaches applying model membrane techniques, well established in our laboratory, have been used to progress in the knowledge of this aspect of cell molecular biology.

The specific aims of this thesis are the following:

- To *in vitro* reconstitute the autophagosome elongation process with a minimal protein ensemble constituted by the human Atg8/ATG3/ATG7 UBL system.

- To investigate the interaction of ATG3 with model membranes and its possible role in the human Atg8 lipidation process.

- To express and purify the transmembrane protein ATG9 in order to explore its involvement in lipid delivery.

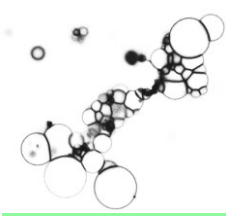

2. Experimental Techniques

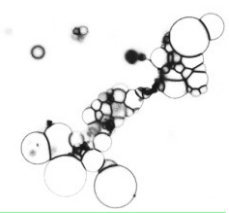

Chapter 2:

Experimental Techniques

2.1 Molecular Biology Methods

Molecular biology techniques make possible to isolate, purify and modify DNA sequences encoding the protein of interest (Sambrook & MacCallum, 2001). In this work, we have applied standard recombinant DNA techniques in order to clone cDNAs of several Atg proteins into bacterial and insect expression vectors as well as to perform mutations in their sequences for analyzing the implication of selected residues in the overall protein function.

2.1.1 DNA Amplification and Cloning

In order to clone the cDNA of interest, a DNA fragment is PCR-amplified and inserted into a self-replicating genetic element, generally a plasmid, usually called the vector. The process can be divided in: 1) PCR Amplification, 2) Digestion, 3) DNA purification, 4) Ligation, 5) Transformation in *E.coli*, 6) Extraction, and 7) Confirmation the presence of the insert in the vector (**Figure 2.1**).

1. PCR Amplification and Purification:

cDNA of interest was PCR-amplified using a MastercyclerPro Thermocycler (Eppendorf AG, Hamburg, Germany) with PfuTurbo DNA Polymerase (Agilent Technologies, Santa Clara, CAL, U.S.A) using the indicated general PCR conditions. Forward and reverse primers, carrying the appropriate restriction sites allowing ligation in the target vectors, were synthesized by Sigma Aldrich (Madrid, Spain). The PCR product was subjected to purification using QIAquick Gel Extraction Kit (Qiagen, California, U.S.A.).

2. Digestion:

Both PCR product and target vector were digested with the same restriction enzymes (New England Biolabs, Canada) for 1 hour at 37 ºC. To avoid self-ligation, the vector was subjected to dephosphorylation using shrimp alkaline phosphatase (USB Corp, Cleveland, OH, U.S.A) for 1 hour at 37 ºC. Restriction enzymes and alkaline phosphatase were heat-inactivated for 20 min at 65 ºC.

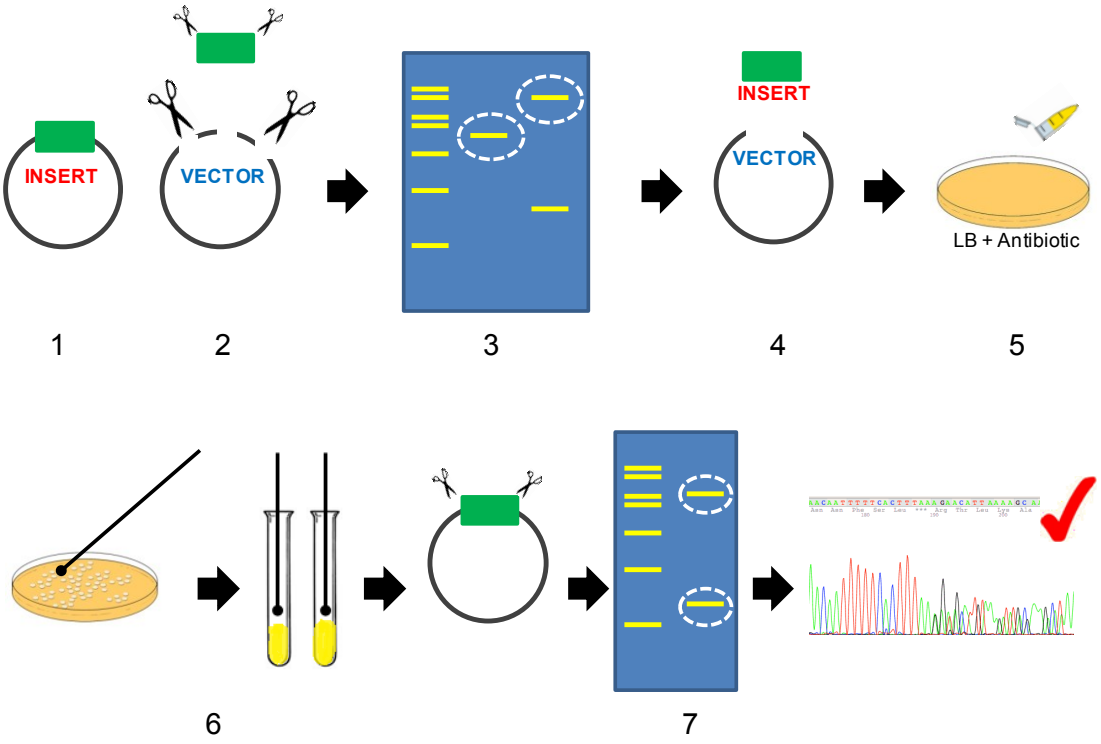

Figure 2.1. General cloning steps. (1) PCR amplification, (2) Digestion, (3) Purification, (4) Ligation, (5) Transformation in *E.coli*, (6) DNA isolation and (7) Checking for the presence of insert. See details in text.

3. Purification of Digestion Products:

Digestion products were diluted in Loading Dye Solution (Thermo Scientific, Waltham, MA, U.S.A); loaded on 1-2% agarose gels and then gel purified using the QIAquick Gel Extraction Kit (Qiagen, California, U.S.A.).

4. Ligation:

Ligations were performed at 16 ºC overnight using T4 DNA ligase in 10x T4 DNA Ligase Buffer (Roche, Basel, Switzerland).

5. Transformation in *E.coli*:

For transformation of ligation products, ligation mixture was added to 50 µl of XL10-Gold Ultracompetent Cells (Agilent Technologies, Santa Clara, CAL, U.S.A). Cells were first incubated on ice for 15 min, and then heat-shocked for 90 s in a bath at 42 ºC. The mixture was immediately transferred to an ice bucket and incubated for 2 min to allow cell recovery. Next the mixture was placed in a tube with 1 ml Luria Broth (LB) medium and incubated with gentle stirring at 37 ºC for 45 min. Finally, cells were spun down in a benchtop centrifuge at 8,000 xg for 1 min. The pellet was resuspended in 50 µl LB, plated in an agar plate with the appropriate antibiotic and incubated at 37 ºC overnight.

6. Confirmation the Presence of the Insert in the Vector:

If present, several colonies were randomly picked from the agar plate and grown overnight at 37 ºC in 5 ml LB medium containing the appropriate antibiotics. For isolation of plasmidic DNA, cells were subjected to alkaline lysis followed by DNA purification using a miniprep spin kit (Qiagen, California, U.S.A) following the manufacturer's instructions. DNA concentration was determined by measuring the absorbance of the sample at 260 nm (A_{260}), and its purity from the A_{260}/A_{280} ratio in a NanodropTM spectrophotometer (Thermo Scientific, Waltham, MA, U.S.A). DNAs were digested with appropriate restriction enzymes at 37 ºC for 1 h and subjected to electrophoresis to check that the insert was present. Any mutation introduced during PCR amplification was discarded by sequencing (Secugen S.L, Madrid, Spain).

2.1.2 Site-directed Mutagenesis

In vitro site-directed mutagenesis is an invaluable technique for determining the contribution of individual amino acids to the structure and function of a given protein. Over the past two decades, highly effective simple methods for making site-directed mutations without subcloning have been developed (Fisher & Pei, 1997). In this work, we have used Stratagene Quikchange Site-Directed Mutagenesis Kit (Agilent Technologies, Santa Clara, CAL, U.S.A) to perform point mutations in ATG3.

The basic procedure utilizes an initial template double-stranded DNA (dsDNA) and two synthetic oligonucleotide primers containing the desired mutation (**Table 2.1**). The oligonucleotide primers, each complementary to opposite strands of the vector, are extended during temperature cycling by PCR using PfuTurbo DNA polymerase

(Agilent). Incorporation of the oligonucleotide primers generates a mutated plasmid containing staggered nicks. Following temperature cycling, the product is treated with DpnI. The DpnI endonuclease (target sequence: 5´-Gm6ATC-3´) is specific for methylated and hemimethylated DNA and is used to digest the parental DNA template and to select for mutations containing synthesized DNA. The nicked vector containing the desired mutations is then transformed into XL10-Gold Ultracompetent Cells (Agilent).

In the following protocol (**Protocol 1**), the general procedure used in this work to perform point mutations in ATG3 is shown. However, for particular cases where the reaction failed, the protocol was modified by dropping the primer concentration, increasing the template concentration, or decreasing the PCR annealing temperature.

Primers		Sequence
ATG3 K9D/K11D	**Forward**	5´-GATTAATACTGTGGCGGGAGCGGCACTGG-3´
	Reverse	5´-CCAGTGCCGCTCCCGCCACAGTATTAATC-3´

Table 2.1. Designed oligonucleotides for recombinant ATG3 mutations.

Protocol 1. Site-directed Mutagenesis

1. Mutagenic primers are designed using Stratagene´s web-based primer design program (http://www.stratagene.com/cprimerdesign.com) which basically designs primers with a melting temperature (Tm) of at least 78 ºC and centers the mutation in the middle.
2. Mix:
   - 0.5 µl Forward primer (2.5 pmoles/µl)
   - 0.5 µl Reverse primer (2.5 pmoles/µl)
   - 0.5 µl template DNA (10 ng/µl)
   - 0.5 µl 40 mM dNTP mix (10 mM each)
   - 0.5 µl Pfu Turbo Polymerase (2.5 U/µl)
   - 5 µl Polymerase buffer (5X)
   - 17.5 µl sterilized H2O
3. PCR program:
   - 5 min 95 ºC
   - Repeat x18
     - 30 s 95 ºC
     - 1 min 55 ºC
     - 2 min 72 ºC
   - 7 min 72 ºC

4. *DpnI* digestion is performed by adding 0.25 µl of *DpnI* (20 U/µl) to the reaction mixture, and incubating at 37 ºC for 1 h.
5. The final reaction product is transformed into competent cells. Generally, 1 µl is added into 50 µl of XL10-Gold Ultracompetent cells.
6. Finally a colony is picked, the DNA is amplified by miniprep and sequenced to verify the presence of the mutation and to discard any PCR-introduced mutation.

2.2 Recombinant Protein Expression and Purification

2.2.1 Protein Expression

Plasmids of LC3, GATE-16, GABARAP, ATG3 and their corresponding mutant forms were transformed onto *E. coli* BL21 (DE3) cells. Information about bacterial strains used for hATG9 expression are detailed in **Chapter 5**. Proteins were expressed as Glutathione S-transferase (GST)-tagged fusion proteins. First, cells were picked from a *E.coli* BL21 (DE3) glycerol stock into a 100 ml flask containing LB-Ampicillin (Amp) medium, and were incubated in an orbital shaker at 37 ºC overnight. The culture was escalated by adding 10 ml of the overnight saturated culture to 1 l LB-Amp medium, and the mixture was incubated at 37 ºC to 0.6-0.8 Optical Density (OD_{600}), then Isopropil-β-D-1-tiogalactopiranósido (IPTG) was added to start the induction of the recombinant protein expression. Due to differences in protein expression levels and susceptibility to proteolysis, different induction and expression times were optimized for each protein (**Table 2.2**). After IPTG addition, samples were incubated in an orbital shaker for the indicated times and bacteria were collected by centrifugation (5000 xg for 20 min, 4 ºC) in a Beckman Coulter centrifuge using a JLA-9.100 rotor (Beckman Coulter, Fullerton, California, U.S.A). The supernatant was discarded and the pellet was stored at -80 ºC for the purification steps.

Protein	Expression Conditions
LC3/GATE-16	3 h at 37 ºC
GABARAP	4 h at 20 ºC
ATG3	18 h at 18 ºC

Table 2.2. Conditions for expression of recombinant proteins.

2.2.2 Purification of GST-tagged Proteins (LC3, GATE-16, GABARAP and ATG3)

In order to start with the purification procedure, cells were subjected to the disruption and lysate clearance steps. Bacterial pellets were resuspended in appropriate Lysis buffer [10 mM PBS, 20 mM Tris-HCl pH 7, 150 mM NaCl, supplemented with freshly prepared 1 mg/ml lysozyme (Sigma- Aldrich), 1 mM Dithiothreitol (DTT)(Sigma-Aldrich), bacterial protein inhibitors (Roche, Basel, Switzerland) and 2.5 µg/ml DNAase (Sigma-Aldrich)]. The mixture was then incubated at 4 ºC in an orbital shaker for 40 min to allow disruption of the bacterial cell wall by lysozyme. Samples were then subjected to sonication on ice, to avoid overheating, 10 s on/10 s off 40 cycles twice. After cell disruption, the resultant suspension was centrifuged at 30000 xg for 30 min at 4 ºC in a Beckman Coulter centrifuge using JA-25-50 rotor (Beckman Coulter, Fullerton, California, U.S.A). The pellet was discarded and the supernatant was filtered through 0.45 µm and 0.2 µm filters, and finally kept on ice for subsequent purification steps.

GST-tagged LC3, GATE-16, GABARAP and ATG3 were purified by affinity chromatography using Glutathione Sepharose 4B beads (GE Healthcare). For each 4 l bacterial culture, 1 ml beads was required. Beads were first washed three times with ten bed volumes of distilled water and then five times with Lysis buffer by centrifugation. The bacterial supernatant was mixed with washed beads and the mixture was incubated for 3 h in an orbital rotator at 4 ºC to allow binding of Glutathione S-Transferase to glutathione. The beads with bound proteins were packed in a gravity flow column (Biorad), and the Flow-Through (FT) was removed. After that the column is washed with 10 bed volumes of each buffer described in **Table 2.3**. Then, 50 µl (Stock: 2000 units/ml) PreScission protease (GE Healthcare, Waukesha, WI, USA) were added to the beads in a 2 ml final volume. The mixture was transferred to a 15 ml falcon tube and incubated for 4 h in an orbital rotator at 4 ºC to allow efficient protease cleavage. The cleaved protein was eluted from the gravity flow column with Prescission buffer and two fractions of 4 ml were collected. After that another 4 ml Prescission buffer were added to the column with the beads and it was stored overnight at 4 ºC. Finally, the next day two more 4 ml fractions were eluted and subjected to SDS-PAGE analysis and Coommassie Blue staining. Protein enriched fractions were concentrated up to the desired.

Buffer		Buffer composition
Washing buffer	1	PBS1x pH 7.4 + 1 mM DTT
	2	PBS1x/TRIS 50 mM pH 8.7 + 1 mM DTT
	3	PBS1x/TRIS 50 mM, NaCl 500 mM pH 8.7 + 1 mM DTT
Prescission buffer		50 mM TRIS, 150 mM NaCl, 1 mM EDTA, pH 7.5 + 1 mM DTT.

Table 2.3. Buffer solutions used in GST-tagged proteins purification.

2.3 Baculovirus Expression Vector System

Microbial expression systems have been widely used for recombinant protein production. Well-known examples are the production of insulin, using *Escherichia coli* and the production of bovine growth hormone using *Saccharomyces cerevisiae* (Swartz, 2001). Many complex proteins, such as functional monoclonal antibodies or highly glycosylated proteins require post-translational processing for which the metabolic machinery is only available in higher eukaryotic or mammalian cells (Butler, 2006). While mammalian cells are the best to produce these proteins, they are also more costly for large scale production and can lead to immune reactions when used in therapeutic production. Another way of getting proteins is by extracting them from plants or animals directly, but that makes the process very expensive and leads to the sacrifice of many animals. Also, this method of production requires the often very difficult protein isolation from a plant or animal. The baculovirus expression vector system (BEVS) was developed in the 1980s. This system can be used to express proteins in insect cell lines and produce valuable and functional proteins that are similar to mammalian cell proteins. Proteins produced by BEVS can reduce the production time, as it takes a relatively short time to obtain a recombinant *Autographa californica* multiple nucleopolyhedrovirus (AcMNPV) for expressing a protein. Thus, the BEVS provides an intermediate approach between microbial and mammalian expression systems that is cost- and quality-effective. However a major problem with BEVS is the production of excess reactive oxygen species (ROS) e.g. superoxide radical (O2 •-) and hydroperoxide radical (•OH) resulting in oxidative stress following viral infection of the cell. These oxidative stresses result in earlier cell death that reduces protein production.

2.3.1 Baculovirus as Expression Vector

The Baculovirus (BV) infection in cell culture can be divided into three phases, namely *early phase*, or the reprogramming of the cells for virus replication, followed by the *late phase* for BV production, and then the *very late phase* for Occluded Virus (OV) production. The early phase lasts for about the first six hours post infection (hpi). During this time the cells undergo significant changes, e.g., cytoskeleton re-arrangements, host chromatin dispersion within the nucleus and cell enlargement. These changes occur primarily due to new proteins expressed following viral infection. The late phase lasts from 6 hpi to approximately 20-24 hpi. This stage mainly accounts for Baculovirus production. The very late phase begins at approximately 20 hpi. The production of OVs mainly occurs in this phase and can be marked by the presence of occlusion bodies in the nucleus. Polyhedra occlusion bodies have a crystalline nature and tend to give a highly refractive appearance to the group of infected cells or plaques.

The two most commonly used BV are *Bombyx mori* nucleopolyhedrovirus (BmNPV) and *Autographa californica* multiple nucleopolyhedrovirus (AcMNPV). Both of these viruses have a genome of approximately 130 kbp. The polyhedrin gene (polh) is expressed at very high levels during a separate and final phase of infection and this gene product is found to be non-essential for virus replication in cell culture (Smith *et al.*, 1983a). Thus, the first recombinant baculovirus was developed by replacing the polh gene with a heterogeneous gene under the control of the polh promoter (Miller *et al.*, 1983; Pennock *et al.*, 1984; Smith *et al.*, 1983b) and this is still used for most baculovirus expression vectors. This is also due to the fact that the polyhedron gene has a very strong promoter, leading to the accumulation of recombinant protein to levels as high as 50 % of the total cell protein. Also, expression vectors have been developed with multiple copies of this promoter that can be used to simultaneously express several recombinant proteins (Belyaev *et al.*, 1995).

Moreover, the rod shape of the nucleocapsids of Baculovirus can accommodate large viral DNA genomes, thereby allowing for DNA insertions at least as large as 15 kbp. BV vectors are relatively simple to use as they are independent of helper-virus. Construction of recombinant Baculovirus is easier than cloning and isolating stable cell lines and they do not infect mammalian cells, therefore providing a much safer expression system.

2.3.2 Insect Cell Lines

Insect cell lines have intermediate properties between mammalian cell lines and bacterial cell lines. Insect cells can perform post-translational protein folding like mammalian cells. However, it has been recognized that the protein processing pathways of insect cell lines differ from mammalian cell lines. For instance, the N- and O-linked glycosylations happen in a fundamentally different manner. Furthermore, protein production is dependent on the insect cell line, some insect cell lines just may not be able to produce a functional protein, while others can successfully carry out the protein processing (Harrison & Jarvis, 2007). The three most commonly used insect cell lines for BV expression are BTI-TN-5B1-4 (H5; High Five cells), which are derived from the eggs of *Trichoplusia ni*, Sf-21 cells, which were heterogeneously derived from pupal ovarian tissue of *Spodoptera frugiperda*, and Sf-9 cells, which were cloned from the Sf-21 cell line to maximize β-galactosidase production during BV expression. The Sf-21 and Sf-9 cell lines are most commonly used for transfection, viral amplification and protein expression while H5 are primarily used for protein expression (Murhammer, 2007).

2.3.3 Recombinant Protein Expression Using the Baculovirus-Insect Cell System

For the expression of recombinant hATG9 and hATG7 using the Baculovirus expression system the following cell lines, vectors and general procedures are required.

A) Eukaryotic Cells

In order to generate, amplify and express the recombinant Baculoviruses (rBV) the cell line High Five TM (H5) (BTI-TN-5B1-4) (Invitrogen) was used. This cell line is an isolated cell clon of *Trichoplusia ni*. H5 cells were cultured in TC-100 medium (GIBCO) supplemented with 10% Fetal Calf Serum (FCS), penicillin (100 U/ml), streptomycin (100 µg/ml), gentamycin (50 µg/ml) and fungizone (1 µg/ml).

B) pFastBacHTa and pFastBac1

These plasmids were used to generate the hATG7 and hATG9 CT, and the hATG9 FL rBVs respectively. Heterologous genes (hATG7 and hATG9) cloned in this plasmid are under control of the polyhedrin gene promotor, and are flanked by specific sites for the recombinant gene transposition into the bacmid. Recombinant proteins produced through this vector contain a 6xHis sequence in their N-terminal end and a 16-aminoacid linker that includes a Tobacco Etch Virus nuclear-inclusion-a endopeptidase (TEV protease) cleavage site.

C) Baculovirus

This virus was generated through genetic manipulation of an isolated *Autographa californica* polyhedrovirus (AcPHV). Production of the recombinant baculoviruses was achieved from BV FastBac strain (Invitrogen). The produced rBV express the corresponding proteins (hATG7 or hATG9) fused to an N-terminal 6xHis tag.

D) Bac to Bac System

rBV were generated with a Bac-to-Bac system (Invitrogen) following the manufacturer´s instructions. This method is based on the transposition of the recombinant genes into the infective genome of the Baculovirus, which is present in a vector (called bacmid) multiplied in the *E. coli* DH10Bac strain (Luckow *et al.*, 1993). Once the relevant sequence is cloned in the donor plasmid (pFastBacHTa), this plasmid will be used to transform DH10Bac bacteria where the recombinant gene transposition into the bacmid will take place. Then, the recombinant bacmid containing the relevant gene is selected, and the rBV are generated by H5 cell transfection with these bacmids. Finally, rBV are amplified through H5 cell infection with the bacmid-transfected cell supernatant (**Figure 2.2**).

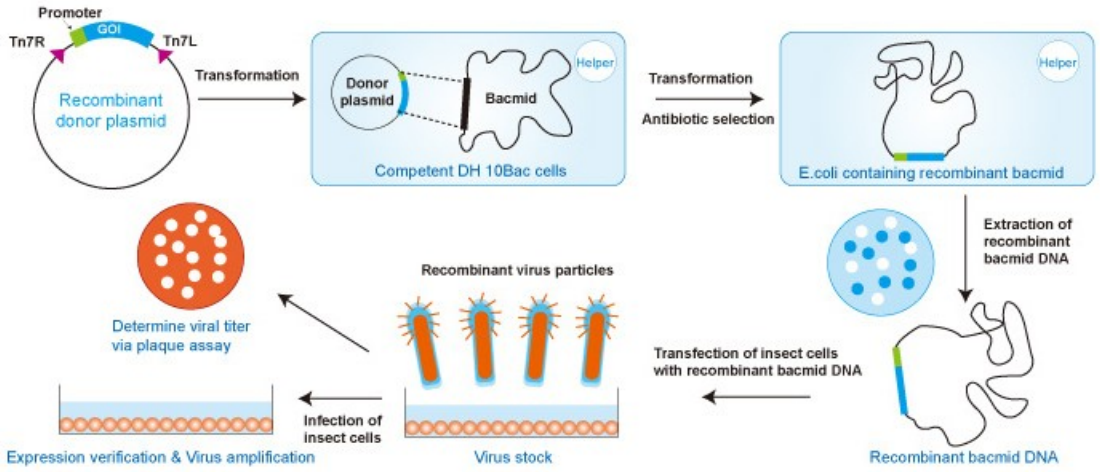

Figure 2.2 Schematic view of the recombinant Baculovirus (rBV) production.

2.3.4 hATG7 Protein Cloning

A plasmid containing human ATG7 (hATG7-PGEX-6P-2) sequence was kindly provided by Dr. Isei Tanida (National Institute of Infectious Diseases, Tokyo, Japan).

hATG7 sequence was amplified using the designed oligonucleotides, hATG7 cloning forward and hATG7 cloning reverse (**Table 2.4**), and subsequently digested with the restriction enzymes EcoRI and SalI to clone the fragment into a pFastBac-HTa vector.

Thereupon the ligation product was used to transform *E. coli* DH5α cells to keep the DNA and check the reaction efficiency. The presence of the correct sequence was checked by agarose gel and sequencing.

DH10Bac cells contain the required bacmid for the next insect cell infection and are used to select the correct transposition of the hATG7 gene from the donor plasmid to the bacmid. Hence, DH10Bac cells were transformed with the hATG7-pFastBac-HTa plasmid. Blue-white screening was performed to select the white colonies that contain the bacmid with the hATG7 sequence inside. Next the bacmid was isolated, purified and finally the presence of the corresponding sequence was confirmed by PCR. hATG7-containing bacmid was stored at 4 ºC.

Oligonucleotide		Sequence
hATG7 cloning	**Forward**	5´-CCCCGGAATTCATGGCGGCAG-3´
	Reverse	5´-GCGCGTCGACCTCAGATGGTCTCATCGTCGCTC-3´
hATG7 Sequencing	**1**	5´-GGTCCAAGGTCCGGTCTCTGG-3´
	2	5´-GTAAGCCCAAGGCTCTGGCAG-3´
	3	5´-CCCTGGTTACAAGCTTGGCTGC-3´

Table 2.4. Designed oligonucleotides for recombinant hATG7 cloning and sequencing.

2.3.5 hATG9 Protein Cloning

A plasmid containing human ATG9 (ATG9 FL 441) sequence was kindly provided by Dr. Sharon Tooze (Cancer Research UK, London Research Institute, London, UK).

Two different constructs were amplified (hATG9 FL and hATG9 CT) using specific oligonucleotides (**Table 2.5**). The resulting fragments were subsequently digested with the restriction enzymes NcoI and SalI (hATG9 CT), and BamHI and SalI (hATG9 FL) to clone the fragment into a pFastBac-HTa and pFastBac1 vectors respectively. Thereupon the ligation products were used to transform *E. coli* DH5α cells to keep the DNA and check the reaction efficiency. The presence of the correct sequence was checked by agarose gel and sequencing.

DH10Bac cells contain the required bacmid for the next insect cell infection and are used to select the correct transposition of the hATG9 FL and hATG9 CT genes from the donor plasmid to the bacmid. Hence, DH10Bac cells were transformed with the hATG9 CT-pFastBac-HTa or hATG9 FL-pFastBac1 plasmid. Blue-white screening was performed to select the white colonies that contain the bacmid with the correct sequence inside. Next the bacmid was isolated, purified and finally the presence of the corresponding sequence was confirmed by PCR. hATG9-containing bacmids were stored at 4 ºC.

Oligonucleotide		Sequence
hATG9 CT cloning	**Forward**	5´-CGCGCCATGGCCCGGGCCCTGGAGATTATAGACTTC-3´
	Reverse	5´-GCGCGTCGACTATACCTTGTGCACCTGAGGG-3´
hAT9 FL Fragment 1	**Forward**	5´-GGCTCCCTTATCACCATCCTGG-3´
	Reverse	5´-GCGCGTCGACTATACCTTGTGCACCTGAGGG-3´
hATG9 FL Fragment 2	**Forward**	5´-GCGCGGATCCATGGCGCAGTTTGACACTGAATAC-3´
	Reverse	5´-CCCGGCTCCCGCTTCAGCACCTC-3´

Table 2.5. Designed oligonucleotides for recombinant hATG9 FL and CT cloning and sequencing.

2.3.6 Transfection with Recombinant Bacmid

A 75% confluent p60 plate of H5 insect cells was transfected following the steps: 4 µg hATG7-pFastBac-HTa, hATG9 CT-pFastBac-HTa or hATG9 FL-pFastBac1 were incubated with 30 µl lipofectine in a 1:2.5 lipofectine:vector proportion for 30 min at RT. Then, the mixture was added over the cell culture and incubated for 5 h at 28 ºC. Finally, the lipofectine:vector mix was removed and replaced by TC-100 medium supplemented with 5% FCS. Transfected cells were incubated for 5-6 days at 28 ºC until cytophatic effect was observed.

At this stage, the culture supernatant was collected, centrifuged for 10 min at 3000 rpm and 4 ºC, and then stored as **1st Recombinant Baculovirus stock (P1)** at 4 ºC. It contains the first population of viruses with the recombinant gene incorporated in their genome. In addition, the pellet fraction was used to analyze the recombinant protein expression by SDS-PAGE and Western Blot.

Once it was known that hATG7, hATG9 CT and hATG9 FL were being expressed, the next action was to amplify the P1 stock to get a **2nd Recombinant Baculovirus Stock (P2)** that contains a higher virus titer. Two 80% confluent p150 plates were infected with a Multiplicity of Infection (MOI) 1-5 PFU/cell (20 µl of P1 stock), and incubated for 4-5 days at 28 ºC until the cytophatic effect was evident. As in the case of P1 stock, the supernatant was stored at 4 ºC. This P2 stock is used for the next steps of H5 cells infection to produce the proteins on a large scale.

For the purpose of determining the optimal quantity of virus and time of infection to get the best protein expression, virus and time titration were performed. Different

quantities of P2 stock were used to infect confluent wells of a M6 plate and also some infection times were tested. hATG7, hATG9 CT and hATG9 FL expression quality was checked by SDS-PAGE.

2.3.7 Purification of 6xHis-tagged Human ATG7 and ATG9-CT

48 h after hATG7 or hATG9-rBV infection, H5 cells were collected and centrifuged at 500 xg for 5 min at 4 ºC. Then the supernatant was removed and the cell pellet washed with cold PBS and subjected to a new centrifugation. The pellet was stored at -80 ºC for the following protein purification steps.

Cell pellets were resuspended in ATG7 Lysis buffer [50 mM Tris-HCl pH 8, and 150 mM NaCl supplemented with freshly prepared 1 mM TCEP (Sigma-Aldrich) and EDTA-free protein inhibitors (Roche, Basel, Switzerland)]. The mixture was incubated at 4 ºC on ice for 30 min to allow cell disruption. Samples were then subjected to sonication on ice, to avoid overheating, 5x 40 s on/60 s off cycles. After cell disruption, the resultant suspension was centrifuged at 30000 xg for 30 min at 4 ºC in a Beckman Coulter centrifuge using a JA-25-50 rotor (Beckman Coulter, Fullerton, California, U.S.A). The pellet was discarded and the supernatant was finally kept on ice.

6xHis-tagged full-length hATG7 or hATG9-CT were purified by affinity chromatography using “Talon Metal Affinity Resin” (Clontech). For each 10 p150 plates of insect cell culture, 1 ml beads was required. Beads were first washed three times with 10 bed volumes of distilled water and then 5 times with 10 bed volumes of ATG7 Lysis buffer followed by centrifugation for 5 min at 1000 xg. The cell supernatant was mixed with washed beads and the mixture was incubated for 3 h in an orbital-rotator at 4 ºC to allow binding of 6xHis-tagged proteins to cobalt-containing beads. The beads with bound proteins were collected by centrifugation (1000 xg, 5 min, 4 ºC), the supernatant was removed and the beads with bound proteins were subjected to a washing step. The cobalt resin was washed 5 times with 10 bed volumes of Washing buffer (50 mM Tris-HCl pH 8, 150 mM NaCl, 1 mM TCEP and 5 mM Imidazole). The protein was eluted using Elution buffer (50 mM Tris-HCl pH 8, 150 mM NaCl, 1 mM TCEP and 500 mM imidazole supplemented with EDTA-free protein inhibitors) and 10 fractions of 0.5 ml were collected for SDS-PAGE analysis and Coomassie-Blue staining. Fractions enriched in hATG7 protein were concentrated in Amicon Ultra Centrifugal Filter Units (Millipore) up to a 500 µl-volume, and they were loaded into a Superdex 200 Increase 10/300 GL size exclusion column (GE Healthcare) equilibrated

in Superdex Elution buffer (50 mM Tris-HCl pH 8, 150 mM NaCl and 1 mM DTT supplemented with protein inhibitors). Sample elution was performed at a 0.3 ml/min flow-rate at 4 ºC. Protein elution was followed by monitoring UV absorbance at 280 nm, and 0.5-ml fractions were collected. Peak protein fractions were analyzed by SDS-PAGE and Coomassie-Blue staining. Finally, fractions containing pure hATG7 were concentrated in Amicon Ultra Centrifugal Filter Units (Millipore) up to the desired concentration.

2.4 Membrane Lipid Model Systems

Numerous model membrane systems have been developed for studying the properties of pure lipids, lipid mixtures, and reconstituted lipid-protein systems. A variety of model membrane systems is required as no single system is suitable for all the techniques used in their study. These model systems can be grouped as (1) monolayers, (2) planar bilayers, and (3) liposomes or vesicles (Gennis, 1989). In the present work two of them have been used: i) lipid vesicles or liposomes, and ii) lipid monolayers. A detailed explanation of their principal applications and their preparation procedures is given.

2.4.1 Lipid Vesicles (Liposomes)

A lipid structure in a bilayer configuration enclosing an aqueous solution is called a liposome. Liposomes are spontaneously generated when dispersing cylindrical-shaped lipids in aqueous solutions, thus they constitute a convenient source of lipidic model membranes. Depending on the treatment, liposomes can be prepared to have a single or several bilayers or lamellae, being unilamellar vesicles the principal system used in this work (**Figure 2.3**). However, research with both kinds of vesicles and various biophysical techniques provides essential information for our understanding of most membrane processes.

Liposomes have been extensively used for measuring fusion, fission, solubilisation, leakage, lipid flip-flop, lipid-protein binding, protein-protein binding and many more events. An interesting application is the use of liposomes for drug administration in medical treatments. By enclosing drug molecules within liposomes,

side effects can be reduced and a more specific and gradual drug release within the target area can be achieved (Gregoriadis, 1978, 2008). Nowadays, liposomes as drug carriers are largely been tested in anticancer therapies [See (Allen & Cullis, 2013; Dass, 2008; Noble *et al.*, 2014) for recent reviews on the methodology and liposome applications in cancer treatment].

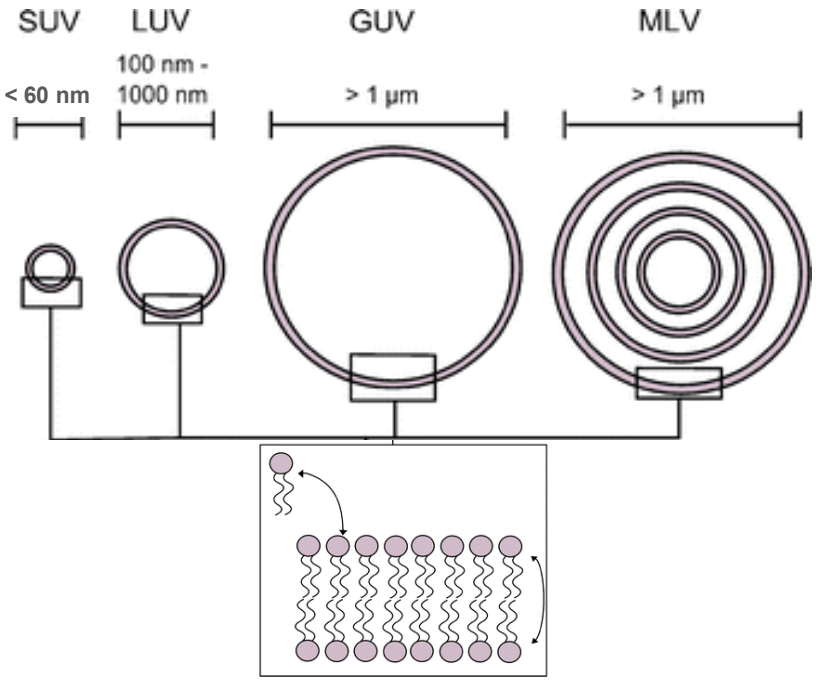

Figure 2.3. Outline of the phospholipid organization in vesicles of various sizes (SUV, LUV, GUV and MLV).

2.4.2 Multilamellar Vesicles (MLVs)

In the early 60´s, the British haematologist Alec Bangham and collaborators characterised the first known liposomes in Cambridge by looking at lecithin dispersions under electron microscopy (Bangham & Horne, 1964). As he pointed out, some "spherulites" containing concentric lamellae were formed. Vesicles were formed either by hand-shaking or by sonication, the latter inducing the formation of vesicles with fewer lamellae. These vesicles are nowadays commonly known as multilamellar vesicles (MLVs) and mostly used in lipid biophysical studies for the characterization of lipid phases either by differential scanning calorimetry (DSC), nuclear magnetic resonance (NMR) or x-ray diffraction techniques. After lipid hydration and sample shaking, MLVs are spontaneously formed usually containing between 7 and 10 concentric bilayers, each of them separated by a thin water layer. Vesicles are

heterogeneous in size, displaying an average diameter of around 700 nm but ranging from 100 to 5000 nm (**Figure 2.3**).

MLV generation is the simplest and fastest of all liposome formation methods. A detailed protocol for multilamellar vesicle preparation used in the present work is described (**Protocol 2**).

Protocol 2. Multilamellar Vesicles (MLVs)

1. Pure lipid stocks are prepared by dispersing lipids in powder in chloroform/methanol (2:1 v/v) to the desired concentration.
2. The desired amount of lipid is pipetted from the stock in organic solution into a glass test tube.
3. The organic solvent is evaporated under a nitrogen gas flow.
4. To completely remove any traces of organic solvent, the sample is placed into a high vacuum desiccator for 2 h to obtain a solvent-free dried lipid film at the bottom of the test tube.
5. Finally the lipid is hydrated by pipetting the desired amount of an aqueous solution at a temperature above the lipid main phase transition temperature and the suspension is shaken by vigourous vortexing for lipid detachment from the bottom of the test tube. By increasing temperature, the lipid is hydrated faster and, when preparing vesicles with a mixture of lipids, a more homogeneous lipid composition through the vesicles can be expected by maintaining every lipid in the fluid phase state. This method is often enough for MLV preparation.

2.4.3 Large Unilamellar Vesicles (LUVs)

MLVs are easy and fast to prepare, but they have an important drawback. When treating vesicles with a solubilising agent, or when looking at a protein effect upon binding to the vesicle, only the effects of interaction with lipids on the external bilayer can be achieved, thus making difficult data analysis and interpretation. To overcome this issue, unilamellar vesicles are generally used (**Figure 2.3**). Unilamellar vesicles are classified according to their size, those with an average diameter of less

than 60 nm being named SUVs (small unilamellar vesicles), those with an average diameter between 100 and 500 nm are LUVs (large unilamellar vesicles) and those with larger, micrometer-ranged diameters, are GUVs (giant unilamellar vesicles). Apart from their size, they differ from each other in the method of preparation.

Large unilamellar vesicles present, in contrast to small vesicles, low curvature stress and so, when preparing LUVs containing a mixture of lipid species, a homogeneous lipid distribution through both monolayers in stable lipid vesicles is generally obtained. In this way, LUVs represent a very good model system for most studies. LUVs are generally prepared by mechanical extrusion of MLV suspensions through polycarbonate porous filters of the desired pore size (Mayer *et al.*, 1986). A detailed protocol (**Protocol 3**) follows:

Protocol 3. Large Unilamellar Vesicles (LUVs)

1. Steps 1-5 of MLV preparation protocol (**Protocol 1**)
2. The MLV solution is subjected to 10 freeze/thaw cycles in order to reduce the number of lamellae in the vesicles. This is obtained as a result of placing the vesicles in liquid nitrogen for 1 min, then placing these vesicles in a water bath at a temperature above that of the lipid with the highest main transition temperature. Finally the suspension is vortexed before starting the next cycle.
3. Vesicles are extruded 10 times through polycarbonate filters of the desired diameter (usually between 0.1 and 0.4 μm), using a high-pressure extruder (nitrogen gas flow). The extruder can be connected to a water bath in order to maintain the vesicles at a high temperature if necessary.
4. The concentration of the vesicle suspension is assayed using the Fiske method (**Protocol 6**), because some lipid can be lost in the process.
5. Finally it is important to check vesicle size using dynamic light scattering (DLS) (see **Section 2.6**)

2.4.4 Small Unilamellar Vesicles (SUVs)

Due to their small diameter (smaller than 60 nm) SUVs present a high curvature stress, which induces a lipid enrichment in the external monolayer as compared to the

inner one (Szoka & Papahadjopoulos, 1980). Their curvature stress makes these vesicles good model membranes for the study of membrane fusion and/or fission related processes (Nieva *et al.*, 1989), because they may be subjected to such stress conditions *in vivo*. Small unilamellar vesicles are usually prepared by sonication of MLV suspensions. This is basically done either by bath sonication or probe tip sonication, in the latter case probes are immersed in the MLV suspension for sonication. In this way, large MLV are broken down into small unilamellar vesicles. In the present work, small unilamellar vesicles have been prepared by probe tip sonication. Thus, the protocol for SUV generation is that of the MLV but with final sonication of the vesicles for 20 min (10 s on/ 10 s off). Finally, SUV preparation is centrifuged at 14500 rpm, 10 min to remove aggregates and traces of the sonicator tip. SUV generation can be directly observed as the vesicle solution becomes transparent.

2.4.5 Giant Unilamellar Vesicles (GUVs)

Giant unilamellar vesicles are nowadays one of the most promising model systems in the study of membrane heterogeneity. Their size, in the order of 5-100 micrometers as prepared by electroformation, i.e. comparable to a cell, allows performing direct microscopy on individual vesicles. The generation of giant vesicles was first described in 1969 by John P. Reeves and Robert M. Dowben exposing dry lipid films to aqueous solutions at temperatures above that of the lipid main phase transition temperature for 24 hours (Reeves & Dowben, 1969). Giant vesicles were spontaneously generated but with very low total lipid yield and a very heterogeneous size distribution.

In 1986, Miglena I. Angelova and Dimiter S. Dimitrov developed a new method for the generation of giant vesicles based on the exposure of dry lipid films to an aqueous solution under electric fields, which is the most generally applied procedure in the present (Angelova & Dimitrov, 1986; Angelova *et al.*, 1992) (**Figure 2.4**). As in the initial procedure, the aqueous solution is kept at temperatures higher than that of the lipid with the highest main phase transition, but the method is much faster and a higher amount of homogeneous size vesicles can be obtained. Vesicle generation under electric fields is strongly dependent on the lipid composition, aqueous solution ionic strength and pH, and on the electric voltage and frequency conditions (Bagatolli, 2003). In particular, only very low ionic strengths can be used in the buffers to prepare GUVs

under this procedure. However, the approach has considerably evolved and nowadays even the generation of giant vesicles from erythrocyte membranes in physiological salt solutions is possible (Montes *et al.*, 2007).

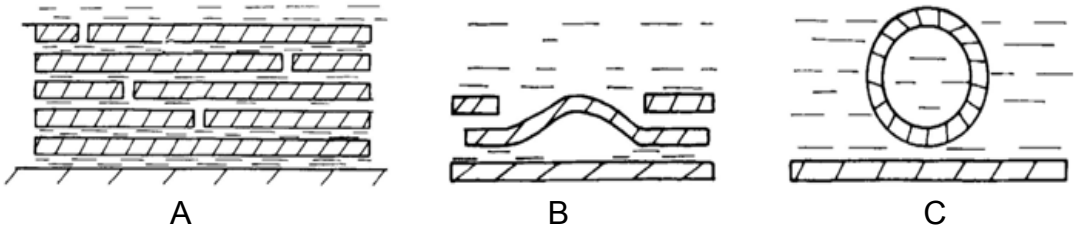

Figure 2.4 Outline of GUV electroformation. The electric field makes the lipid films **(A)** to grow/fuse **(B)** and detach **(C)** yielding GUV. [Adapted from Angelova and Dimitrov (1986)]

Regarding the present work, an important application for giant vesicles is the study of lipid lateral segregation by direct confocal microscopy of individual vesicles. With this aim two vesicle generation procedures have been applied to obtain: i) giant vesicles in solution, or ii) giant vesicles attached to a platinum wire for direct microscopy measurements. A general overview for both procedures is given. For a detailed specification on buffer, electric field or microscopy conditions in a particular assay see Materials & Methods in the corresponding chapter.

2.4.5.1 GUV in Solution

GUV in solution are formed and subsequently translated to visualization chambers (**Protocol 4**). To enable their visualization, a high density sucrose solution is encapsulated in vesicles so that when transferred to chambers with an iso-osmotic solution, they sediment at the bottom of the chamber and can be imaged.

Protocol 4. Giant Unilamellar Vesicles in solution

1. Pure lipid stocks are prepared by diluting commercially available lipids in powder into a chloroform/methanol (2:1 v/v) organic solution to a 0.2 mM concentration.

2. 3 µl of the appropriate stock solution are added onto the surface of different platinum electrodes in a specially designed chamber (Industrias Técnicas ITC, Bilbao, Spain) containing four holes with two platinum electrodes each.

3. The chamber is introduced into a high vacuum desiccator for 2 h to remove any remaining solvent traces.

4. The chamber is then equilibrated for 15 min at the desired temperature by an incorporated water bath.

5. Next, the platinum wires are covered with a 300 mM sucrose solution previously equilibrated at the desired temperature.

6. The chamber holes are covered with a glass held in place with vacuum grease to avoid evaporation during electroformation.

7. The platinum electrodes are connected to a generator and the desired electric field (870 mV) is applied for approximately 2 h. Vesicles are then generated enclosing sucrose. Temperature during preparation is always higher than that of the lipid with the highest main phase transition temperature.

8. The applied frequency (10 Hz) is decreased for 1 h 30 min to induce vesicle detachment from the electrodes.

9. The electric field and water bath are disconnected and the vesicles left 30 min for equilibration.

10. The vesicle solution is then transferred to microscopy chambers, which have been pre-treated with BSA (10 mg/ml) and contain an iso-osmotic aqueous solution or buffer without sucrose. In this way, vesicles sediment due to the higher density of the enclosed sucrose, and this allows direct fluorescent confocal microscopy measurements to be performed.

2.4.5.2 GUV for Direct Microscopy

GUV for direct microscopy measurements are formed in home-made chambers and remain attached to a platinum wire where they are formed (**Figure 2.5**). The chamber is directly placed under the microscope.

The procedure for the generation of GUVs attached to a platinum wire is very similar to that for giant vesicles in solution but with two main variants: A) A special chamber for direct microscopy supplied by Luis A. Bagatolli (Odense, Denmark) has been used for this purpose, and B) vesicles are prepared in the desired aqueous or buffer solution, and there is no need for sucrose to be encapsulated (**Protocol 5**).

Figure 2.5. Homemade chamber and PTFE circular wells for the formation of GUV attached to a platinum wire.

Protocol 5. GUVs attached to a platinum wire for direct microscopy

1. Pure lipid stocks are prepared by diluting commercially available lipids in powder into a chloroform/methanol (2:1 v/v) organic solution to a 0.2 mM concentration. The desired percentage of a fluorescent dye (approximately 0.2%) is added to the lipid stock to allow the direct visualization of vesicles in a confocal fluorescence microscope.

2. 3 µl of the appropriate stock solution are added onto the surface of different platinum electrodes attached to specially designed polytetrafluoroethylene (PTFE) circular wells.

3. The round units containing the wires are introduced into a high vacuum desiccator for 2 h to remove any remaining solvent traces.

4. Then, the units are fitted into specific holes within a specially designed homemade chamber (**Figure 2.5**) to which a glass cover slide has been previously attached by the use of epoxy glue. Once fitted, the platinum wires stay in direct contact with the glass cover slide.

5. The chamber is then equilibrated to the desired temperature for 15 min by an incorporated water bath.

6. Then the platinum wires are covered with the buffer solution, previously equilibrated at the desired temperature, and closed with perfectly fitting caps to avoid evaporation during electroformation.

7. The chamber is connected to a generator through the platinum electrodes and the desired electric field is applied for 2 h following a detailed protocol of voltage and frequencies e.g: 6 min 0.22 V/ 20 min 1.9 V/ 90 min 5.3 V.

8. After this step, the electric field and water are disconnected and vesicles are left to equilibrate for 30 min.

9. The chamber is finally moved to the microscope and direct confocal fluorescence microscopy is performed on vesicles attached to the platinum wire.

2.4.6 Lipid Monolayers

Another model system for the study of lipid-lipid and/or lipid-protein interactions are monomolecular films at the air-water interface, the so-called lipid monolayers. An important advantage of this system compared to vesicles is that neither curvature nor fluctuation effects are present, and furthermore, there is a complete control of the surface pressure, lipid composition and molecular packing at any time. Its main detriment is the uncertainty of applying of data from lipid monolayers to biological membrane bilayers. However, very precise information about lipid-lipid interaction behaviour can be obtained, a virtually impossible task using *in vivo* measurements in cell cultures.

Lipid monolayers can be prepared in a fast and easy way. A monolayer is generated by spreading a lipid solution, previously prepared by diluting lipids in highly volatile organic solutions such as pure chloroform or chloroform/methanol mixtures, on top of an aqueous solution. Due to their amphipathic nature, lipids self-organize with their hydrophilic headgroups in contact with the water environment and their acyl chains towards the air. Once generated, different measurements within the monolayer are performed based on the accurate control of its surface pressure by the use of a Langmuir balance. This is commonly done by the Wilhelmy method, using a suspended probe located at the air-water interface that measures any deviation from water surface tension, e.g. those induced by the presence of the monolayer (**Figure 2.6**).

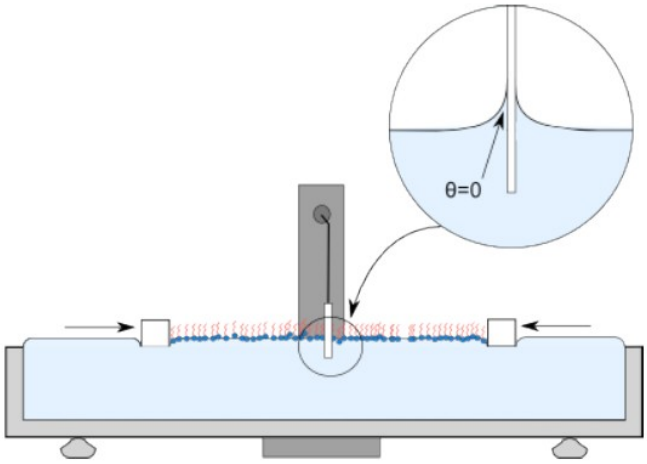

Figure 2.6. A lipid monolayer at the air-water interface of a Langmuir trough. Zoomed area: contact angle on the Wilhelmy plate at the interface. [Taken from NIMA Technology (UK)].

A special section in the current chapter (**Section 2.7**) has been introduced for a detailed overview on Langmuir balance-based approaches on lipid monolayers, applications and their methodological aspects.

2.5 Phospholipid Assay (FISKE Assay)

A well-established method has been applied for phospholipid assay based on the quantitation of inorganic phosphorous, an approach based on the initial procedure developed in 1925 by Cyrus H. Fiske and Yellapragada SubbaRow (Fiske & Subbarow,

1925) and later modified (Bartlett, 1959 and Böttcher *et al.*, 1961). Briefly, the approach consists of hydrolysing the phospholipids until the lipid phosphate group is free to interact with specific reagents that will colour the solution in a concentration-dependent manner (**Protocol 6**).

Protocol 6. Phospholipid assay (FISKE assay)

1. A phosphorous calibration curve must be set up from which the exact lipid sample concentration will be determined. 0, 25, 50, 75 and 100 nmol phosphorous are respectively pipetted into duplicate separate test tubes from a 1 mM NaH_2PO_4 standard solution, which will be used to construct the calibration curve.

2. The sample is then pipetted into separate tubes (at least triplicate) to contain theoretically 50 nmol lipid phosphorous, which will be in the centre of the calibration curve. When pipetting samples in organic solution, Hamilton syringes are used.

3. To each tube, 500 µl of a 60% perchloric acid ($HClO_4$) are pipetted. The tubes are vigourously vortexed and introduced into a heating block at 205 ºC for 45 min. In this way phospholipid hydrolysis is achieved leaving free inorganic phosphate.

4. Tubes are collected, cooled down to room temperature and the following solutions are pipetted:

   - 4 ml 1X ammonium heptamolybdate solution $[(NH_4)_6Mo_7O_{24}.4H_2O]$.
   - 500 µl 10% (v/v) ascorbic acid (added while vortexing).

   The inorganic phosphate reacts with molybdate, which subsequently reacts with the ascorbic acid giving a yellow-coloured solution.

5. The tubes are introduced into a boiling water bath and left for 6 min. During that period, the solution colour is blue-shifted depending on the amount of phosphorous.

6. Finally, tubes are cooled in water and absorbance at 812 nm measured for each of the samples. In the present work a Ultrospec 500 pro spectrophotometer from Amersham Biosciences (Piscataway, NJ, USA) was used for this purpose.

7. To obtain the sample phospholipid concentration, the standard absorbance is plotted against the phosphorous concentration and adjusted to a straight line. The slope of the curve and the sample absorbance are used to find out the sample concentration.

2.6 Vesicle Size Measurement by Dynamic Light Scattering (DLS)

Vesicle size measurements were performed using the quasi-elastic light scattering (QELS) technique, commonly known as dynamic light scattering (DLS), that is related to the Brownian motion of particles in solution. By the use of a laser beam focused within a small area in the solution, a measurement of the intensity fluctuations from the scattered light of sample particles crossing through the focused area is performed. The particles, vesicles in our case, scatter the light and this is recorded and related to the hydrodynamic radius (Rh) of the vesicle by the Stokes-Einstein equation:

$$D = k_B T/6\pi\rho R_h$$

Equation 2. Stokes-Einstein equation.

where: D is the diffusion coefficient, k_B is the Boltzmann constant = 1.38 x 10^{-23} m^2 kg s^{-2} K^{-1}, T is temperature, ρ is viscosity of the medium and R_h is the hydrodynamic radius of spherical particles

The scattered light provides a correlation function from which, by the use of several algorithms, a vesicle size distribution in solution can be obtained (**Figure 2.7**). This value is accompanied by a polydispersity index (PDI), which gives information on the size heterogeneity of the sample. The PDI varies between 0 and 1, where values close to zero indicate homogeneous monodisperse solutions.

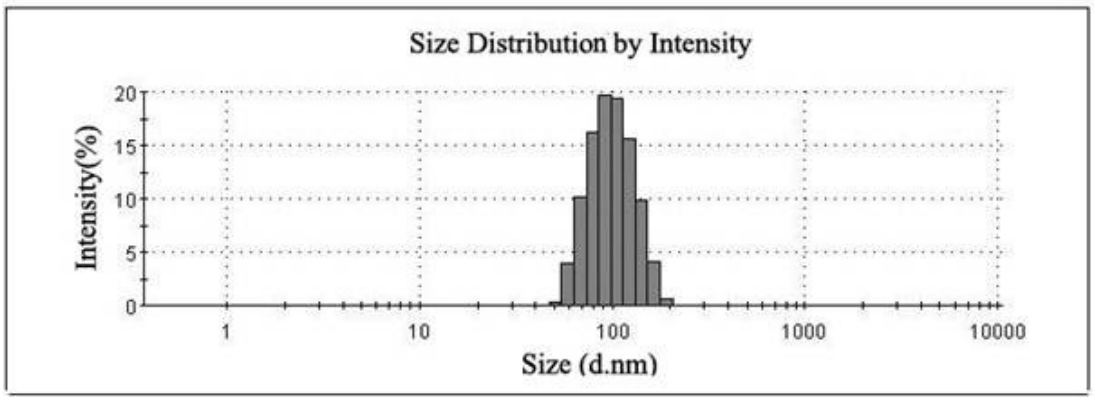

Figure 2.7. Size distribution plot of an egg PC vesicle population prepared using 100 nm polycarbonate filters.

The present measurements have been performed in a Malvern Zeta-Sizer Nano ZS (Malvern, Instruments, UK) with a detection range for sizes between 0.6 nm to 6 μm. We placed 50 μl of the sample (around 0.4 mM in lipid) in standard acryl cuvettes at room temperature with a He-Ne laser beam of 5 mW (λ = 633 nm) as the light source. The light scattered by the vesicles was detected with a photomultiplier placed at 173º to the beam and the results were analyzed by the commercial software of the instrument.

2.7 Langmuir Balance

Due to their amphipathic character, lipids spread on top of a water surface orient their polar headgroups in close contact with the water surface while moving their hydrophobic acyl chains towards the air. In this simple way, a monomolecular lipid film at the air/water interface is generated, in other words, a lipid monolayer. The terms “Langmuir films” and “Langmuir balance” refer to the preparation and characterization of such structures, named after the intensive studies of the American chemist and physicist Irving Langmuir in this field (Langmuir, 1917). For his work in surface chemistry Langmuir was awarded the Nobel Prize in chemistry in 1932.

Langmuir balance measurements represent an important source for the characterisation of lipid-lipid and lipid-protein interactions. In contrast with the use of vesicles or lipid bilayers, Langmuir balance approaches have the advantage of precisely controlling lateral pressure, molecular packing and lipid composition. There are no curvature or fluctuation effects if they are compared to vesicles. Furthermore, the current development of the technique allows for instance direct microscopy measurements by incorporation of fluorescent probes within the monolayer, or transfer of lipid monolayer to solid supports for its analysis under atomic force microscopy, among others. In the present work, Langmuir balance-based approaches have been applied to the study of lipid-protein interaction.

2.7.1 Surface Pressure Measurements

Langmuir balance approaches are based on the measurement of the water surface tension by means of a suspended solid probe. The probe is referred to as the

"Wilhelmy plate" with regard to Ludwig Wilhelmy, who first provided a way for measuring surface tension in 1863 (Wilhelmy, 1863). The Wilhelmy plate is very thin and usually made of platinum or filter paper, but other materials have been as well used: quartz, glass or mica. As explained, the Wilhelmy plate measures surface tension, which is the excess of free cohesive energy present at a gas-liquid interface. Water molecules are exposed to forces from surrounding molecules, which are balanced in the bulk of a water solution due to the equal attraction in every direction. However, at a gas-liquid interface, water molecules in the interface are not subjected to attractive forces in every direction, and thus, an excess cohesive energy is generated which is called the surface free energy. This excess energy can be related to surface tension as force/length by means of the forces detected by the plate (probe) partly introduced into the gas-liquid interface as depicted in **Figure 2.8**, which can be further related with surface pressures. The overall forces detected by the solid probe are:

Total force = Weight of the probe + probe buoyancy + surface tension

Equation 3. Overall forces detected by the Langmuir balance solid probe.

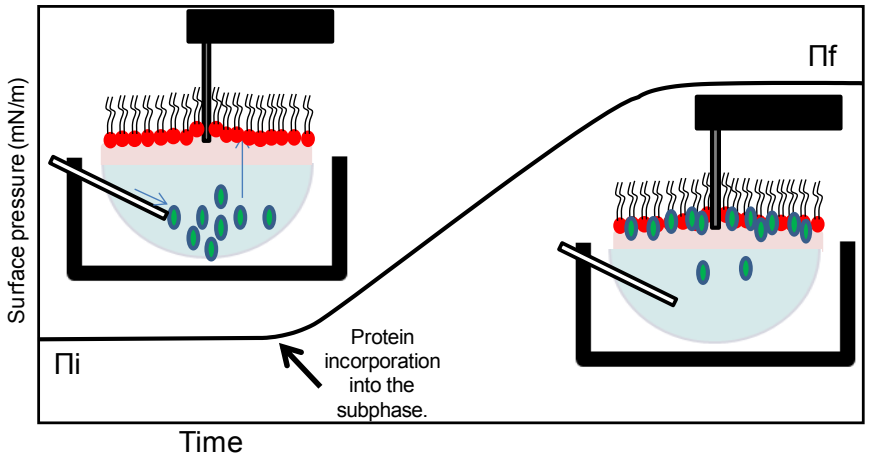

Figure 2.8. Schematic representation of the process of protein insertion into a lipid monolayer. Experimental set-up for lipid monolayers experiment. Before adding the protein, the initial pressure of the monolayer is adjusted to the desired value (πi). The protein inserts into the monolayer increasing the surface pressure until reaching the equilibrium (πf).

Before measurement, the pressure detected by the probe is adjusted to zero, thus discarding the weight force. The probe´s buoyancy reflects the applied force of displaced water molecules upon probe immersion acting upwards, and is as well discarded as the probe is maintained at a constant depth during the measurement. Thus, the overall force can be reduced to surface tension, which is described on the

following equation:

$$F = 2(w + t)(\gamma)(\cos \Theta)$$

Equation 4. Reduced equation of the overall force.

where: w,t = width and thickness of the probe, γ = surface tension, Θ = contact angle.

When introducing the probe in the aqueous solution, a meniscus is formed, resulting in a contact angle of zero degrees as shown in **Figure 2.6**. In this way, the equation can be reduced to:

$$\gamma = \text{Force/Perimeter}$$

Equation 5. Surface tension.

or force/length which is given in the following units (dynes/cm = mN/m).

Water molecules give rise to one of the highest surface tensions due to their high intermolecular attractive forces, 72.8 mN/m at 22 ºC and 1 atm. The presence of amphipathic molecules at the air-water interface disrupts the cohesive energy of water molecules, decreasing the water surface tension, this reduction being known as the surface pressure (π) with same units but opposite sign.

$$\pi = \gamma_o - \gamma$$

Equation 6. Surface pressure.

In conclusion, all the Langmuir balance measurements are performed following changes of surface pressure. Typically, a lipid solution in a highly volatile organic solvent (usually pure chloroform or chloroform/methanol (2:1 v/v)) is spread onto the surface of an aqueous solution (the air-liquid interface). As the solvent is evaporated, lipids organise themselves with the polar headgroup towards the aqueous solution and the hydrophobic chain towards the air. As the lipid spreads over the available surface area it decreases the water surface tension, i.e. increases the surface pressure. In this way, for instance for lipid-protein interaction studies, a lipid monolayer is prepared by spreading the desired amount of lipid into an air-water interface at a controlled surface pressure. Protein is subsequently incorporated into the subphase and lipid-protein interaction followed in terms of surface pressure changes upon incorporation or

adsorption of the protein into the monolayer (**Figure 2.8**). In this respect, it is to be stressed that cell membranes are proposed to have a surface pressure of around 30 mN/m (Janmey & Kinnunen, 2006; Marsh, 1996), although this value can vary largely.

A methodological overview on the preparation of Langmuir films can be found in Cruz & Pérez-Gil, (2007). Precise methodological conditions for each of the experiments carried out in the present work will be specifically found in the Materials & Methods section of the corresponding chapter.

2.8 Equilibrium Sucrose Gradient Centrifugation of Liposomes

Liposome floatation assays are widely applied for studying the affinity and lipid specificity of proteins binding to membranes (Landeta et al., 2011; Yethon et al., 2003). In the liposome float-up experiment, the vesicles and bound proteins are enriched by density gradient centrifugation. In general, large unilamellar or multilamellar vesicles are the best model membrane systems for these studies. Another commonly used and more sensitive technique is the vesicle sedimentation, but many membrane-interacting proteins have a tendency to aggregate or oligomerize, which results in their sedimentation in the absence of liposomes. In this situation, membrane binding of such proteins cannot be reliably examined by vesicle sedimentation assays and liposome floatation assays, which are not that sensitive to protein oligomerization/aggregation, can be used instead.

Liposome floatation assay starts with the incubation of the proteins with liposomes at 37 ºC. Then the sample is adjusted to 1.4 M sucrose using a sucrose stock solution prepared in prescission buffer and loaded at the bottom of a discontinuous sucrose gradient (medium layer of 0.8 M, upper layer of 0.5 M sucrose). The sample is centrifuged at 4 ºC for 3 h at 100000 rpm in a Beckman Optima TLX benchtop ultracentrifuge, using a TLA 120.2 rotor. During ultracentrifugation, due to their lower density, liposomes and liposome-bound proteins float up to the top fraction of the gradient whereas free protein remains at the bottom of the tube (**Figure 2.9**). Aliquots of 250 µl were taken starting from the bottom (a total of 4 samples) and added to 50 µl 6X Loading Buffer (LB). Then the samples (25 µl) were analyzed by 10-15% SDS-PAGE gels stained with Coommassie Blue or by Western-blotting.

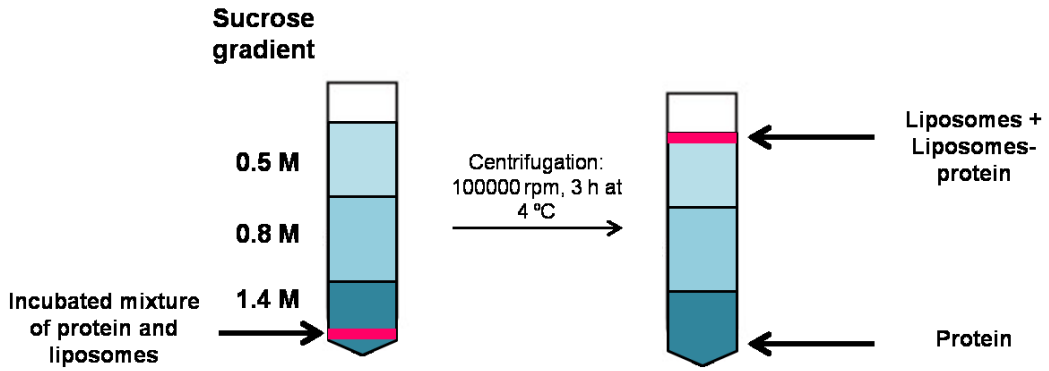

Figure 2.9. Schematic representation of an equilibrium sucrose gradient centrifugation assay. Before centrifugation (left side) a sucrose gradient is generated and the sample is in the bottom of the test tube. After centrifugation, liposomes and protein bound to liposomes float up and free protein remains in the bottom of the tube.

2.9. Vesicle Aggregation Measurements

Lipid vesicles are found to aggregate under a variety of conditions. Aggregation is usually assayed as an increase in turbidity (A_{400}) of the vesicle suspension that can be followed spectrophotometrically (**Figure 2.10**). The vesicle aggregation may be a first step for vesicle-vesicle fusion so turbidity measurements can be used as a first approach in the study of fusion events. This assay has been performed in a spectrophotometer Uvikon 922 (Kontron, Augsburg, Germany) as described in the following protocol (**Protocol 7**).

Protocol 7. Vesicle Aggregation Assay

1. LUV or SUV at the desired lipid composition are prepared as previously described (**Protocol 3**).
2. A Fiske assay is performed to determine the exact lipid concentration (**Protocol 6**).
3. In 1 ml quartz cuvettes, 600 µl final volume of buffer (previously equilibrated at the desired temperature) containing 0.4 mM liposomes is added under continuous stirring at 37 ºC.
4. After 5 min stabilization, the corresponding amount of protein is added to the cuvette in the smaller possible volume.
5. Absorbance at 400 nm is recorded to obtain the aggregation time course.

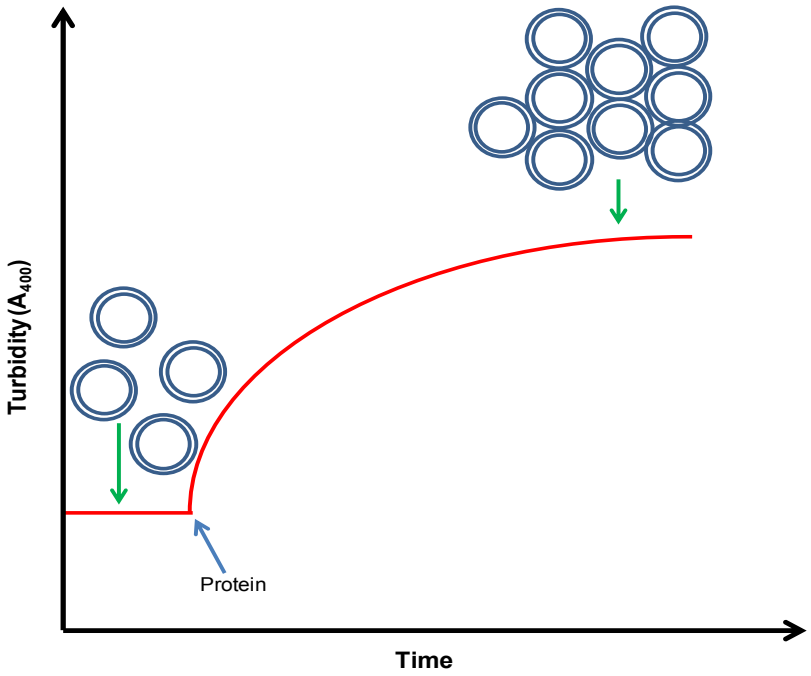

Figure 2.10. Schematic overview of a time-course of an aggregation assay. Initially vesicles scarcely scatter light. Upon protein addition, aggregation occurs and turbidity increases, thus light scattering increases in parallel.

2.10 Protein Analysis

2.10.1 Protein Concentration Measurements

Protein concentration was quantified using either the biscinchoninic acid (BCA) protein assay (Thermo Scientific) or absorbance measurements at 280 nm.

2.10.1.1 Biscinchoninic Acid Assay (BCA)

The reaction that leads to BCA color formation is strongly influenced by four amino acid residues (cysteine or cystine, tyrosine, and tryptophan) in the amino acid sequence of the protein. However, the universal peptide backbone also contributes to color formation, helping to minimize variability caused by protein compositional differences. In the first step, known as the biuret reaction, the chelation of copper with protein in an alkaline environment takes place to form a light blue complex. In the second step, BCA reacts with the reduced (cuprous) cation that was formed in step one.

The BCA/copper complex is water-soluble and exhibits a strong linear absorbance at 562 nm with increasing protein concentrations. The assay was performed using the standard test tube protocol and a set of prediluted bovine serum albumin (BSA) protein assay standards.

2.10.1.2 Absorbance at 280 nm

Proteins in solution absorb ultraviolet light with absorbance maxima at 280 nm, due to the presence of amino acids with aromatic rings. Secondary, tertiary, and quaternary structure all affect absorbance, therefore factors such as pH or ionic strength can alter the absorbance spectrum. Following the Lambert-Beer equation with a theoretically calculated extinction coefficient, the protein concentration can be estimated.

$$A = \varepsilon c l$$

Equation 7. Lambert-Beer equation.

where A is absorbance, ε is the molar extinction coefficient, c is the concentration and l is the path length.

2.10.2 Protein Electrophoresis

Protein separation was achieved by SDS-PAGE in 10-15% (w/v) acrylamide gels. Samples were mixed with Laemmli loading buffer (6x) supplemented with β-mercapthoethanol and heated at 90 ºC for 10 min. Broad-range and precision (unstained and pre-stained) standards (Bio-Rad) were used as molecular weight markers. Electrophoresis was performed at 150 V in running buffer (3.028 g Tris, 14.41 g glycine, 1 g SDS and H_2O to 1 L). For quick protein visualization, the gel was stained for at least 10 min in a solution containing 0.1% (v/v) Coomassie Brilliant Blue R-250, 40% (v/v) methanol and 10% (v/v) acetic acid. Background staining was eliminated by washing with 10% (v/v) acetic acid solution and images were taken on a Gel DocTM EZ Imager (Bio-Rad).

2.10.3 Western Blotting

Transfer of proteins from an SDS-PAGE gel to nitrocellulose membranes (Bio-Rad) was performed with a Trans-Blot® (Bio-Rad) equipment. A gel sandwich with Trans-Blot filter papers and a nitrocellulose membrane was prepared and hydrated with transference buffer (2.25 g Glycine, 5.81 g Tris pH 8, 0.375 g SDS, 200 ml MetOH and H_2O to 1L). Protein transfer was performed at 22 V for 30 min at room temperature. After protein transfer, membranes were blocked with 5% skim milk in PBS and incubated with the specific primary (1:1000) and secondary (1:2000) antibodies, the latter tagged with a horse-radish peroxidase (HRP). Membrane washing was followed by protein detection in a Curix 60 processor with the SuperSignal™ West Pico Chemiluminescent Substrate (Thermo Scientific). The intensity of the sample signal was quantified in a GS-800 densitometer (Bio-Rad).

2.11 Circular Dichroism

Circularly polarised light can be understood as a combination of two electromagnetic radiation components of equal magnitude that rotate counter-clockwise (left-handed) and clockwise (right-handed), respectively. When a sample is irradiated with light, an absorption process is produced. If both components are equally absorbed by the sample, the transmitting light will be polarised circularly. However, if there is a differential absorption of the left- and right- handed components, the resulting light will be elliptically polarised. Circular dichroism (CD) spectroscopy measures the differences in the absorption of the left- and right- handed components of circularly polarised light (Martin & Schilstra, 2008). This technique is used to study molecules of all types and sizes but it is in the analysis of the secondary structures of macromolecules where it finds its main application. The peptide bond is the primary chromophore contributing to the absorption of light in the far-UV spectra (from 170 to 250 nm). Moreover, the specific organization of the peptide bonds in the protein gives rise to isolated absorbing units that present unique spectral features. Thus, alpha-helix, beta-sheet and random-coiled structures produce each a characteristic shape and magnitude in the CD spectrum (**Figure. 2.11**). CD spectroscopy in the far-UV was used to obtain a quantitative estimate of the average secondary structure of Atg8 homologues, ATG3 and ATG7.

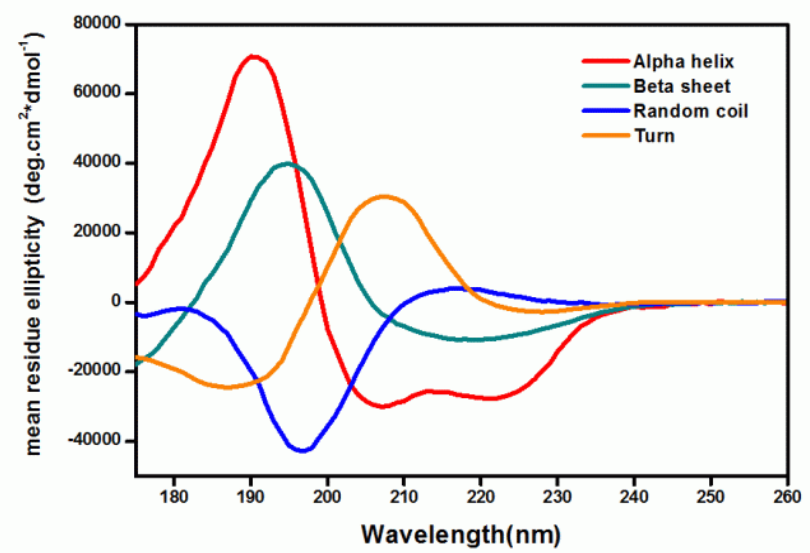

Figure 2.11. Far-UV spectra associated with various types of secondary structure. Different secondary structure elements display characteristic CD spectra: α-helical proteins have negative bands at 222 nm and 208 nm and a positive band at 193 nm. Proteins with well defined antiparallel β-pleated sheets have negative bands at 218 nm and positive bands at 195 nm. Finally, disordered proteins have very low ellipticity above 210 nm and negative bands near 195 nm.

2.12 Fluorescence Spectroscopy Techniques

2.12.1 Lipid Mixing Assay

Fluorescence energy transfer (FRET) is a distance-dependent interaction between the electronic excited states of two dye molecules in which excitation is transferred from a donor molecule to an acceptor molecule without emission of a photon. The efficiency of FRET is dependent of the inverse sixth power of the intermolecular separation, thus it can only occur when fluorophores are very close to each other.

In order to study vesicle-vesicle fusion, lipid mixing between vesicles was monitored using a FRET pair of fluorescently labeled lipids, a methodology developed by Struck et al. (Struck *et al.*, 1981). 7-nitrobenz-2-oxa-1,3-diazol-4-yl (NBD) was used as the energy donor and rhodamine (Rho) as the energy acceptor. The energy transfer takes place because the emission spectra of the donor (465 nm) and the acceptor excitation (560 nm) spectra are overlapped. Each of the two fluorophores is coupled to the free amino group of a phosphatidylethanolamine to provide an analogue that can be incorporated into a lipid vesicle bilayer. When both fluorescent lipids are in LUV at

the appropriate surface densities (ratio of fluorescent lipid to total lipid), efficient energy transfer is observed. When such vesicles are fused with a population of unlabelled vesicles by the addition of a fusion inducing agent, the two probes mix with the other lipids present to form a new membrane. This mixing reduces the surface density of the fluorophores and the energy transferred between molecules decreases, thus the fusion can be measured as an increase of NBD (donor) fluorescence (**Figure 2.12**) (**Protocol 8**).

Using this system, the lipid mixing induced by the Ubiquitin Like System (UBL) and ATG3 has been studied.

Protocol 8. Total Lipid Mixing Assay

1. Prepare two LUV populations, population 1 with no fluorescent probes and population 2 with 1.5 mol% NBD and 1.5 mol% Rho (**Protocol 3**)
2. Determine the lipid concentration with the lipid phosphorous assay (**Protocol 6**).
3. In 1 ml quartz cuvettes, the two populations are mixed in a 1:4 (population 1: population 2) ratio to a 0.4 mM total concentration.
4. After 5 min stabilization, proteins are added and NBD fluorescence was recorded at 530nm.

Protocol 9. Inner Lipid Mixing Assay

1. Prepare two LUV populations, population 1 with no fluorescent probes and population 2 with 1.5 mol% NBD and 1.5 mol% Rho (**Protocol 3**).
2. Prepare a fresh 100 mM stock solution of sodium dithionite (keep in the dark at 4 ºC) in the same buffer than the vesicles.
3. Place population 2 in a 1 ml quartz cuvette and add small amounts (1 – 3 ul) of dithionite to the sample until the fluorescence is quenched to half of initial value.
4. The vesicle suspension is immediately passed through a Sephadex G-25 column to remove dithionite. Steps 3 and 4 should be done as quickly as possible because some dithionite can penetrate the vesicles.

5. Determine the lipid concentration with the lipid phosphorous assay (**Protocol 6**).

6. In 1ml quartz cuvettes, the two populations are mixed in a 1:4 (population 1: population 2) ratio to a 0.4 mM total concentration.

7. Add proteins and record NBD fluorescence at 530 nm.

   Fluorescence is followed in an AmincoBowman Series 2 spectrofluorimeter under the following conditions:

   λ_{ex} = 465 nm
   λ_{em} = 530 nm
   Interference filter at 515 nm
   0% fusion = Initial fluorescence of vesicles with maximum NBD-Rho energy transfer.
   100% release = Fluorescence after complete vesicle solubilisation with 1 mM n-octyl-β-D-glucopyranoside (OG) detergent.

To calculate the amount of lipid mixing the following equation is used:

$$\text{Lipid mixing \%} = [(F - F_0)/(F_{100} - F_0)]^* 100$$

Equation 8. Lipid Mixing % calculation.

Where: F = Fluorescence at equilibrium
F_0 = Fluorescence of vesicles at time zero
F_{100} = Maximum fusion (Fluorescence after OG addition)

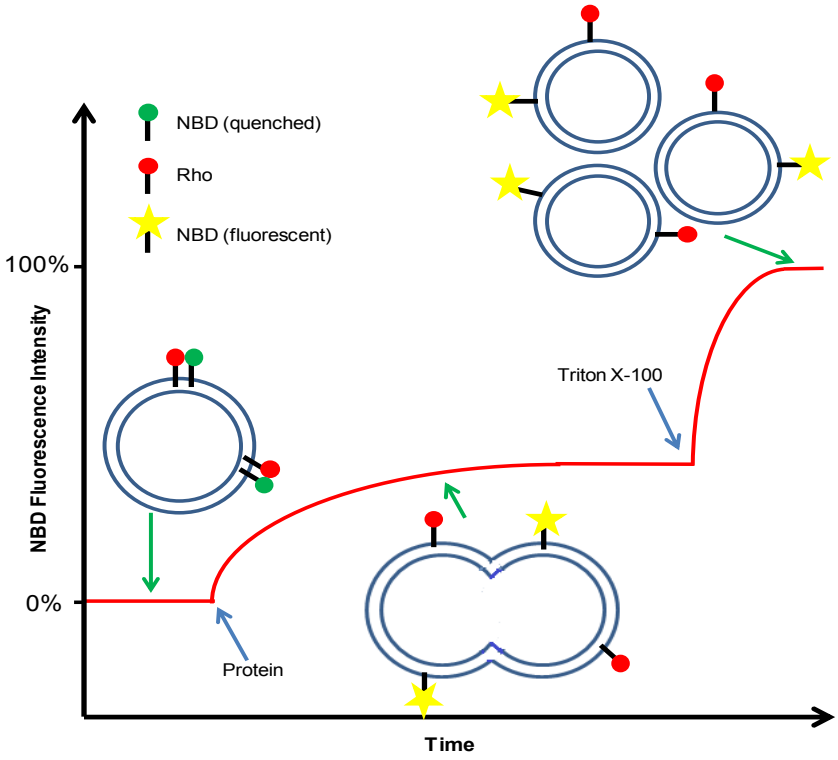

Figure 2.12. Schematic overview of an inter-vesicle lipid mixing assay. Initially there are two populations of vesicles, one with and the second without the FRET pair. Upon protein addition, when fusion occurs lipids are mixed and rhodamine cannot quench NBD. Triton X-100 is added to achieve vesicle solubilisation, under these conditions 100% lipid mixing value is obtained.

2.12.2 Aqueous Contents Mixing Assay

Intervesicular contents mixing was monitored using the 8-aminonapthalene-1,3,6 trisulfonic acid (ANTS)/ p-xylene-bis-pyridinium bromide (DPX) assay. ANTS emission was monitored at 530 nm with the excitation wavelength set at 360 nm (slits, 2 nm). A 470 nm cut-off filter was placed between the sample and the emission monochromator to avoid scattering interference. 0% vesicle contents mixing was set by using a 1:1 mixture of ANTS and DPX liposomes. 100% mixing of contents corresponded to the fluorescence of the vesicles containing coencapsulated ANTS and DPX. Details for the intervesicular lipid mixing and contents mixing assays can be found in Goñi et al, 2003. (**Figure 2.13**)

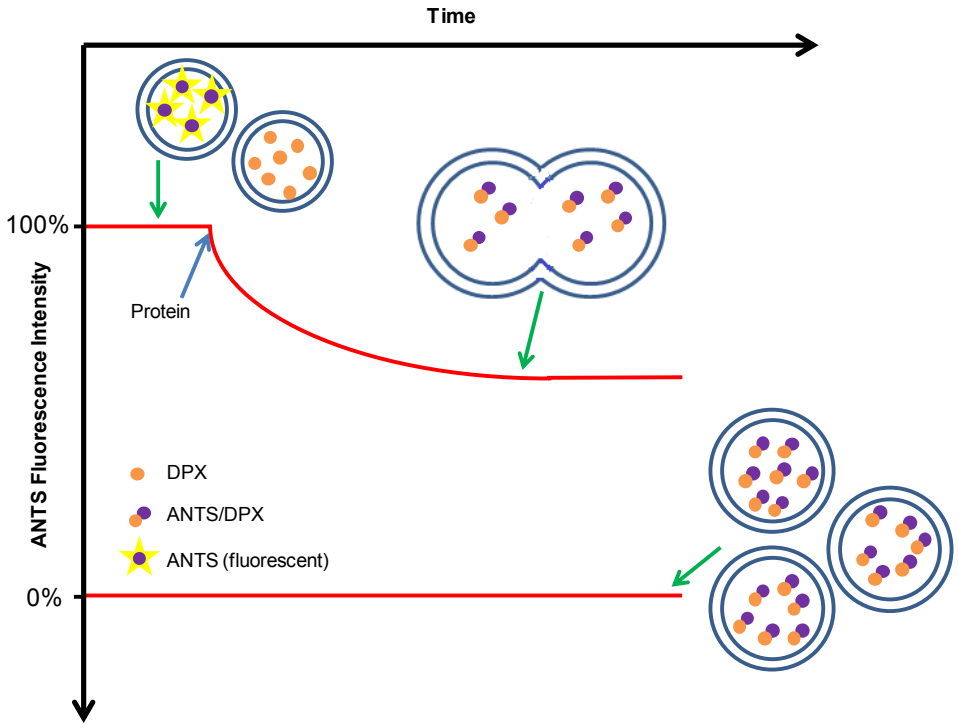

Figure 2.13. Schematic overview of an inter-vesicular aqueous contents mixing assay. Initially there are two populations of vesicles, one with ANTS and the second one with DPX. Upon protein addition, when complete fusion occurs the aqueous contents of the vesicles are mixed , and DPX can quench ANTS. 100% fusion value is obtained measuring the fluorescence of a vesicle population containing both molecules in the same proportion.

2.12.3 Vesicle Contents Efflux Measurement (Leakage) Assay

This technique measures the ability of particular molecules to permeabilise the vesicle lipid bilayer. It is a simple approach in which vesicles are prepared enclosing fluorescent molecules. Upon specific molecule incubation, permeabilisation is followed by changes in fluorescence. If vesicles are incubated with a detergent, a possible permeabilisation could be followed by externalisation of entrapped fluorescent molecules through unstable solubilised vesicle regions. In the present study, the ability of ATG3 to produce vesicle leakage in the process of vesicle aggregation, and the possible leakage in vesicle fusion processes were tested by following the externalisation of the well-known low-molecular weight ANTS and its quencher DPX fluorescent molecules.

The basis of this approach is depicted in **Figure 2.14**. By entrapping both ANTS and DPX inside the vesicles, their close proximity allows DPX to interact with ANTS quenching its fluorescence. Upon externalisation, both molecules are diluted into the external medium and they hardly interact, inducing an increase of ANTS fluorescence. Thus, by following ANTS fluorescence, vesicle bilayer permeabilisation, or solubilisation in our case, can be followed. This approach was initially developed in 1985 (Ellens *et al.*, 1985) to measure vesicle fusion, a situation in which both molecules where entrapped into separate vesicle populations and their fusion followed in terms of ANTS fluorescence quenching upon fusion and ANTS-DPX interaction [see (Goñi *et al.*, 2003; Nieva *et al.*, 1989)]. A full description of the assay conditions is given in the **Protocol 10**.

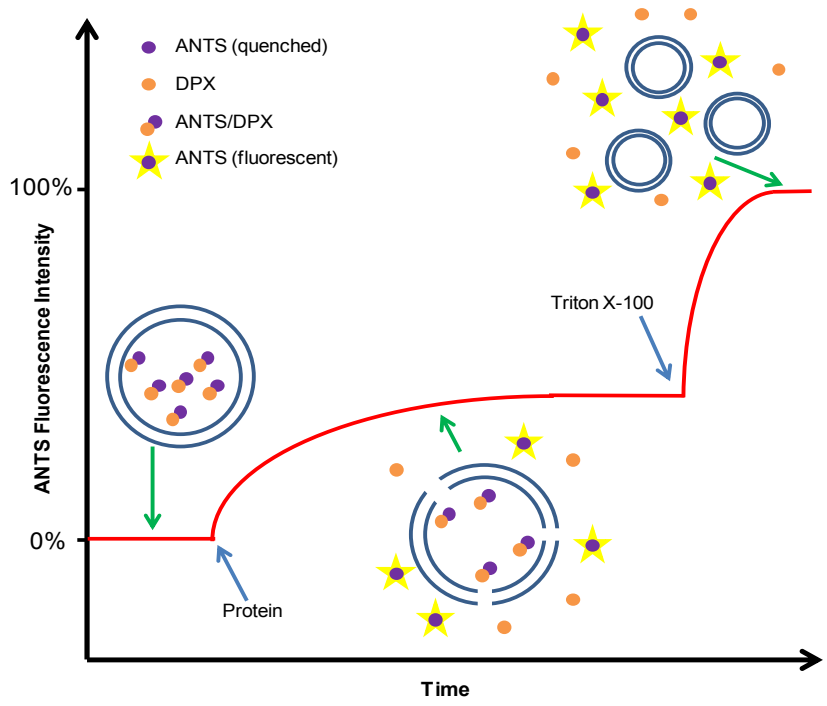

Figure 2.14. Schematic overview of the ANTS/DPX leakage assay. Upon incorporation of the protein into the membrane, vesicle-enclosed ANTS and DPX are externalised through membrane defects. An increase on ANTS fluorescence is observed. Triton X-100 is generally added for complete vesicle solubilisation into mixed vesicle lipid/surfactant/Triton X-100 micelles that gives the 100% leakage value (i.e. maximum ANTS fluorescence).

Protocol 10. Vesicle Contents Efflux Measurement (Leakage) Assay

1. 100 nm large unilamellar vesicles (LUVs) are prepared as previously described (**Protocol 3**) in the following buffer containing both ANTS and DPX.

- For experiments with ATG3: 20 mM ANTS, 70 mM DPX, 40 mM NaCl, 50 mM Tris-HCl (pH 7.5).
- For experiments with UBL System: 20 mM ANTS, 70 mM DPX, 1 mM $MgCl_2$, 40 mM NaCl, 50 mM Tris-HCl (pH 7.5).

A high DPX/ANTS ratio is used to ensure complete quenching inside vesicles. Samples are covered with aluminium foil to protect fluorescent molecules from bleaching.

2. The vesicle suspension is passed through a Sephadex G-25 column to remove non-entrapped ANTS and DPX. A previously adjusted isosmotic buffer solution is used for this process:

- For leakage experiments with ATG3: 50 mM Tris-HCl, 175 mM NaCl, 1 mM DTT (pH 7.5) for leakage experiments with Atg3.
- For UBL system experiments: 50 mM Tris-HCl, 150 mM NaCl, 1 mM $MgCl_2$, 1 mM DTT (pH 7.5) for UBL system experiments.

3. Lipid concentration is determined as previously described (**Protocol 6**).

4. The permeabilizing agent is added to 0.4 mM vesicles in 1 ml quartz cuvettes with continuous stirring and leakage is followed in terms of ANTS fluorescence in a QuantaMaster spectrofluorometer (Photon Technology International, Birmingham, New Jersey) under the following conditions:

λ_{ex} = 355 nm
λ_{em} = 520 nm
Interference filter at 450 nm
0% release = Initial fluorescence of intact vesicles.
100% release = Fluorescence after complete vesicle solubilisation with 1 mM Triton X-100.

To calculate the amount of leakage the following equation is used:

$$\text{Leakage \%} = [(F - F_0)/(F_{100} - F_0)]^* 100$$

Equation 9. Leakage % calculation.

Where: F = Fluorescence at equilibrium
F_0 = Fluorescence at time zero
F_{100} = Maximum leakage (Fluorescence after Triton X-100 addition)

2.13 Cryo-electron Microscopy

Cryo-electron microscopy (cryo-EM), is a form of transmission electron microscopy (EM) where the sample is studied at cryogenic temperatures (generally liquid nitrogen temperatures). Nowadays, cryo-EM is gaining users in structural biology.

The main advantage of cryoelectron microscopy stems from the fact that this technique allows the observation of specimens that have not been stained or fixed in any way, showing them in their native form. This is in contrast to X-ray crystallography, which requires crystallizing the specimens, which can be a difficult task, and placing them in non-physiological environments, which can occasionally lead to functionally irrelevant conformational changes.

In this electron microscopy derived technique, the way in which sample is prepared is one of the main advantages. The sample could be frozen from its native conditions, generally in an aqueous environment (aqueous buffer). The biological material is spread on an electron microscopy grid and is preserved in a frozen-hydrated state by rapid freezing, usually in liquid ethane near liquid nitrogen temperature. By maintaining samples at or below liquid nitrogen temperature, they can be introduced into the high-vacuum of the electron microscope column. Most biological samples are extremely radiation-sensitive, so they must be imaged with low-dose techniques. Usefully, the low temperature of cryo-electron microscopy provides an additional protective factor against radiation damage.

For our observations the samples were placed in the controlled environment of the vitrification chamber of Vitrorobot (FEI) at room temperature, where the relative humidity was kept close to saturation to prevent water evaporation form the sample. A 5 µl drop of the aqueous solution was placed on carbon-coated holey film supported by a TEM copper grid. Most of the liquid was removed by careful blotting with absorbent filter paper to create a thin liquid film. The sample was then rapidly plunged into liquid ethane and cooled by liquid nitrogen to its melting temperature to obtain a vitrified film. The vitrified specimen was stored under liquid nitrogen and transferred into the electron microscope (Jeol JEM-2200FS) operating at 200 kV. Images were collected under low-dose conditions with a CCD camera (UltraScan 4000, Gatan) with an underfocus in the range of 3-5 µm at magnifications of 40000-60000 x. This technique was performed in collaboration with D. Gil and M. Valle at CIC-Biogune (Zamudio, Spain).

2.14 Fluorescence Confocal Microscopy

The development of confocal microscopy during the late 70´s resulted in one of the major advances in optical microscopy. Specifically, fluorescence confocal microscopy allows analysing the fluorescence coming from an individual thin in-focus plane of the sample, and this enables the construction of real three-dimensional (3D) images. To discard fluorescence coming from out-of-focus planes, and in contrast to common epifluorescence microscopy, confocal imaging is achieved by introducing a pinhole next to the detector that allows only fluorescence coming from the in-focus plane to reach the detector. **Figure 2.15** shows a schematic picture of the central components of a fluorescence confocal microscope. Essentially, a laser beam is used as the excitation light, which is focused into a dichroic mirror, that selects the light to be directed through an objective into a small spot within the sample. However, this is not enough to build a 3D image of the specimen being measured. For this purpose, special mirrors are introduced to scan the laser beam on the x-y plane, thus building a special confocal microscopy known as laser scanning confocal microscopy. In this way, by precisely controlling the z sample movement, three dimensional images can be constructed.

In the present work, laser scanning confocal microscopy has been applied to observe the binding of protein to GUV and for immunofluorescent localization of proteins in cells.

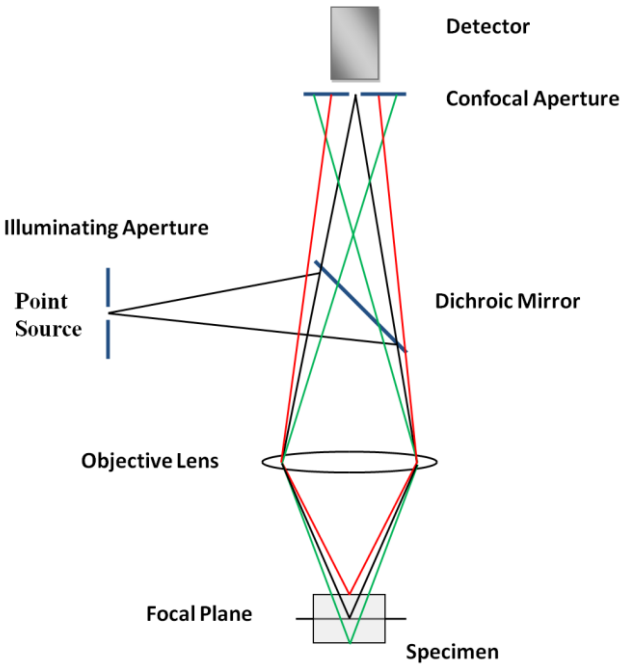

Figure 2.15. Components of fluorescence confocal microscope.

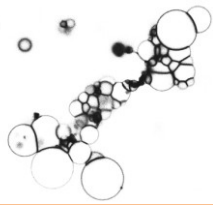

3. Lipid geometry and bilayer curvature modulate LC3/GABARAP-mediated model autophagosomal elongation

CHAPTER 3:

Lipid geometry and bilayer curvature modulate LC3/GABARAP-mediated model autophagosomal elongation

3.1 Introduction

Macroautophagy, “autophagy” in this context, is an intracellular degradation pathway conserved in all eukaryotes (Mizushima & Komatsu, 2011). This process does not only provide nutrients to maintain vital cellular functions under amino-acid limiting conditions, but also plays an important role in a wide range of physiological processes (Boya *et al.*, 2013). Not surprinsingly, impaired autophagic function seems to underlie a wide range of pathological conditions (Choi *et al.*, 2013). During autophagy portions of the cytosol and even entire organelles are sequestered by double-membrane structures called autophagosomes (AP). Eventually, AP fuse with the lysosomal system where the inner membrane and the cargo are degraded. One outstanding question is how the AP membrane is formed and elongated. The most widely accepted hypotheses propose the formation of a core pre-autophagosomal structure, named isolation membrane or phagophore, upon which adhesion and fusion of further membrane structures would occur (Hamasaki *et al.*, 2013; Rubinsztein *et al.*, 2012; Shibutani & Yoshimori, 2014).

To date, at least 35 autophagy-related genes (*ATG*) have been identified and related to the process (Homma *et al.*, 2011; Xie & Klionsky, 2007). Among them, the Atg8 family of ubiquitin-like proteins are among the late autophagosome-specific proteins to bind the AP (Suzuki *et al.*, 2001). Conjugation of Atg8 to PE at the autophagosomal membrane is essential for AP elongation (Ichimura *et al.*, 2000; Xie *et*

al., 2008) but the underlying mechanism of AP growth remains essentially unknown.

While most studies have been focused on the Atg8 conjugation system derived from *S. cerevisiae*, the role of Atg8 homologues in higher eukaryotes is less well characterized (Yang & Klionsky, 2010). Remarkably, whereas yeast has a single Atg8 gene, mammals have up to seven homologs (Shpilka *et al.*, 2011), which can be divided into LC3 and GABARAP subfamilies. Members of both subfamilies have overall similar structures (Coyle *et al.*, 2002; Kouno *et al.*, 2005), are localized to autophagosomal membranes (Kabeya *et al.*, 2000; Tanida *et al.*, 2002a) and are all-essential for the autophagic process (Sou *et al.*, 2008; Weidberg *et al.*, 2010). However, far from being simply redundant members of a protein family, specific members are suggested to act at different stages of AP biogenesis (Weidberg *et al.*, 2010).

Several authors have approached autophagy, and particularly the fusion processes leading to autophagosomal growth, using model membrane systems consisting of vesicles of defined lipid compositions and purified proteins. Nakatogawa *et al.* (Nakatogawa *et al.*, 2007) showed in this kind of systems that yeast Atg8 can trigger liposome tethering and hemifusion, while Weidberg *et al.* (Weidberg *et al.*, 2011) found that mammalian ortologues of Atg8 have the same activities. Furthermore Nair and coworkers (Nair *et al.*, 2011) described how the *in vitro* fusion activity of Atg8-like proteins depended strongly on the presence of high amounts of phospatidylethanolamine (in the 50% mol range). These studies have elicited the interest of investigators on the role of specific lipids and their corresponding synthesizing enzymes in the process of AP formation. Because of the important role of PI3P in autophagy (Dooley *et al.*, 2014; Noda *et al.*, 2010b), this area of research has recently attracted considerable attention and a variety of other lipids have been involved (Chu *et al.*, 2013; Dall'Armi *et al.*, 2013; Vicinanza *et al.*, 2015). However, how the various membrane lipid species modulate AP biogenesis, particularly at the level of autophagic membrane elongation, remains largely unexplored. The ever-increasing number of ATG proteins and the potential combinatorial interactions among them and with cellular factors make the autophagy network very complex and difficult to dissect and analyse in intact cells. In this regard, compositionally defined *in vitro* reconstituted systems are increasingly being used to reveal fundamental information concerning the mechanism of action of individual autophagy proteins and their regulatory factors (Zens *et al.*, 2015). Here we used two minimal reconstituted systems, based on a minimal set of recombinant proteins together with synthetic vesicles of defined lipid compositions, to gain further insight into the the ability of human Atg8 homologues (LC3, GABARAP and GATE-16) to mediate membrane fusion. Our *in vitro* studies shed light on the role of the

various human Atg8 proteins during AP elongation and identify selected lipids as potent modulators of the process.

3.2 Materials and Methods

3.2.1 Materials

Egg phosphatidylcholine (PC), bovine liver phosphatidylinositol (bl-PI), heart cardiolipin (CL), 1,2-dioleoyl-*sn*-glycero-3-phosphatidylethanolamine (DOPE), lysophosphatidylcholine (LPC), egg diacylglycerol (DAG), 1,2-dioleoyl-*sn*-glycero-3-phosphatidylethanolamine-N-(lissamine rhodamine B sulfonyl) (Rho-PE), 1,2-dioleoyl-*sn*-glycero-3-phosphatidylethanolamine-p-maleimidomethyl-cyclohexanecarboxamide (PEmal) and 1-oleoyl-2-{6-[(7-nitro-2-1,3-benzoxadiazol-4-yl)amino]hexanoyl}-*sn*-glycero-3 phosphatidylethanolamine (NBD-PE) were purchased from Avanti Polar Lipids (Alabaster, AL). NaCl, Tris Base, $MgCl_2$, Triton X-100 and n-octyl-β-D-glucopyranoside were obtained from Calbiochem (Darmstadt, Germany**).** *N*-(7-nitrobenz-2-oxa-1,3-diazol-4-yl)-1,2-dihexadecanoyl-*sn*-glycero-3-Phosphatidylethanolamine (NBD-PE), (1,3,6 aminonaphtalene-trisulfonate (ANTS) and p-xilene-bisdipicolinic acid (DPX) were purchased from Molecular Probes (Eugene, OR). Dithiothreitol (DTT) and tris(2-carboxyethyl)phosphine (TCEP) were purchased from Sigma-Aldrich (St. Louis, MO).

3.2.2 DNA Constructs and Site-directed Mutagenesis

Plasmids for expression of human ATG7, human ATG3 and the various homologues of Atg8 (human LC3B, human GATE-16 and human GABARAP) were kindly provided by Dr. Isei Tanida (National Institute of Infectious Diseases, Tokyo, Japan). Note that each Atg8 homologue was a truncated form ending in the reactive C-terminal glycine such that no ATG4-mediated pre-processing was necesary. Wild-type plasmids were mutated by site-directed mutagenesis to obtain $LC3^{G120C}$, $GATE\text{-}16^{C15SG117C}$ ($GATE^{G117C}$ for simplicity) and $GABARAP^{G117C}$ by TopGeneTech (Montreal, Canada) and confirmed by sequencing.

3.2.3 Expression and Purification of Recombinant Proteins

Proteins were purified from soluble fractions of bacterial extracts obtained in the absence of detergents, and were >90% pure as evaluated by Coomassie-stained SDS-PAGE. ATG7 was expressed by baculoviral infection of HighFive (H5) insect cells. ATG7 in pFASTBAC HTa plasmid DNA was used to transform DH10Bac *E. coli* for transposition into the bacmid. We used blue/white colony selection to identify colonies containing the recombinant bacmid and they were confirmed by PCR. The recombinant bacmid was then isolated and purified using Macherey Nagel endotoxin-free DNA purification kit. H5 insect cells were transfected with purified bacmid using Lipofectamine from Invitrogen (Waltham, MA) in TC-100 insect media (Sigma-Aldrich) supplemented with the appropiate antibiotics. When the transfected cells demonstrated signs of late stage infection (typically around 72 h), the medium containing the free virus was collected. We repeated cycles of transfection and virus collection to amplify the viral stock. Cells were collected after 48 h infection followed by centrifugation at 5,000 xg for 10 min. The pellet was resuspended and sonicated in a breaking buffer consisting of 50 mM Tris pH 8, 150 mM NaCl and freshly prepared 1 mM TCEP and protease inhibitors. The lysate was cleared by 30 min centrifugation at 30,000 xg and loaded on cobalt resin (Clontech, Mountain View, CA) for 3 h at 4 ºC. Protein was eluted with 500 mM imidazole, concentrated up to 500 µl using YM-30 microcons (Millipore, Darmstadt, Germany) and loaded onto a Superdex TM200HR 10/30 size exclusion column (GE Healthcare, Buckinghamshire, UK) equilibrated in 50 mM Tris pH 8, 150 mM NaCl, supplemented with freshly added 1 mM DTT and protease inhibitors. Purified protein was kept at 4 ºC. Plasmids of ATG3, LC3, GATE-16, GABARAP and their corresponding mutant forms were transformed onto *E. coli* BL21 (λDE3) cells. Cells were grown to OD_{600}=0.8 and induced with 0.5 mM IPTG for 3 h at 37 **º**C in the case of GATE-16 and LC3, 4 h at 20 ºC in the case of GABARAP, and 18 h at 18 ºC in the case of ATG3. Following centrifugation at 5,000 xg for 10 min, the pellet was resuspended and sonicated in breaking buffer (PBS with protease inhibitors mixture and 1 mM DTT). The lysate was cleared by 30 min centrifugation at 30,000 xg, loaded on glutathione-agarose (Sigma-Aldrich) and incubated for 3 h at 4 ºC. Proteins were eluted by cleavage with PreScission Protease (GE Healthcare) in Precission Buffer (50 mM Tris (pH 7.5), 150 mM NaCl, 1 mM EDTA) with freshly added 1 mM DTT, for 4 h at 4 ºC. In the case of cysteine C-terminal mutants 1 mM TCEP was used instead of DTT to avoid interference with the thiol-maleimide coupling. Proteins were aliquoted, flash-frozen and stored at -80 °C until further use.

3.2.4 Liposome Preparation

The appropriate lipids were mixed in organic solution, and the solvent was evaporated to dryness under a stream of N_2. The sample was then kept under vacuum for 2 h to remove solvent traces. The lipids were swollen in appropiate buffers. Small unilamellar vesicles (SUVs) were prepared from the swollen lipids by sonication with a probe tip sonicator (MSE Soniprep 150 (MSE, UK)) for 10 min (10 s on and off cycles) at 10-20 μm amplitude. The vials were kept on ice during the process to avoid overheating. When large unilamellar vesicles (LUVs) were required, swollen lipids were subjected to 10 freeze/thaw cycles and then extruded using 0.05 μm pore-size Nuclepore (San Diego, CA) filters, as described by Mayer et al (Mayer *et al.*, 1986). Vesicle size was checked by quasielastic light scattering, using a Malvern Zeta-Sizer 4 spectrometer (Malvern Instruments, Worcestershire, UK). LUVs had an average diameter of 80 nm and SUVs had an average diameter of 50 nm. Lipid concentration was determined by phosphate analysis (Fiske & Subbarow, 1925).

3.2.5 Dynamic Light Scattering Measurements

To determine size-distribution profiles of the liposomes, the samples were properly diluted with the conjugation reaction buffer and subjected to DLS measurements at 37 ºC using a Zetasizer Nano-S system (Malvern Instruments).

3.2.6 *In vitro* Enzymatic Lipidation Reaction

To recreate PE-conjugation *in vitro,* purified ATG7 (1 μM), ATG3 (1 μM), and LC3 or one of its homologues (10 μM) were mixed with liposomes (0.4 mM total lipid) in the presence of 1 mM DTT and 5 mM ATP in conjugation buffer (50mM Tris pH 7.5, 150 mM NaCl and 1 mM $MgCl_2$) and incubated at 37 °C for 90 min. The reaction was stopped with 6x SDS-PAGE sample buffer and heated at 90 °C for 5 min. Samples were run on SDS-PAGE gels and visualized with Coomassie Blue stain (Thermoscientific; Waltham, MA).

3.2.7 Lipidation of LC3 and Homologues with PEmal

To reconstitute LC3-PE conjugation *in vitro* without the use of ATG7, ATG3 or

PE, purified $LC3^{G120C}$, $GATE\text{-}16^{G117C}$ or $GABARAP^{G117C}$ (10 μM each) were incubated with 15% PEmal-containing liposomes at a final lipid concentration of 0.4 mM in conjugation buffer. The reaction mixture was incubated at 37 ºC for 90 min and visualized by SDS-PAGE.

3.2.8 Aggregation Assays

Liposome aggregation was monitored in an Uvikon 922 (Kontron, Augsburg, Germany) spectrophotometer as an increase in turbidity (absorbance at 400 nm) of the sample. All assays were carried out at 37 ºC with continuous stirring.

3.2.9 Lipid Mixing and Aqueous Contents Mixing Assays in Large Unilamellar Vesicles

A fluorescence resonance energy transfer assay was used to monitor intervesicular membrane lipid mixing (Struck *et al.*, 1981). The appropriate LUVs containing 1.5 mol% NBD-PE and 1.5 mol% Rh-PE were mixed with 9-fold excess of unlabeled LUVs. NBD-PE emission was monitored in a QuantaMaster spectrofluorometer (Photon Technology International, Birmingham, New Jersey) in a thermostatically controlled 1 cm path length cuvette with constant stirring at 37 °C. NBD emission was monitored at 530 nm with the excitation wavelength set at 467 nm (slits, 2 nm). A 515 nm cut-off filter was placed between the sample and the emission monochromator to avoid scattering interference. Inner monolayer lipid mixing was measured using asymmetrically labeled membrane vesicles produced by the quenching of the outer leaflet NBD-PE fluorescence upon addition of sodium dithionite (Xu *et al.*, 2005). Dithionite was removed by gel filtration in Sephadex G-25M, using conjugation buffer for elution.

Intervesicular content mixing was monitored by the ANTS/DPX assay (Ellens *et al.*, 1985). ANTS emission was monitored at 530 nm with the excitation wavelength set at 360 nm (slits, 2 nm). A 470 nm cut-off filter was placed between the sample and the emission monochromator to avoid scattering interference. 0% vesicle content mixing was set by using a 1:1 mixture of ANTS and DPX liposomes. 100% mixing of contents corresponded to the fluorescence of the vesicles containing coencapsulated ANTS and DPX. Details for the intervesicular lipid mixing and contents mixing assays can be found in Goñi *et al.* (2003).

3.2.10 Vesicle Contents Leakage Assay

Leakage of vesicle contents was monitored by the ANTS/DPX assay (Ellens *et al.*, 1985). ANTS emission was monitored at 530 nm with the excitation wavelength set at 360 nm (slits, 2 nm). A 470 nm cut-off filter was placed between the sample and the emission monochromator to avoid scattering interference. To establish the 100% leakage signal, Triton X-100 was added to a concentration of 1%. Details for the vesicle contents leakage assay can be found in Goñi *et al.*, (2003).

3.2.11 Cryo-electron Microscopy (Cryo-EM)

For the Cryo-EM studies, conjugation reactions were performed as explained above. Grids were prepared following standard procedures and observed at liquid nitrogen temperatures in a JEM-2200FS/CR transmission electron microscope (JEOL Europe, Croissy-sur-Seine, France) operated at 200 kV. An in-column omega energy filter helped to record images with improved signal to noise ratio by zero-loss filtering. The energy selecting slit width was set at 9 eV. Digital images were recorded on UltraScan4000 CCD camera under low-dose conditions at a magnification of 55,058 obtaining a final pixel size of 2.7 Å/pixel.

3.3 Results

3.3.1 Production of UBL System Proteins and Detection of UBL System Reaction Intermediates

The Atg8 UBL conjugation system has been well studied in the past few years. Different steps in the conjugation reactions have also been characterized in yeast, and using both mammalian and yeast proteins jointly. Recently, a new study (Nath *et al.*, 2014) first reconstituted the system using only mammalian proteins, most of them from human origin. However, no reports about this system with the whole human set of proteins have been published. Thus, we tried to reconstitute and characterize the behaviour of the human UBL system. We used LC3B, GATE-16 and GABARAP as human Atg8 homologues, as well as human ATG7 and ATG3.

Among these proteins ATG7, the E1-like enzyme, was expressed in bacteria, *E. coli* strains. Many different strains and as many different constructs with a variety of tags were tested to get protein expression but without success. Most of the references about ATG7 protein are related to the yeast homologue, because in higher organisms ATG7 seems to be very unstable and requires some modifications in the expression process. Thus in order to obtain the human full length ATG7, we decided to switch to a more sophisticated expression system, such as insect cells. Baculovirus expression system is closer to the mammalian expression and implements more post-translational modifications than bacteria to obtain better protein expression results. ATG7 was cloned into a pFastBac-Hta vector and expressed in insect cells.

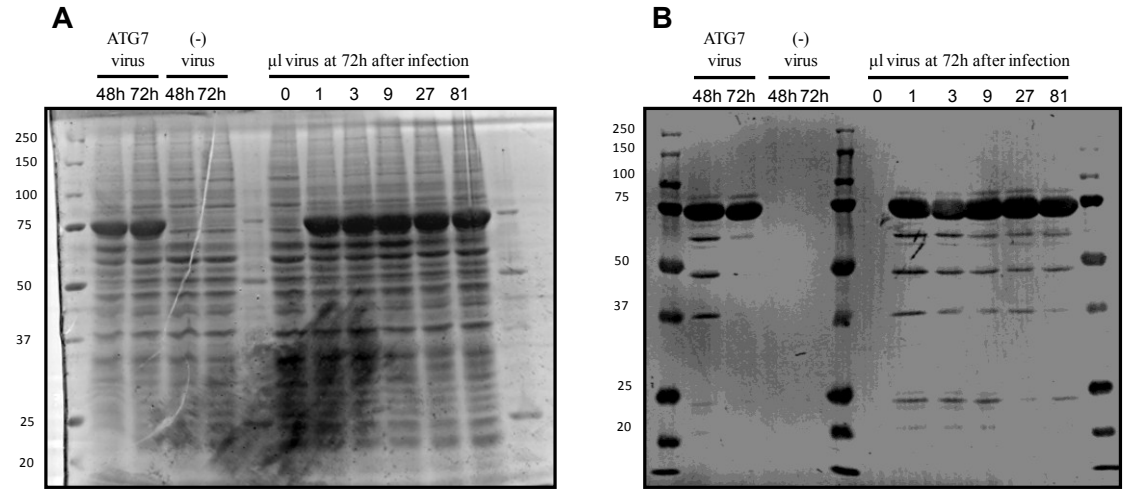

Figure 3.1. Infection time and MOI optimization for ATG7 expression. ATG7 expression was followed by SDS-PAGE **(A)** and Western Blotting anti-His **(B)**, under different infection times and MOI. ATG7 is observed as a band around 75 kDa. Molecular masses are shown in kDa on the left-hand side.

Expression was optimized in terms of infection time and MOI (**Figure 3.1**), obtaining a satisfactory amount of polypeptide. Protein was purified using cobalt beads and size exclusion chromatography to clean the sample and verify the oligomeric state of the protein (**Figure 3.2 A-B**). Enough amount of protein in its dimeric state was obtained (**Figure 3.2 D**). Nevertheless, ATG7 was very unstable and tended to be proteolytically degraded in a short period of time. Freshly added protease inhibitors were necessary to conserve the protein after each purification step, and to store it.

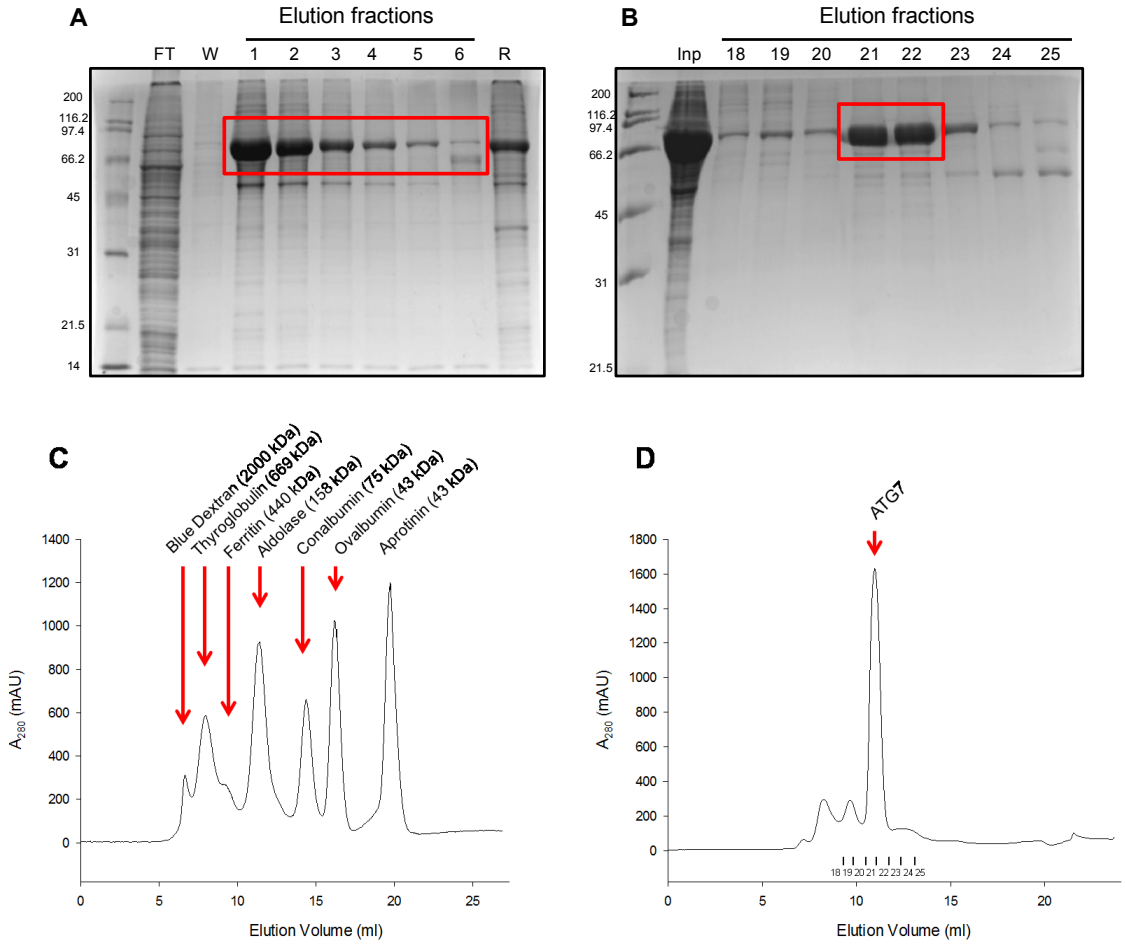

Figure 3.2. ATG7 purification. (A) SDS-PAGE of cobalt affinity chromatography. **(B)** SDS-PAGE of the size exclusion chromatography using Superdex 200 Increase column. (FT: Flow-Through; W: Wash; R: Resin after elution; Inp: Input). Molecular masses are shown in kDa on the left-hand side. **(C)** Size exclusion calibration chromatogram. **(D)** Size exclusion ATG7 chromatogram. ATG7 is indicated by a red rectangle in both A and B. Red arrows denote each chromatography peak.

Atg8 human homologues LC3B, GATE-16 and GABARAP were expressed and purified in three different versions (**Figure 3.3**). In this study, all three proteins were

expressed with the C-terminal Gly exposed in order to bypass the cleavage by ATG4. These versions are denoted with the original name of the proteins in the following experiments. Another version used as a negative control of the lipidation reaction was the deletion mutant of the exposed C-terminal Gly, called as LC3ΔG, GATE-16ΔG and GABARAPΔG. In addition, with the aim of mimicking the conjugation reaction of these proteins without the other components of the system, we designed mutants of the C-terminal Gly to Cys (LC3G120C, GATE-16G117C and GABARAPG117C). In this manner, the protein could covalently bind a maleimide modified PE by itself. The set of the different protein versions (**Figure 3.3**) were expressed in their GST-tagged form in *E. coli* BL21 (DE3) and purified using Glutathione Sepharose beads (**Figure 3.4 A-C**). Human ATG3, the E2-like enzyme, was expressed, as well as Atg8 human homologues, in *E. coli* BL21 (DE3) with a GST tag, and purified in the same way (**Figure 3.4 D**).

Next, circular dichroism (CD) was used to assess the secondary structure and the correct folding of the recombinant purified Atg proteins. Results are shown in **Figure 3.4 F**. As expected from previously reported data of these proteins, LC3, GATE-16, GABARAP and ATG3 gave rise to CD spectra with minima near 205 nm compatible with a mix of α-helix and intrinsically disordered structures. By contrast, the CD spectra of ATG7 displayed substantial helicity, showing minima at 222 and 208 nm.

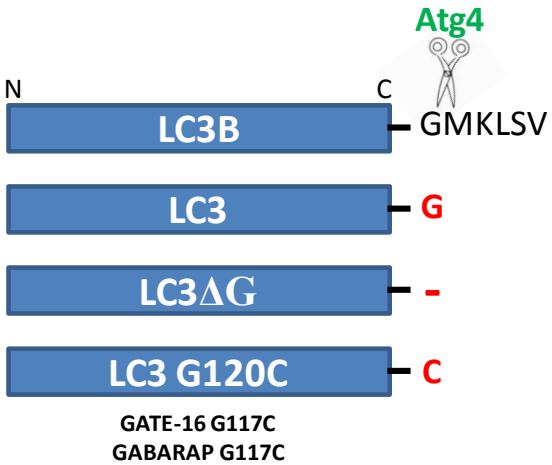

Figure 3.3. Schematic representation of the Atg8 homologue versions. From top to bottom, LC3 wild type, LC3 with the C-terminal Gly exposed the negative control without the C-terminal Gly, and finally the substitution mutant LC3 with a Cys in its C-terminal end.

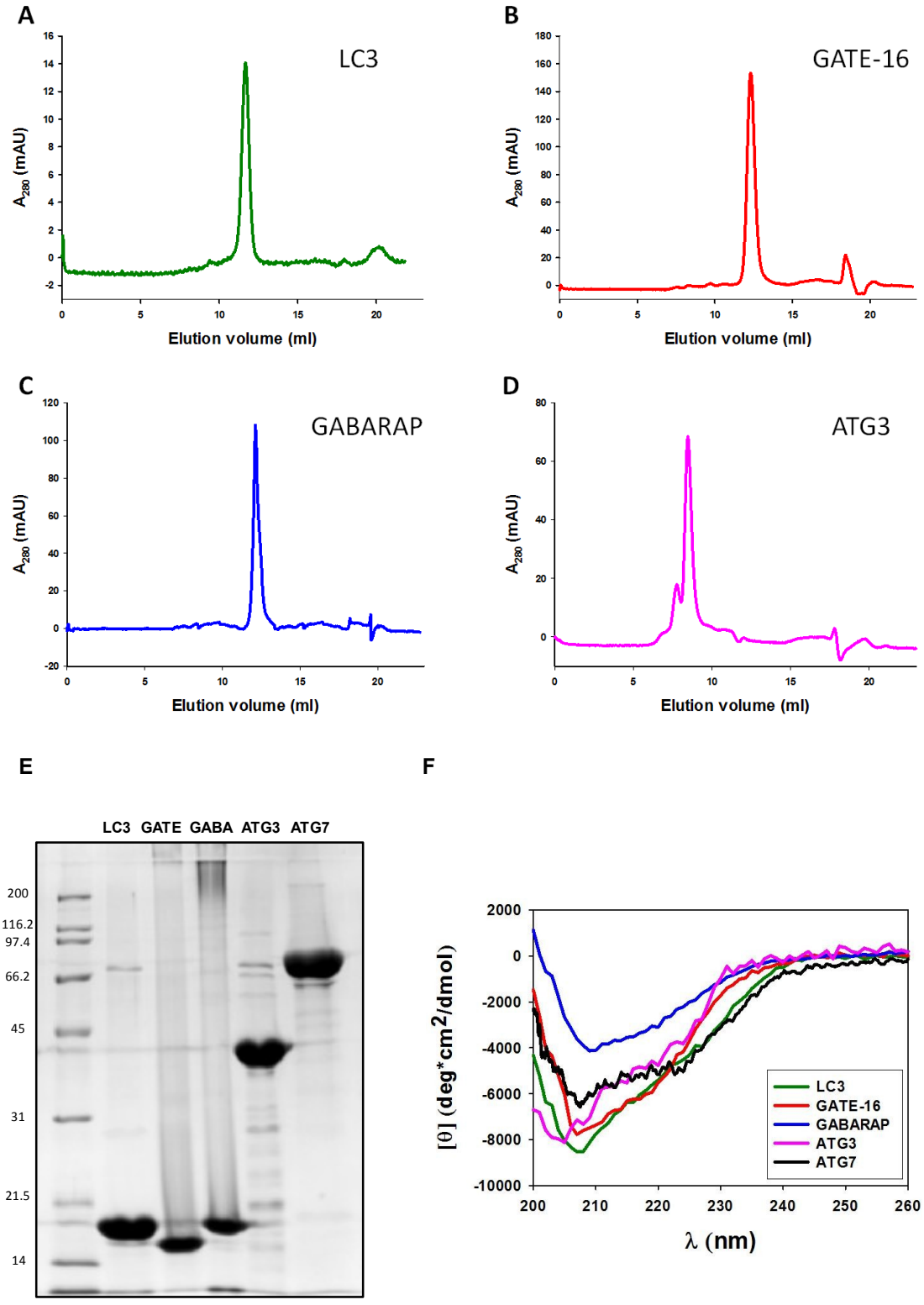

Figure 3.4. Expression and purification of human LC3, GATE-16, GABARAP and ATG3. **(A-D)**, After elution from gluthatione beads, ATG proteins were subjected to size exclusion chromatography on a Superdex 75 10/300 GL column. **(E)** After SEC, all proteins were >90% pure as evaluated by Coomassie-stained SDS-PAGE. Molecular masses are shown in KDa on the left-hand side. **(F)** Circular dichroism (CD) analysis of ATG proteins in 50 mM Na_2HPO_4, 20 mM KCl, pH 7.0.

The entire system behaviour was checked by detection of the first reaction intermediates ATG7-LC3 and ATG3-LC3, before the lipidation occurred and triggered different membrane tethering or fusion events. Proteins bind through a thioester bond. Two different reactions were set up, one with the first two components of the system, ATG7 and LC3, and the next one with the addition of ATG3, both of them in the presence of ATP and $MgCl_2$. The appearance of the ATG7-LC3 intermediate product at different time points was followed by non-reducing SDS-PAGE (**Figure 3.5 A**) and Western blotting (**Figure 3.5 B**) in the presence and absence of ATP. ATG7-LC3 was detected only in the presence of ATP, complex concentration increasing with time (**Figure 3.5**). The presence of ATG7 and LC3 in this band was also checked by mass spectrometry. Moreover, an additional larger product was detected but its origin is unknown.

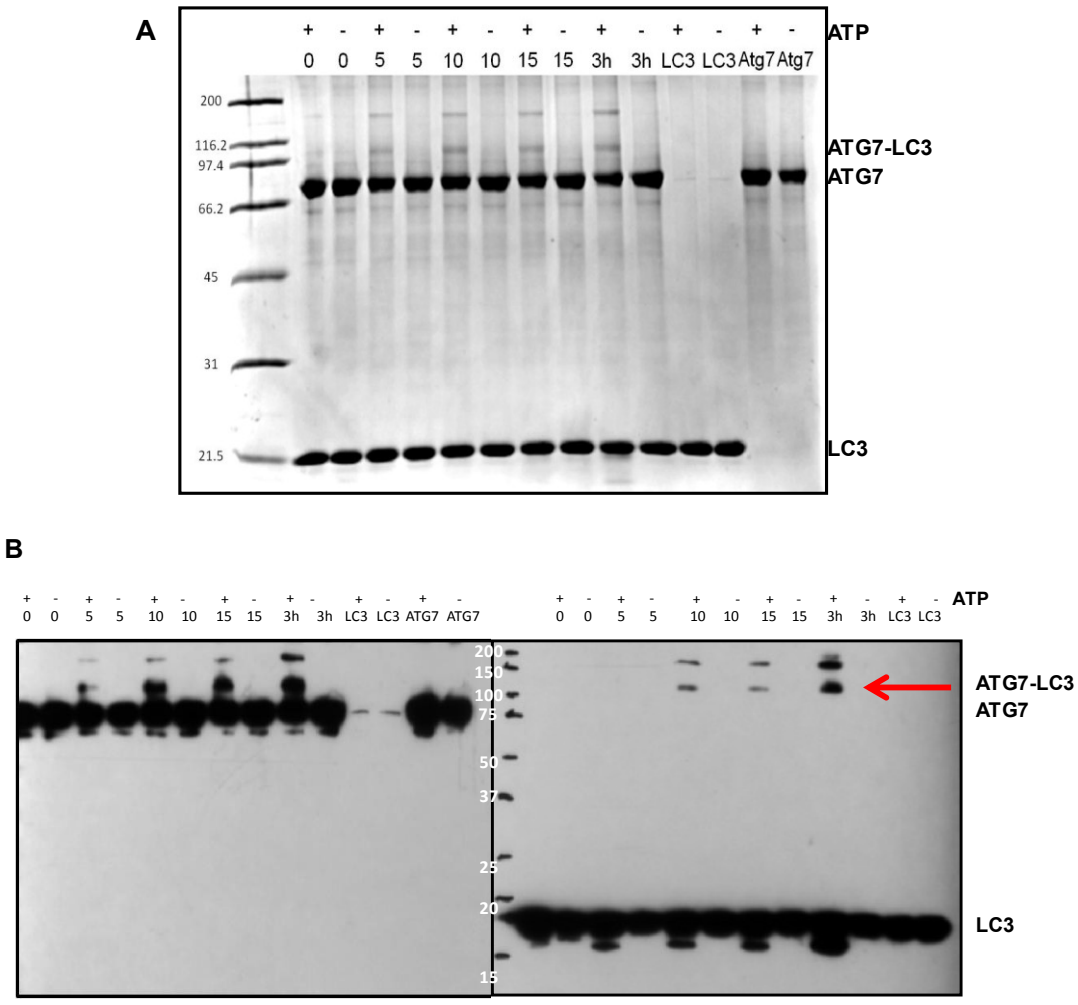

Figure 3.5. ATG7-LC3 intermediates. ATG7 (2 μM) and LC3 (8 μM) were incubated with 1 mM $MgCl_2$ and 0.2 mM DTT at 4 ºC in the presence or absence of 1 mM ATP. The reaction intermediate formation was followed at different times, either by SDS PAGE **(A)** or anti-ATG7 or anti-LC3 Western Blotting **(B)**. Molecular masses are shown in kDa on the left-hand side.

When the third component of the system was added to the reaction under the same working conditions, an extra band appeared in the non-reducing SDS-PAGE (**Figure 3.6 A**) and Western Blot (**Figure 3.6 B**), corresponding to the ATG3-LC3 intermediate. This product was only observed in the presence of ATP (**Figure 3.6**).

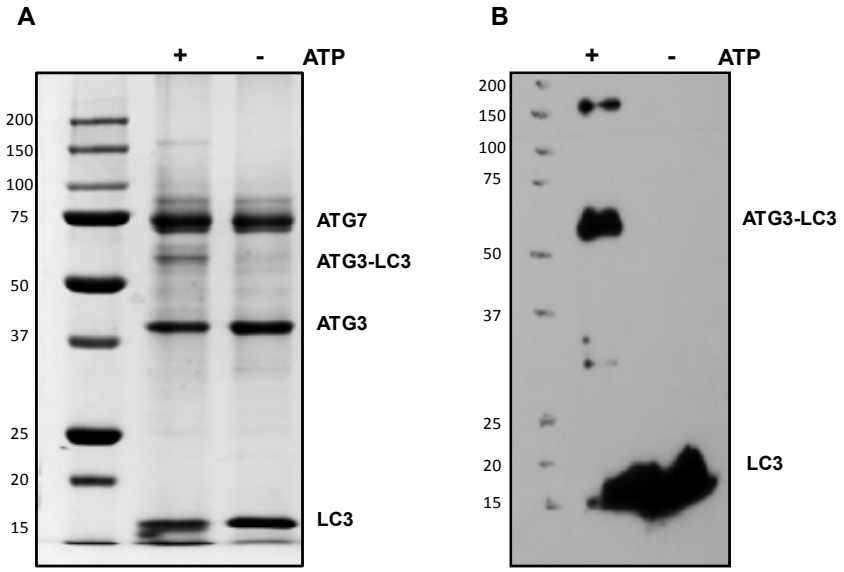

Figure 3.6. ATG3-LC3 intermediates. ATG7 (2 μM), ATG3 (2 μM) and LC3 (8 μM) were incubated with 1 mM $MgCl_2$ and 0.2 mM DTT at 4 ºC in the presence or absence of 1mM ATP. The second reaction intermediate formation was followed at different times, either by SDS PAGE **(A)** or anti-LC3 Western Blotting **(B)**. Molecular masses are shown in kDa on the

3.3.2. Reconstitution of the Lipidation Reaction

After activation by ATG4B, covalent attachment of Atg8 to PE is mediated by a ubiquitin-like chain of enzymatic steps involving the E1-like ATG7 and the E2-like ATG3 (**Figure 3.7 C**). These reactions can be reconstituted *in vitro*, using recombinant purified proteins, liposomes and ATP (Ichimura *et al.*, 2004; Nakatogawa & Ohsumi, 2012). In order to study the role of these protein-lipid complexes in membrane tethering and fusion processes, we first tried to reconstitute the enzymatically-driven lipidation reaction of the human Atg8 proteins, LC3, GABARAP or GATE-16 (**Figure 3.7 A-B**).

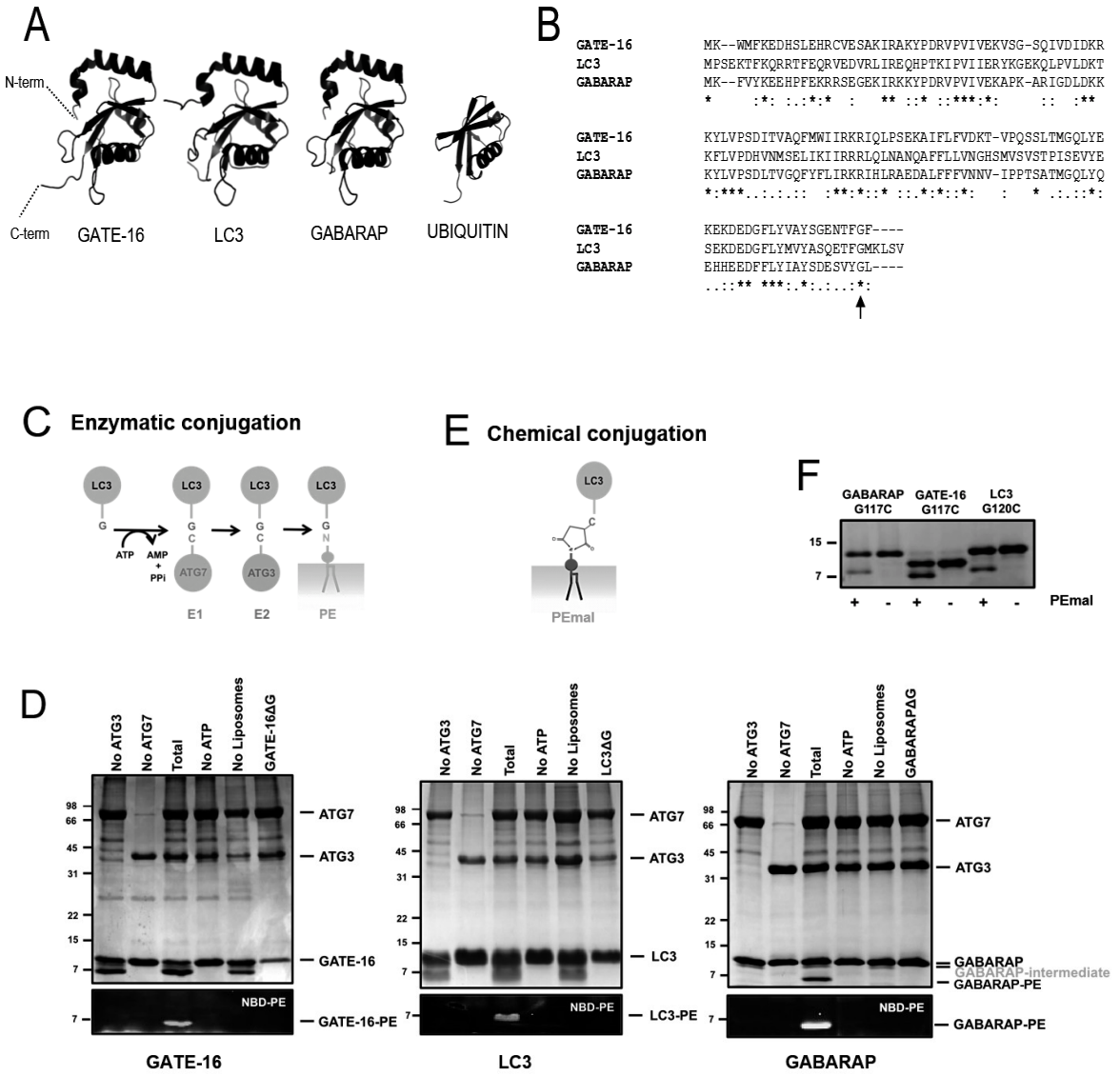

Figure 3.7. In vitro reconstitution of the lipidation reaction. (A) Crystal structures of the indicated human Atg8 family members and ubiquitin. All Atg8s share a similar ubiquitin-like fold with two additional amino-terminal α helices. GATE-16 (Protein Data Bank (PDB): 1EO6), LC3B (PDB: 1V49), GABARAP (PDB: 1KOT) and ubiquitin (PDB: 1UBI). Helix shape represents an α helix; arrow shape represents a β sheet; arrowhead represents the carboxyl termini of β sheets. **(B)** ClustalW sequence alignment of human GATE-16 (data base accession no. P60520), LC3B (Q9GZQ8) and GABARAP (Q6IAW1)**.** The black arrow indicates the conserved glycine residue present at the C terminus of the processed forms of the Atg8-like proteins. **(C)** Outline representation of the enzymatic conjugation of LC3/GABARAP to PE. **(D)** Conjugation of recombinant LC3, GATE-16 and GABARAP with phosphatidylethanolamine (PE). Reaction media contain 1 μM ATG7, 1 μM ATG3, 10 μM Atg8 homologues, 1 mM DTT, 5 mM ATP and 0.4 mM LUV [PC/DOPE/bl-PI/NBD-PE (35/45/10/10 mol ratio)]. Each reaction mixture was incubated at 37 ºC for 90 min, run on 12.5% SDS–PAGE gels and visualized by CBB-staining (top panels) or using a VersaDoc MP 4000 Imaging System (bottom panels). In CBB-stained gels lipidated forms of GATE-16 and LC3 are undistinguishable from the adelynated intermediates (compare lanes 1, 3 and 5 from the right). In the case of GABARAP, the adelynated intermediate appears immediately below the non-lipidated form (GABARAP-intermediate) and clearly distinguishable from the lipidated form (GABARAP-PE).

Conjugation of proteins to NBD-PE results in the appearance of a fluorescent faster migrating band corresponding to the lipidated form of the protein. Molecular masses are shown in kDa on the left-hand side. For negative controls, Atg8 homologues lacking the reactive C-terminal glycine (ΔG) or reactions lacking either ATG7, ATG3, ATP or LUVs were used. **(E)** Outline representation of the chemical conjugation of LC3/GABARAP to PEmal. **(F)** Chemical conjugation of recombinant LC3BG120C, GATE-16G117C and GABARAPG117C. The indicated recombinant proteins (10 μM) were incubated at 37 ºC for 90 min with 0.4 mM LUV [PC/DOPE/PEmal/bl-PI (35/40/15/10 mol ratio)]. Cross-linking of the proteins to the maleimide-functionalized lipid results in the appearance of a faster migrating band corresponding to the lipidated form of the protein. For negative control liposomes lacking PEmal were used. Molecular masses are shown in kDa on the left-hand side.

Reaction systems including ATG7, ATG3, ATP and liposomes led to the formation of a faster migrating band readily visualized by Coomassie Brilliant Blue (CBB)-staining (**Figure 3.7 D, upper panels**). The latter was particularly well-resolved for the GABARAP case. However for LC3 and GATE-16 this band was undistinguishable from the presumably adenylated form of the protein that appears in the presence of ATP and ATG7 (Nath *et al.*, 2014) (**Figure 3.7 D, upper panels**). To confirm the lipidation reaction, conjugation reactions were prepared with liposomes containing 10% NBD-PE. In each case, reactions led to the formation of a fluorescent faster migrating band representing the lipidated products of LC3/GABARAP subfamilies (**Figure 3.7 D, lower panels**).

Alternatively to the enzyme-driven reaction LC3 homologues can also be chemically lipidated (Nair *et al.*, 2011; Weidberg *et al.*, 2011) (**Figure 3.7 E**). Here the C-terminal glycine of the proteins is replaced by a cysteine residue and then linked to PE carrying a reactive maleimide on its headgroup (PEmal). Structurally this linkage differs from the native coupling by the addition of the maleimide ring, however, these maleimide-anchored conjugates have been reported to be functionally active and are generally considered as useful mimetic analogues to the naturally coupled proteins. Conjugation of the corresponding C-terminal mutants to PEmal-containing liposomes caused the appearance of a faster migrating band in SDS-PAGE, similar to the lipidated forms obtained using the enzymatic-conjugation machinery (**Figure 3.7 F**).

Taken together these experiments indicate that the production of the lipidated products for the three proteins used in this study can be detected, in the context of the whole conjugation enzymatic system as well as using a chemically modified lipid.

3.3.3. Effect of Human LC3 Homologues on Liposome Clustering *in vitro*

In the course of autophagosome maturation membrane tethering should be essential both in the recruitment of vesicles targeting the expanding phagophore and in the closure of the autophagosome itself. In fact, yeast Atg8-PE was proven to induce liposome aggregation *in vitro* (Nakatogawa *et al.*, 2007), shedding some light on the possible role of this protein during AP biogenesis. As an initial test for analyzing the functional activity of LC3 homologues, we evaluated their ability to induce liposome aggregation *in vitro.* As shown in **Figure 3.8**, of the three proteins tested, GATE-16 and GABARAP induced a marked liposome aggregation, measured as an increase in absorbance at 400 nm (**Figure 3.8 A**) and by visual observation under the light microscope (**Figure 3.8 C**). This effect was not observed in the absence of ATG7. LC3 had a small effect under the same conditions.

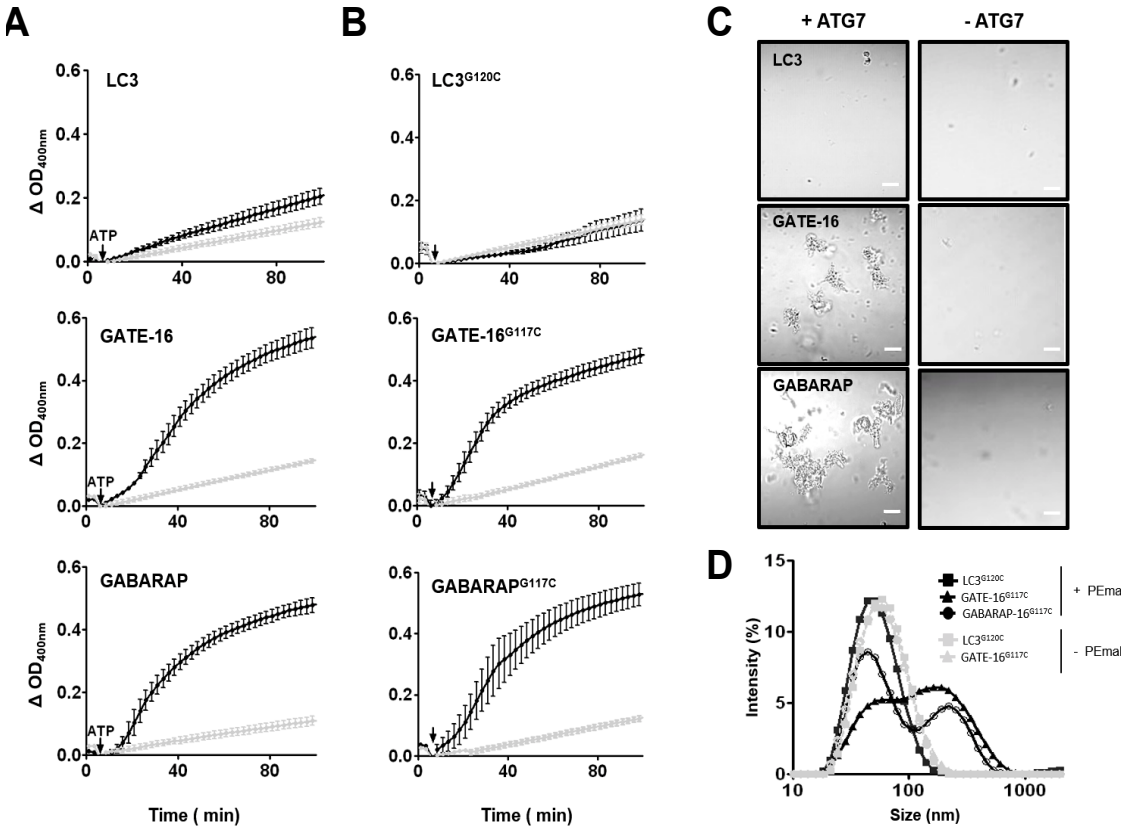

Figure 3.8. Membrane tethering activities by human autophagic proteins. **(A, C)** Enzymatic conjugation reactions (maleimide-free) were performed as described in **Figure 1 C** followed by changes in absorbance at 400 nm, 37 ºC and observation under a light microscope (bar=10 µm). Liposomes were composed of PC/DOPE/bl-PI (35/55/10 mol ratio). For a negative control, ATG7 was excluded from the reaction (grey trace). **(B, D)** Chemical conjugation to PEmal was performed as described in Fig. 1D followed by measurements of changes in the absorbance at 400 nm, 37 ºC. Aggregate size distribution was measured by DLS at 37 ºC. In B and D liposomes were composed of PC/DOPE/PEmal/bl-PI (35/40/15/10 mol ratio). For negative controls, liposomes lacking PEmal were used (grey traces).

We also evaluated the capacity of the PEmal-anchored homologues to induce liposome aggregation. Again only GATE-16-PEmal and GABARAP-PEmal were able to induce efficient liposome aggregation according to either turbidimetric (**Figure 3.8 B**) or dynamic light-scattering measurements (**Figure 3.8 D**). Interestingly, PEmal conjugates induce liposome aggregation at similar rates than their enzymatically conjugated counterparts, supporting the reliable use of this chemical model.

These results are consistent with the growing number of evidences indicating a membrane tethering activity for autophagy-related ubiquitin molecules and might represent the first evidence of such an *in vitro* activity for the GABARAP homologue. LC3-PEmal was shown to efficiently induce membrane tethering *in vitro* (Weidberg *et al.*, 2011). The fact that in our system this protein lacked this activity may result from differences in the experimental system, particularly differences in the lipidic composition of the LUVs that included phosphatidylserine and cholesterol in their case.

3.3.4. Effect of Human LC3 Homologues on Membrane Fusion

Liposome aggregation could simply represent membrane tethering, but it could also be an indication of hemifusion (i.e., fusion of the outer leaflets of adjacent membranes, while inner leaflets remain intact) or even of complete fusion (i.e., the merger of both inner and outer leaflets) of apposed membranes (Chernomordik & Kozlov, 2008). Previous studies with an *in vitro* reconstituted system similar to ours reported that yeast Atg8 mediates membrane hemifusion, but not complete fusion (Nakatogawa *et al.*, 2007). In a different study, mammalian forms of LC3 and GATE-16, artificially linked to PEmal, were shown to induce full membrane fusion (lipid mixing) (Weidberg *et al.*, 2011). In order to clarify the situation we initially used a intervesicular lipid-mixing assay based on fluorescence resonance energy transfer (FRET) from NBD-PE to Rho-PE (Struck *et al.*, 1981). When the two dyes are present at an appropriate concentration in the same liposome, the fluorescence of NBD is quenched by rhodamine. Upon fusion of these LUVs with unlabeled LUVs and subsequent probe dilution in the bilayer the distance between the two dyes increases, resulting in a dequenching of NBD fluorescence. As shown in **Figure 3.9 A**, when the two LUV populations were subjected to the conjugation reaction, a significant increase in fluorescence was observed with GATE-16-PE and GABARAP-PE proteins. Importantly, lipid mixing was not observed in the absence of ATG7. In agreement with the inefficient capacity of LC3-PE to tether liposomes, only a small increase in NBD fluorescence was recorded in this case.

We then investigated whether GATE-16/GABARAP-PE induced lipid mixing resulted from complete membrane fusion or membrane hemifusion. To this aim, we prepared asymmetrically labeled liposomes by adding the membrane-impermeable reductant sodium dithionite to the liposome suspension to selectively quench the fluorescence of NBD in the outer leaflet (Xu *et al.*, 2005). Thus any observed lipid mixing arises from intervesicular mixing of inner monolayer lipids, i.e. from full membrane fusion. Both GATE-16-PE and GABARAP-PE stimulated NBD fluorescence of dithionite-treated liposomes in a time-dependent manner, indicating that fusion of the inner leaflets of apposed membranes, i.e., complete fusion of vesicles, had occurred (**Figure 3.9 A**). As expected, the intensity of the fluorescence signal corresponding to fusion of inner monolayer lipids is about one-half of the one indicating total lipid mixing. Note that fusion of inner monolayers exhibits a longer lag time than total lipid mixing which is particularly clear for GABARAP. The phenomenon occurs because total lipid mixing includes hemifusion, that is an obligatory step previous to inner monolayer mixing, i.e complete fusion (Basañez *et al.*, 1996a; Ibarguren *et al.*, 2010; Villar *et al.*, 2001). These results indicate that the observed membrane fusion elicited by human GATE-16 and by GABARAP *in vitro*, in the context of a minimal human conjugation machinery, consists of full membrane fusion events. Since in the process of vesicle-vesicle fusion a pore connecting the vesicle inner spaces is opened, intervesicular mixing of aqueous contents should occur. This was tested, and confirmed, using the ANTS/DPX fluorescence quenching couple (**Figure 3.9 B**). Note that the extent of contents mixing corresponds roughly with that of inner monolayer lipid mixing (**Figure. 3.9 A**) at a given time. Most biological fusion events occur in such a way that vesicle contents are not leaked out. This is also the case in our model fusion system (**Figure 3.9 C**).

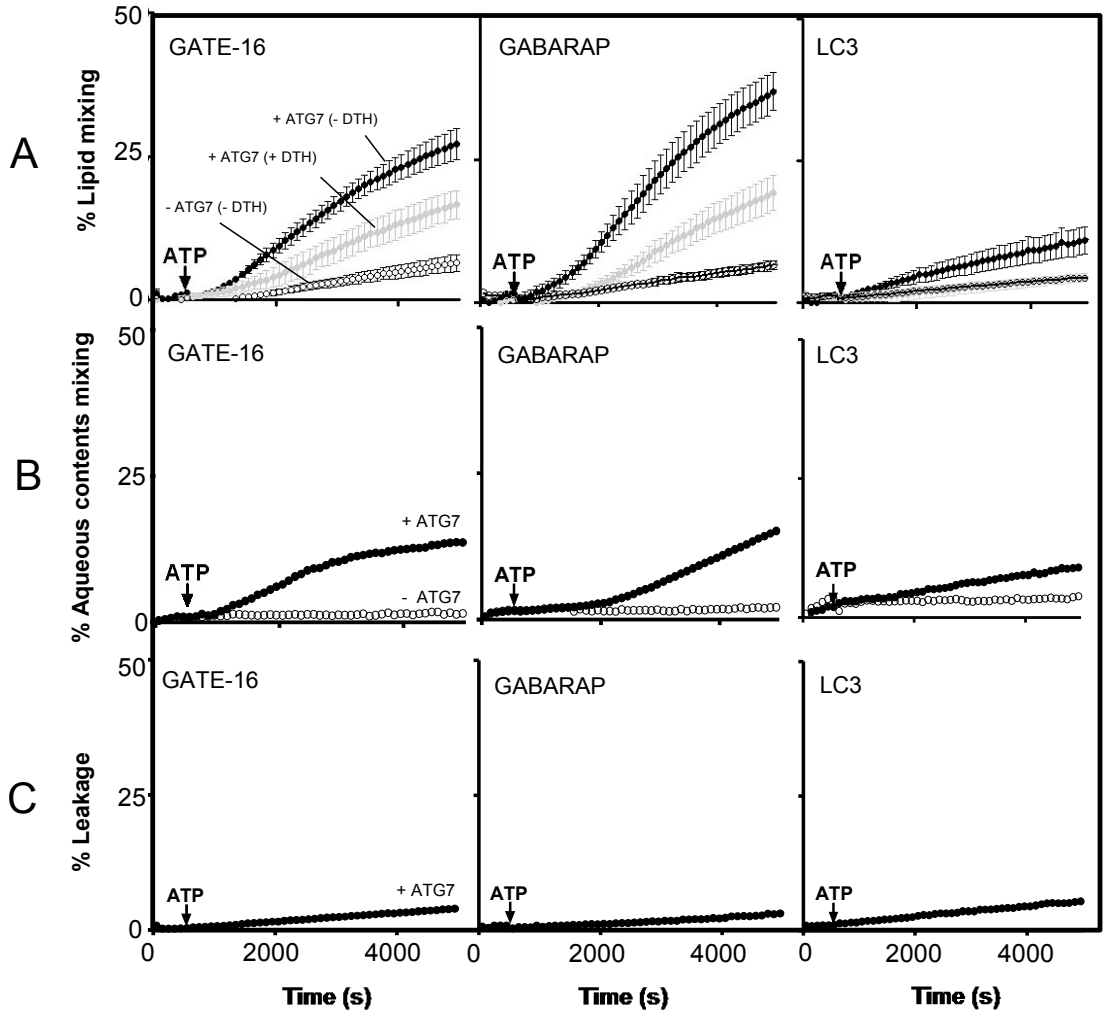

Figure 3.9. Membrane fusion induced by enzymatically conjugated LC3/GABARAP-PE. **(A)** Time courses of total (●) and inner lipid (●) mixing induced by ATG7 (1 μM), ATG3 (1 μM) and the indicated Atg8 human homologues (10 μM) in liposomes (0.4 mM) composed of PC/DOPE/bl-PI (35/55/10 mol ratio). Lipid mixing was monitored by the NBD/Rhodamine lipid dilution assay. For inner monolayer lipid mixing NBD + Rho-liposomes were pre-treated with the appropriate amounts of sodium dithionite to quench NBD fluorescence of the outer leaflet. Unlabeled and (NBD + Rho)-labeled liposomes (9:1) were mixed and incubated for 5 min before ATP addition. The extent of lipid mixing was quantified on a percentage basis according to the equation: $(F_t-F_0/F_{100}-F_0)$ x100 where F_t is the measured fluorescence of protein-treated LUVs at time t, F_0 is the initial fluorescence of the LUV suspension before protein addition, and F_{100} is the fluorescence value after complete disruption of LUVs by addition of 30 mM β-octylglucoside (OG). Each curve represents the average and S.E. of three independent experiments. For negative controls, ATG7 was excluded from the reactions (○). **(B)** Time course of intervesicular aqueous content mixing. Proteins and lipids as in (A). Content mixing (●) was monitored by the ANTS/DPX mixing assay; 100% mixing was determined using LUVs containing coencapsulated ANTS and DPX. ATG7 was excluded from the reactions for negative controls (○). **(C)** Time courses of fusion-related vesicle content leakage. Proteins and lipids as in (A). Vesicle leakage (●) was monitored by the ANTS/DPX leakage assay; 100% leakage signal was obtained by adding 1% Triton X-100.

To obtain a morphological evidence of fusion, we analyzed the morphology of liposomes by cryo-EM. As shown in **Figure 3.10**, in the case of conjugation reactions including GATE-16 and GABARAP homologues, formation of much larger vesicles was observed at the end of the fusion reaction, clearly suggesting repetitive fusion events. These results strongly support our conclusion that GATE-16-PE and GABARAP-PE cause fusion of liposomes. In control experiments, no increase in liposome size was observed in the absence of ATG7. Moreover, consistent with the biochemical results suggesting that LC3 is a weaker inducer of membrane fusion in the *in vitro* system used here, liposome size increased less markedly. However, a significant number of liposomes lost their spherical shape and appeared as elongated structures that may derive from either deformation of single vesicles and/or fusion events between no more than 2-3 vesicles.

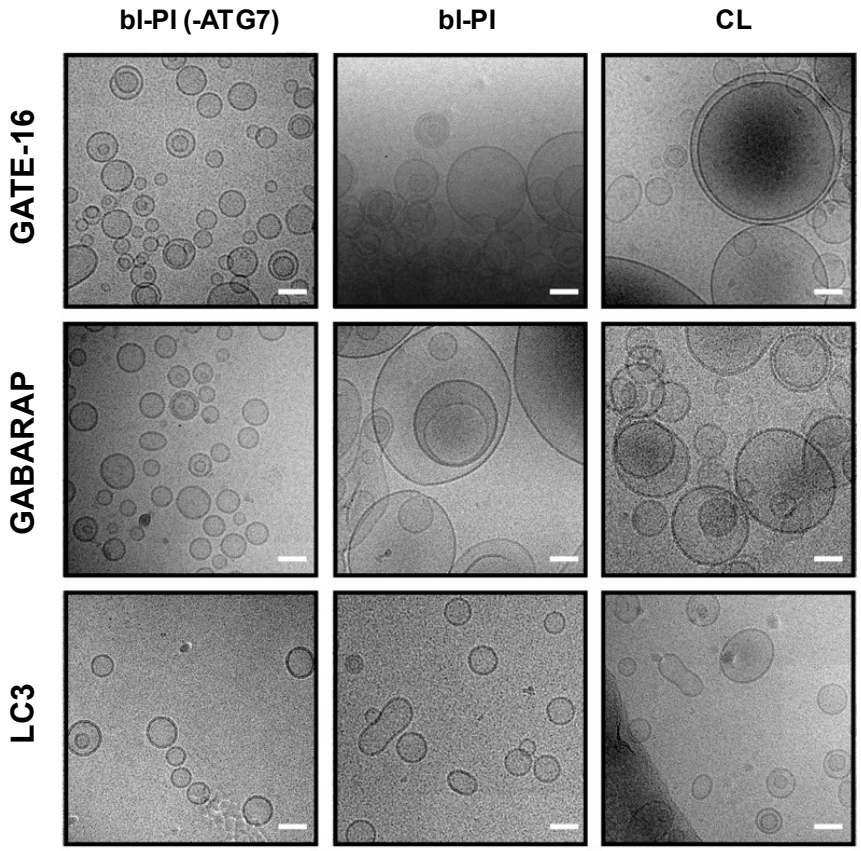

Figure 3.10. Fusion-dependent increase in vesicle size analyzed by cryo-EM. Typical cryo-EM images of liposomes treated with human autophagic proteins. Enzymatic conjugation reactions including the indicated LC3 homologues (30 μM), ATG3 (3 μM), ATG7 (3 μM), and 3 mM ATP were performed in conjugation buffer for 1 hour at 37 ºC and the products examined by cryo-EM. Liposome (LUVs) compositions: PC/DOPE/bl-PI (35/55/10 mol ratio), column 1 and 2, or PC/DOPE/CL (35/55/10 mol ratio), column 3. In all cases, liposome concentration was 1.2 mM. In control experiments (column 1) ATG7 was excluded from the reaction. The same scale (bar=50 nm) was used in all images.

3.3.5. The Role of Specific Lipids in LC3- and GATE-16/GABARAP-Promoted Fusion

According to the widely accepted stalk-pore fusion model (Basañez *et al.*, 1996b, 1998; Chernomordik *et al.*, 1995; Goñi & Alonso, 2000; Ibarguren *et al.*, 2010; Villar *et al.*, 2001), fusion is thought to start with the formation of a non-lamellar lipidic stalk, a local connection between the contacting monolayers of two membranes. The stalk then extends connecting the facing monolayers (hemifusion) before pore formation (fusion) occurs. The model predicts that addition of inverted cone-shaped lipids (i.e. positive curvature-inducing lipids) such as lyso-phosphatidylcholine (LPC) to contacting membrane leaflets should prevent formation of hemifused intermediates whereas cone-shaped lipids such as diacylglycerol (DAG) or cardiolipin (CL) (i.e lipids with a negative intrinsic curvature) should promote formation of hemifusion intermediates (Chernomordik *et al.*, 1995). As shown in **Figure 3.11 A**, substituting bl-PI for CL (10 mol%) strongly promoted GATE/GABARAP-PE-induced lipid mixing. Addition of DAG (10 mol%) further promoted intervesicular lipid mixing and LPC (10%) totally inhibited it (**Figure 3.11 A**).

Furthermore fusion pore formation and content mixing occurred as well with lipidated GATE-16 and GABARAP proteins. Consistent with what it was observed in lipid mixing experiments, CL strongly potentiates mixing of aqueous contents (**Figure 3.11 B**). Again vesicle fusion was accompanied by only a residual leakage of vesicular content (data not shown). For all lipid composition tested vesicle size was centered around 80 nm as assessed by DLS measurements (data not shown).

Vesicle radius has been proven to modulate LC3/GABARAP lipidation *in vitro* (Nath *et al.*, 2014). In their study, Melia and coworkers showed that ATG3 contains a membrane inserting, curvature-sensitive domain and that the conjugation of the Atg8-family proteins occurs preferentially on highly curved membranes *in vivo.* In addition to promoting the lipidation process, membrane curvature may also facilitate the fusion process itself (Ahyayauch *et al.*, 2005; de Arcuri *et al.*, 1999), inducing autophagosome elongation on the curved edge of the growing isolation membrane. To address the effect of vesicle radius on the process of membrane fusion, we chose the maleimide system, as it allows the evaluation of membrane fusion elicited by LC3 homologues independently of ATG3. To this aim, labelled and non-labelled PC/DOPE/bl-PI liposomes containing 15% PE-mal were prepared either by sonication (SUVs) or by extrusion through polycarbonate membranes 0.05 µm pore size (LUVs). As shown in **Figure 3.12**, decreasing liposome membrane radius from 40 to 25 nm markedly

stimulates total lipid mixing induced by artificially coupled GATE-16-PEmal and GABARAP-PEmal (compare panels 3.12 A and B).

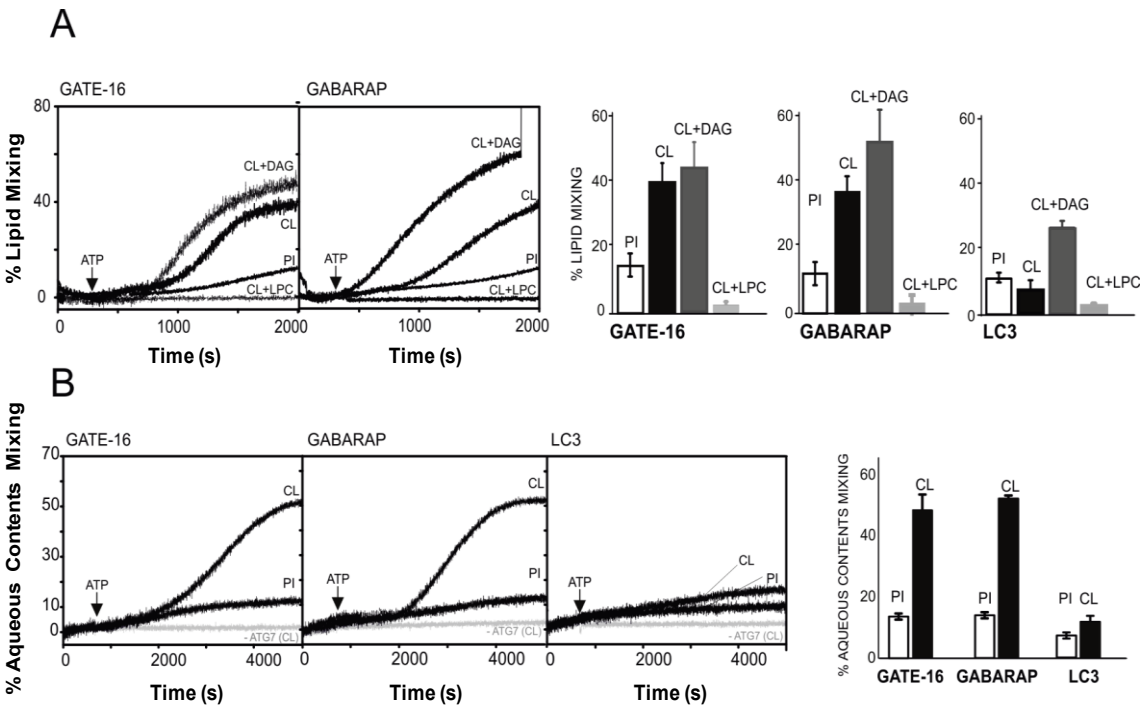

Figure 3.11. Effect of lipids modifying the membrane intrinsic curvature on membrane fusion induced by LC3/GABARAP-PE conjugates. (A) Representative time courses (left panels) and comparison at t=2000 s (right panels) of intervesicular total lipid mixing induced by ATG7 (1 μM), ATG3 (1 μM) and the indicated Atg8 human homologues (10 μM) in liposomes (0.4 mM) with the basic lipid composition PC/DOPE (35/55 mol ratio) to which either bl-PI (+10 mol ratio), CL (+10 mol ratio), CL+DAG (+10 +10 mol ratio) or CL+LPC (+10+10 mol ratio) was added. **(B)** Representative time courses (left panels) and comparison at t=2000 sec (right panel) of aqueous contents mixing for the same reactions as in A. Lipid mixing and content mixing assays were performed as described in **Fig. 3**. ATG7 was excluded from the reaction in control experiments (grey traces). Liposomes and proteins were incubated for 5 min before ATP addition. Each curve represents the average and S.E. of three independent experiments.

Hardly a stimulatory effect was observed in the case of LC3-PEmal, although it was efficiently conjugated to PEmal. Consistent with what was observed previously for enzymatically-conjugated GATE-16 and GABARAP, substitution of PI by CL strongly enhances lipid-mixing induced by GATE-16-PEmal and GABARAP-PEmal (compare panels 3.12 B and C). Again inclusion of CL did not affect particle size (data not shown). These results add to the growing body of evidence supporting an important role of both vesicle radius and membrane intrinsic curvature during autophagosome biogenesis (Antonny, 2011; Fan *et al.*, 2011; Knorr *et al.*, 2014).

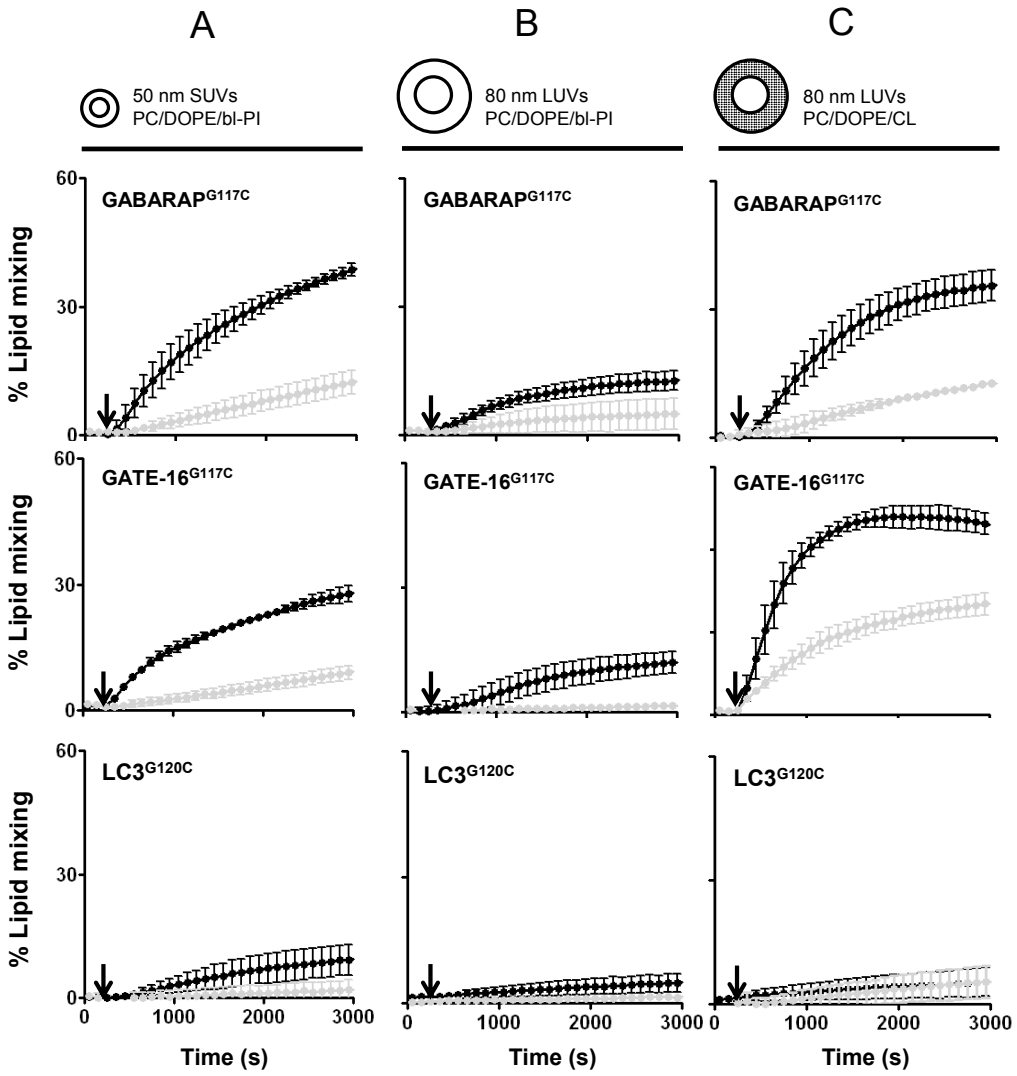

Figure 3.12. Effect of vesicle diameter and lipid composition on membrane fusion elicited by LC3/GABARAP-PEmal conjugates. Time courses of total (●); and inner (●); lipid mixing induced by the indicated proteins (10 μM) in liposomes (total lipid 0.4 mM) of different sizes (sonicated A, or extruded, B and C) and different lipid compositions: PC/DOPE/PEmal/bl-PI (35/40/15/10 mol ratio) **(A, B)** or PC/DOPE/PEmal/CL (35/40/15/10 mol ratio) **(C)**. The arrow marks the moment of protein addition. Each curve represents the average and S.E. of three independent experiments.

The fusogenic potential of Atg8-PEmal has been shown to be highly dependent on the concentration of PE in the target membrane (Nair *et al.*, 2011). In that study, a reduction of PE concentration from 55 to 30% made Atg8-PEmal unable to fuse liposomes despite the fact that coupling of Atg8 to maleimide was equally efficient in both cases. We evaluated whether reducing the PE content in our liposomes had an impact on GABA/GATE-PE-dependent vesicle fusion. In agreement with the previous report, GATE-PEmal and GABA-PEmal were hardly able to fuse liposomes containing 30% PE (**Figure 3.13 A-B**). However, substitution of bl-PI by cone-shaped lipid

molecules such as CL or DAG promoted vesicle fusion, nearly to the extent observed with 55% DOPE. With enzymatically conjugated GATE and GABARAP proteins (**Figure 3.13 C-D**) vesicle fusion is significantly impaired by reduction of DOPE to 30%, probably due to a drop in the efficiency of the lipidation reaction. However, incorporation of CL and DAG into the vesicles sustained potent vesicle fusion, even in the context of a limiting DOPE concentration.

DAG and CL fatty acid composition could be an important factor influencing fusion. The beef heart CL used here is mainly tetra-linoleoyl, while egg DAG contains mainly saturated and mono-unsaturated fatty acids. In principle, for a given fatty acid composition, the intrinsic negative curvature of DAG is higher than that of CL, but this could be compensated by the different unsaturation in both lipids. We have resolved the ambiguity by assaying separately CL and DAG in our fusion assay (**Figure 3.13 A-B**). Both for GATE-16 and GABARAP, with either 30% or 55% PE, DAG is more potent than CL in increasing the fusion rate, thus the headgroup appears to be more important than the fatty acid composition in our case.

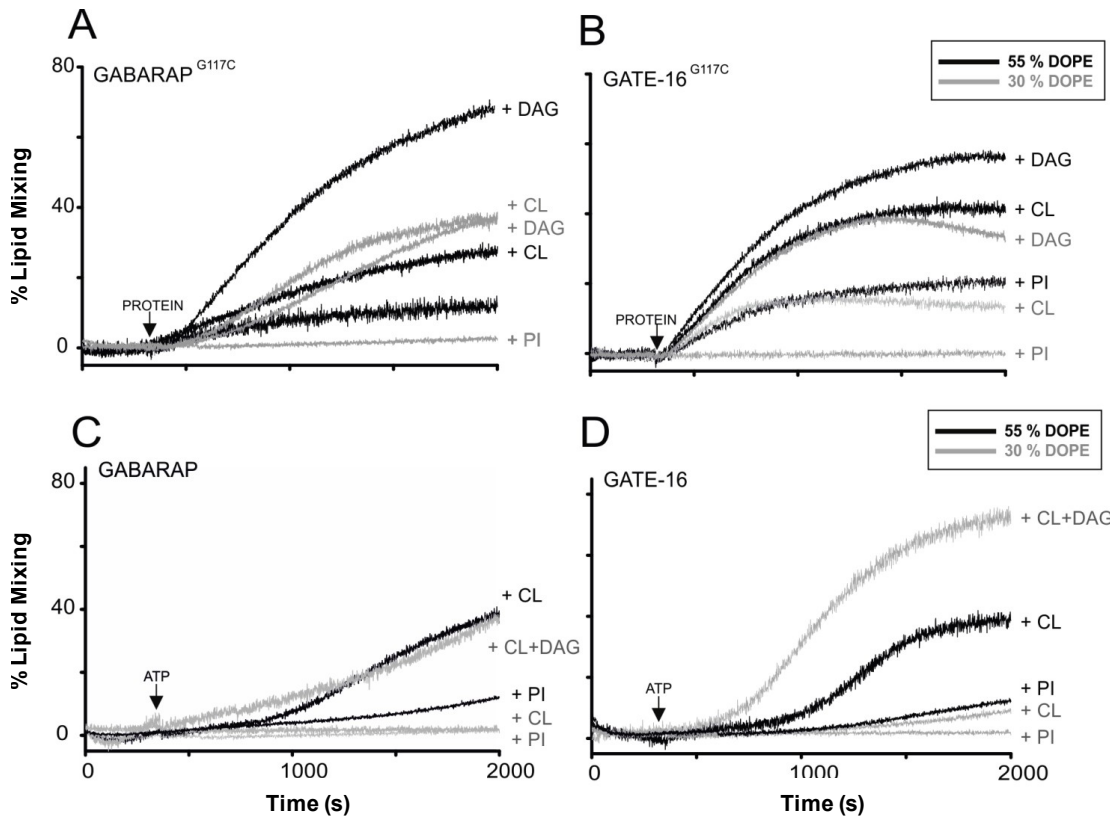

Figure 3.13. CL- and DAG-sustained membrane fusion under PE limiting concentrations. Time courses of total lipid mixing induced by the indicated proteins (10 μM) in liposomes (0.4 mM) of different lipid compositions. **(A)** and **(B)** panels (chemical conjugation): with the basic lipid composition PC/DOPE/PEmal (45/30/15 mol ratio, grey lines) to which either bl-PI (+10 mol ratio), CL (+10 mol ratio) or DAG (+10 mol ratio) were used; or basic lipid composition of PC/DOPE/PEmal (35/40/15 mol ratio, black lines) to which either bl-PI (+10 mol ratio), CL (+10 mol ratio) or DAG (+10 mol ratio) were used. **(C)** and **(D)** panels (enzymatic conjugation): with the basic lipid composition of PC/DOPE (60/30, grey lines) to which either bl-PI (+10 mol ratio), CL (+10 mol ratio) and CL+DAG (+10+10 mol ratio) were used or the basic lipid composition of PC/DOPE (35/55, black lines) to which either bl-PI (+10 mol ratio) or CL (+10 mol ratio) were added. Liposomes and proteins were incubated for 5 min before ATP addition. Traces are representative of at least three independent experiments.

3.4 Discussion

The Atg8 ubiquitin-like conjugation system plays a central role in autophagy. However, despite its likely importance during autophagosome formation, its mode of action is only incompletely understood. This is particularly true in the case of higher eukaryotes and information regarding mammalian LC3/GABARAP subfamilies is just recently starting to emerge (Mizushima *et al.*, 2003; Tanida *et al.*, 2002b, 2004; Yang & Klionsky, 2010). In this study we used two reconstituted liposomal systems to learn

more about the molecular mechanisms by which human LC3 and GABARAP subfamilies trigger AP biogenesis. Using these simplified and biochemically accessible model systems, we systematically explored the membrane activities of human Atg8 homologues in the context of different lipid compositions. Our data provide new insight into several aspects of the human autophagy machinery, namely on the nature of the fusion process leading to AP elongation, and the role of lipid instrinsic curvature in the process. From the methodological point of view, our results fully validate the use of chemically lipidated Atg8 homologue.

3.4.1 The Fusion Mechanism

According to the current view, phagophore expansion requires the supply and subsequent fusion of membranal material of yet uncharacterized origin. In this regard, several studies have involved both yeast Atg8 (Nakatogawa *et al.*, 2007; Xie *et al.*, 2008) and human LC3 and GATE-16 (Weidberg *et al.*, 2011) in the fusion processes underlying phagophore expansion. However the molecular mechanism is still obscure. The liposomal assays applied here allowed us to explicitly test the capacity of the different homologues for inducing membrane fusion *in vitro*, in the absence of other cellular proteins.

The ensemble of the data is compatible with a fusion mechanism based on the “stalk hypothesis” (Basañez *et al.*, 1996b, 1998; Chernomordik & Kozlov, 2008; Chernomordik *et al.*, 1995; Goñi & Alonso, 2000; Ibarguren *et al.*, 2010; Villar *et al.*, 2001; Xu *et al.*, 2005), according to which the formation of a lipidic intermediate, the stalk, with a non-lamellar structure, is the limiting step in the fusion event. The canonical form of stalk-mediated fusion requires the independent demonstration of vesicle aggregation, intervesicular mixing of total membrane lipids, mixing of inner monolayer lipids and mixing of aqueous contents in the absence of vesicular content leakage or spill-out. Ideally aggregation, total lipid mixing, inner lipid mixing, and contents mixing should start in the said order, i.e should exhibit increasing lag times. All these predictions have been demonstrated in our case, particularly for GATE-16 and GABARAP (**Figure 3.8 and Figure 3.9**). Moreover the proposed stalk architecture demands that lipids with an intrinsic negative curvature (e.g. DAG, CL) must facilitate stalk formation, thus membrane fusion (Basañez *et al.*, 1996b, 1998). This is also amply demonstrated by our data, as well as the opposite, inhibitory effect of positive intrinsic-curvature lipids (e.g lyso PC) (**Figure 3.11**). The same considerations on intrinsic lipid curvature apply to the requirement of high proportions of PE in the vesicle

composition (**Figure 3.13**). We can thus conclude that, at least in the *in vitro* situation, Atg8 proteins induce AP growth via stalk-mediated fusion events.

In the cell environment, the AP is seen to grow by elongation, i.e along a main axis. In our case the most effective Atg8 analogs, namely GATE-16 and GABARAP, give rise to a spectacular growth of vesicles, leading to roughly spherical structures (**Figure 3.10**), while LC3, a much less efficient fusogen, gave rise to elongated, peanut-shaped structures, reminiscent of the growing AP in cell images. The reason why LC3 is less effective than the other two, and why it originates elongated vesicles deserves further study. At least part of the answer will rely in the yet unknown mechanisms of AP growth regulation (Moreau *et al.*, 2011; Nair *et al.*, 2011). At the present time, we cannot rule out the possibility that, being less effective, LC3 is more physiologically relevant in AP elongation.

3.4.2 Proteins and Lipids

Both SNAREs and viral fusion proteins contain a transmembrane domain, which is critical for their fusion activity (Langosch *et al.*, 2007; Xu *et al.*, 2011, 2005). Atg8 homologues do not present such a transmembrane domain and yet are capable of inducing full membrane fusion when anchored only to one membrane leaflet via PE. Several models have been proposed including that self-oligomerization of Atg8-PE molecules would drive membrane tethering and hemifusion through a yet uncharacterized mechanism (Nakatogawa *et al.*, 2007). Alternatively, it has been shown that peptides representing the N-terminus of LC3 and GATE are sufficient to drive full membrane fusion when artificially linked to PEmal (Weidberg *et al.*, 2011). An additional, non-exclusive possibility is that the asymmetric insertion of this N-terminal region would promote positive curvature and tension in the outer leaflet of the membrane thus promoting hemifusion and eventually fusion (Zimmerberg & Kozlov, 2006). Amphipathic proteins devoid of transmembrane domains can induce vesicle fusion, e.g muscle glyceraldehyde 3-phosphate dehydrogenase (Morero *et al.*, 1985). Determining membrane structures of LC3/GABARAP proteins, particularly at the fusogenic state, will likely broaden our understanding of Atg8-driven membrane fusion.

According to a growing body of evidence, AP biogenesis is a lipid-modulated process (Chu *et al.*, 2013; Dall'Armi *et al.*, 2013; Sentelle *et al.*, 2012; Vicinanza *et al.*, 2015). However, with the exception of the relatively well characterized role of PI3P, little is known about the specific role that each lipid species plays during the different steps

of AP biogenesis. Here we obtained direct evidence that intrinsic-curvature modifying lipids (DAG, LPC, CL) act in concert with autophagic proteins to modulate the fusion of vesicles *in vitro*. This observation is compatible with a model in which the local generation or transfer of these lipids from the ER or mitochondria to the isolation membrane may regulate phagophore expansion *in vivo*. Interestingly the PLD1 pathway, which produces phosphatidic acid (PA), a cone-shaped lipid, has been reported to promote autophagy (Dall'Armi *et al.*, 2010). Furthermore, another study showed that DAG generation is required for the initiation of *Salmonella*-induced autophagy (Shahnazari *et al.*, 2010). In both cases, however, the underlying mechanism is not known. What still needs to be determined is the lipid composition of the phagophore as well as the lipid changes that accompany AP biogenesis *in vivo*. In this regard, reliable autophagosome purification procedures in conjunction with lipidomic approaches should help to understand the specific roles of lipids in autophagy.

In agreement with a recent report (Nath *et al.*, 2014), we observe that both human LC3 and GABARAP subfamilies can be enzymatically lipidated *in vitro* (**Figure 3.7 D**), even in the absence of the ATG12-ATG5-ATG16L1 complex. However both systems are essential for proper AP biogenesis *in vivo*, and several *in vitro* studies (Hanada *et al.*, 2007; Sakoh-Nakatogawa *et al.*, 2013) indicated that the ATG12-ATG5-ATG16L1 complex functions, at least in part, facilitating the transfer of Atg8/LC3 from ATG3 to PE. Whether human ATG12-ATG5-ATG16L1 complex promotes lipidation of GABARAP subfamily in a similar manner to LC3 needs to be tested and will be addressed in future studies.

As an alternative to the enzymatically-driven reaction the chemical conjugation approach enables direct conjugation of proteins to PE lipids (**Figure 3.7 F**), thus bypassing the requirement for the conjugation machinery. Although the enzymatic conjugation is more physiologically relevant, chemically-conjugated versions of LC3/GABARAP subfamilies are easily prepared and are increasingly being used in both mechanistic (Nair *et al.*, 2011; Weidberg *et al.*, 2011) and structural (Ma *et al.*, 2010) studies. Here we report that PEmal conjugates faithfully recapitulate key features of their naturally conjugated homologues, supporting the reliable use of these artificial complexes. In fact PEmal conjugates show faster aggregation and fusion kinetics than the enzymatically-conjugated proteins, consistent with the fact that they are not conjugated through a relatively complex ubiquitin-like reaction comprising multiple steps (compare lag times between enzymatic and chemical conjugation reactions).

4. Human ATG3 membrane association induces tethering of negatively-charged membranes

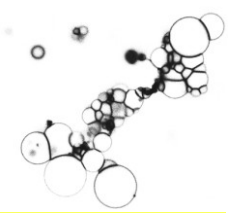

CHAPTER 4:

Human ATG3 membrane association induces tethering of negatively-charged membranes

4.1 Introduction

Macroautophagy is a bulk degradation pathway conserved among eukaryotic cells (Tooze *et al.*, 2010). A double membrane structure called autophagosome engulfs organelles or cytoplasmic portions and subsequently delivers the material into the lysosome for degradation (He & Klionsky, 2009). Autophagosome formation requires more than 30 proteins acting in a hierarchical manner (Lamb *et al.*, 2013). Among these proteins an ubiquitin-like (UBL) system triggers the covalent attachment of Atg8 (LC3 and GABARAP subfamilies in mammals) to phosphatidylethanolamine (PE) in the autophagosomal membrane (Sou *et al.*, 2006; Tanida *et al.*, 2004). Atg8 conjugation requires the involvement of additional enzymes such as Atg7 and Atg3. These proteins catalyze the mentioned process, Atg3 being responsible for transferring Atg8 to the membrane (Hong *et al.*, 2011; Kaiser *et al.*, 2012). Once in the membrane Atg8 participates in autophagosome formation, maturation and closure. It has been described that mammalian Atg8-like proteins (LC3, GATE-16 and GABARAP) induce membrane tethering and fusion *in vitro* (Landajuela *et al.*, 2016; Nakatogawa *et al.*, 2007; Weidberg *et al.*, 2011).

Human ATG3, the E2-like enzyme for Atg8 conjugation, contains some disordered regions that allow its classification among the intrinsically disordered proteins (Popelka *et al.*, 2014). This property is found in proteins that participate in cell

processes requiring quick responses such as autophagy. Atg3 shows two regions for its interaction with Atg7 and Atg8, respectively the HR and FR regions (Yamada *et al.*, 2007). These two domains act together with the catalytic cysteine (Cys264) to catalyse ATG3-LC3 binding and thus redirect LC3 to the membrane (Sakoh-Nakatogawa *et al.*, 2013). For this purpose, it was described that Atg3 N-terminus was the protein region responsible for membrane detection and interaction (Hanada *et al.*, 2009). Specifically, a predicted N-terminal amphiphatic helix was indicated to be a membrane-curvature sensing domain (Nath *et al.*, 2014). However, it was also proposed that the Atg5-Atg12/Atg16 complex promotes a more efficient recruitment of Atg3 to membranes (Romanov *et al.*, 2012; Walczak & Martens, 2013), due to the ability of Atg3 to interact with Atg12 (Metlagel *et al.*, 2013; Radoshevich *et al.*, 2010). Atg16 promotes localization of the Atg12-Atg5 conjugate to membranes *in vivo* (Fujita *et al.*, 2008), in order to allow Atg8-PE conjugation and also tethering of GUV *in vitro* (Romanov *et al.*, 2012). Atg12-Atg5 complex induces a reorientation of Atg3 catalytic cysteine toward a threonine residue so that Atg3 conjugase activity is stimulated (Klionsky & Schulman, 2014; Sakoh-Nakatogawa *et al.*, 2013). Apart from its specific role in autophagy, the possible implication of Atg12 conjugation to Atg3 in the regulation of mitochondrial homeostasis and cell death has been proposed (Radoshevich *et al.*, 2010).

In this context, a question remains about what determines the movement of ATG3 to the membrane. Some proteins contain domains that detect specific membrane lipids, e.g. phosphoinositides, or membrane curvature (BAR and amphipathic helices) (Lemmon, 2008; McMahon & Gallop, 2005). An amphiphatic helix was proposed to be the responsible of the specific membrane recognition by ATG3 (Nath *et al.*, 2014).

Here we study the properties of ATG3 interaction with membranes in order to obtain a better understanding on how the lipidation process could be regulated by protein-lipid interactions. We show that human ATG3 interacts with PE-containing membranes through its N-terminal region and that this binding can be enhanced by the presence of negatively-charged phospholipids in the membrane. Furthermore, ATG3 recognizes preferentially highly curved vesicles, but the presence of anionic phospholipids suppresses the necessity of this curvature. We also have demonstrated that ATG3 has the ability to aggregate liposomes *in vitro*, a novel activity for this autophagic protein.

4.2 Experimental Techniques

4.2.1 Materials

QL22 and QF27 peptides were synthesized and purchased from ProteoGenix SAS (Schiltigheim, France). Egg phosphatidylcholine (PC) was purchased from Lipid Products (South Nutfield, UK). 1,2-dioleoyl-sn-glycero-3-phosphoethanolamine (DOPE), bovine liver phosphatidylinositol (PI), heart cardiolipin (CL), brain phosphatydilserine (PS), egg phosphatidyldglycerol (PG), egg Phosphatidic Acid (PA), 1,2-dioleoyl-sn-glycero-3-phosphoethanolamine-N-(lissamine rhodamine B sulfonyl) (Rho-PE), ovine wool cholesterol (Chol) and 1,2-dihexadecanoyl-sn-glycero-3-phosphocholine (DPPC) were purchased from Avanti Polar Lipids, Inc. (Alabaster,AL). Anti-ATG3 antibody and goat anti-mouse IgG-HRP were from Santa Cruz Biotechnology, Inc. (Dallas, TX). Anti-GABARAP monoclonal antibody was from MBL International (Medical & Biological laboratories Co. Ltd.). Alexa Fluor® 488 dye was purchased from Molecular Probes (Eugene, OR). All other reagents were of analytical grade.

4.2.2 DNA Constructs and Site-directed Mutagenesis

Plasmids for expression of human ATG3 were kindly provided by Dr. Isei Tanida (National Institute of Infectious Diseases, Tokyo, Japan). A double mutant for Lys to Asp (ATG3 K9D/K11D) at positions 9 and 11 of ATG3 was made using QuikChange site-directed mutagenesis kit (Stratagene). Specifically designed ATG3 primers purchased from Sigma Aldrich (Madrid, Spain) were used (See **Table 2.1**). Mutations were confirmed by DNA sequencing (Secugen S.L, Madrid, Spain).

4.2.3 Recombinant Protein Expression and Purification

All ATG3 variants were purified from soluble fractions of bacterial extracts obtained in the absence of detergents, and were >90% pure as evaluated by Coomassie-stained SDS-PAGE. *E.coli* BL21 (DE3) cells were transformed with appropriate plasmids, grown to OD_{600}=0.8 and induced with 0.5 mM IPTG for 18 h at 20 ºC. Following centrifugation at 4,500 xg for 15 min, the pellet was resuspended and sonicated in breaking buffer (PBS with protease inhibitors mixture and 1 mM DTT).

After removal of cellular debris by centrifugation at 30,000 xg for 30 min at 4 ºC, the sample supernatant fraction was incubated with 1 ml Glutathione Sepharose 4B (GE Healthcare) for 3 h at 4 °C to bind GST tagged proteins. Then, PreScission Protease (GE Healthcare) was added at 100 units/ml in 2 bed volumes of PreScission Buffer [50 mM Tris (pH 7.5), 150 mM NaCl, 1 mM EDTA] with freshly added 1 mM DTT and cleavage was performed for 4 h at 4 °C. Cleaved protein was eluted and purified proteins were stored in 20% glycerol at -80 °C.

4.2.4 Monolayer Surface Pressure Measurements

Lateral pressure experiments were carried out in a multi-well Delta Pi-4 Langmuir balance (Kibron Inc., Helsinki, Finland) under constant stirring. Proteins induced changes in surface pressure at the air-water interface and protein-lipid monolayer interactions were studied at 25 ºC (same results were obtained at 37 ºC, data not shown). Monolayers were formed by spreading a small amount of the lipid mixtures in chloroform:methanol (2:1 v/v) solution on top of assay buffer, until the desired initial surface pressure was reached. Proteins were injected with a micropipette through a hole connected to the subphase. The assay buffer was 20 mM HEPES [4-(2-hydroxyethyl)-1-piperazineethanesulfonic acid] (pH 7.4), 150 mM NaCl, 1 mM $MgCl_2$, 0.2 mM DTT.

4.2.5 Liposome Preparation

The appropriate lipids were mixed in organic solution and the solvent was evaporated to dryness under a N_2 stream. Then the sample was kept under vacuum for 2 h to remove solvent traces. The lipids were swollen in PreScission buffer, except in leakage assay experiments, where the corresponding buffer was used (see leakage assay section). Large unilamellar vesicles (LUVs) were prepared from swollen lipids, subjected to 10 freeze/thaw cycles, and then extruded using 0.1 µm pore size Nuclepore filters as described by Mayer *et al.*, (1986). Small unilamellar vesicles (SUVs) were obtained by sonicating multilamellar vesicles (MLVs) with a probe tip sonicator (MSE Soniprep 150 (MSE, UK)) for 10 min (10 s on, 10 s off) on ice. Vesicle size was checked by quasi-elastic light scattering using a Malvern Zeta-Sizer 4 spectrometer (Malvern Instruments, Worcestershire, UK). LUVs had an average

diameter of 100 nm and SUVs an average diameter of 50 nm. Lipid concentration was determined by phosphate analysis (Böttcher *et al.*, 1961).

4.2.6 Sucrose Gradient Centrifugation of Liposomes

ATG3 purified as indicated (10 μM) was incubated with 3 mM liposomes (containing 0.05% Rho-PE for detection) for 1 h at 37 ºC in 200 μl PreScission buffer. The protein/lipid mix was diluted to 300 μl in PreScission buffer containing 2.4 M sucrose. Then the reaction mix was transferred to a centrifuge tube. A 2.4 M sucrose layer was overlaid with 400 μl PreScission buffer containing 0.8 M sucrose and 300 μl PreScission buffer containing 0.5 M sucrose. Sucrose step gradients were centrifuged in a TLA-120.2 rotor at 100,000 xg for 3 h at 4 ºC. Four 250-μl fractions were pipette starting from the bottom. The top fraction (T) contained liposomes as determined by the rhodamine fluorescence, and the bottom fraction (B) contained the unbound protein. Both fractions were analyzed by SDS-PAGE and Western blotting.

4.2.7 Aggregation Assays

All assays were carried out at 37 ºC with continuous stirring, in a 1 ml cuvette with 600 μl of 50 mM Tris, 150 mM NaCl, 1 mM DTT buffer (pH 7.5). All experiments were performed at a vesicle concentration equivalent to 0.4 mM phosphate and 10 μM ATG3 were used unless otherwise stated. Lipid aggregation was monitored in an Uvikon 922 spectrophotometer (Kontron instruments, Groß-Zimmern, Germany) as an increase in turbidity (absorbance at 400 nm) of the sample.

4.2.8 Alexa Fluor 488 Protein Labeling

Purified proteins were first concentrated to 4-5 mg/ml (protein concentration should be at least 2 mg/ml for optimal results) and dialyzed against 0.1 M sodium bicarbonate pH 8.2, 150 mM NaCl buffer to remove any amine-containing substances that will interfere with the conjugation reaction. Then 10 μl of the reactive dye solution (10 mg/ml of the amine-reactive compound dissolved in dimethylsulfoxide) was slowly added to the protein solution. The reaction mixture was incubated for 2 h at 37 ºC with continuous stirring. A Sephadex G-25 chromatography column was used to separate

the conjugate from unreacted labelling reagent, with PreScission buffer as the eluent. The degree of labelling was determined measuring the absorbance of the protein-dye conjugate at 280 nm and at 488 nm for the dye. Labelled samples were subjected to SDS-PAGE and visualized using a VersaDoc MP 4000 Imaging System.

4.2.9 Giant Unilamellar Vesicle (GUV) Preparation

GUVs were prepared using the electroformation method developed by Angelova & Tsoneva, (1999). For direct visualization under the microscope a homemade chamber was used (Fidorra *et al.*, 2006). Transferred GUVs were formed in a PRETGUV 4 chamber supplied by Industrias Técnicas ITC (Bilbao, Spain). Stock solutions of lipids (0.2 mM total lipid containing 0.2 mol% Rho-PE) were prepared in chloroform:methanol (2:1, v/v), 3 µl of the lipid stocks were added onto the surface of Pt electrodes and solvent traces were removed by evacuating the chamber under high vacuum for at least 2 h.

4.2.10 Direct Visualization of GUVs

The Pt electrodes were covered with 400 µl of 50 mM Tris-HCl, 150 mM NaCl, 1 mM EDTA and 1mM DTT, pH 7.5. The Pt wires were connected to an electric wave generator (TG330 function generator, Thurlby Thandar Instruments, Huntington, UK) under alternating current (AC) field conditions (500 Hz, 0.031 VRMS for 6 min; 500 Hz, 0.281 VRMS for 20 min, and 500 Hz, 0.623 VRMS for 1 h 30 min) at 37°C. After GUV formation, the chamber was placed on an inverted confocal fluorescence microscope (Nikon D-ECLIPSE C1, Nikon, Melville, NY). The excitation wavelengths were 488 nm for ATG3-Alexa488 and 561 nm for Rho-PE. The images were collected using band-pass filters of 593 ± 20 nm for Rho-PE, and of 515 ± 15 nm for Alexa488. Then 1 µM ATG3-Alexa488 was added to study the ATG3 effect on the GUVs. All these experiments were performed at room temperature. Image treatment was performed using the EZ-C1 3.20 software (Nikon).

4.2.11 Observation of Transferred GUVs

The Pt electrodes were covered with 400 µl of a 300 mM sucrose solution, previously heated at 37 °C. The Pt electrodes were connected to a generator (TG330

function generator, Thurlby Thandar Instruments) under AC field conditions (10 Hz, 1 VRMS for 2 h, followed by 2.5 Hz, 1 VRMS, 1h 30 min) at 37 °C. Finally, the AC field was turned off and the vesicles (in 300 mM sucrose) were collected from the PRETGUV 4 chamber with a pipette and transferred to chambers pretreated with bovine serum albumin (BSA) (2 mg/ml) and containing an equiosmolar buffer solution of 50 mM Tris-HCl, 150 mM NaCl, 1 mM EDTA and 1mM DTT, pH 7.5. Due to the different density between the two solutions, the vesicles sedimented at the bottom of the chamber, and this facilitated observation under the microscope. Finally, ATG3-Alexa488 at 1 μM was added to study the ATG3 effect on the GUVs. The excitation wavelengths were 488 nm for ATG3-Alexa488 and 561 nm for Rho-PE; and the emission was collected using 515 ± 15 nm and 593 ± 20 nm band-pass filters, respectively. All these experiments were performed at room temperature. Image treatment was performed using the EZ-C1 3.20 software (Nikon).

4.2.12 Lipid Mixing Assay

A fluorescence resonance energy transfer assay was used to monitor intervesicular membrane lipid mixing (Struck et al., 1981). 0.4 mM LUVs containing 1.5 mol% NBD-PE and 1.5 mol% Rho-PE were mixed with 9-fold excess of unlabeled LUVs in 50 mM Tris-HCl (pH 7.5), 150 mM NaCl, 1 mM EDTA and 1mM DTT buffer. NBD-PE emission was monitored in a QuantaMaster spectrofluorometer (Photon Technology International, Birmingham, New Jersey) in a thermostatically controlled 1-cm path length cuvette with constant stirring at 37 °C. NBD emission was monitored at 530 nm with the excitation wavelength set at 467 nm (slits, 2 nm). A 515 nm cut-off filter was placed between the sample and the emission monochromator to avoid scattering interference. 10 μM ATG3 were used unless otherwise stated in 1 ml final volume.

4.2.13 Vesicle Contents Leakage Assay

Leakage of vesicle contents was monitored by the ANTS/DPX assay (Ellens et al., 1985). ANTS emission was monitored at 530 nm with the excitation wavelength set at 360 nm (slits, 2 nm). A 470 nm cut-off filter was placed between the sample and the emission monochromator to avoid scattering interference. To establish the 100% leakage signal, Triton X-100 was added to a concentration of 1%. Details for the vesicle contents leakage assay can be found in Goñi et al., (2003).

4.3 RESULTS

4.3.1 ATG3 Interaction with Model Membranes

ATG3 was proposed to direct human Atg8 homologues (LC3, GATE-16 and GABARAP) to the membrane to complete their lipidation process. Some studies demonstrated an important implication of the Atg3 N-terminal region in membrane recognition (Hanada *et al.*, 2009). Particularly, a predicted N-terminal amphiphatic alpha-helix (**Figure 4.1**) would be responsible for this recognition and also acts as a membrane curvature sensor (Nath *et al.*, 2014). Based on these observations, we decided to analyze the interaction of ATG3 with membranes in more detail. ATG3 K9D/K11D mutant was created and analyzed to discern the involvement of this region and particularly of the mutated residues in ATG3 interaction with membranes.

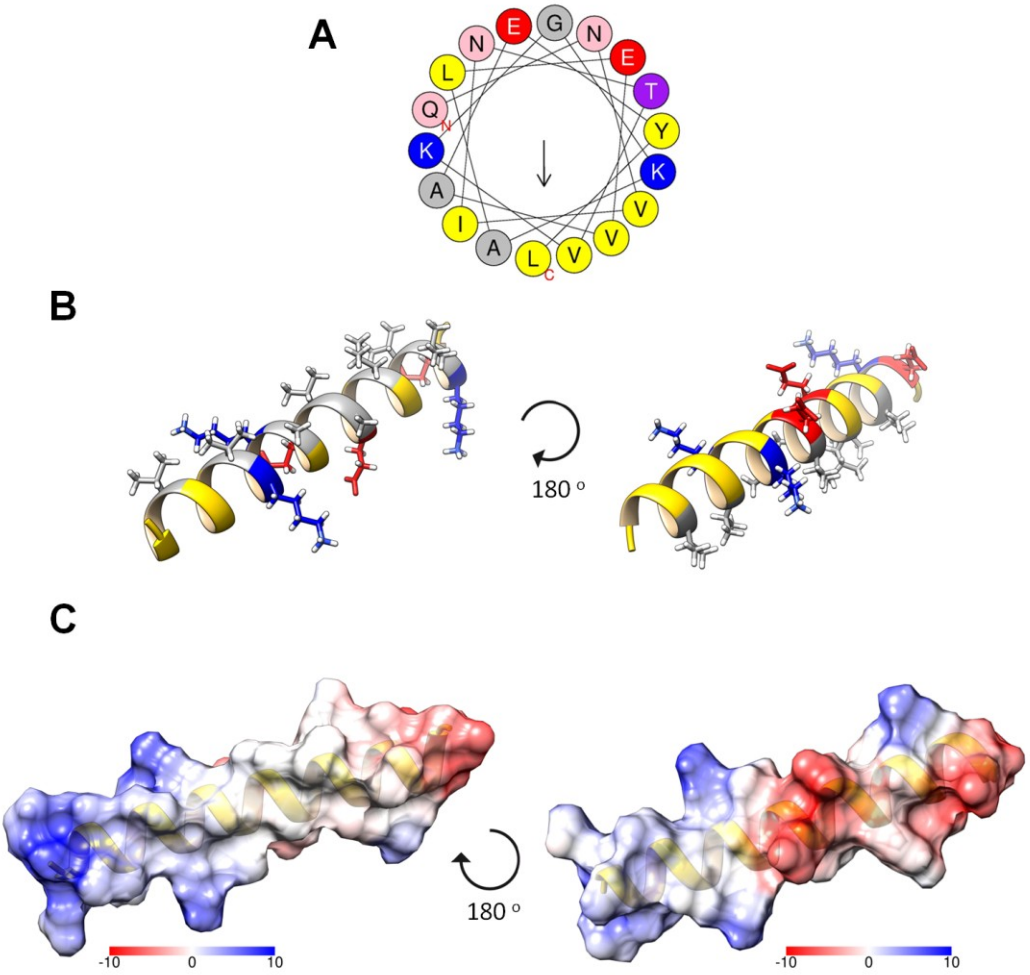

Figure 4.1. Predicted structure of ATG3 N-terminal amphiphatic α-helix. (A) Helical wheel representation of the predicted N-terminal amphipathic helix (amino acids 2–20) of human ATG3 (wheel generated in Heliquest). **(B)** Ribbon diagram of the hydrophobic (left) and hydrophilic (right) faces. Hydrophobic (Leu, Ala, Val), negatively-charged (Glu) and positively-charged (Lys) residues are coloured grey, red and blue respectively. **(B)** Electrostatic surface diagram of the ATG3 N-terminal α-helix. Both hydrophobic and hydrophilic faces are represented, and the color code indicated below each image.

To this aim, we first decided to explore the ability of ATG3 to interact and insert into lipid monolayers using a Langmuir balance. A rapid and dose-dependent increase of lateral pressure at the air-water interface was observed when ATG3 was injected into the aqueous phase (**Figure 4.2 A** left panel). This increase indicates that ATG3 is adsorbing onto the air-water interface and thus it is a surface-active molecule. A similar trend was observed for ATG3 K9D/K11D (**Figure 4.2 A** right panel). Both wild type and mutant ATG3 reach a similar plateau value of ~23 mN/m at 0.2 and 0.3 μM protein concentration, respectively.

ATG3 was able to insert into lipid monolayers extended at an initial surface pressure ≥ 23 mN/m, above the maximum Δπ caused by adsorption of ATG3 at an air-water interface. Compositions of PC:DOPE (70:30 mol ratio), PC:DOPE:CL (60:30:10 mol ratio) and PC:DOPE:PA (50:30:20 mol ratio) were used to test the affinity of ATG3 for monolayers containing different anionic phospholipids (**Figure 4.2 C** left panel). The protein (0.2 μM) was injected into the subphase and the increase in surface pressure was monitored in real time. A change in the lateral pressure at equilibrium (Δπ) was observed in all cases. The protein change in Δπ decreases linearly for both proteins with the increase in initial pressure (π_0), i.e. insertion becomes more difficult when the initial lateral pressure is higher. In order to obtain a quantitative measure of ATG3 insertion into lipid monolayers, critical surface pressure (π_c) values were determined. Above a certain π_0 value insertion is no longer observed (**Figure 4.2 C**). Extrapolation of the Δπ versus π_0 lines to Δπ=0 provides the so-called critical surface pressure π_c, above which no protein insertion occurs. π_c values for wild type and mutant ATG3 are shown in **Table 4.1**. These values are close to or above the usually accepted average value of ~30–35 mN/m for the lateral pressure of lipid monolayers in the cell membranes (Marsh, 1996). The increase in surface pressure obtained with PC:DOPE:CL and PC:DOPE:PA was considerably higher than that obtained with PC:DOPE monolayers. This result suggests a preference of ATG3 to insert into negatively-charged monolayers. Atg3 causes a larger surface pressure increase in PA-containing monolayers as compared to CL-containing monolayers even though the net electrical charge must be the same in both cases (**Figure 4.2 B** left panel). However, ATG3 K9D/K11D (0.3 μM) did not show any preference for monolayers containing anionic phospholipids (**Figure 4.2 C** right panel).

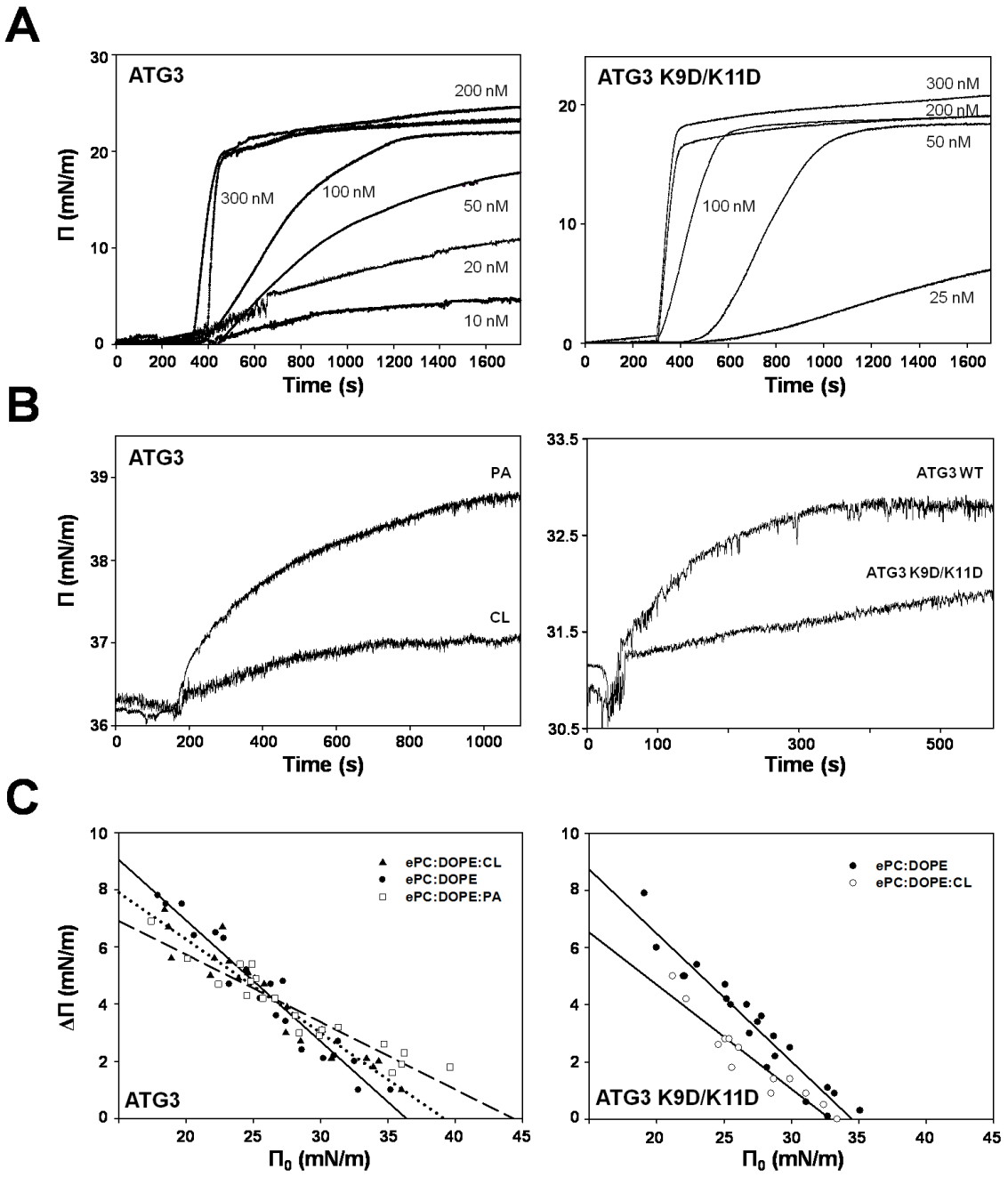

Figure 4.2. ATG3 and ATG3 K9D/K11D insertion into lipid monolayers. (A) Representative time courses of adsorption of ATG3 (left) or ATG3 K9D/K11D (right) at an air-water interface. **(B)** Representative time courses of increase in lateral pressure after ATG3 (0.2 μM) insertion into PC:DOPE:CL (60:30:10 mol ratio) or PC:DOPE:PA (50:30:20 mol ratio) monolayers (left). Representative time courses of increase in lateral pressure after ATG3 or ATG3 K9D/K11D insertion into PC:DOPE:CL (60:30:10 mol ratio) monolayers (right). **(C)** Maximum increase in lateral pressure after ATG3 (left) or ATG3 K9D/K11D (right) insertion into lipid monolayers. Lipids were: [●] PC:DOPE (70:30 mol ratio), [▲] PC:DOPE:CL (60:30:10 mol ratio), [□] PC:DOPE:PA (50:30:20 mol ratio) (left). Data reported as a function of initial lateral pressure.

Lipid Composition	π_c
ePC:DOPE (70:30)	36.4 mN/m (± 1.23)
ePC:DOPE:CL (60:30:10)	39.2 mN/m (± 1.67)
ePC:DOPE:PA (50:30:20)	44.3 mN/m (± 1.94)
ATG3 K9D/K11D (ePC:DOPE)	34.5 mN/m (± 0.81)
ATG3 K9D/K11D (ePC:DOPE:CL)	32.9 mN/m(± 1.29)

Table 4.1. Critical surface pressures (π_c) of ATG3 interaction with lipid monolayers of different compositions. Data derived from experiments as shown in **Figure 4.2 C**. The tendency line associated standard error is given for each π_c.

The interaction of ATG3 with a simplified model, such as lipid bilayers, was assessed next. Using liposomes as model membranes, we can reproduce the composition and curvature of cell membranes. For this purpose we performed liposomal float up assays. A fixed concentration of ATG3 (10 μM) was incubated with liposomes (1:300 protein:lipid ratio) of different lipid compositions. Then the mixture was subjected to an equilibrium sucrose gradient centrifugation where the vesicles have the capacity to float up, and the amount of protein interacting with these liposomes was examined. Fractions from the top (T) and bottom (B) of the gradient were subjected to SDS-PAGE and Western Blot analyses.

According to previous studies with the UBL system, 55% DOPE was required for get an optimal lipidation of LC3, and also aggregation and fusion of vesicles (Nair *et al.*, 2011). As ATG3 is thought to be responsible for bringing over Atg8 homologues to the membrane, the preference of this protein for membranes with different DOPE amounts and the influence of negatively-charged phospholipids on this interaction was tested. ATG3 bound DOPE-containing membranes, but no significant difference was observed between 30% and 55% DOPE (**Figure 4.3 A**). However, when an anionic phospholipid (10% CL in this case) was included in the lipid composition, the affinity of ATG3 for the membrane increased significantly (**Figure 4.3 A**). Moreover, even in the presence of CL no difference between 30% and 55% of DOPE was observed. ATG3 K9D/K11D was not able to bind vesicles of any composition tested (**Figure 4.3 A**). These results suggest that ATG3 has a marked preference to interact with negatively-charged membranes, and that its N-terminal positively-charged residues play an important role in this interaction.

Melia and coworkers (Nath *et al.*, 2014) showed that mouse ATG3, basically identical to human (97.5% identity), contains a predicted N-terminal amphiphatic helix

that could be a membrane curvature sensor. In order to know if the human ATG3 possesses this property, we compared the binding of ATG3 to vesicles of different sizes such as LUV (100 nm diameter) and SUV (50 nm diameter). We observed an increase in the binding of ATG3 to 30% or 55% DOPE-containing SUV as compared to LUV with the same electrically neutral composition (**Figure 4.3 B**). Nevertheless, in vesicles with anionic phospholipids present in the membrane no curvature preference of ATG3 was sensed (**Figure 4.3 B**). Hence, ATG3 could behave as a membrane curvature sensor when neutral membranes were present, however the incorporation of negatively-charged phospholipids could by-pass the curvature effect.

Similar floatation experiments were performed to figure out whether or not ATG3 displayed the same affinity for any anionic phospholipid. In fact, ATG3 showed a very strong affinity for PA and CL, although the binding to liposomes with PI, PG or PS was also significantly higher than the one to neutral membranes (**Figure 4.3 C**). Considering that PA and CL, which gave the higher rates of binding, are the only conical shape phospholipids among those tested, we could suggest a dual requirement for ATG3 interaction with membranes, namely defects in lipid packaging generated by cone-shaped phospholipids, and net negative charges in the membrane. Insertion of proteins into pure lipid bilayers may also rely on the transient appearance of hydrophobic patches on the bilayer surface, which might provide access points. The occurrence of these patches may be promoted by the presence of lipids in the bilayer that promote negative curvature and facilitate the lamellar-to-inverted hexagonal phase transition such as PE, PA, DAG or CL. Aerolysin (Alonso *et al.*, 2000), adenilate cyclase toxin (Martín *et al.*, 2004) or CTP:phosphocholine cytidyltransferase (Jamil *et al.*, 1993) interaction with membranes are favoured by the incorporation of this kind of lipids, as could also be in the case of ATG3.

To evaluate the relevance of the electrostatic component in ATG3 binding to membranes the above experiments were carried out with increasing NaCl concentrations. For ATG3 we observed the same amount of binding to vesicles with NaCl concentrations from 150 mM to 1 M, further suggesting that the electrostatic component is not the main factor in ATG3-membrane interaction. (**Figure 4.3 D**).

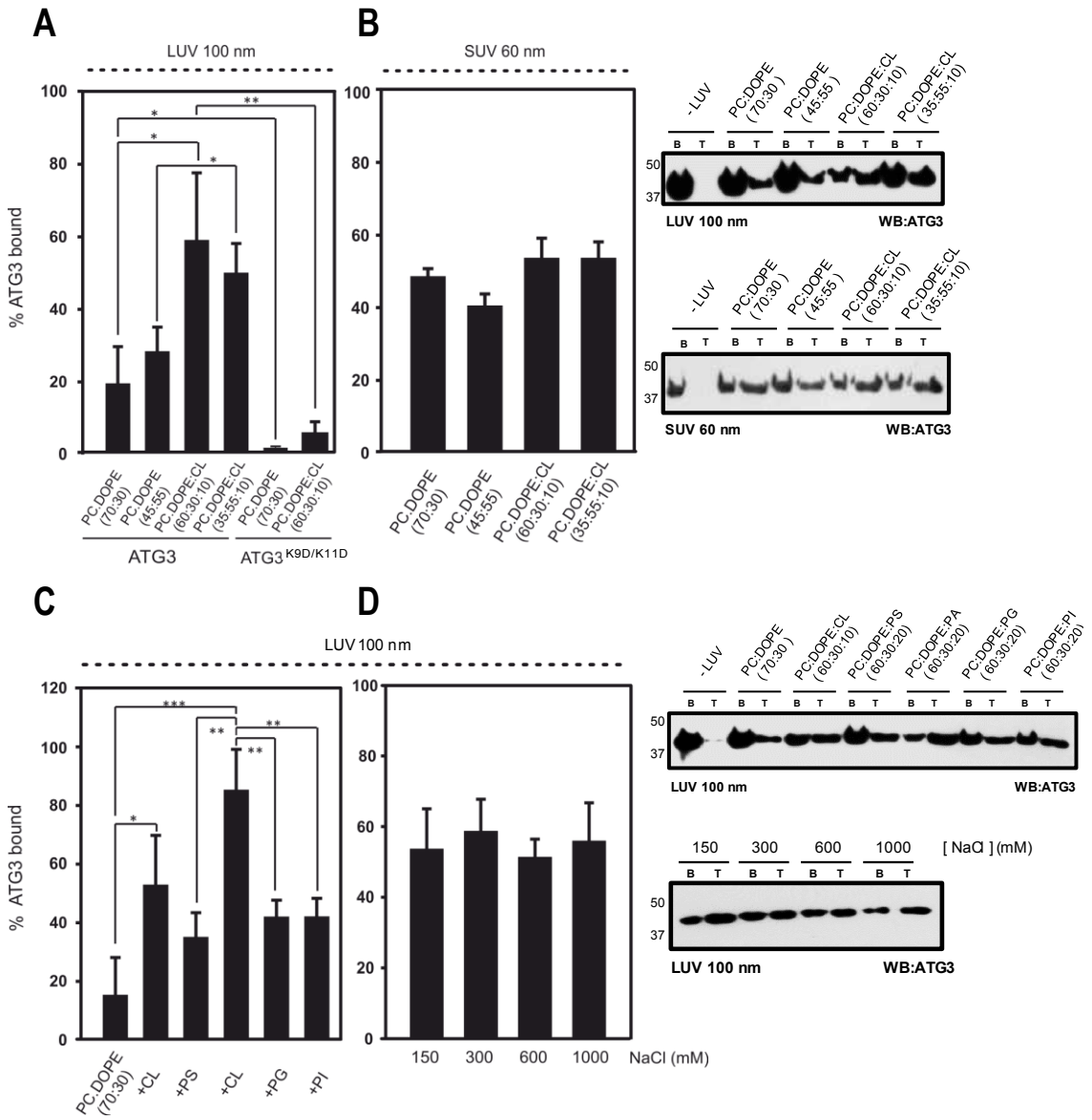

Figure 4.3. ATG3 interacts with negatively-charged phospholipid vesicles. The liposome-bound protein fraction was analyzed after floatation sucrose density gradient centrifugation by SDS-PAGE/immunoblot analysis and quantified by densitometric integration of the peaks. **(A)** 10 μM ATG3 was incubated with 3 mM LUVs composed of PC:DOPE (70:30 or 45:55 mol ratio) or PC:DOPE:CL (60:30:10 and 35:55:10 mol ratio). ATG3 K9D/K11D was also shown. **(B)** Effect of vesicle size reduction on ATG3 interaction. ATG3 (10 μM) incubated with SUV containing 30% or 55% DOPE with or without CL **(C)** Atg3 interaction with LUV containing different anionic phospholipids. **(D)** ATG3 (10 μM) binding to liposomes (3 mM) composed of PC:DOPE:CL after incubation with increasing NaCl concentration (150 mM to 1M). Molecular mass is shown in kDa on the left-hand side. Data shown as mean ± SEM (n = 3); **p = 0.001-0.01, ***p < 0.001.

In order to test to what extent could the ATG3 N-terminal predicted α-helix reproduce the behavior of the full protein in the interaction with model membranes, we designed two different peptides respectively of 22 (QL22) and 27 (QF27) amino acids corresponding to this helix. These peptides are predicted to fold into a helix in the protein. They are expected to be water-soluble (**Figure 4.4 A**). According to circular dichroism both peptides showed a non-defined structure (random coil) in solution

(**Figure 4.4 B**). Moreover, due to the capacity of some peptides to fold in the presence of membranes, Langmuir balance studies and floatation experiments were performed. Both peptides showed the ability to interact with neutral and anionic lipid monolayers although with critical pressures π_c well below those found for the whole protein (**Figure 4.4 C**) but they did not interact in any case with lipid bilayers (**Figure 4.4 D**). This may suggest that (a) the peptides were in the unfolded conformation, an in that conformation they cannot bind lipid bilayers, or (b) even if they could adopt the α-helical structure in the presence of lipids, they cannot by themselves become inserted in bilayers.

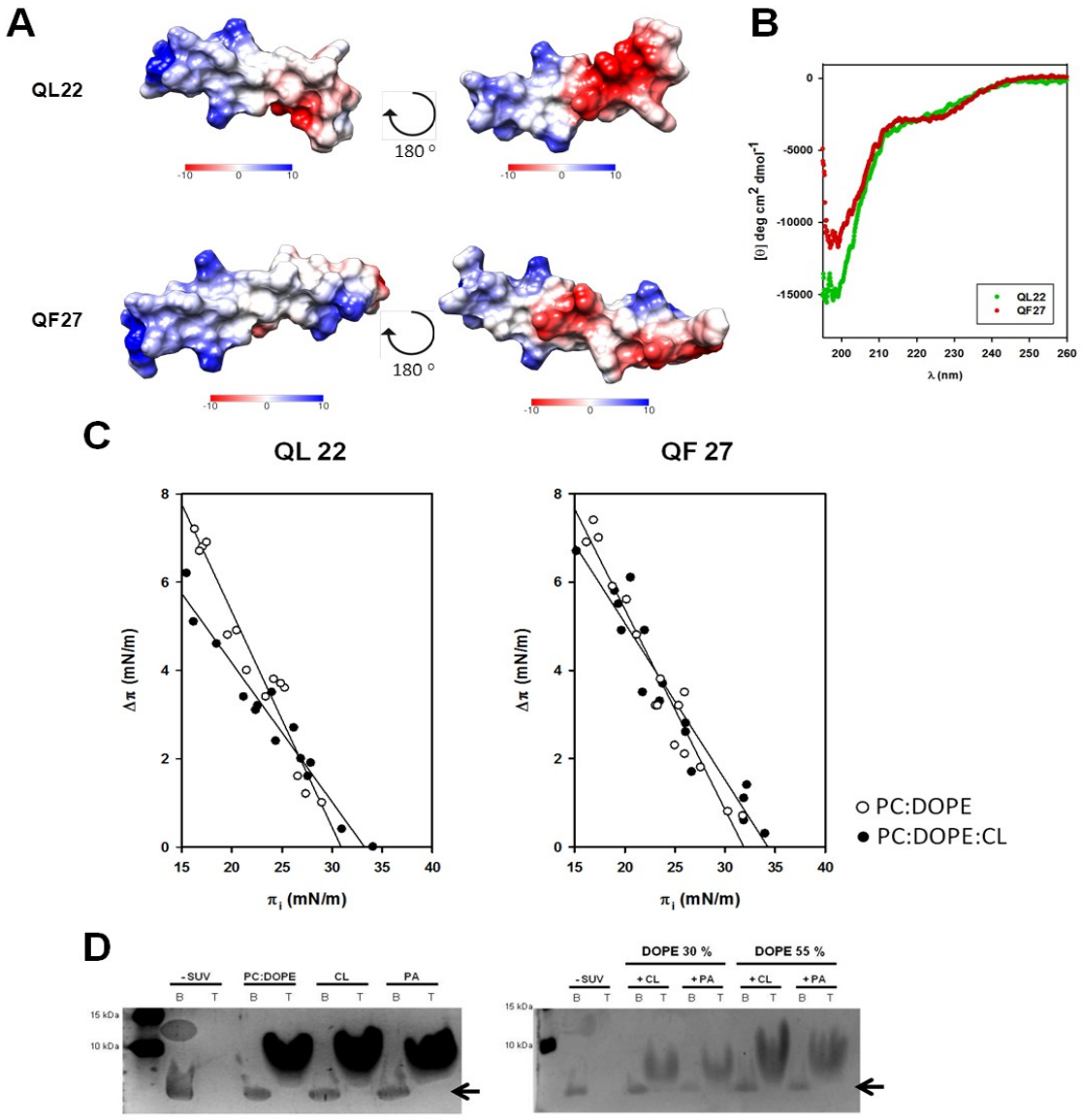

Figure 4.4. ATG3 N-terminal peptides do not reproduce ATG3 full length protein interaction with membranes. (A) Surface electrostatics of the predicted structures of QL22 and QF27 peptides generated by QUARK. **(B)** Secondary structure analysis of both peptides analyzed by circular dichroism. **(C)** Maximum increase in lateral pressure after QL22 and QF27 peptide insertion into lipid monolayers. Lipids were: [○] PC:DOPE (70:30 mol ratio) or [●] PC:DOPE:CL (60:30:10 mol ratio). Data reported as a function of initial lateral pressure π_i. **(D)** QL22 and QF27 binding to liposomes. Lipid compositions are shown in the panel. The peptide position in the gel is indicated by the arrow.

To summarize, the above results suggest that human ATG3 interacts with membranes containing physiological concentrations of DOPE, binds preferentially to negatively-charged membranes, and the membrane association is improved by defects in the membrane structure. The presence of anionic phospholipids decreases or suppresses the preference for highly curved vesicles, whereas the anionic lipids with a negative intrinsic curvature clearly facilitate ATG3 interaction with membranes. Furthermore mutations of Lys residues 9 and 11 in the predicted N-terminal α-helix revealed their importance in the protein binding to lipid vesicles.

4.3.2 ATG3 Induces Aggregation of Liposomes but no Intervesicular Lipid Mixing

ATG7/ATG3/LC3 UBL system is involved in the autophagosome elongation. In this process vesicle tethering and fusion is essential. It is usually understood that the full responsibility of the latter processes falls on the last reaction component, LC3. The other components (ATG7 and ATG3) are considered to act only in the previous conjugation reactions. However, since ATG3 interacts with membranes this protein could contribute, to some extent, to the aggregation and fusion of vesicles. This hypothesis was tested as detailed below.

First, vesicles of different lipid compositions were incubated in presence of ATG3. Aggregation was monitored continuously in a spectrophotometer as an increase in sample turbidity (absorbance at 400 nm) (Goñi *et al.*, 2003). ATG3 was observed to cause vesicle aggregation of electrically neutral vesicles [PC:DOPE (70:30 mol ratio)] and, at higher rates, of negatively-charged liposomes (containing PA, CL or PI) (**Figure 4.5 C**). Just as in the interaction of ATG3 with vesicles assay (**Figure 4.3**) this protein showed the best tethering rate with PA-containing liposomes. In all cases, aggregation is ATG3 concentration dependent, at least between 1 μM and 10 μM. Furthermore, the activity of ATG3 K9D/K11D was tested in parallel experiments and no vesicle aggregation was observed even with anionic vesicles (**Figure 4.5 B**).

Confocal images of liposome aggregates confirmed the turbidity results. 10 μM ATG3 was incubated with liposomes of different lipid compositions, and after 1 h images were taken in a confocal microscope. Very little aggregation was observed with the PC:DOPE composition, while extensive liposome aggregation was seen with CL- or PA-containing vesicles (**Figure 4.5 A**). Our negative controls, buffer only or ATG3 K9D/K11D did not show any amount of vesicle tethering.

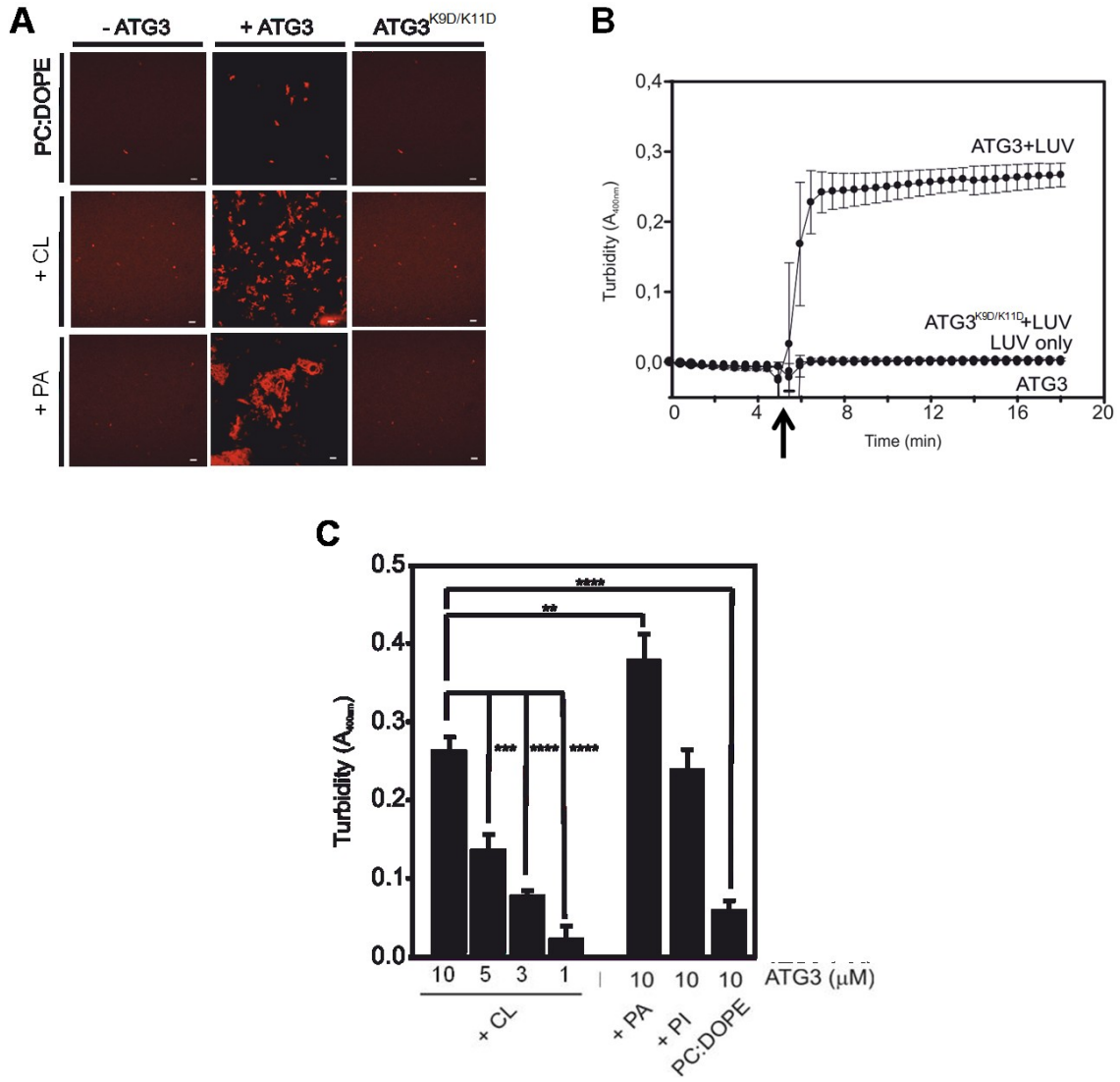

Figure 4.5. ATG3-promoted vesicle aggregation. (A) Representative images of ATG3-induced LUV aggregation of different lipid compositions PC:DOPE (70:30 mol ratio), PC:DOPE:CL (60:30:10 mol ratio) and PC:DOPE:PA (50:30:20 mol ratio). **(B)** Time-course of ATG3 (10 μM) LUV aggregation. PC:DOPE:CL (60:30:10 mol ratio) lipid composition was used. Arrow indicates time of ATG3 addition. Each curve is the mean ± SE of three experiments. **(C)** Effect of different lipid composition and ATG3 concentration on LUV aggregation. Lipid compositions are indicated for each bar. Bars represent mean ± SE (n = 3) of ΔA_{400}. ***P ≤ 0.001, **P ≤ 0.01, *P ≤ 0.05 of unpaired t-test.

Once aggregation was monitored, lipid mixing and release of vesicle contents assays were performed in order to assess the possible contribution of this protein to the fusion processes in autophagosome elongation, but ATG3 did not exhibit any of those activities under our experimental conditions (**Figure 4.6 A-B**).

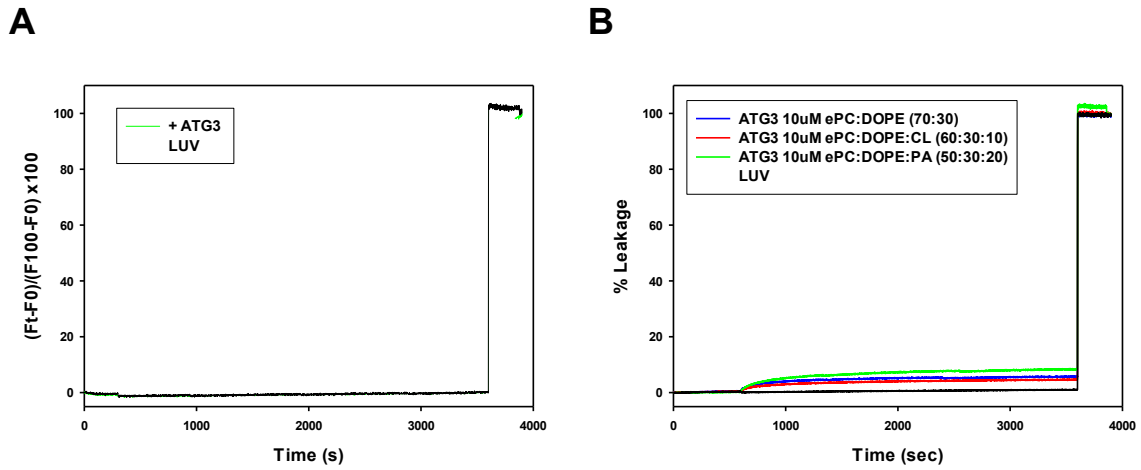

Figure 4.6. (A) Time courses of total lipid mixing induced by ATG3 (10 μM) in liposomes (0.4 mM) composed of PC:DOPE:CL (45:55:10 mol ratio). Lipid mixing was monitored by the NBD/Rhodamine lipid dilution assay. Unlabeled and (NBD + Rho)-labeled liposomes (9:1) were mixed and incubated for 5 min before ATG3 addition. The extent of lipid mixing was quantified on a percentage basis according to the equation: $(F_t-F_0/F_{100}-F_0)$ x100 where F_t is the measured fluorescence of protein-treated LUVs at time t, F_0 is the initial fluorescence of the LUV suspension before protein addition, and F_{100} is the fluorescence value after complete disruption of LUVs by addition of 30 mM β-octylglucoside. **(B)** Time courses of vesicle content leakage induced by ATG3 (10 μM). Lipid compositions are shown in the panel. Vesicle leakage was monitored by the ANTS/DPX leakage assay; 100% leakage signal was obtained by adding 1% Triton X-100.

The above results demonstrate a novel activity for ATG3, namely vesicle tethering. This new activity would be in part performed by its N-terminal α-helix as a membrane anchor, but some other region of the protein might also be involved. Further investigation is required to discern the regions of the protein involved. Our observations could suggest a possible contribution of ATG3 to the tethering of vesicles preceding fusion events in autophagosome elongation, while the fusion ability would only remain in the final effector of the UBL system, Atg8. These aggregation and fusion processes could occur in negatively-charged and highly curved membrane regions such as the edge of the isolation membrane where could exist a relatively enrichment of this proteins.

4.3.3 ATG3 Interaction with Negatively-charged GUV

Giant unilamellar vesicles (GUVs) constitute a cell-sized model membrane system that allows direct visualization of particular membrane-related phenomena, such as domain formation or protein interaction, at the level of single vesicles using fluorescence microscopy-related techniques. We used this method to know whether ATG3 was able to interact with GUVs of different lipid compositions, had any lipid preference when binding GUVs, and could reproduce the aggregation activity with much larger vesicles.

GUVs with different lipid compositions were electroformed in sucrose solution and then transferred to a visualization chamber with an equiosmolar buffer. Then Alexa488-labeled ATG3 or ATG3 K9D/K11D (1 μM) was incubated with Rho-PE-labeled GUVs and the mixture was observed under the microscope. ATG3-Alexa 488 was clearly seen bound to the membranes (**Figure 4.7 A**). In GUV containing some other negatively-charged phospholipids colocalization of Rho-PE and ATG3-Alexa 488 was also detected, indicating the interaction of ATG3 with all these vesicles (**Figure 4.8**). A preferential association of ATG3 to the GUV-GUV contact sites was observed (**Figure 4.7 B**). In contrast, no ATG3 interaction was observed in the absence of anionic phospholipids (electrically neutral vesicles) (**Figure 4.7 A**). To further analyse the preference of ATG3 for anionic phospholipids, GUV with segregated domains were electroformed. Asymmetric distributions of CL within the membrane of single vesicles were engineered by incorporating CL into lipid mixtures that are known to phase separate into two distinct liquid phases. Ternary mixtures of DOPC/DPPC/cholesterol have a large region of their phase diagram wherein these membranes demix to form liquid-ordered (L_o) and liquid-disordered (L_d) domains (Veatch & Keller, 2003). The L_d phase of these model membranes is rich in DOPC due to its unsaturated hydrocarbon tails, and the L_o phase is rich in the saturated DPPC. Cholesterol partitions into both phases but is slightly enriched in the L_o domains compared to the L_d phase. GUVs composed of DOPC:DPPC:cholesterol (37.5:37.5:25 mol ratio) at 22 °C are within this region of liquid-liquid phase separation. Domains of these two liquid phases coalesce to form two large domains on the vesicle surface, one of each phase. 10 mol% DOPC for 10 mol% CL were exchanged based upon two assumptions: that CL, due to its high degree of chain unsaturation, will also prefer to partition into the L_d phase, and that despite such a significant change in lipid composition, the membrane will still be in a region of phase space for liquid-liquid phase coexistence (Beales *et al.*, 2011). ATG3-Alexa488 bound preferentially to regions of the membrane that are rich in CL (labeled

with Rho-PE) (**Figure 4.8 C**). Thus, ATG3 interaction with GUVs is determined by the presence of negatively-charged lipids on their surface.

However, GUV containing CL were not labeled with ATG3 K9D/K11D-Alexa 488. In fact, the vesicles were seen as dark objects against a green (Alexa) background (**Figure 4.7 D**)

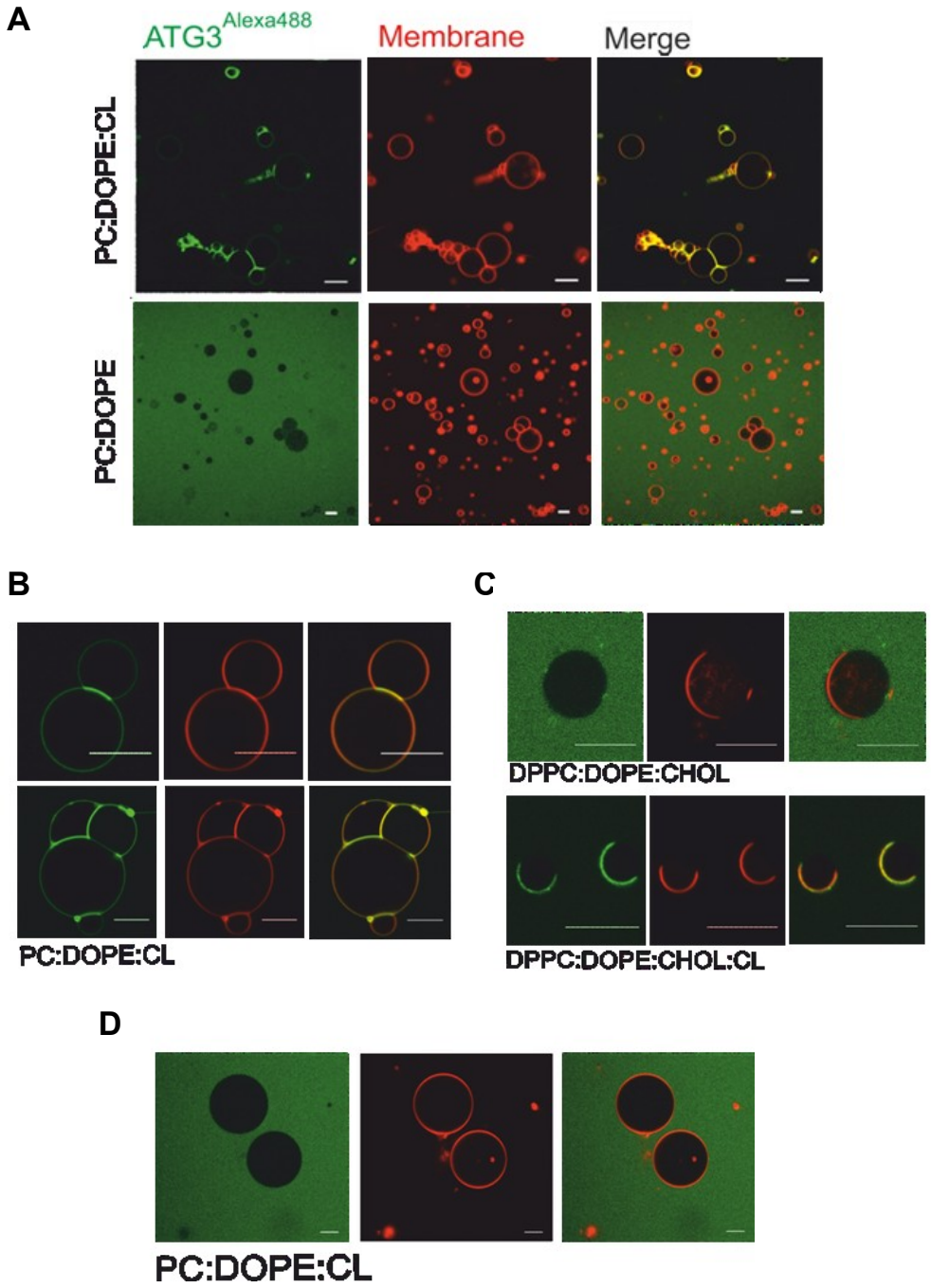

Figure 4.7. Confocal microscopy of representative GUVs. (A) ATG3 interaction with CL-containing or non-containing GUV. Membrane labelled with Rho-PE and protein represented as ATG3-Alexa 488. Merge: yellow indicates colocalization of both probes. Lipid composition is given at the left-hand side. **(B)** ATG3 preferential localization in GUV contact sites. **(C)** ATG3 binding to GUV with segregated domains. Two different lipid domains are clearly seen, one of them containing CL and labelled with Rho-PE. **(D)** ATG3 K9D/K11D does not interact with PC:DOPE:CL (60:30:10 mol ratio) GUV. Lipid compositions are given in each panel. Scale bars: 10 μm

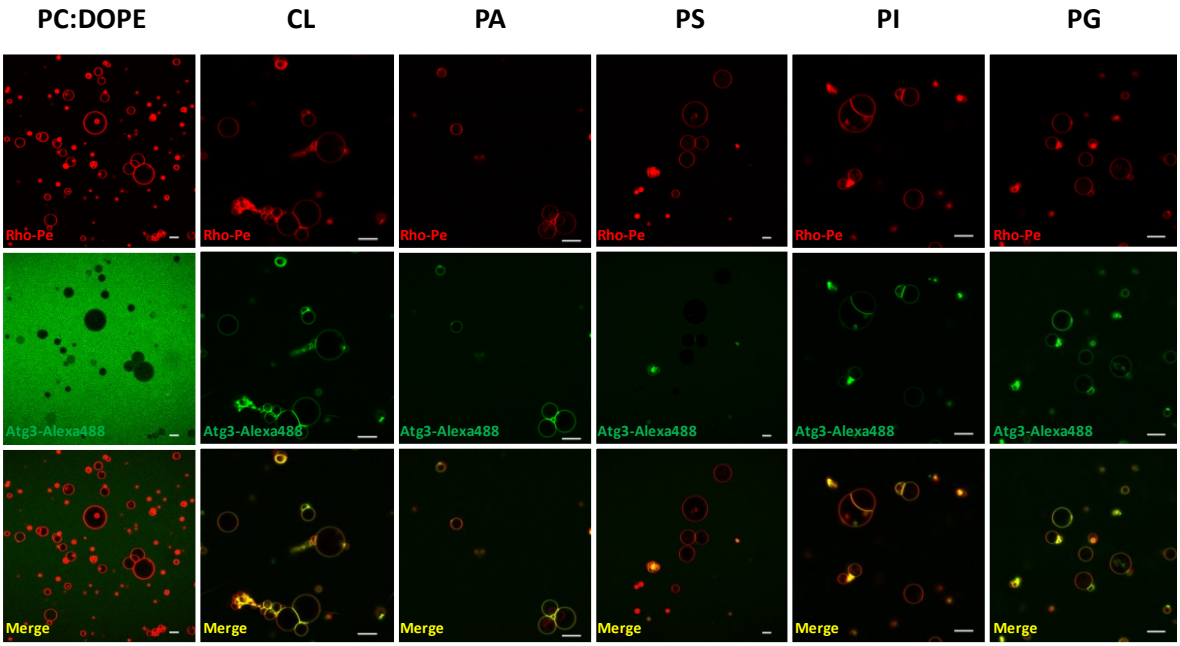

Figure 4.8. ATG3 interaction with negatively charged GUVs. Different anionic phospholipids are incorporated to GUVs (labeled with Rhodamine-PE) and protein (labeled with Alexa-488) incorporation to them was observed by confocal microscopy. Merge: yellow indicates colocalization of both probes. Scale bars: 10 μm.

ATG3 aggregation experiments could also be reproduced in GUV. A different methodology was used to form GUV in order to obtain them as close as possible to allow the protein-induced tethering. In this case, PC:DOPE:CL (60:30:10 mol ratio) GUV were electroformed and directly visualized in a Nikon confocal microscope. Upon addition of ATG3-Alexa 488 (1 μM) GUV tended to aggregate and precisely the flattened areas between tightly aggregated GUV appeared enriched in ATG3-Alexa 488 (**Figure 4.9** upper panels). Controls made with ATG3 K9D/K11D-Alexa 488 and buffer did not show any event of GUV tethering (**Figure 4.9** lower panels).

These results suggest that ATG3 interaction with membranes does not require a high vesicle curvature (GUV curvature is practically zero), instead the electrostatic interaction with anionic phospholipids and the intrinsic negative membrane curvature generated by conic-shape lipid molecules.

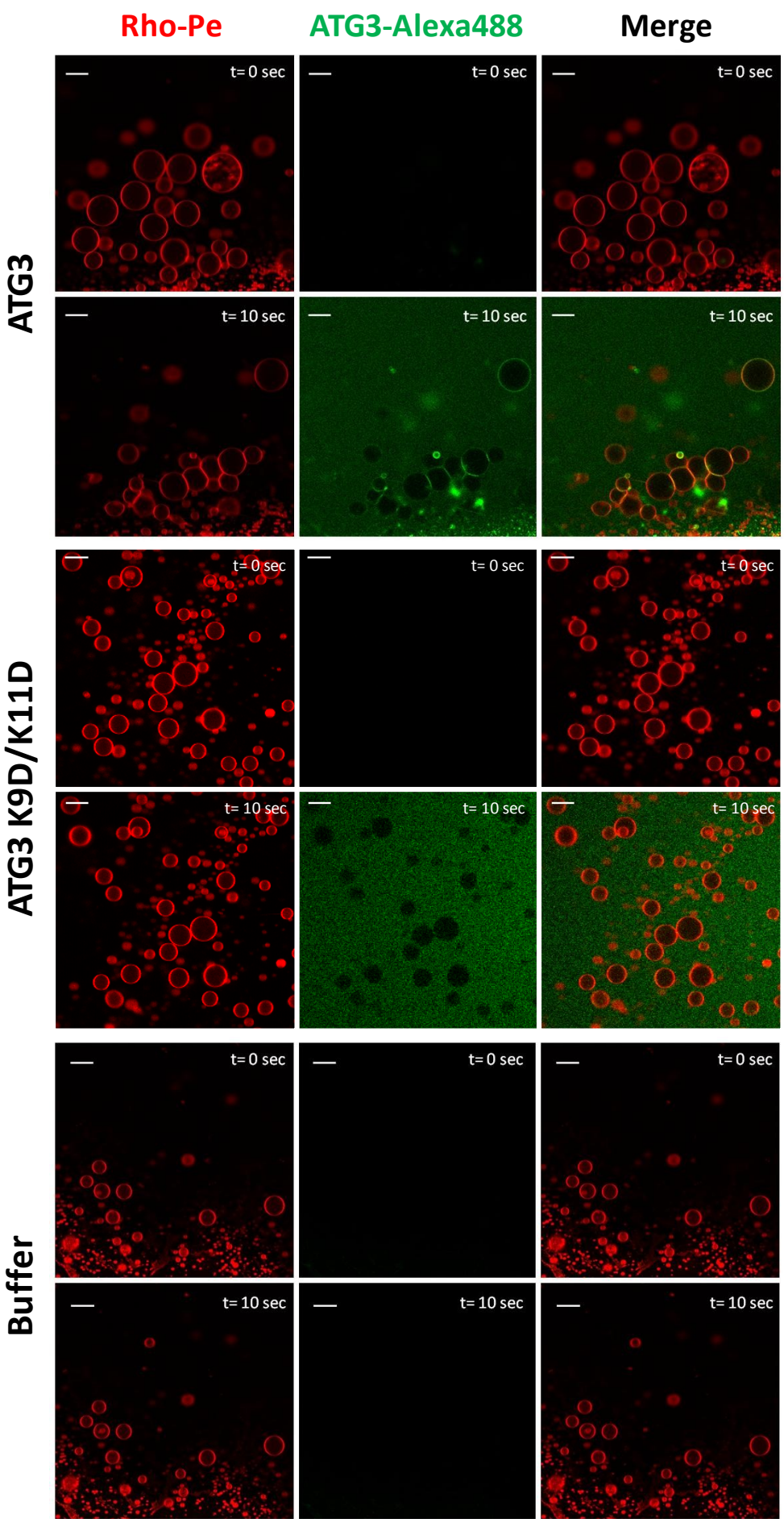
Rho-Pe
ATG3-Alexa488
Merge
ATG3
ATG3 K9D/K11D
Buffer
t= 0 sec
t= 10 sec

Figure 4.9. ATG3-induced GUV aggregation. PC:DOPE:CL (60:30:10 mol ratio) vesicles stained with Rho-PE were used. After ATG3-Alexa488 addition (t=10 s) vesicle aggregation was observed (upper panels). Protein (labeled in green) is localized preferentially to vesicle contact sites. Merge: yellow indicates colocalization of both probes. ATG3 K9D/K11D-Alexa488 or buffer do not induce any effect on the GUVs.

4.3.4 ATG3 Interaction with Membranes could Govern GABARAP Lipidation

Atg3 was proposed to direct LC3 to the membrane for lipidation *in vitro* and also to act together with the Atg5-Atg12/Atg16 system to perform the same task *in vivo* (Hanada *et al.*, 2007; Walczak & Martens, 2013). In this context, lipid composition changes could modify the lipidation rate of Atg8 homologues (Ichimura *et al.*, 2004; Nath *et al.*, 2014; Sou *et al.*, 2006). The effect of adding negatively-charged lipids, or lipids with a negative intrinsic curvature, that facilitate ATG3 binding to membranes, on GABARAP lipidation was analysed. For this purpose *in vitro* lipidation assays incubating ATG7, ATG3 and GABARAP in the presence of liposomes, ATP and $MgCl_2$ were performed. The lipidation product was followed by SDS-PAGE gels and its subsequent CBB staining or Western blotting. GABARAP was used as the human Atg8 homologue in this experiments because the lipidated band of LC3 and GATE-16 was undistinguishable from the presumably adenylated form of the protein. The increased affinity of ATG3 for anionic monolayers (**Figure 4.10 A**) and vesicles (**Figure 4.10 B**) was also associated to an enhanced lipidation as observed in **Figure 4.10 C-D**. Moreover higher lipidation ratios were observed when lipids such as PA and CL, with a high negative intrinsic curvature, were incorporated to the liposomes. This suggests that ATG3 membrane interaction could govern the lipidation efficiency of the Atg8 homologues. This does not rule out a similar involvement of ATG7 in the regulation of Atg8 lipidation, for which no experimental data are available.

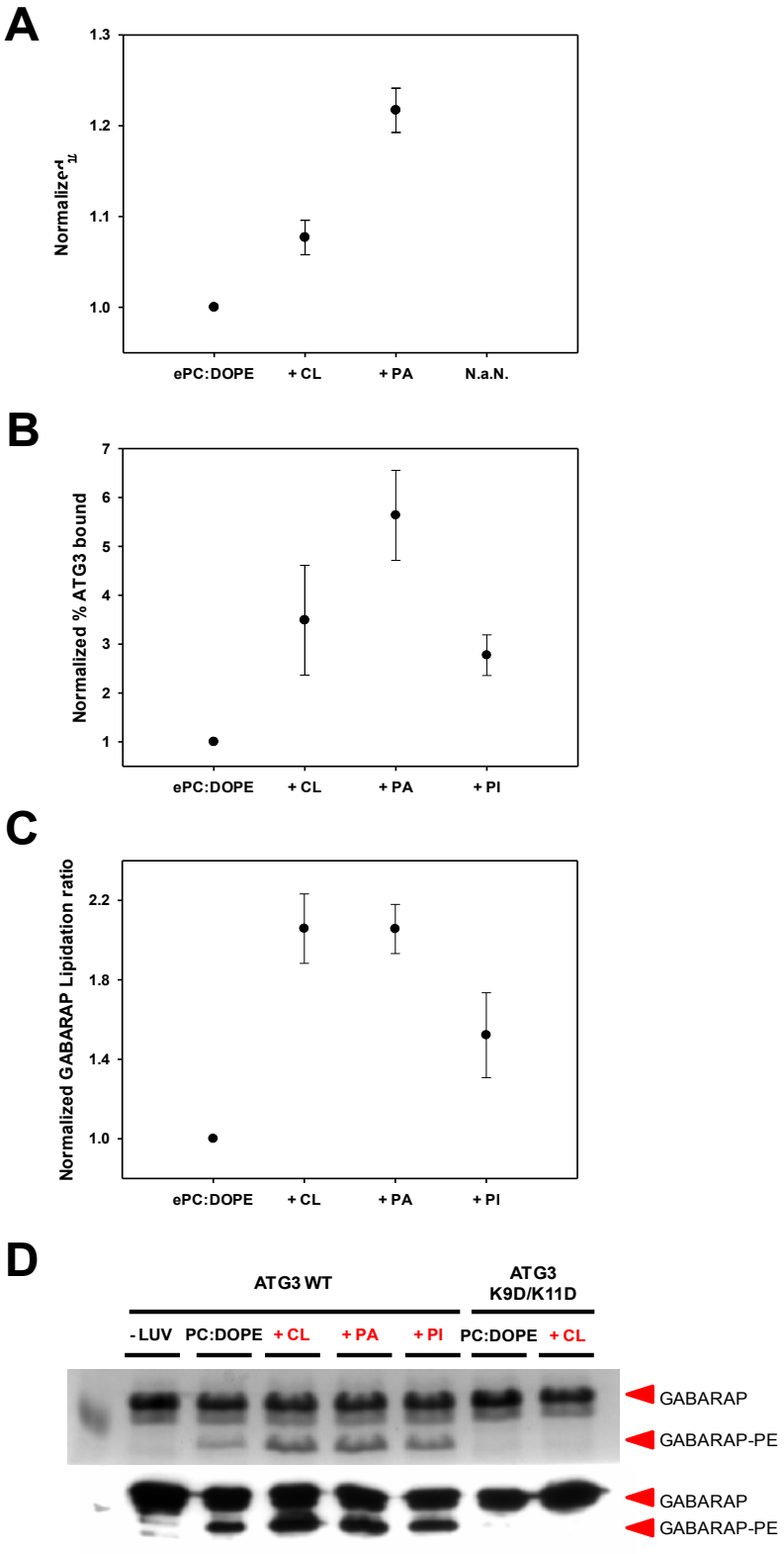

Figure 4.10. ATG3 governs GABARAP lipidation ratio. (A) ATG3 binding to lipid monolayers. Data from **Figure 4.2 C** normalized to the PC:DOPE value **(B)** ATG3 binding to liposomes of different lipid compositions. Data from **Figure 4.3 C** normalized to PC:DOPE. **(C)** GABARAP lipidation ratio using different lipid compositions. Data obtained from gels as shown in D normalized to the PC:DOPE value. Average values of two experiments. **(D)** Coomassie blue staining (upper panel) and anti-GABARAP Western blotting (lower panel) of the *in vitro* lipidation reaction using different lipid compositions. Lipid compositions are detailed in each panel. Red arrows indicate lipidated and non-lipidated forms of GABARAP.

4.4 Discussion

The autophagy machinery is the subject of study in several contexts due to its essential role in cell life survival and its controversial function in apoptosis. A large amount of proteins have been discovered that participate in autophagy control, more precisely in the formation, elongation and closure of the autophagosome. In this process, the protein Atg8 (and its mammalian homologues LC3, GATE-16 and GABARAP) triggers the aggregation and fusion of vesicles with the nascent autophagosome. The way in which Atg8 is brought to the membrane has been studied but little is known on how the proteins involved in this process recognize specific sites in the membrane. Some studies showed that Atg3 is the protein involved in the transport and recognition of PE as Atg8 substrate (Oh-oka *et al.*, 2008), and also that another UBL system involved in autophagy, Atg5-Atg12/Atg16, interacts with membranes and improves the rate of Atg8 lipidation through interaction with Atg3 (Romanov *et al.*, 2012).

According to a growing body of evidence, changes in membrane properties such as surface charge or lipid packaging directly affect protein binding. The physical properties of different lipid acyl chains or headgroups can favor different membrane curvatures (McMahon & Boucrot, 2015; McMahon & Gallop, 2005). For example, lysophosphatidic acid (LPA) and phosphatidic acid (PA), which are interconverted by lysophosphatidic acid acyl transferase and phospholipase A2 activity respectively, favour opposite curvatures (Kooijman *et al.*, 2003). In addition, flippases (that transfer lipids from one leaflet to the other) give rise to membrane asymmetry (Pomorski & Menon, 2006), and enzymes that change lipid headgroup size will influence the area occupied by the lipids and thus affect membrane curvature. The access to the membrane could also be favoured by inverted cone-shaped lipids that impart negative curvature to bilayer leaflets and as the result they lower the surface pressure at the interface, i.e. aerolysin-membrane interaction (Alonso *et al.*, 2000). In addition, lipid headgroups are the attachment sites for peripheral membrane proteins. The main acidic phospholipids in mammalian cell membranes are phosphatidylserine, phosphatidic acid and phosphatidylinositol. These negatively-charged lipids are particularly important directing the membrane association of phospholipid-binding domains. At least 10 different globular domain types bind phospholipids at the membrane surface. The interactions of these domains with the membrane surface fall into two broad classes: some are highly specific and involve stereospecific recognition of particular membrane components; others are non-specific and involve a general

physical property of the membrane (such as charge, amphiphilicity, or curvature) (Antonny, 2011).

For Atg3 it was demonstrated to interact with membranes in part through its N-terminal region. It was also suggested that the predicted N-teminal amphiphatic helix would be responsible for this attachment, and also that this helix would be a membrane curvature sensor (Nath *et al.*, 2014).

4.4.1 ATG3-membrane Interaction

This work was focused on a better understanding of ATG3-membrane interaction. Using Langmuir balance measurements (**Figure 4.2**) and liposome floatation assays (**Figure 4.3**) we show that ATG3 binds to PE-containing membranes and in particular to negatively charged membranes. Incorporation of anionic phospholipids to the liposome compositions substantially increases ATG3 binding to these vesicles (**Figure 4.3 A**). It was reported by Nath *et al.*, (2014b) that ATG3 contains a membrane curvature sensor in its structure. We report here that curvature recognition by ATG3 is only noticed when neutral membranes are present, because no change is observed in ATG3 binding when the size of anionic-lipid containing liposomes decreases (**Figure 4.3 B**). Furthermore, ATG3 attachment to membranes relies on two components, electrostatic and hydrophobic interactions due to membrane defects. This result is consistent with the notion that mutations in the N-terminal amphiphatic helix, including polar and hydrophobic residues, alter ATG3 interaction efficiency (Nath *et al.*, 2014). Our results with ATG3 K9D/K11D mutant (**Figure 4.3 A**) strongly support the idea that these two lysines, located between the hydrophobic and polar faces of the helix represent an important anchor for ATG3 binding, probably related to the increased binding capacity in the presence of anionic phospholipids. Moreover, comparing the different negatively-charged phospholipids we observe that lipid packaging defects in the membrane may be important for ATG3 interaction (**Figure 4.3 C**). Both CL and PA possess a high negative intrinsic curvature, and when incorporated to bilayers they create membrane defects where ATG3 can easily insert. According to this, the electrostatic component would favor protein binding but it would not be the only force driving this association.

Furthermore, when approaching to a cell system using cell-sized model membranes (GUV), where no membrane curvature is present, ATG3 recapitulates the same properties showed in small vesicles (**Figure 4.7**).

BAR domains and amphiphatic α-helices are considered to be the best examples of membrane curvature-sensing domains in proteins. BAR domains sense membrane curvature by insertion of an amphiphatic helix to membrane defects and also by electrostatic interactions with negative charges in the membrane (Madsen *et al.*, 2010), whereas amphiphatic α-helices such as ALPS motifs just insert their hydrophobic face into lipid packing defects (Bigay *et al.*, 2005; Mesmin *et al.*, 2007). In this case ATG3 exhibits both requirements, electrostatics and intrinsic curvature of the membrane lipids. According to the snorkel model, lysines at the interface of the polar and nonpolar faces of the helix favor the association to flat membranes and the electrostatic interaction with them (Mishra *et al.*, 1994), and this would also explain ATG3 ability to bind negatively-charged vesicles. Hence, mutations of lysine residues to aspartic acid in ATG3 K9D/K11D mutant cause an electrostatic repulsion between these amino acids and the negative charges of the membrane (lipid polar head groups and phosphate). The same Lys mutated to Ala just causes a decrease in binding to anionic vesicles but not to neutral membranes. In the autophagy context, ATG3 would not be the only protein that is proposed to sense membrane curvature through an amphiphatic helix, also Barkor is involved in detecting this curvature in PI3P-enriched membranes (Fan *et al.*, 2011; Wilz *et al.*, 2011).

Moreover, in an attempt to extrapolate our *in vitro* findings to physiological conditions in cells, there are evidences suggesting that autophagosome biogenesis is a lipid-modulated process (Dall'Armi *et al.*, 2013). While the role of phosphoinositides (PI3P) in autophagy progression is well known (Dooley *et al.*, 2014; Vicinanza *et al.*, 2015), little information on the participation of other lipid species during the different steps of autophagosome biogenesis is reported (Chu *et al.*, 2013; Sentelle *et al.*, 2012). A combined action between lipids and autophagic proteins should lead to phagophore expansion. The participation of PA and other cone-shaped lipids (DAG) in autophagy and also in membrane fusion/fission processes has been proposed (Ibarguren *et al.*, 2010). Previous studies in our group have suggested a possible role of intrinsic-curvature modifying lipids such as CL, DAG and LPC in promoting GATE-16 and GABARAP mediated vesicle fusion *in vitro* (Landajuela *et al.*, 2016). DAG generation was shown to be required for the initiation of *Salmonella*-induced autophagy (Shahnazari *et al.*, 2011). Moreover, the PLD1 pathway, that produces PA, a cone-shaped lipid, has been also reported to promote autophagy (Dall'Armi *et al.*, 2010). The lipid composition of the pre-autophagosomal membrane is not yet known but further efforts to discern it would open a new window to understand how elongation would occur.

4.4.2 ATG3 Aggregation

During autophagosome formation and elongation, a large amount of vesicles containing proteins and lipidic material are fused with the forming autophagosome. In this process some Atg and other proteins are involved, i.e the Atg7/Atg3/Atg8 UBL system. Atg8 homologues are the final effectors of the system and are well studied that mediates the tethering and fusion of liposomes *in vitro* (Landajuela *et al.*, 2016). It is also known that other proteins e.g. SNARES participate in this action (Moreau *et al.*, 2013). Here, we report a novel function for ATG3, namely the vesicle aggregation capacity. We demonstrate that Atg3 can tether vesicles when it binds them (**Figure 4.5** and **4.9**). The aggregation potential would be related to the anionic charge and intrinsic curvature of the membrane, but further work has to be performed to find the specific protein regions involved in this activity. In this context, ATG3 might be cooperating with Atg8 in the aggregation process before vesicle fusion in the pre-autophagosome elongation.

Other studies have reported a regulation of the lipidation ratio of Atg8 and their mammalian homologues by changes in the lipid composition of the membrane (Ichimura *et al.*, 2004; Landajuela *et al.*, 2016; Nath *et al.*, 2014; Sou *et al.*, 2006). According to this, we suggest in this work that ATG3 would be the responsible for bringing Atg8 homologues the membrane *in vitro*. As we have shown, the incorporation of CL, PA or PI to the liposomes improves ATG3 association to the membrane and also enhances the lipidation ratio of GABARAP (**Figure 4.10**). Nevertheless, other proteins participate in this process *in vivo* such as the Atg5-Atg12/Atg16 system, and further experiments with these other partners should be performed to discern the precise role of each protein.

In conclusion, the data shown on ATG3 interaction with membranes should clarify the mechanism by which the lipid composition of the autophagosomal membrane could facilitate the redirection of the autophagy machinery to some regions, in order to undertake the elongation process. However, the lipid composition of the phagophore and the number of proteins recruited to it should be further investigated for a better understanding of how phagophore elongates. This would allow discovering new potential targets implicated in macroautophagy that could also be explored in cancer progression therapies.

5. Preliminary results on hATG9 purification in *E. coli* and insect cells, and its implication in lipid delivery

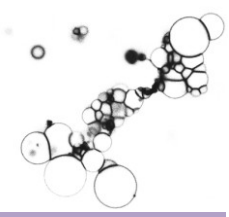

CHAPTER 5:

Preliminary results on hATG9 purification in *E. coli* and insect cells, and its implication in lipid delivery

5.1 Introduction

Cellular homeostasis requires equilibrium between protein degradation and protein synthesis. For this purpose, eukaryotic cells have two main different mechanisms for degrading components, the ubiquitin-proteasome system in order to degrade proteins, and autophagy for degrading proteins and organelles. Autophagy is responsible to maintain energy levels and provide amino acids under starvation or cellular stress, thus it is involved in several disorders such as cancer, Parkinson´s or Alzheimer´s diseases.

The main event in autophagy is the formation of a double-membrane compartment, named autophagosome, which engulfs the unnecessary material. After that, fusion with the lysosome occurs to degrade the sequestered contents. Despite the identification of more than 30 Atg proteins required for normal autophagy there are still many key questions open (Lamb *et al.*, 2013). For instance, the origin of the membrane that gives rise to autophagosome formation and the way in which this newly formed structure elongates and closes have to be elucidated (Tooze & Yoshimori, 2010).

Among the Atg proteins Atg9 is the only transmembrane protein essential for autophagosome formation (Lang *et al.*, 2000; Noda *et al.*, 2000). It is composed by six conserved transmembrane domains with its N- and C-terminal regions exposed to the

cytoplasm (Tooze, 2010). An N-glycosilation site was described in the first luminal loop (Young *et al.*, 2006) (**Figure 5.1**). As the only multispanning membrane protein in this system so far, Atg9 is considered to play a key role in the trafficking of membrane material along the autophagosome formation and elongation process. In yeast, Atg9 can be observed as punctate structures scattered through the cytoplasm and partially colocalizing with a perivacuolar site, known as the PAS (Mari & Reggiori, 2007; Reggiori *et al.*, 2005). These puncta correspond to highly motile Atg9-containing vesicles of 30-60 nm and they are increased upon rapamycin treatment (Yamamoto *et al.*, 2012). Furthermore, Atg23 and Atg27 are required for Atg9 trafficking through the Golgi (Backues *et al.*, 2015; Yen *et al.*, 2007), and under starvation Atg9 was demonstrated to be embedded in the autophagosomal outer membrane (Yamamoto *et al.*, 2012). Another evidence of the Atg9 involvement in autophagosome elongation resides in the upregulation of Atg9 expression when a protein as Atg16 (essential for phagophore growth) is not present in *Dictyostelium discoideum*. This indicates that cells overexpress other proteins involved in the elongation process such as Atg9 to compensate the lack of Atg16 (Xiong *et al.*, 2015). Moreover, a recent publication shows the participation of Atg9 in the phagophore nucleation through its interaction with proteins such as Atg13 or Atg17, which are members of the Atg17-Atg29-Atg31 complex, probably involved in fusion processes that give rise to the autophagosome nucleation and elongation (Ragusa *et al.*, 2012; Sekito *et al.*, 2009; Stanley *et al.*, 2014; Suzuki *et al.*, 2015)

In contrast, human ATG9 (hATG9) resides in the trans-Golgi Network (TGN), and late and recycling endosomes under basal conditions (Orsi *et al.*, 2012). When autophagy is induced, it redistributes from the TGN to endosomal membranes, where LC3 is present, in a ULK1-dependent manner (Young *et al.*, 2006). Despite this fact, ATG9 does not completely colocalize with autophagosomes but it transiently interacts with them. The latter would be a difference between the yeast and mammalian homologues, and it could be explained because hATG9 is rapidly recycled from the autophagosome.

Taking this into account, ATG9 vesicles could contribute to the regulation of autophagosome size, thus participating in the delivery of lipid material and/or proteins in the elongation step to the forming autophagosome. The continuous movement of these vesicles in the cytoplasm and their transient incorporation to the autophagosome would recapitulate a process of material delivery. Moreover, due to the high hATG9 C-terminal domain size (almost half of the entire protein), this could be the region through which ATG9 performs its function. Here we have made a first approach to purify

hATG9 and its C-terminal domain in *E. coli* to test their possible participation in lipid or vesicle delivery during autophagosome formation. In a preliminary study, we have observed the presence of phospholipids in ATG9 C-terminal-enriched fractions. In addition a eukaryotic system was also used to purify the above-cited two versions of ATG9 with improved results, thus opening a possibility to obtain the protein in sufficient amounts to perform *in vitro* experiments.

5.2 Materials and Methods

5.2.1 Materials

NaCl, Tris Base, $MgCl_2$, Triton X-100 and n-octyl-β-D-glucopyranoside were obtained from Calbiochem (Darmstadt, Germany). Dithiothreitol (DTT) and Tris(2-carboxyethyl)phosphine (TCEP) were purchased from Sigma-Aldrich (St. Louis, MO). Anti-ATG9 FL (STO219) and anti-ATG9 CT (STO215) antibodies were kindly provided by Dr. Sharon Tooze (Cancer Research UK, London Research Institute, London, UK). Goat anti-rabbit and anti-6xHis antibodies were from Clontech (Mountain View, CA). Ni-NTA Agarose was purchased from Qiagen (Hilden, Germany).

5.2.2 DNA Constructs

Plasmids for expression of human ATG9 (pCMV6XL4-hATG9) were kindly provided by Dr. Sharon Tooze (Cancer Research UK, London Research Institute, London, UK). ATG9 C-terminal domain was generated as a deletion mutant from ATG9. Specifically designed ATG9 primers for mutations, cloning and sequencing, purchased from Sigma Aldrich (Madrid, Spain) were used (See Section 2.3.5). Mutations were confirmed by DNA sequencing (Secugen S.L, Madrid, Spain).

5.2.3 Expression and Purification of Recombinant Proteins

hATG9 C-terminal (ATG9 CT) fragment was purified from soluble fractions of bacterial extracts obtained in the absence of detergents, and purity was evaluated by Coomassie-stained SDS-PAGE. Full length ATG9 (ATG9 FL) and ATG9 CT were also expressed by baculoviral infection of HighFive (H5) insect cells. ATG9 FL and ATG9 CT in pFASTBAC HTa and pFASTBAC1 plasmids respectively were used to transform

DH10Bac *E. coli* for transposition into the bacmid. Blue/white colony selection was used to identify colonies containing the recombinant bacmid and they were confirmed by PCR. The recombinant bacmid was then isolated and purified using Macherey Nagel endotoxin-free DNA purification kit. H5 insect cells were transfected with purified bacmid using Lipofectamine from Invitrogen (Waltham, MA) in TC-100 insect media (Sigma-Aldrich) supplemented with the appropriate antibiotics. When the transfected cells demonstrated signs of late stage infection (typically around 72 h), the medium containing the free virus was collected. Repeated cycles of transfection and virus collection were performed to amplify the viral stock. Cells were collected after 48 h infection followed by centrifugation at 5,000 xg for 10 min. The pellet was resuspended and sonicated in a breaking buffer consisting of 50 mM Tris pH 8, 150 mM NaCl and freshly prepared 1mM TCEP and protease inhibitors. The lysate was cleared by 30 min centrifugation at 30,000 xg and loaded on cobalt resin (Clontech, Mountain View, CA) for 3 h at 4 ºC. Protein was eluted with a gradient of 0-500 mM imidazole.

ATG9 CT plasmid was transformed onto *E. coli* one shot BL21 Star (DE3) cells. Cells were grown to OD_{600}=0.6 and induced with 0.5 mM IPTG overnight at 18 ºC. Following centrifugation at 5,000 xg for 10 min, the pellet was resuspended and sonicated in breaking buffer [50 mM sodium phosphate, 300 mM NaCl, 1 mM DTT, 0.1 mM PMSF, 1 mg/ml lysozyme and EDTA-free protease inhibitors (Roche), pH 8.0]. The lysate was cleared by 30 min centrifugation at 30,000 xg, loaded on Ni-NTA beads (Sigma-Aldrich) and incubated for 3 h at 4 ºC. Proteins were eluted with elution buffer (50 mM sodium phosphate, 525 mM NaCl, 250 mM imidazole, pH 6.0 and freshly added 1 mM DTT). The eluted fractions were loaded onto SDS-PAGE gels and subjected to CBB-staining and Western blotting. Then these fractions were dialyzed against 20 mM Pipes, 137 mM NaCl, 3 mM KCl (pH 6.8) and loaded into a Hiload 16/600 Superdex-75 size exclusion column. The protein was eluted with the same buffer used for the dialysis.

5.2.4 Lipid Extraction from Protein Samples

Lipid extraction for mass spectrometry analysis was performed as follows: 500 µl protein sample was mixed with 6 ml chloroform:methanol (2.5:1) in a glass tube and kept on ice. The mixture was sonicated for 10 s at 22 microns and kept at room temperature for phase stabilization. The sample was filtered using 0.22 µm filters (GV filters, Millipore) and transferred to glass centrifuge tubes with 0.2 volumes of K_4EDTA (pH 6). The mix was subjected to 200 rpm, 15 min at 4 ºC centrifugation. After that, two

different phases were observed, aqueous (top) and organic (bottom), the latter containing the extracted lipids. The organic phase was transferred to another glass tube and dried under N_2 at 37 ºC. Then the sample was resupended in 100 µl chloroform:methanol:water (5:5:1), transferred to an HPLC vial with 40 µl lipid standard and dried under N_2 gas flow. Finally, the sample was resuspended in 18 µl chloroform:methanol:water (90:9.5:0.5) for its application to HPLC and mass spectrometry.

5.2.5 Mass Spectrometry Analysis of Lipids

Mass spectrometry was used for the lipid analysis of ATG9 CT and PITPα protein samples. Samples obtained from lipid extraction and a control sample containing only the lipid standards were subjected to the mass spectrometer-associated HPLC, in order to separate the different compounds and proceed to mass spectrometry analysis.

The HPLC solvents were:

A: 135 ml chloroform, 14 ml methanol, 1 ml water and 51 µl ethylamine.
B: 30 ml chloroform, 35 ml methanol, 5 ml water, 30 ml acetonitrile and 45 µl ethylamine.

2 µl samples were used for each mass spectrometry analysis, and the following analyses were performed for each sample:

Analysis Number	Analysis Name	Observations
1	Q1-	Solvent A equilibration
2	Q1-	Solvent A equilibration
3	Q1-	Solvent A equilibration
4	Q1- PIP	Standards
5	Q1+	Standards
6	241 PI	Standards
7	184 PC	Standards
8	153 PA	Standards
9	196 PE	Standards
10	87 PS	Standards
11	Q1-	Solvent A wash
12	Q1-	Solvent A wash
13	Repeat 4-10 for each sample	Analysis 4-10 for each extracted sample

Table 5.1. Detailed description of the analyses performed by mass spectrometry.

In order to detect the presence of PG in the analysed samples, a different program was used. A new PG standard was incorporated to the samples and the following program with a specific analysis for PG was run:

Analysis Number	Analysis Name	Observations
1	Q1-	Solvent A equilibration
2	MI-PG	Standards
3	Q1-	Solvent A equilibration

Table 5.2.Specific program for PG detection by mass spectrometry.

Mass Spectrometry analysis was performed on a Shimadzu IT-TOF LC/MS/MS system hyphenated with a five-channel online degasser, four-pump, column oven and autosampler with cooler (Prominence HPLC, Shimadzu). To identify and quantify molecular species we used accurate mass (mass accuracy 5 ppm) and tandem MS, as well as comparison with appropriate lipid standards. IT-TOF mass spectrometer operation conditions: ESI interface voltage +4.5kv for positive ESI and -4kv for negative ESI, heat block temperature 230 ºC, nebulising gas flow 1.4 L/min, CDL temperature 210 ºC, drying gas pressure 100 psi. All solvents used for lipid extraction and LC/MS/MS analysis are LC-MS grade from Fisher Scientific.

5.2.6 Cell Inmunofluorescence

Hi5 cells were plated on 12 mm glass disks and infected as detailed in **Section 2.3.6**. At 24, 48 or 72 h post-infection cells were washed twice with PBS 1X and fixed with 3% *p*-formaldehide solution for 10 min. After fixation cells were permeabilised using 0.01% (v/v) Triton-X-100 in PBS 1X for 3 min and blocked with 10% FCS in PBS 1X for 1 h at room temperature. Following this step, the glasses were incubated with anti-6xHis, anti-ATG9 FL or anti-ATG9 CT for 1 h at 37 ºC. After 6 washes with PBS 1X, they were incubated with Alexa-488 conjugated goat anti-rabbit or anti-mouse antibodies under the same conditions. Nuclei were stained using 4',6- Diamidino-2-phenilindol (DAPI, Sigma) and the glasses were fixated to the glass slides with ProLong (Invitrogen). The samples were visualized using a confocal fluorescence microscope (Nikon D-ECLIPSE C1, Nikon, Melville, NY). Image treatment was performed using the EZ-C1 3.20 software (Nikon).

5.3 Results

5.3.1 ATG9 CT Bacterial Expression, Purification and Lipid Mass Spectrometry Analysis

hATG9 is a multispanning membrane protein required for normal autophagy. As stated in the **Introduction section**, ATG9 might deliver lipids as membrane material for autophagosome formation and elongation. As ATG9 consists of 6 transmembrane domains a difficult expression and purification was envisaged. In order to manage this issue, a construct was designed containing the C-terminal domain which covered almost half of the protein (36.9 kDa) (**Figure 5.1**). This C-terminal domain does not contain any putative transmembrane domain, so it could be predicted as a large soluble region of the protein that might be at least partially responsible for the ATG9 function.

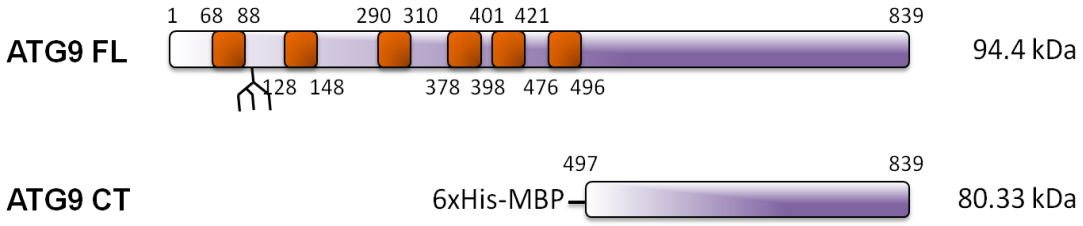

Figure 5.1. Outline of Atg9 FL and CT proteins. The orange sections correspond to the transmembrane regions. Violet denotes exposed regions.

Many different constructs, plasmids, tags, bacterial strains and expression conditions were tested for ATG9 FL and CT expression, but just one of them was considered as relatively satisfactory. No expression of ATG9 FL was detected under any condition tested, perhaps because this protein may be toxic when overexpressed in a bacterial system. However, the ATG9 CT construct cloned in a pEXP11085-HisMBP plasmid was slightly expressed in *E. coli* One shot BL21 Star (DE3), although high degradation was observed. This HisMBP tagged ATG9 CT fragment was affinity purified using Ni-NTA beads and a subsequent pass through a size exclusion column. The eluted fractions were loaded onto SDS-PAGE gels and protein was detected by CBB-staining and Western blotting (Anti-His and Anti-ATG9 CT antibodies) (**Figure 5.2 A-B**). Together with a large amount of degraded protein some ATG9 CT remained intact in certain fractions but probably not in its monomeric state, because the protein

eluted as a larger protein in the column. Finally, a monoQ chromatography was performed to obtain some purer fractions of the ATG9 CT fragment (**Figure 5.2 C-D**). Further modifications of the expression conditions and purification protocol were tested but no better results were obtained.

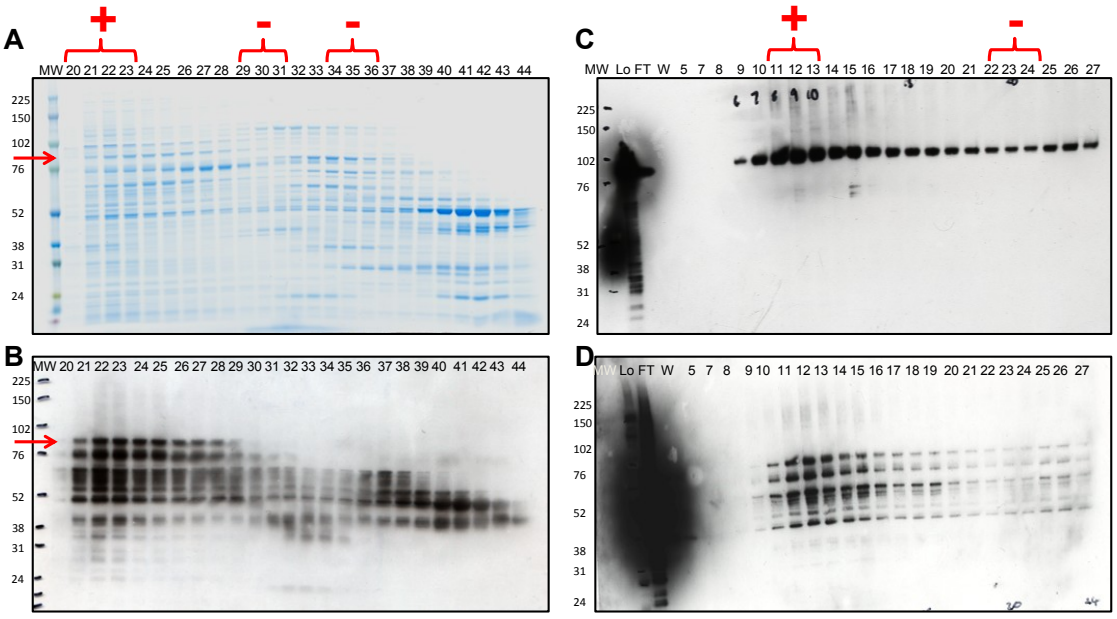

Figure 5.2. ATG9-CT purification steps. (A) Gel filtration chromatography SDS-PAGE stained with coomassie blue. A small band between 76 and 102 kDa markers corresponds to ATG9 CT. **(B)** Anti-6xHis Western blot of the gel filtration chromatography fractions. Protein degradation could be observed. **(C)** MonoQ chromatography of ATG9 CT-containing fractions selected from the gel filtration. Anti-ATG9 CT Western blot. **(D)** MonoQ chromatography of ATG9 CT-containing fractions selected from the gel filtration. Anti-6xHis western blotting. The square brackets with a positive sign are the ATG9 CT-containing fractions subjected to mass spectrometry, whereas those that are indicated with a negative sign are the ATG9 CT-non containing fractions. Molecular weight markers are shown at the left-hand side of each panel. The ATG9 CT position in the gel is indicated by a red arrow. Molecular masses are shown in kDa on the left-hand side.

A preliminary study of the presence of lipids associated to the ATG9 CT domain was performed by mass spectrometry. To this aim we divided the elution fractions from the size exclusion and monoQ chromatography into ATG9 CT-containing and non-containing fractions, subjecting both types of samples to a modified Folch lipid extraction. At the end of the lipid extraction a mix of lipid standards was added to the samples to have an internal standard and an estimation of the detection quality and lipid quantity. Phosphatidylglycerol was the only lipid class found associated to ATG9. Different species of phosphatidylglycerol were detected in all the ATG9 CT-containing fractions (**Figures 5.3** and **5.4**), the mol% distribution of each species being the same

in all the fractions (**Figures 5.4** and **5.5**). Nevertheless, the ATG9 CT-non-containing fractions did not show any presence of phospholipids (**Figures 5.3** and **5.4**). Detection of PG in the sample could be explained because it is the predominant phospholipid in bacterial membranes. Moreover in order to have a positive control of a lipid carrier protein, we purified PITPα (Phosphatidylinositol Transfer Protein alpha) and, as described (Garner *et al.*, 2012), phosphatidylglycerol and phosphatidylserine were detected (**Figure 5.6**). Taking this into account, we would suggest that the ATG9 CT might be in contact with membranes either continuously or transiently. The presence of lipids in the protein sample might indicate, as in the case of PITP, a lipid carrier function, and the ATG9 CT-associated lipids might recapitulate some contacts with the membrane. However further improvements in the expression and purification of ATG9 CT should be performed to confirm the above results.

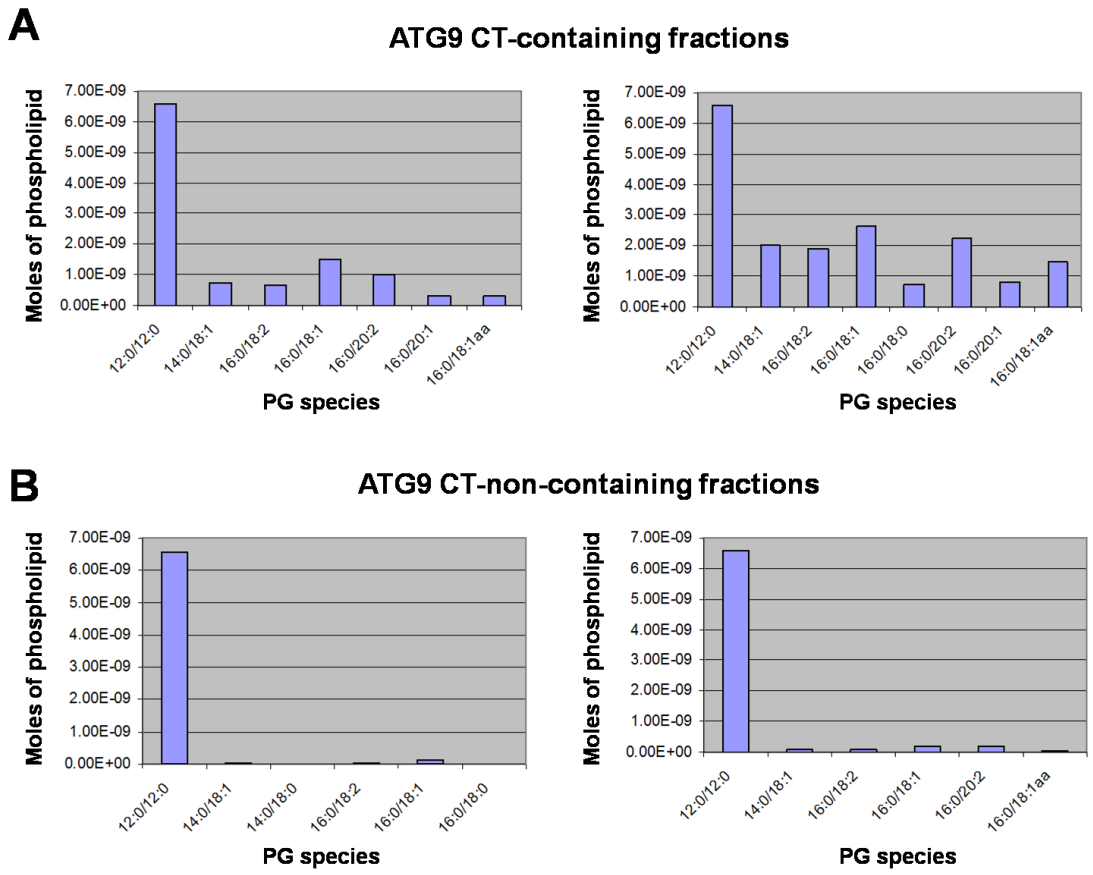

Figure 5.3. Mass spectrometry analysis of phospholipids in ATG9 CT protein sample. **(A)** Two different ATG9 CT-containing fractions were analysed and the main PG species detected. **(B)** Two different ATG9 CT-non-containing fractions analysed by mass spectrometry. Only trace amounts of phospholipids were detected. 12:0/12:0 PG species represents the internal standard added to each sample.

A

Gel Filtration. ATG9 CT-containing fractions	nmoles	mol %
16:0/20:2	1.971	17.085
16:0/18:1	1.662	14.406
16:0/18:1aa	1.367	11.845
16:0/20:1aa	1.196	10.365
14:0/18:1	0.947	8.206
16:0/18:2	0.940	8.150
18:0/20:2aa	0.885	7.668
16:0/20:1	0.458	3.968
16:0/18:0	0.295	2.555
18:0/20:2	0.244	2.114
16:0/18:0aa	0.234	2.030
12:0/18:0	0.212	1.835
16:0/20:0aa	0.202	1.747
18:0/20:1aa	0.199	1.728
14:0/18:0	0.165	1.433
16:0/20:2aa	0.123	1.063
Total	11.099	96.200

B

MonoQ. ATG9 CT-containing fractions	nmoles	mol %
16:0/20:2	2.650	17.185
16:0/18:1	2.299	14.904
16:0/18:1aa	1.890	12.254
16:0/20:1aa	1.654	10.723
14:0/18:1	1.309	8.490
16:0/18:2	1.300	8.431
18:0/20:2aa	1.224	7.933
16:0/20:1	0.633	4.106
16:0/18:0	0.373	2.415
18:0/20:2	0.337	2.188
16:0/18:0aa	0.323	2.091
12:0/18:0	0.293	1.899
16:0/20:0aa	0.279	1.807
18:0/20:1aa	0.276	1.788
14:0/18:0	0.211	1.369
16:0/20:2aa	0.170	1.100
Total	15.220	98.683

C

Gel filtration. ATG9 CT non-containing fractions	nmoles	mol %
16:0/18:2	0.039	27.998
16:0/18:1	0.090	64.267
16:0/18:0	0.011	7.736
Total	0.140	100.000

Figure 5.4. PG species detected by mass spectrometry. Main species detected in samples from gel filtration **(A)** and monoQ chromatography **(B)** containing and non-containing ATG9 CT **(C)** nmoles detected and the % of the total of the sample for each species are detailed.

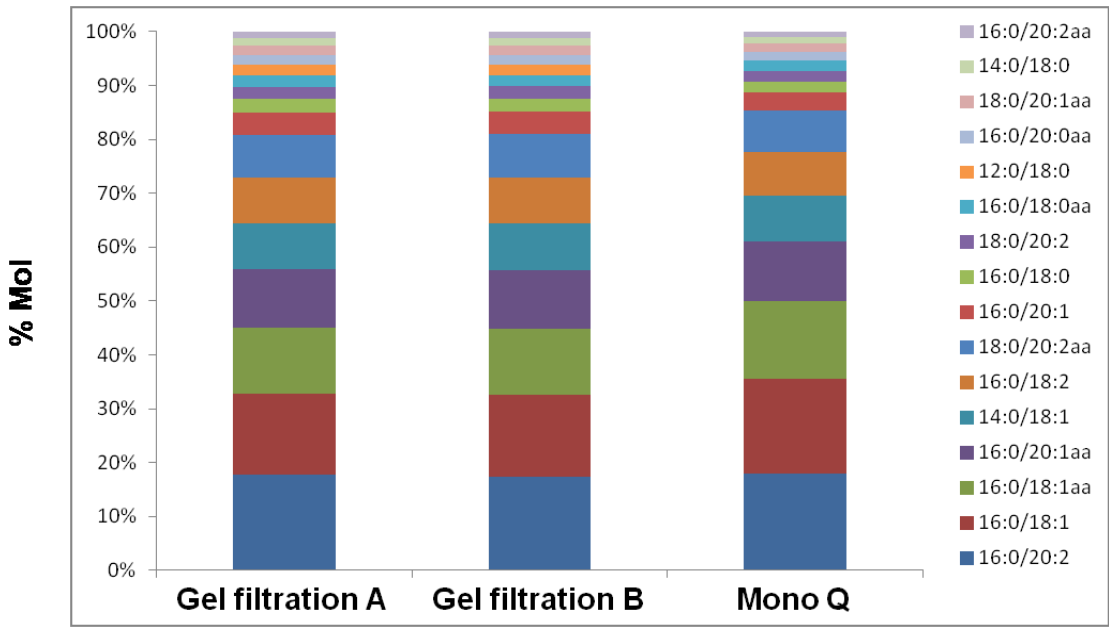

Figure 5.5. PG species detected in ATG9 CT fractions. Each bar corresponds to a different sample analysed by mass spectrometry. PG species are coloured and ordered according to their relative abundance.

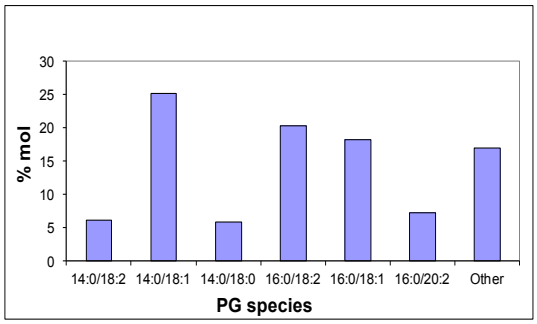

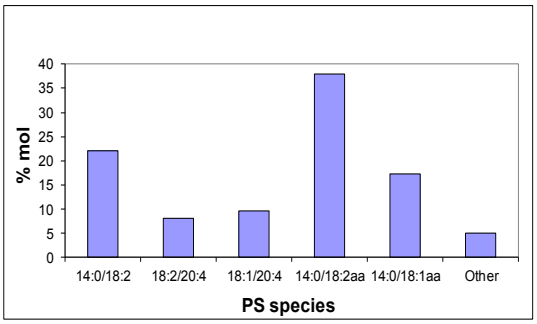

PG

Lipid	mass	area	ug	mole	%
12:0/12:0	609	8.08E+07	4	6.56814E-09	
14:0/18:2	717	6.28E+07	3.108910891	4.336E-09	6.171791688
14:0/18:1	719	2.57E+08	12.72277228	1.76951E-08	25.1869166
14:0/18:0	721	5.91E+07	2.925742574	4.0579E-09	5.775944178
16:0/18:2	745	2.15E+08	10.64356436	1.42867E-08	20.33541118
16:0/18:1	747	1.94E+08	9.603960396	1.28567E-08	18.30003411
16:0/20:2	773	7.90E+07	3.910891089	5.05937E-09	7.20142378
Other					17.02848
				Total	**5.82917E-08**	**82.97152154**

PS

Lipid	mass	area	ug	mole	mole %
12:0/12:0	622	1.56E+06	4	6.43087E-09	
14:0/18:2	730	6.14E+06	15.74358974	2.15666E-08	21.99162172
18:2/20:4	806	2.52E+06	6.461538462	8.0168E-09	8.174802039
18:1/20:4	808	2.96E+06	7.58974359	9.39325E-09	9.578380733
14:0/18:2aa	716	1.04E+07	26.66666667	3.72439E-08	37.97799759
14:0/18:1aa	718	4.72E+06	12.1025641	1.68559E-08	17.18815653
Other					5.0890414
			Total	**9.30765E-08**	**94.91095862**

Figure 5.6. Mass spectrometry analysis of phospholipids in PITP protein sample.

5.3.2 ATG9 FL and CT Expression in Insect Cells

The results of ATG9 CT expression in bacteria and its possible association with membranes encouraged us to try other expression systems in order to reproduce and pursue our observations. The human origin of ATG9 indicates that we would get the best expression in a mammalian system, but the good results obtained for ATG7 expression (**Chapter 3**) led us to use insect cells. The Baculovirus expression system incorporates more post-translational modifications in proteins than the prokaryotic cells.

ATG9 FL and ATG9 CT were cloned into pFastBac1 and pFastBacHta plasmids respectively for overexpression in insect cells. Both of them were successfully expressed and optimization of the infection time and MOI were performed (**Figures 5.7** and **5.8 A-B**).

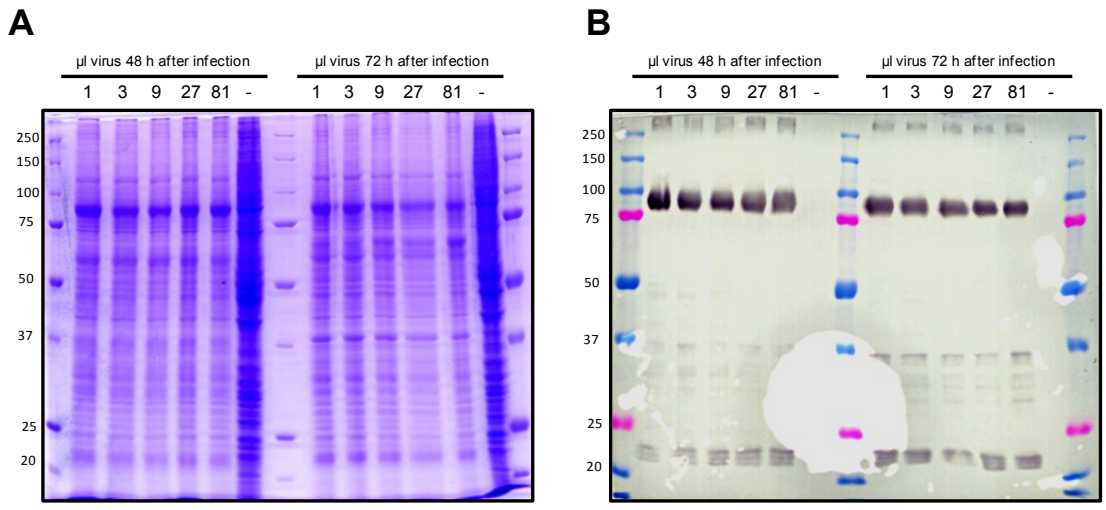

Figure 5.7. ATG9 FL expression in insect cells. Infection time and MOI optimization for ATG9 FL expression. ATG9 FL expression was followed by SDS-PAGE **(A)** and Western blotting anti-Atg9 FL **(B)**, under different infection times and MOI. ATG9 FL is observed as a band around 90 kDa. Molecular masses are shown in kDa on the left-hand side.

Then ATG9 CT containing a His-tag in its N-terminal end was subjected to purification using cobalt beads. Unfortunately the protein was insoluble and remained almost completely in the pellet fraction after cell disruption (**Figure 5.8 B**). Some attempts with lower expression temperatures and the use of detergents in the purification process were tried in order to obtain soluble ATG9 CT but no improvements were observed. The insolubility of the protein would reside in the incorporation to inclusion bodies or the association to cell membranes that would bring it the pellet fraction upon cell disruption.

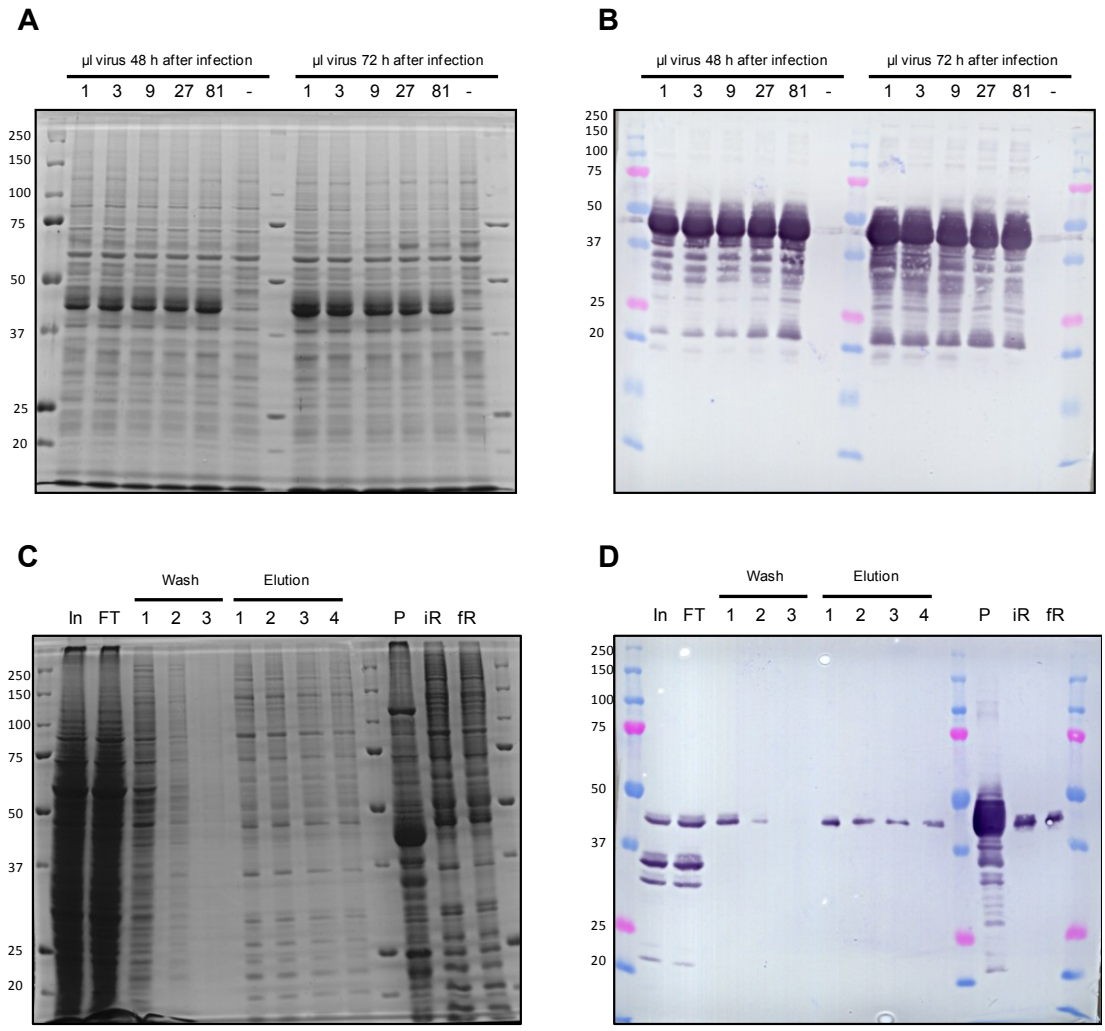

Figure 5.8. ATG9 CT expression and purification from insect cells. (A, B) Infection time and MOI optimization for ATG9 CT expression. ATG9 CT expression was followed by SDS-PAGE **(A)** and anti-ATG9 CT Western blotting **(B)**, under different infection times and MOI. **(C)** SDS-PAGE gel of ATG9 CT purification using Ni-NTA beads. **(D)** Anti-ATG9 CT Western blotting of the nickel affinity purification of ATG9 CT. ATG9 CT is observed as a band around 45 kDa. Molecular masses are shown in kDa on the left-hand side. (FT: Flow-Through; P: Pellet; iR: Resin before elution; fR: Resin after elution; In: Input).

With the purpose of detecting the localization of the protein within the cell after overexpression, cell immunofluorescence was performed. Anti-His and anti-ATG9 CT antibodies were used to visualize the protein and DAPI for the nuclei. It could be observed that ATG9 CT was located mainly associated to cell membranes which partly explained its behaviour as an insoluble protein during its purification (**Figure 5.9** upper panels). ATG9 FL-expressing insect cells were also subjected to immunofluorescence to know where the protein was located. ATG9 FL showed the same behaviour as the CT fragment, appearing associated to membranes, with only a small fraction in the cytoplasm (**Figure 5.9** lower panels).

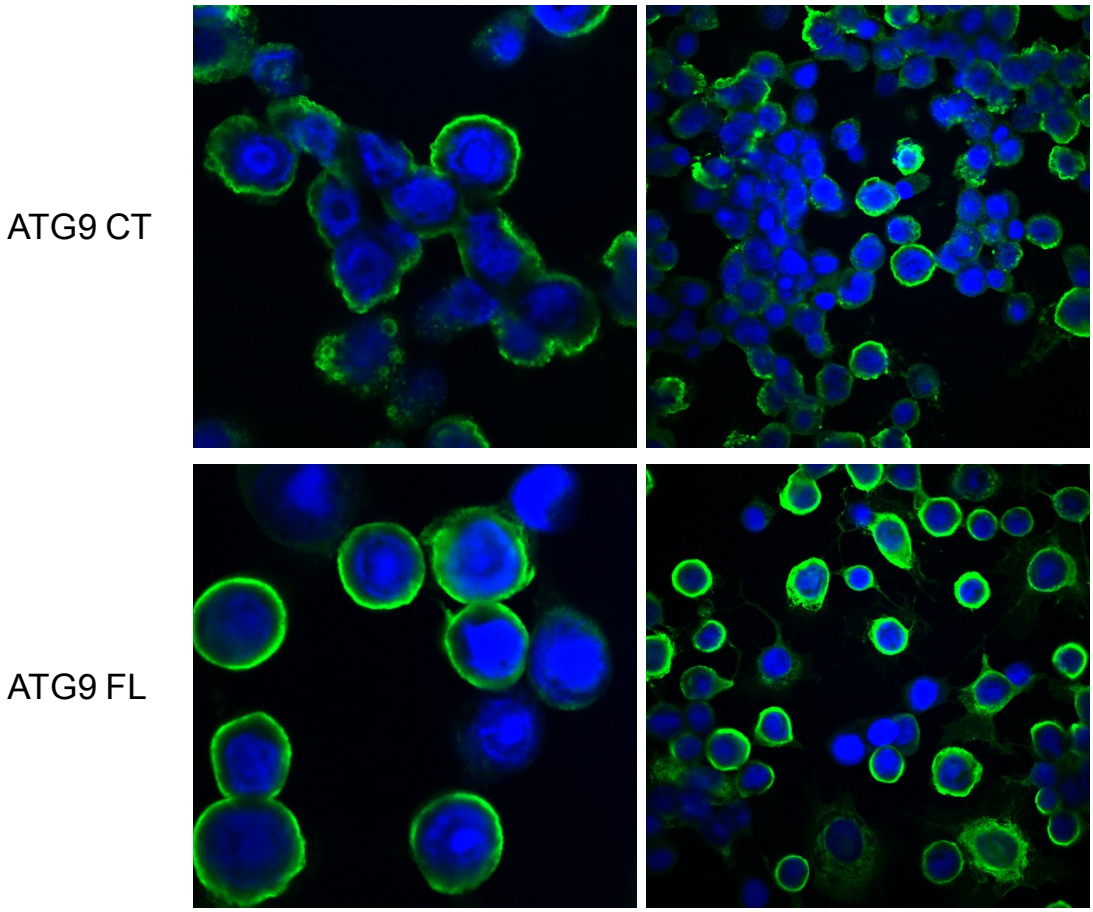

Figure 5.9. ATG9 FL and CT cells inmunofluorescence. ATG9 CT (green, upper panels), and ATG9 FL (green, lower panels) expressed in Hi5 insect cells were immunofluorescence labelled. The localisation of both proteins in cells was detected by confocal microscopy. Cell nuclei are labelled with DAPI (blue).

In light of the above results we conclude that the use of insect cells as a more sophisticated system to express ATG9 may be satisfactory, but the purification of the full length or C-terminal fragment would need some modifications and improvements due to the membranous character of this protein.

5.4 Discussion

ATG9 is an essential and scarcely studied protein involved in cell macroautophagy. The role of this protein has been mainly explored *in vivo*, but little information about its function is available. Yeast autophagy is the most used system for the study of Atg9, revealing important results about the movement of the protein from a pool of very motile vesicles around the cytoplasm to the outer autophagosomal membrane (Yamamoto *et al.*, 2012). Atg9 function in mammals has been less investigated, although some studies about the trafficking of Atg9 between TGN and recycling endosomes (Young *et al.*, 2006), and the transient association to the autophagosome have been emerged. Because of this lack of knowledge on Atg9 function *in vivo*, and complete absence of data on Atg9 *in vitro*, this protein is an interesting object in the field of cell autophagy.

As mentioned in the **Introduction section**, Atg9 is the only transmembrane protein described so far in autophagy (Lang *et al.*, 2000; Noda *et al.*, 2000). The cytosolic C-terminal domain of the protein covers almost 40 kDa (**Figure 5.1**), which might indicate that the protein would act through this region. Furthermore, according to the published data Atg9 might be involved in the delivery of membrane material to the autophagosome nucleation and growth through fusion events of ATG9 vesicles (Stanley *et al.*, 2014; Suzuki *et al.*, 2015).

In this chapter, we have contributed to the *in vitro* study of ATG9 function. We first tried to express the full length and the C-terminal domain of ATG9 in *E. coli*, in order to perform studies with model membranes. Unfortunately we only got low expression levels of ATG9 CT with some degradation of the protein and purification of ATG9 CT was poor (**Figure 5.2**). Thus, we were unable to use the protein for the assays with model membranes, instead it was checked whether this fragment of protein could really be associated to membranes and perhaps could contain bound lipids. For this purpose, mass spectrometry of the lipids extracted from ATG9 CT-containing fractions was performed and compared with PITPα as a positive control of a lipid carrier protein (**Figure 5.6**). The results showed that PG was present in the samples where ATG9 CT domain was present (**Figures 5.3-5**) which might indicate a possible association of this region to the membrane or even that the fragment acts as a lipid carrier, in the way of the PITPα protein. However, the lack of purity of the samples does not allow us to establish a more solid conclusion about how ATG9 could participate in the delivery of lipids for autophagosome elongation.

We also tried to express and purify ATG9 FL and CT from insect cells, a more evolved organism that incorporates some more post-translational modifications to the proteins. High expression of both variants was achieved (**Figures 5.7** and **5.8 A-B**) but ATG9 CT was not soluble for its purification (**Figure 5.8 C-D**). Despite of the insolubility of the protein, further attempts to solubilise ATG9, either with detergents or otherwise, must be performed in order to obtain an appropriate amount of protein to carry out *in vitro* studies. Moreover, extraction or purification of ATG9-containing vesicles directly from cells could reveal the lipid composition of these vesicles and shed light on how this could contribute to the autophagosome membrane lipidome.

To sum up, ATG9 is an interesting and important protein to be studied both *in vivo* and *in vitro* due to its transmembrane character. In the present study we have taken the first steps in the recombinant ATG9 expression and purification for its future use with model membranes in order to perform aggregation or fusion assays. Moreover we have also obtained preliminary results on the presence of phosphatidylglycerol associated to the C-terminal domain of ATG9. Future experiments in this context could be very relevant in the understanding of ATG9 structure-function.

6. Overview and Conclusions

Resumen y Conclusiones

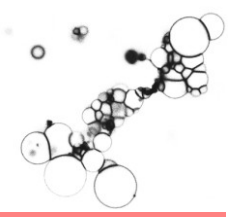

CHAPTER 6:

Overview and Conclusions

Overview

Cell homeostasis requires a correct balance between catabolic and anabolic processes. Many different pathways are involved in biosynthetic functions or possess catabolic responsibilities. Autophagy can participate in both kinds of pathways, being essential to degrade unnecessary or damaged organelles (catabolism) and also to produce new building blocks through mobilization of diverse cellular energy and nutrient sources such as lipids, carbohydrates or iron (anabolism) under normal or starvation conditions. Autophagy participates also in a large variety of physiological processes such as viral infection, cell differentiation and development, or immunity, causing certain disorders when it is deregulated (Wirawan *et al.*, 2012).

As a regulation process of many housekeeping events in the cell, autophagy is connected to several human disorders, especially to neurodegenerative diseases such as Huntington´s, Parkinson´s and Alzheimer´s diseases (Lynch-Day *et al.*, 2012; Martinez-Vicente *et al.*, 2010; Nixon *et al.*, 2005). These disorders are related to the accumulation of protein aggregates that would not occur under normal autophagy conditions. Moreover, cancer, aging and other metabolic disorders are somehow regulated by autophagy and therefore it is a promising target for the prevention and treatment of these conditions (Choi *et al.*, 2013; Levine & Kroemer, 2008).

In the autophagy signalling pathway several proteins are involved, mainly participating in complexes that regulate specific steps in the formation of a double membrane organelle called autophagosome. This one is the key event taking place in

autophagy, although the lipid source for this newly formed membrane is still unknown (Tooze & Yoshimori, 2010). Mitochondria, plasma membrane, Golgi or ER are postulated to supply materials for the initial nascent membrane (Mari *et al.*, 2011). The material susceptible to be degraded is enclosed in this pre-formed compartment which grows by adhesion and fusion of other membrane structures. Finally, autophagosome closes in a recently described scission process (Knorr *et al.*, 2015) and fuses with the lysosome to degrade the trapped material. Several studies have proposed the specific participation of two UBL systems (Atg8/Atg3/Atg7 and Atg5-Atg12/Atg16), among the various Atg proteins, in vesicle fusion processes that give rise to the phagophore extension (Nair *et al.*, 2011; Romanov *et al.*, 2012; Walczak & Martens, 2013; Weidberg *et al.*, 2011). Others have described the presence of a unique autophagic transmembrane protein (Atg9) that is essential for autophagy in yeast and mammalian organisms (Noda *et al.*, 2000; Webber *et al.*, 2007).

However how the autophagosome grows and is finally sealed are key open questions that are now being studied. For this reason the subject of study in this thesis has been to contribute to a better understanding of the autophagosome elongation process and also to reproduce its growth *in vitro*. To this aim, biophysical techniques and model membranes have been handled to (i) analyze the role of the human Atg8/ATG3/ATG7 UBL system in vesicle tethering and fusion processes and how they can be modulated by lipids, and (ii) to characterize the lipid-protein interactions of the autophagic protein ATG3. Moreover a preliminary study of ATG9, a promising transmembrane protein probably involved in lipid delivery for autophagosome growth, has been performed.

Lipid Regulation of Fusion Events Triggered by a Reconstituted Minimal Protein System (Atg8/Atg3/Atg7) Involved in Autophagosome Elongation

In the current autophagy model, the most accepted hypothesis about phagophore elongation proposes that small vesicles reach the forming organelle and fuse so that it grows. According to that, yeast Atg8, the final effector of the UBL system, has been demonstrated to participate in vesicle tethering, hemifusion and fusion events *in vitro* (Nair *et al.*, 2011; Nakatogawa *et al.*, 2007). However human Atg8 homologues (LC3 and GATE-16) have only shown fusogenic activity in their artificially conjugated forms (Weidberg *et al.*, 2011). All of them catalyze these processes through their lipidated form (conjugated to PE), that constitutes their way to attach to the membrane.

Taking this into account we have shown here the *in vitro* fusogenic activity of the complete human UBL system comparing it with the artificial one, and demonstrated the lipid geometry and bilayer curvature modulation of the LC3, GATE-16 and GABARAP-induced fusion.

Human Atg8 homologues reproduce the *in vitro* enzymatic lipidation reaction similarly to what was described for yeast (**Figure 3.7 D**). However the lipidation reaction efficiency is apparently lower than in yeast. This fact could be due to the necessity of specific lipid compositions or the presence of the Atg5-Atg12/Atg16 UBL system as it occurs *in vivo*. It might also be due to the fact that 7 human homologues exist versus only one in yeast, a lower activity of each one of them being perhaps required. Furthermore, as recently reported (Nath *et al.*, 2014), a presumably adenylated form of the Atg8 homologues is observed and hampers the detection of LC3-PE and GATE-16-PE conjugates in SDS-PAGE gels by CBB staining or Western blotting. Accordingly we have developed the use of NBD-labeled PE to solve this issue and to allow a correct detection (**Figure 3.7 D**). The chemical lipidation of these proteins resembles closely the enzymatic one.

To gain information on the initial steps of the fusion process, vesicle tethering assays were performed. According to the commonly accepted stalk-fusion pore model (Basañez *et al.*, 1998; Chernomordik & Kozlov, 2008; Chernomordik *et al.*, 1995; Khattari *et al.*, 2015; Siegel, 1999), membranes first approach and make local contacts in order to remove the water in between. GATE-16 and GABARAP, in our experimental context, show a high membrane aggregation activity in both the enzymatic and chemical conjugation systems, whereas LC3 is less active than its homologues (**Figure 3.8**).

The vesicle tethering activity itself does not recapitulate hemifusion nor fusion of membranes. Prior *in vitro* studies with the recombinant yeast Atg8 reported that this protein mediates membrane hemifusion, but not complete fusion (Nakatogawa *et al.*, 2007). Closer to our system, Weidberg *et al.*, (2011) showed that mammalian LC3 and GATE-16, artificially attached to PEmal, induced full membrane fusion, and moreover Nair *et al.*, (2011) showed that Atg8 and LC3 require high contents of DOPE to drive membrane hemifusion. In our enzymatic system both GATE-16 and GABARAP induce intervesicular total lipid mixing, inner lipid mixing and aqueous content mixing, that correlates with the capacity of these proteins to mediate full membrane fusion (**Figure 3.9**). Similar results display the chemically lipidated forms of GATE-16 and GABARAP (**Figure 3.12**). This fact allows us to conclude that the proteins are correctly folded after

the chemical conjugation and faithfully reproduce the activity of the wild type forms. As previously suggested and shown in our experiments, not all the different human Atg8 homologues display the same *in vitro* activity. This could indicate the participation of each protein at different time points during phagophore growth or even under different physiological conditions. These results indicate perhaps the first evidence of the *in vitro* fusion activity of GABARAP, and also provide a complete *in vitro* study of the fusogenic potential of three human Atg8 homologues acting through their corresponding enzymatic machinery.

As other membrane-related processes, vesicle fusion can be notably regulated by lipids. Many evidences on how lipids with different morphologies and intrinsic curvatures modulate fusion events have been described (Basañez *et al.*, 1996b, 1998). In Atg8-driven membrane fusion the incorporation of cone-shaped lipids with a negative intrinsic curvature such as cardiolipin or diacylglycerol stimulates intervesicular lipid mixing and the mixing of aqueous contents, whereas the addition of inverted cone-shaped lipids completely inhibits both processes (**Figure 3.11**). These results are consistent with the stalk-fusion pore model which assumes that the inclusion of lipids with negative intrinsic curvature favours the hemifusion intermediate and thus fusion event progression. In this context and in contrast to studies that suggest that non-physiological DOPE concentrations (55%) are necessary to promote fusion by these proteins (Nair *et al.*, 2011), our chemical conjugation system shows vesicle fusion under physiological amounts of DOPE (30%) supplemented by 10% of a conical-shape lipid (**Figure 3.13**). Furthermore, the predicted fusion events that govern autophagosome elongation would take place in highly curved regions on the edge of the isolation membrane, perhaps with a specific lipid composition, or enriched in fusogenic proteins, and small vesicles would participate. Consistent with this GATE-16 and GABARAP promote membrane fusion to a greater extent when vesicle size decreases (**Figure 3.12**). Interestingly a spectacular growth of liposomes shown by cryo-EM is promoted by our human Atg8 homologues-induced membrane fusion events, thus providing a rough visual reproduction of the autophagosome elongation process *in vitro* (**Figure 3.10**). Further experiments combining our system with Atg5-Atg12/Atg16 would provide a better understanding of the *in vivo* features of the process.

ATG3, the E2-like Enzyme of the UBL System, Interacts with and Tethers Negatively-charged Membranes, Possibly Governing the Human Atg8-Homologue Lipidation

Given the participation of the human Atg8 homologues in vesicle fusion processes involved in autophagosome elongation, the question arises of how these proteins sense or are recruited to this forming membrane. Previous studies have suggested that both Atg3, the last enzyme involved in the Atg8 UBL system, and the Atg5-Atg12/Atg16 system are involved in membrane recognition and catalyze the lipidation process *in vivo* (Nath *et al.*, 2014; Romanov *et al.*, 2012; Sakoh-Nakatogawa *et al.*, 2015). Other proteins involved in autophagy have been described to recognize specific lipids or features in the membrane, such as phosphoinositides (WIPI1-2) (Dooley *et al.*, 2014) or membrane curvature (Barkor) (Fan *et al.*, 2011), that facilitate the lipidation or fusion processes respectively. In this context, a recent paper has shown that mouse ATG3 possesses a predicted N-terminal amphiphatic α-helix that would act as a membrane curvature sensor, and that mutations in this region modulate the lipidation ratio of GABARAP-L1 *in vitro* and *in vivo* (Nath *et al.*, 2014). This provides evidence that ATG3 participates in membrane recognition in order to cause Atg8 lipidation. According to this, we have used biophysical techniques to assay the affinity of human ATG3 to model membranes in order to gain further knowledge of how this protein detects and interacts with the membrane previously to Atg8 lipidation.

ATG3 shows a strong affinity to negatively-charged membranes compared to neutral ones as the Langmuir balance, floatation and GUV studies reveal (**Figures 4.2, 4.3 and 4.8**). In addition the presence of anionic phospholipids in the membrane eliminates the high DOPE (55%) and small-sized vesicle requirements for ATG3 binding proposed by Nath *et al.*, (2014) (**Figure 4.3 A-B**). Additionally a high preference for cone-shaped and negatively-charged lipids such as CL and PA is observed (**Figure 4.3 C**), suggesting a dual component in ATG3-membrane interaction, electrostatics (negative charge) and membrane defects (created by lipids with negative intrinsic curvature). Consistent with these results and assuming that human ATG3, almost identical to mouse ATG3, contains the same predicted amphiphatic helix in its N-terminal region, the implication of this α-helix in the membrane association was assessed. Two lysines (K9 and K11) delimiting the hydrophobic and hydrophilic faces of the helix might accommodate in between the polar headgroups (near the phosphates) and the hydrophobic tails of the phospholipids in the membrane, i.e. at the membrane-water interface. ATG3 K9D/K11D mutant loses the ability of the wild-type

protein to bind neutral or anionic vesicles, probably due to charge repulsion with the negative environment in the region mentioned above (**Figure 4.3 A**). However, peptides covering this ATG3 N-terminal helix do not reproduce the complete protein activity (**Figure 4.4**), as a likely consequence of the involvement of other regions of the protein, or perhaps because the isolated peptides do not exhibit an α-helical conformation.

There are publications indicating that the presence of negatively-charged phospholipids (i.e. PI, PS or PG) in model membranes favours the lipidation ratio of Atg8 *in vitro* (Ichimura *et al.*, 2004; Oh-oka *et al.*, 2008). Nevertheless, only one associates ATG3 binding to membranes with the efficiency of Atg8-PE conjugation (Nath *et al.*, 2014). Consistent with these evidences, we also proposed the role of ATG3 in directing Atg8 homologues to the membrane through insertion of the predicted α-helix, and moreover suggest that the ATG3 affinity for negatively-charged cone-shaped lipids might govern GABARAP lipidation efficiency at least *in vitro* (**Figure 4.10**). Some other components have been related to the conjugation machinery *in vivo* (Fujita *et al.*, 2008; Hanada *et al.*, 2007; Romanov *et al.*, 2012).

Different proteins including human Atg8 homologues, as we have demonstrated, participate in tethering and fusion processes along the AP growth (Diao *et al.*, 2015; Landajuela *et al.*, 2016; Romanov *et al.*, 2012). Additionally, as shown above (**Chapter 3**), these events can be modulated by the lipid composition of specific regions in the membranes. In this context ATG3 might participate in the vesicle fusion processes that accompany phagophore elongation. This proposal is based on the novel ATG3 activity proposed in this work, vesicle tethering. ATG3 promotes aggregation of anionic membranes and, to a lesser extent, of neutral membranes (**Figure 4.5**). Just as in ATG3-membrane interaction, the tethering activity is modulated by lipids that generate inverted hexagonal phases in the membrane (CL or PA) (**Figure 4.5 C**), and does not require highly curved membranes. However intervesicular lipid mixing or leakage is not observed (**Figure 4.6**) suggesting that ATG3 would help only in the vesicle approaching step that precedes full fusion.

From a different perspective, in the autophagosome elongation pathway the continuous arrival of new vesicles or even of lipids alone is currently proposed. For this purpose one or a few proteins should manage the movement of these vesicles to the growing organelle. ATG9 has been proposed to participate in this process and further *in vitro* experiments with model membranes should be performed in connection with

our preliminary results on recombinant human ATG9 expression and lipid binding by ATG9 C-terminal domain (**Figures 5.3-8**).

In summary the findings in this thesis shed light on the role of three different human Atg8 homologues in the fusion events taking place during autophagosome elongation. The enzymatically PE-conjugated forms of LC3, GATE-16 and GABARAP induce liposome fusion and this process can be modulated by the lipid geometry and membrane curvature, features that could be present in the edge of the nascent phagophore and rightly match with the proposed stalk-fusion model. Additionally ATG3, a component of the enzymatic reaction that produces the PE-conjugated forms, interacts specifically with anionic membranes, appears to modulate the lipidation efficiency and shows vesicle-tethering activity, all of which might be related to the fusion steps in autophagosomal growth catalyzed by the above-mentioned Atg8 homologues. Finally, preliminary results might suggest a possible involvement of the transmembrane protein ATG9 in the lipid delivery process that has been proposed for phagophore elongation.

Conclusions

1) LC3, GATE-16 and GABARAP human Atg8 homologues, enzymatically or chemically PE-conjugated, induce complete vesicle-vesicle fusion events modulated by the lipid geometry and membrane curvature. This process constitutes a minimal *in vitro* reconstitution model of the human autophagosome elongation process.

2) ATG3, the E2-like enzyme in the Atg8 conjugation system, strongly interacts with negatively-charged membranes through its predicted N-terminal amphiphatic α-helix, and also induces tethering of anionic vesicles. ATG3 governs GABARAP lipidation efficiency through its preferential interaction with anionic and cone-shaped lipids *in vitro*.

3) Recombinant ATG9 and ATG9 C-terminal domain can be expressed in insect cells associated to cell membranes. Mass spectrometry analysis of the recombinant ATG9 C-terminal domain-containing fractions shows the presence of phosphatidylglycerol. This might indicate the attachment of this domain to the membrane and/or the participation of ATG9 in lipid delivery during phagophore growth.

CAPÍTULO 6:

Resumen y Conclusiones

La homeostasis celular requiere un correcto balance entre los procesos catabólicos y anabólicos, en los cuales están involucradas diferentes rutas de señalización celular. La autofagia puede participar en ambos tipos de señalización, y es esencial tanto en la degradación de orgánulos innecesarios o dañados (catabolismo), como en la producción de nuevos elementos básicos a través de la movilización de energía celular y fuentes de nutrientes como lípidos, carbohidratos o hierro (anabolismo). La autofagia también esta implicada en una gran variedad de procesos fisiológicos tales como la inmunidad, la protección frente a infecciones virales, la diferenciación y el desarrollo celular, y puede causar incluso diversas patologías cuando está desregulada (Wirawan *et al.*, 2012).

La autofagia es un proceso mediante el cual se regulan muchos eventos esenciales en la célula, por lo que está implicada en el desarrollo de varias enfermedades humanas, especialmente neurodegenerativas, como son el Alzheimer, la enfermedad de Huntington y el Parkinson (Lynch-Day *et al.*, 2012; Martinez-Vicente *et al.*, 2010; Nixon *et al.*, 2005). Los desajustes que se producen en estas enfermedades están relacionados con la acumulación de agregados proteicos que no ocurrirían en condiciones normales de autofagia. Además, el cáncer, envejecimiento y otras alteraciones metabólicas están también reguladas en mayor o menor medida por la autofagia, lo que la convierte en una prometedora diana para la prevención y tratamiento de estos procesos. (Choi *et al.*, 2013; Levine & Kroemer, 2008).

Se han descrito muchas proteínas involucradas en la ruta de señalización de la autofagia, las cuales participan principalmente en forma de complejos que regulan

etapas específicas en la formación de un orgánulo de doble membrana denominado autofagosoma. Éste es considerado el evento principal que tiene lugar en la autofagia, y aunque aún se desconoce la procedencia del material lipídico de esta nueva membrana (Tooze & Yoshimori, 2010), se han propuesto la membrana plasmática u orgánulos como la mitocondria, el retículo endoplasmico o el Golgi como donantes. (Mari *et al.*, 2011). El material susceptible de ser degradado es atrapado dentro del nuevo orgánulo, el cual crece gracias a la adhesión y fusión de otras estructuras membranosas en forma de vesículas. Finalmente, el autofagosoma se cierra mediante un proceso de escisión recientemente descrito (Knorr *et al.*, 2015), y se fusiona con el lisosoma tras lo cual se degrada el material contenido en su interior. Varios estudios han propuesto que, de entre todas las proteínas Atg, dos sistemas UBL (Atg8/Atg3/Atg7 y Atg5-Atg12/Atg16) participan en los procesos de fusión que dan lugar a la extensión del fagóforo (Nair *et al.*, 2011; Romanov *et al.*, 2012; Walczak & Martens, 2013; Weidberg *et al.*, 2011). Por otro lado, también se ha descrito la presencia de una única proteína Atg con carácter transmembrana (Atg9), que es esencial para la autofagia tanto en levaduras como en mamíferos (Noda *et al.*, 2000; Webber *et al.*, 2007).

Sin embargo, la manera en la que el autofagosoma crece y finalmente se cierra es todavía una pregunta sin resolver, y continúa siendo objeto de profundo estudio. Por este motivo, el objetivo de esta tesis ha sido contribuir a conocer mejor el proceso de elongación del autofagosoma, así como reproducir su crecimiento *in vitro*. Para ello se han empleado técnicas biofísicas y membranas modelo para (i) analizar el papel del sistema UBL humano Atg8/ATG3/ATG7 en los procesos de agregación y fusión de vesículas, y cómo estos pueden ser modulados por lípidos, y (ii) caracterizar las interacciones lípido-proteína de la proteína autofágica ATG3. Además, se ha realizado un estudio preliminar de ATG9, una prometedora proteína transmembrana probablemente involucrada en el transporte de lípidos necesario para el crecimiento del autofagosoma.

Regulación lipídica de los eventos de fusión catalizados por el sistema mínimo proteico reconstituido (Atg8/Atg3/Atg7) involucrado en la elongación del autofagosoma

En el modelo actual de autofagia, la hipótesis más aceptada sobre la elongación del fagóforo propone que pequeñas vesículas llegarían al orgánulo emergente y se fusionarían para que éste creciese. De acuerdo con esto, se ha

demostrado que Atg8 de levaduras, el efector final del sistema UBL, participa en eventos de agregación, hemifusión y fusión *in vitro* (Nair *et al.*, 2011; Nakatogawa *et al.*, 2007). Sin embargo, los homólogos humanos de Atg8 (LC3 y GATE-16) solo han mostrado actividad fusogénica en sus formas unidas químicamente, o sea, artificialmente a PE (Weidberg *et al.*, 2011). Es importante señalar que todas estas proteínas catalizan los procesos mencionados a través de su forma lipidada, unida a PE, lo cual constituye su principal manera de asociarse a la membrana. Teniendo todo esto en cuenta, en este trabajo hemos descrito la actividad fusogénica *in vitro* del sistema UBL completo, la hemos comparado con el artificialmente lipidado, y hemos demostrado que la geometría lipídica y la curvatura de la membrana modulan la fusión inducida por LC3, GATE-16 y GABARAP.

Los homólogos humanos de Atg8 sufren la reacción de lipidación enzimática de manera similar a lo descrito en levaduras (**Figura 3.7 D**). Sin embargo, la eficiencia de la reacción es aparentemente menor que en el sistema de levaduras. Este hecho podría deberse a la necesidad de una composición lipídica específica o a la presencia del sistema UBL Atg5-Atg12/Atg16, tal y como sucede *in vivo*. Por otro lado, existen 7 homólogos humanos de Atg8 mientras que en levaduras solo existe uno, por lo que la baja eficiencia podría deberse a que quizá se requiera la presencia de varios homólogos, con una menor actividad de cada uno de ellos. Además, recientemente se ha descrito (Nath *et al.*, 2014) una posible forma adenilada de los homólogos de Atg8, la cual dificulta la detección de los conjugados LC3-PE y GATE-PE en los geles SDS-PAGE. Para solucionar este problema y conseguir una correcta detección hemos desarrollado el uso de PE marcada con NBD (**Figura 3.7 D**). La lipidación química de estas proteínas es semejante a la enzimática.

Con el objetivo de obtener más información acerca de los primeros momentos del proceso de fusión, se han realizado ensayos de agregación de vesículas. Según el modelo de fusión actualmente aceptado, denominado “modelo de tallo” (del inglés *stalk*) (Basañez *et al.*, 1998; Chernomordik & Kozlov, 2008; Chernomordik *et al.*, 1995; Khattari *et al.*, 2015; Siegel, 1999), las membranas inicialmente se aproximan y establecen contactos locales para eliminar las moléculas de agua que se encuentran entre ellas. En nuestras condiciones experimentales, GATE-16 y GABARAP muestran una alta actividad de agregación tanto en el sistema de conjugación enzimática como en el químico. LC3 posee una actividad menor en ambos sistemas (**Figura 3.8**).

La capacidad de agregación de vesículas por sí misma no es indicativa de que la hemifusión o la fusión de membranas haya ocurrido. Estudios previos con la

proteína recombinante de levaduras Atg8 demostraron que ésta es capaz de producir hemifusión, pero no se pudo observar fusión completa (Nakatogawa *et al.*, 2007). Más cercano a nuestro sistema, Weidberg *et al.*, (2011) mostró que LC3 y GATE-16 de mamíferos, artificialmente conjugadas a PEmal, inducen fusión completa de membranas, y además Nair *et al.*, (2011) demostró que Atg8 y LC3 requieren un alto contenido de DOPE en la membrana para inducir hemifusión. En nuestro sistema enzimático tanto GATE-16 como GABARAP inducen mezcla total de lípidos intervesicular, así como mezcla de lípidos de la hemicapa interna y mezcla de contenidos acuosos, lo cual se correlaciona con la capacidad de estas proteínas para producir fusión completa (**Figura 3.9**). Las formas químicamente lipidadas de GATE-16 y GABARAP muestran resultados similares (**Figura 3.12**). Este hecho nos permite concluir que las proteínas están correctamente plegadas después de su conjugación química y reproducen fielmente la actividad de las proteínas salvajes. Como se ha mostrado y sugerido previamente en nuestros experimentos, no todos los homólogos humanos de Atg8 presentan la misma actividad *in vitro*. Esto puede indicar que cada proteína participaría en el crecimiento del fagóforo en distintos momentos o en condiciones fisiológicas diferentes. Estos resultados indican quizá la primera prueba de la actividad fusogénica de GABARAP, y también proporcionan un estudio completo *in vitro* del potencial fusogénico de estos tres homólogos de Atg8 actuando a través de su correspondiente mecanismo enzimático.

Al igual que otros procesos relacionados con las membranas celulares, la fusión de vesículas puede estar considerablemente regulada por lípidos. Existen en la bibliografía muchas pruebas de cómo lípidos con distintas morfologías y curvaturas intrínsecas modulan eventos de fusión (Basañez *et al.*, 1996b, 1998). En la fusión mediada por Atg8, la incorporación de lípidos con forma de cono y curvatura intrínseca negativa (como la cardiolipina o el diacilglicerol), estimula la mezcla intervesicular de lípidos y contenidos acuosos. Por el contrario, la adición de lípidos con forma de cono invertido inhibe ambos procesos (**Figura 3.11**). Estos resultados están de acuerdo con el modelo de fusión de tallo, el cual supone que la inclusión de lípidos con curvatura intrínseca negativa favorece el intermediario de hemifusión y por lo tanto la progresión del proceso de fusión. En este contexto, y en contra de estudios que sugieren que son necesarias concentraciones no fisiológicas de DOPE (55%) para promover la fusión desencadenada por estas proteínas (Nair *et al.*, 2011), nuestro sistema de conjugación química muestra fusión de vesículas con cantidades fisiológicas de DOPE (30%) suplementadas con un 10% de un lípido con forma cónica (**Figura 3.13**). Además, nuestros estudios sugieren que los eventos de fusión involucrados en la elongación del

autofagosoma tendrían lugar en las regiones altamente curvadas que se generan en el borde de la membrana emergente, las cuales estarían enriquecidas en proteínas y lipidos fusogénicos, y cuya aparición podría incluso verse favorecida por la unión de vesículas pequeñas. De acuerdo con esto último, la fusión observada para GATE-16 y GABARAP es mayor cuanto menor es el tamaño de las vesículas (**Figura 3.12**). Por último, nuestros experimentos de cryo-EM muestran el espectacular crecimiento de liposomas promovido por los procesos de fusión inducidos por nuestros homólogos humanos de Atg8, y ofrecen una reproducción visual aproximada de la elongación del autofagosoma *in vitro* (**Figura 3.10**). Futuros experimentos combinando nuestro sistema con el sistema Atg5-Atg12/Atg16 proporcionarán un mejor entendimiento de las características del proceso *in vivo*.

ATG3, la enzima homóloga de E2 del sistema UBL, interacciona y agrega vesículas cargadas negativamente, probablemente dirigiendo la lipidación de los homólogos humanos de Atg8

Una vez establecido que los homólogos de Atg8 participan en los procesos de fusión que provocan la elongación del autofagosoma, se plantea la pregunta de cómo detectan las proteínas la membrana emergente y son dirigidas hacia ella. Estudios previos en este campo sugieren que tanto Atg3 (la última enzima implicada en el sistema UBL de Atg8), como el sistema Atg5-Atg12/Atg16 están involucrados en el reconocimiento de la membrana y catalizan el proceso de lipidación *in vivo* (Nath *et al.*, 2014; Romanov *et al.*, 2012; Sakoh-Nakatogawa *et al.*, 2015). También se ha descrito que otras proteínas implicadas en la autofagia reconocen lípidos específicos, como fosfatidilinositoles (WIPI1-2) (Dooley *et al.*, 2014), o características específicas de la membrana, como la curvatura (Barkor) (Fan *et al.*, 2011). De esta manera, dichas proteinas facilitarían la lipidación o los procesos de fusión respectivamente. En este contexto, un artículo reciente ha indicado que la proteína ATG3 de ratón posee una posible α-hélice N-terminal anfipática que actuaría como sensor de curvatura de membrana. Mutaciones en esta región modulan la lipidación de GABARAP-L1 *in vitro* e *in vivo* (Nath *et al.*, 2014). Estos estudios proporcionan una prueba de que ATG3 participa en el reconocimiento de la membrana para promover la lipidación de Atg8. De acuerdo con esto, hemos empleado técnicas biofísicas para analizar la afinidad de ATG3 humana por membranas modelo, con el objetivo de entender cómo esta proteína detecta la membrana e interacciona con ella durante el paso previo a la lipidación de Atg8.

Nuestros estudios con la balanza de Langmuir, de flotación de liposomas y GUV muestran que ATG3 tiene una fuerte afinidad por membranas cargadas negativamente en comparación con membranas neutras (**Figuras 4.2, 4.3** y **4.8**). Además, la presencia de fosfolípidos aniónicos en la membrana elimina el requerimiento, propuesto por Nath *et al.*, (2014), de altas concentraciones de DOPE (55%) y vesículas de pequeño tamaño para la unión de ATG3 (**Figura 4.3 A-B**). Además, se observa una alta preferencia por lípidos con forma cónica y cargados negativamente, como son CL y PA (**Figura 4.3 C**), lo que sugiere un doble componente en la interacción de ATG3 con la membrana: fuerza electrostática (carga negativa) y defectos en la membrana (creados por lípidos con curvatura intrínseca negativa). De acuerdo con estos resultados y suponiendo que ATG3 humana (casi idéntica a ATG3 de ratón) contiene la misma α-hélice anfipática predicha en su extremo N-terminal, se estudió la implicación de esta hélice en la interacción de la proteína con la membrana. Las dos lisinas (K9 y K11) que delimitan las caras hidrofóbica e hidrofílica de la hélice se acomodarían entre los grupos polares (cerca de los fosfatos) y las colas hidrofóbicas de los fosfolípidos en la membrana, es decir, en la interfase membrana-agua. El mutante de ATG3 K9D/K11D pierde la capacidad de unirse a vesículas tanto neutras como aniónicas, probablemente por la repulsión de carga con el ambiente negativo en la región mencionada anteriormente (**Figura 4.3 A**). Sin embargo, los péptidos sintéticos que cubren la secuencia de esta hélice N-terminal de ATG3 no reproducen la actividad de la proteína completa (**Figura 4.4**), ya sea porque la proteína necesita otras regiones para interaccionar, o quizá porque los péptidos no adoptan la conformación α-hélice.

Diferentes publicaciones indican que la presencia de fosfolípidos cargados negativamente (por ejemplo PI, PS o PG) favorece el rendimiento de la lipidación en membranas modelo *in vitro* (Ichimura *et al.*, 2004; Oh-oka *et al.*, 2008). Sin embargo, sólo un estudio asocia esta unión de ATG3 con membranas a la eficiencia de la conjugación de Atg8 a PE (Nath *et al.*, 2014). A este respecto, en este trabajo proponemos que ATG3 adquiere un papel en la dirección de los homólogos de Atg8 hacia la membrana a través de la inserción de la mencionada α-hélice. Además, sugerimos que la afinidad de ATG3 por lípidos cargados negativamente y con forma cónica podría ser la responsable de la eficiencia de la lipidación de GABARAP *in vitro* (**Figura 4.10**). Otros componentes que participan en el proceso de autofagia celular formarían parte de la maquinaria de conjugación *in vivo* (Fujita *et al.*, 2008; Hanada *et al.*, 2007; Romanov *et al.*, 2012).

Distintas proteínas, incluídos los homólogos humanos de Atg8, participan como hemos demostrado en procesos de agregación y fusión a lo largo del crecimiento del AP (Diao *et al.*, 2015; Landajuela *et al.*, 2016; Romanov *et al.*, 2012). Además, como se ha demostrado (**Capítulo 3**), estos eventos pueden ser modulados por la composición lipídica de regiones específicas en las membranas. En este contexto, podría ser que ATG3 participase en los procesos de fusión de vesículas que acompañan a la elongación del fagóforo. Esta hipótesis está basada en la nueva actividad de ATG3 que hemos observado en este trabajo, la agregación de vesículas. ATG3 promueve la agregación de membranas aniónicas, y en menor medida, de vesículas neutras (**Figura 4.5**). Al igual que ocurre en la interacción de ATG3 con la membrana, la actividad de agregación está modulada por lípidos que generan fases hexagonales invertidas en la membrana (CL o PA) (**Figura 4.5 C**), y no requiere membranas altamente curvadas. Sin embargo, no se observa mezcla de lípidos intervesicular o liberación de contenidos (**Figura 4.6**), lo cual sugiriere que ATG3 únicamente favorecería el paso de aproximación de las vesículas que precede a la fusión completa.

Desde una perspectiva diferente, se ha propuesto que en el proceso de elongación del autofagosoma se da una llegada continua de vesículas o incluso sólo de lípidos. Una o varias proteínas deberían controlar el movimiento de estas vesículas hacia el orgánulo emergente, y se ha propuesto ATG9 como candidata. Sin embargo, en el futuro deberían realizarse experimentos con membranas modelo *in vitro* para validar nuestros resultados preliminares sobre la expresión y unión de lípidos del dominio C-terminal de ATG9. (**Figuras 5.3-8**).

En resumen, los resultados de esta tesis sirven para aclarar el papel de tres homólogos humanos diferentes de Atg8 en eventos de fusión que tienen lugar durante la elongación del autofagosoma. Las formas de LC3, GATE-16 y GABARAP conjugadas enzimáticamente a PE inducen fusión de liposomas y este proceso puede estar modulado por la geometría lipídica y por la curvatura de membrana, características que podrían estar presentes en el borde del fagóforo naciente y que se ajustan debidamente al modelo propuesto de fusión tipo tallo. Además ATG3, uno de los componentes de la reacción enzimática que induce las formas conjugadas a PE, interacciona específicamente con membranas aniónicas, parece modular la eficiencia de la lipidación y muestra actividad de agregación de vesículas, lo cual puede estar relacionado con los eventos de fusión catalizados por los arriba mencionados homólogos de Atg8 durante el crecimiento del autofagosoma. Finalmente, resultados

preliminares pueden sugerir una posible implicación de la proteína transmembrana Atg9 en el transporte de lípidos que parece ocurrir durante la elongación del fagóforo.

Conclusiones

1) Los homólogos humanos de Atg8, LC3, GATE-16 y GABARAP, conjugados a PE enzimáticamente o químicamente, inducen eventos de fusión completa de vesículas lipídicas, modulados por la geometría lipídica y la curvatura de la membrana. Éste constituye el más sencillo modelo reconstituido del proceso humano de elongación del autofagosoma.

2) ATG3, la enzima homóloga de E2 en el sistema de conjugación de Atg8, interacciona fuertemente con membranas cargadas negativamente a través de una hipotética α-hélice anfipática N-terminal, y también induce agregación de vesículas aniónicas. ATG3 dirige la eficiencia de la lipidación de GABARAP a través de su interacción preferencial con lípidos aniónicos y cónicos *in vitro*.

3) La proteína recombinante ATG9 y su dominio C-terminal se pueden expresar asociados a membranas celulares en células de insecto. El análisis por espectrometría de masas de fracciones que contienen el fragmento C-terminal de ATG9 muestra la presencia de fosfatidilglicerol. Esto puede indicar que este dominio se asocia a la membrana y/o que ATG9 participa en el transporte de lípidos durante el crecimiento del fagóforo.

References

Aeffner, S., Reusch, T., Weinhausen, B. & Salditt, T. (2012). Energetics of stalk intermediates in membrane fusion are controlled by lipid composition. *Proc Natl Acad Sci* **109**, E1609–E1618.

Ahyayauch, H., Villar, A. V, Alonso, A. & Goñi, F. M. (2005). Modulation of PI-specific phospholipase C by membrane curvature and molecular order. *Biochemistry* **44**, 11592–600.

Allen, T. M. & Cullis, P. R. (2013). Liposomal drug delivery systems: from concept to clinical applications. *Adv Drug Deliv Rev* **65**, 36–48.

Alonso, A., Goñi, F. M. & Buckley, J. T. (2000). Lipids favoring inverted phase enhance the ability of aerolysin to permeabilize liposome bilayers. *Biochemistry* **39**, 14019–24.

Angelova, M., Soleau, S., Meleard, P., Faucon, F. & Bothorel, P. (n.d.). Preparation of giant vesicles by external AC electric fields. Kinetics and applications. *Trends Colloid Interface Sci VI* 127–131.

Angelova, M. I. & Dimitrov, D. S. (1986). Liposome electroformation. *Faraday Discuss Chem Soc* **81**, 303–311.

Angelova, M. I. & Tsoneva, I. (1999). Interactions of DNA with giant liposomes. *Chem Phys Lipids* **101**, 123–137.

Antonny, B. (2011). Mechanisms of membrane curvature sensing. *Annu Rev Biochem* **80**, 101–23.

de Arcuri, B. F., Vechetti, G. F., Chehín, R. N., Goñi, F. M. & Morero, R. D. (1999). Protein-induced fusion of phospholipid vesicles of heterogeneous sizes. *Biochem Biophys Res Commun* **262**, 586–590.

Backues, S. K., Orban, D. P., Bernard, A., Singh, K., Cao, Y. & Klionsky, D. J. (2015). Atg23 and Atg27 act at the early stages of Atg9 trafficking in S. cerevisiae. *Traffic* **16**, 172–90.

Bagatolli, L. A. (2003). Thermotropic behavior of lipid mixtures studied at the level of single vesicles: giant unilamellar vesicles and two-photon excitation fluorescence microscopy. *Methods Enzymol* **367**, 233–53.

Bangham, A. D. & Horne, R. W. (1964). Negative staining of phospholipids and their structural modification by surface-active agents as observed in the electron microscope. *J Mol Biol* **8**, 660–668.

Bartels, T., Ahlstrom, L. S., Leftin, A., Kamp, F., Haass, C., Brown, M. F. & Beyer, K. (2010). The N-terminus of the intrinsically disordered protein α-synuclein triggers membrane binding and helix folding. *Biophys J* **99**, 2116–24.

Bartke, N. & Hannun, Y. A. (2009). Bioactive sphingolipids: metabolism and function. *J Lipid Res* **50 Suppl**, S91–6.

Bartlett, G. R. (1959). Phosphorus Assay in Column Chromatography. *J Biol Chem* **234**, 466–468.

Basañez, G. (2002). Membrane fusion: the process and its energy suppliers. *Cell Mol Life Sci* **59**, 1478–90.

Basañez, G., Nieva, J. L., Goñi, F. M. & Alonso, A. (1996a). Origin of the lag period in the phospholipase C cleavage of phospholipids in membranes. Concomitant vesicle aggregation and enzyme activation. *Biochemistry* **35**, 15183–7.

Basañez, G., Nieva, J. L., Rivas, E., Alonso, A. & Goni, F. M. (1996b). Diacylglycerol and the promotion of lamellar-hexagonal and lamellar-isotropic phase transitions in lipids: implications for membrane fusion. *Biophys J* **70**, 2299–306.

Basañez, G., Goñi, F. M. & Alonso, A. (1998). Effect of single chain lipids on phospholipase C-promoted vesicle fusion. A test for the stalk hypothesis of membrane fusion. *Biochemistry* **37**, 3901–8.

Beales, P. A., Bergstrom, C. L., Geerts, N., Groves, J. T. & Vanderlick, T. K. (2011). Single vesicle observations of the cardiolipin-cytochrome C interaction: induction of membrane morphology changes. *Langmuir* **27**, 6107–15.

Bejarano, E. & Cuervo, A. M. (2010). Chaperone-mediated autophagy. *Proc Am Thorac Soc* **7**, 29–39.

Belyaev, A. S., Hails, R. S. & Roy, P. (1995). High-level expression of five foreign genes by a single recombinant baculovirus. *Gene* **156**, 229–33.

Berg, J. M., Tymoczko, J. L. & Stryer, L. (2002). Biochemistry. W H Freeman.

Bigay, J., Casella, J.-F., Drin, G., Mesmin, B. & Antonny, B. (2005). ArfGAP1 responds to membrane curvature through the folding of a lipid packing sensor motif. *EMBO J* **24**, 2244–2253.

Böttcher, C. J. F., Van gent, C. M. & Pries, C. (1961). A rapid and sensitive sub-micro phosphorus determination. *Anal Chim Acta* **24**, 203–204.

Boya, P., Reggiori, F. & Codogno, P. (2013). Emerging regulation and functions of autophagy. *Nat Cell Biol* **15**, 713–20.

Burger, K. N. (2000). Greasing membrane fusion and fission machineries. *Traffic* **1**, 605–13.

Butler, M. (2006). Optimisation of the cellular metabolism of glycosylation for recombinant proteins produced by Mammalian cell systems. *Cytotechnology* **50**, 57–76.

Chernomordik, L., Chanturiya, A., Green, J. & Zimmerberg, J. (1995). The hemifusion intermediate and its conversion to complete fusion: regulation by membrane composition. *Biophys J* **69**, 922–9.

Chernomordik, L. V, Melikyan, G. B. & Chizmadzhev, Y. A. (1987). Biomembrane

fusion: a new concept derived from model studies using two interacting planar lipid bilayers. *Biochim Biophys Acta* **906**, 309–52.

Chernomordik, L. V & Kozlov, M. M. (2008). Mechanics of membrane fusion. *Nat Struct Mol Biol* **15**, 675–83.

Choi, A. M. K., Ryter, S. W. & Levine, B. (2013). Autophagy in Human Health and Disease. *N Engl J Med* **368**, 651–662.

Chu, C. T., Ji, J., Dagda, R. K., Jiang, J. F., Tyurina, Y. Y., Kapralov, A. A., Tyurin, V. A., Yanamala, N., Shrivastava, I. H. & other authors. **(2013).** Cardiolipin externalization to the outer mitochondrial membrane acts as an elimination signal for mitophagy in neuronal cells. *Nat Cell Biol* **15**, 1197–1205.

Contreras, F.-X., Sánchez-Magraner, L., Alonso, A. & Goñi, F. M. (2010). Transbilayer (flip-flop) lipid motion and lipid scrambling in membranes. *FEBS Lett* **584**, 1779–1786.

Coyle, J. E., Qamar, S., Rajashankar, K. R. & Nikolov, D. B. (2002). Structure of GABARAP in two conformations: implications for GABA(A) receptor localization and tubulin binding. *Neuron* **33**, 63–74.

Cruz, A. & Pérez-Gil, J. (2007). Langmuir films to determine lateral surface pressure on lipid segregation. *Methods Mol Biol* **400**, 439–57.

Cullis, P. R., de Kruijff, B., Verkleij, A. J. & Hope, M. J. (1986). Lipid polymorphism and membrane fusion. *Biochem Soc Trans* **14**, 242–245.

Dall'Armi, C., Hurtado-Lorenzo, A., Tian, H., Morel, E., Nezu, A., Chan, R. B., Yu, W. H., Robinson, K. S., Yeku, O. & other authors. **(2010).** The phospholipase D1 pathway modulates macroautophagy. *Nat Commun* **1**, 142.

Dall'Armi, C., Devereaux, K. A. & Di Paolo, G. (2013). The Role of Lipids in the Control of Autophagy. *Curr Biol* **23**, R33–R45.

Dass, C. R. (2008). Drug delivery in cancer using liposomes. *Methods Mol Biol* **437**, 177–82.

Diao, J., Liu, R., Rong, Y., Zhao, M., Zhang, J., Lai, Y., Zhou, Q., Wilz, L. M., Li, J. & other authors. **(2015).** ATG14 promotes membrane tethering and fusion of autophagosomes to endolysosomes. *Nature* **520**, 563–6.

Dooley, H. C., Razi, M., Polson, H. E. J., Girardin, S. E., Wilson, M. I. & Tooze, S. A. (2014). WIPI2 Links LC3 Conjugation with PI3P, Autophagosome Formation, and Pathogen Clearance by Recruiting Atg12–5-16L1. *Mol Cell* **55**, 238–252.

de Duve, C. (1963). The lysosome. *Sci Am* **208**, 64–72.

Ellens, H., Bentz, J. & Szoka, F. C. (1985). H+- and Ca2+-induced fusion and destabilization of liposomes. *Biochemistry* **24**, 3099–3106.

Engelman, D. M. (2005). Membranes are more mosaic than fluid. *Nature* **438**, 578–80.

Epand, R. M. (1998). Lipid polymorphism and protein–lipid interactions. *Biochim Biophys Acta - Rev Biomembr* **1376**, 353–368.

Fadok, V. A., Bratton, D. L., Rose, D. M., Pearson, A., Ezekewitz, R. A. & Henson, P. M. (2000). A receptor for phosphatidylserine-specific clearance of apoptotic cells. *Nature* **405**, 85–90.

Fan, W., Nassiri, a. & Zhong, Q. (2011). Autophagosome targeting and membrane curvature sensing by Barkor/Atg14(L). *Proc Natl Acad Sci* **108**, 7769–7774.

Fidorra, M., Duelund, L., Leidy, C., Simonsen, A. C. & Bagatolli, L. A. (2006). Absence of fluid-ordered/fluid-disordered phase coexistence in ceramide/POPC mixtures containing cholesterol. *Biophys J* **90**, 4437–51.

Fisher, C. L. & Pei, G. K. (1997). Modification of a PCR-based site-directed mutagenesis method. *Biotechniques* **23**, 570–1, 574.

Fiske, C. H. & Subbarow, Y. (1925). THE COLORIMETRIC DETERMINATION OF PHOSPHORUS. *J Biol Chem* **66**, 375–400.

Fujita, N., Itoh, T., Omori, H., Fukuda, M., Noda, T. & Yoshimori, T. (2008). The Atg16L complex specifies the site of LC3 lipidation for membrane biogenesis in autophagy. *Mol Biol Cell* **19**, 2092–100.

Fuller, M. (2010). Sphingolipids: the nexus between Gaucher disease and insulin resistance. *Lipids Health Dis* **9**, 113. BioMed Central.

Galluzzi, L., Bravo-San Pedro, J. M. & Kroemer, G. (2016). Autophagy Mediates Tumor Suppression via Cellular Senescence. *Trends Cell Biol* **26**, 1–3.

Garner, K., Hunt, A. N., Koster, G., Somerharju, P., Groves, E., Li, M., Raghu, P., Holic, R. & Cockcroft, S. (2012). Phosphatidylinositol transfer protein, cytoplasmic 1 (PITPNC1) binds and transfers phosphatidic acid. *J Biol Chem* **287**, 32263–76.

Gennis, R. B. (1989). *Biomembranes: molecular structure and function*. Springer-Verlag.

Gilbert, R. J. C. (2015). Protein-lipid interactions and non-lamellar lipidic structures in membrane pore formation and membrane fusion. *Biochim Biophys Acta - Biomembr (In Press*.

Goñi, F. M. & Alonso, A. (2000). Membrane fusion induced by phospholipase C and sphingomyelinases. *Biosci Rep* **20**, 443–63.

Goñi, F. M. Non-permanent proteins in membranes: when proteins come as visitors (Review). *Mol Membr Biol* **19**, 237–45.

Goñi, F. M. (2014). The basic structure and dynamics of cell membranes: an update of the Singer-Nicolson model. *Biochim Biophys Acta* **1838**, 1467–76.

Goñi, F. M., Villar, A. V, Nieva, J. L. & Alonso, A. (2003). Interaction of

phospholipases C and sphingomyelinase with liposomes. *Methods Enzymol* **372**, 3–19.

Goñi, F. M., Montes, L.-R. & Alonso, A. (2012). Phospholipases C and sphingomyelinases: Lipids as substrates and modulators of enzyme activity. *Prog Lipid Res* **51**, 238–66.

Green, D. R. & Levine, B. (2014). To Be or Not to Be? How Selective Autophagy and Cell Death Govern Cell Fate. *Cell* **157**, 65–75.

Gregoriadis, G. (1978). Liposomes in the therapy of lysosomal storage diseases. *Nature* **275**, 695–6.

Gregoriadis, G. (2008). Liposome research in drug delivery: the early days. *J Drug Target* **16**, 520–4.

Hamasaki, M., Shibutani, S. T. & Yoshimori, T. (2013). Up-to-date membrane biogenesis in the autophagosome formation. *Curr Opin Cell Biol* **25**, 455–60.

Hanada, T., Noda, N. N., Satomi, Y., Ichimura, Y., Fujioka, Y., Takao, T., Inagaki, F. & Ohsumi, Y. (2007). The Atg12-Atg5 conjugate has a novel E3-like activity for protein lipidation in autophagy. *J Biol Chem* **282**, 37298–302.

Hanada, T., Satomi, Y., Takao, T. & Ohsumi, Y. (2009). The amino-terminal region of Atg3 is essential for association with phosphatidylethanolamine in Atg8 lipidation. *FEBS Lett* **583**, 1078–1083.

Harrison, R. L. & Jarvis, D. L. (2007). Transforming lepidopteran insect cells for continuous recombinant protein expression. *Methods Mol Biol* **388**, 299–316.

He, C. & Klionsky, D. J. (2009). Regulation Mechanisms and Signaling Pathways of Autophagy. *Annu Rev Genet* **43**, 67–93.

He, C., Song, H., Yorimitsu, T., Monastyrska, I., Yen, W.-L., Legakis, J. E. & Klionsky, D. J. (2006). Recruitment of Atg9 to the preautophagosomal structure by Atg11 is essential for selective autophagy in budding yeast. *J Cell Biol* **175**, 925–35.

Homma, K., Suzuki, K. & Sugawara, H. (2011). The autophagy database: An all-inclusive information resource on autophagy that provides nourishment for research. *Nucleic Acids Res* **39**, D986–90.

Hong, S. B., Kim, B.-W., Lee, K.-E., Kim, S. W., Jeon, H., Kim, J. & Song, H. K. (2011). Insights into noncanonical E1 enzyme activation from the structure of autophagic E1 Atg7 with Atg8. *Nat Struct Mol Biol* **18**, 1323–30.

Hruban, Z., Spargo, B., Swift, H., Wissler, R. W. & Kleinfeld, R. G. (1963). Focal cytoplasmic degradation. *Am J Pathol* **42**, 657–83.

Hurley, J. H. (2006). Membrane binding domains. *Biochim Biophys Acta* **1761**, 805–11.

Hurley, J. H. & Schulman, B. A. (2014). Atomistic autophagy: the structures of cellular self-digestion. *Cell* **157**, 300–11.

Ibarguren, M., Bomans, P. H. H., Frederik, P. M., Stonehouse, M., Vasil, A. I., Vasil, M. L., Alonso, A. & Goñi, F. M. (2010). End-products diacylglycerol and ceramide modulate membrane fusion induced by a phospholipase C/sphingomyelinase from Pseudomonas aeruginosa. *Biochim Biophys Acta* **1798**, 59–64.

Ichimura, Y., Kirisako, T., Takao, T., Satomi, Y., Shimonishi, Y., Ishihara, N., Mizushima, N., Tanida, I., Kominami, E. & other authors. **(2000).** A ubiquitin-like system mediates protein lipidation. *Nature* **408**, 488–492.

Ichimura, Y., Imamura, Y., Emoto, K., Umeda, M., Noda, T. & Ohsumi, Y. (2004). In vivo and in vitro reconstitution of Atg8 conjugation essential for autophagy. *J Biol Chem* **279**, 40584–92.

Israelachvili, J. N., Marcelja, S. & Horn, R. G. (1980). Physical principles of membrane organization. *Q Rev Biophys* **13**, 121–200.

Jacobson, K., Sheets, E. D. & Simson, R. (1995). Revisiting the fluid mosaic model of membranes. *Science* **268**, 1441–2.

Jamil, H., Hatch, G. M. & Vance, D. E. (1993). Evidence that binding of CTP:phosphocholine cytidylyltransferase to membranes in rat hepatocytes is modulated by the ratio of bilayer- to non-bilayer-forming lipids. *Biochem J* **291**, 419–27.

Janmey, P. a. & Kinnunen, P. K. J. (2006). Biophysical properties of lipids and dynamic membranes. *Trends Cell Biol* **16**, 538–546.

Jia, K. & Levine, B. Autophagy is required for dietary restriction-mediated life span extension in C. elegans. *Autophagy* **3**, 597–9.

Jiang, P. & Mizushima, N. (2014). Autophagy and human diseases. *Cell Res* **24**, 69–79. Nature Publishing Group.

Jo, E., McLaurin, J., Yip, C. M., St George-Hyslop, P. & Fraser, P. E. (2000). alpha-Synuclein membrane interactions and lipid specificity. *J Biol Chem* **275**, 34328–34.

Kabeya, Y., Mizushima, N., Ueno, T., Yamamoto, A., Kirisako, T., Noda, T., Kominami, E., Ohsumi, Y. & Yoshimori, T. (2000). LC3, a mammalian homologue of yeast Apg8p, is localized in autophagosome membranes after processing. *EMBO J* **19**, 5720–8.

Kaiser, S. E., Mao, K., Taherbhoy, A. M., Yu, S., Olszewski, J. L., Duda, D. M., Kurinov, I., Deng, A., Fenn, T. D. & other authors. **(2012).** Noncanonical E2 recruitment by the autophagy E1 revealed by Atg7–Atg3 and Atg7–Atg10 structures. *Nat Struct Mol Biol* **19**, 1242–1249.

Kaiser, S. E., Qiu, Y., Coats, J. E., Mao, K., Klionsky, D. J. & Schulman, B. a. (2013). Structures of Atg7-Atg3 and Atg7-Atg10 reveal noncanonical mechanisms of E2 recruitment by the autophagy E1. *Autophagy* **9**, 778–780.

Khattari, Z., Köhler, S., Xu, Y., Aeffner, S. & Salditt, T. (2015). Stalk formation as a function of lipid composition studied by X-ray reflectivity. *Biochim Biophys Acta* **1848**, 41–50.

Kirisako, T., Ichimura, Y., Okada, H., Kabeya, Y., Mizushima, N., Yoshimori, T., Ohsumi, M., Takao, T., Noda, T. & Ohsumi, Y. (2000). The reversible modification regulates the membrane-binding state of Apg8/Aut7 essential for autophagy and the cytoplasm to vacuole targeting pathway. *J Cell Biol* **151**, 263–76.

Klionsky, D. J. & Schulman, B. a. (2014). Dynamic regulation of macroautophagy by distinctive ubiquitin-like proteins. *Nat Struct Mol Biol* **21**, 336–345.

Knorr, R. L., Nakatogawa, H., Ohsumi, Y., Lipowsky, R., Baumgart, T. & Dimova, R. (2014). Membrane morphology is actively transformed by covalent binding of the protein Atg8 to PE-lipids. *PLoS One* **9**, e115357.

Knorr, R. L., Lipowsky, R. & Dimova, R. (2015). Autophagosome closure requires membrane scission. *Autophagy* **11**, 2134–2137.

Kooijman, E. E., Chupin, V., de Kruijff, B. & Burger, K. N. J. (2003). Modulation of membrane curvature by phosphatidic acid and lysophosphatidic acid. *Traffic* **4**, 162–174.

Kouno, T., Mizuguchi, M., Tanidal, I., Uenol, T., Kanematsu, T., Mori, Y., Shinoda, H., Hirata, M., Kominami, E. & Kawano, K. (2005). Solution structure of microtubule-associated protein light chain 3 and identification of its functional subdomains. *J Biol Chem* **280**, 24610–24617.

Kozlov, M. M. & Chernomordik, L. V. (2015). Membrane tension and membrane fusion. *Curr Opin Struct Biol* **33**, 61–7.

Lamb, C. a., Yoshimori, T. & Tooze, S. a. (2013). The autophagosome: origins unknown, biogenesis complex. *Nat Rev Mol Cell Biol* **14**, 759–774.

Landajuela, A., Hervás, J. H., Antón, Z., Montes, L.-R., Gil, D., Valle, M., Rodriguez, J. F., Goñi, F. M. & Alonso, A. (2016). Lipid geometry and bilayer curvature modultae LC3/GABARAP-mediated model autophagosome elongation. *Biophys J* **110**, 411–422.

Lang, T., Reiche, S., Straub, M., Bredschneider, M. & Thumm, M. (2000). Autophagy and the cvt pathway both depend on AUT9. *J Bacteriol* **182**, 2125–33.

Langmuir, I. (1917). The Constitution And Fundamental Properties of Solids and Liquids. II. Liquids. 1. *J Am Chem Soc* **39**, 1848–1906.

Langosch, D., Hofmann, M. & Ungermann, C. (2007). The role of transmembrane domains in membrane fusion. *Cell Mol Life Sci* **64**, 850–64.

Lemmon, M. a. (2008). Membrane recognition by phospholipid-binding domains. *Nat Rev Mol Cell Biol* **9**, 99–111.

Levine, B. & Kroemer, G. (2008). Autophagy in the pathogenesis of disease. *Cell* **132**, 27–42.

Liang, X. H., Jackson, S., Seaman, M., Brown, K., Kempkes, B., Hibshoosh, H. & Levine, B. (1999). Induction of autophagy and inhibition of tumorigenesis by beclin 1. *Nature* **402**, 672–6.

Lipinski, M. M., Zheng, B., Lu, T., Yan, Z., Py, B. F., Ng, A., Xavier, R. J., Li, C., Yankner, B. A. & other authors. **(2010).** Genome-wide analysis reveals mechanisms modulating autophagy in normal brain aging and in Alzheimer's disease. *Proc Natl Acad Sci U S A* **107**, 14164–9.

Longatti, A., Lamb, C. A., Razi, M., Yoshimura, S., Barr, F. A. & Tooze, S. A. (2012). TBC1D14 regulates autophagosome formation via Rab11- and ULK1-positive recycling endosomes. *J Cell Biol* **197**, 659–75.

Luckow, V. A., Lee, S. C., Barry, G. F. & Olins, P. O. (1993). Efficient generation of infectious recombinant baculoviruses by site-specific transposon-mediated insertion of foreign genes into a baculovirus genome propagated in Escherichia coli. *J Virol* **67**, 4566–79.

Lynch-Day, M. A., Mao, K., Wang, K., Zhao, M. & Klionsky, D. J. (2012). The role of autophagy in Parkinson's disease. *Cold Spring Harb Perspect Med* **2**, a009357.

Ma, P., Mohrlüder, J., Schwarten, M., Stoldt, M., Singh, S. K., Hartmann, R., Pacheco, V. & Willbold, D. (2010). Preparation of a Functional GABARAP–Lipid Conjugate in Nanodiscs and its Investigation by Solution NMR Spectroscopy. *ChemBioChem* **11**, 1967–1970.

Madsen, K. L., Bhatia, V. K., Gether, U. & Stamou, D. (2010). BAR domains, amphipathic helices and membrane-anchored proteins use the same mechanism to sense membrane curvature. *FEBS Lett* **584**, 1848–55.

Mari, M. & Reggiori, F. (2007). Atg9 trafficking in the yeast Saccharomyces cerevisiae. *Autophagy* **3**, 145–8.

Mari, M., Tooze, S. A. & Reggiori, F. (2011). The puzzling origin of the autophagosomal membrane. *F1000 Biol Rep* **3**, 25.

Marsh, D. (1980). Molecular motion in phospholipid bilayers in the gel phase: long axis rotation. *Biochemistry* **19**, 1632–7.

Marsh, D. (1996). Lateral pressure in membranes. *Biochim Biophys Acta - Rev Biomembr* **1286**, 183–223.

Martín, C., Requero, M.-A., Masin, J., Konopasek, I., Goñi, F. M., Sebo, P. & Ostolaza, H. (2004). Membrane restructuring by Bordetella pertussis adenylate cyclase toxin, a member of the RTX toxin family. *J Bacteriol* **186**, 3760–5.

Martin, S. R. & Schilstra, M. J. (2008). Circular dichroism and its application to the study of biomolecules. *Methods Cell Biol* **84**, 263–93.

Martinez-Vicente, M., Talloczy, Z., Wong, E., Tang, G., Koga, H., Kaushik, S., de Vries, R., Arias, E., Harris, S. & other authors. **(2010).** Cargo recognition failure is responsible for inefficient autophagy in Huntington's disease. *Nat Neurosci* **13**, 567–76.

Mayer, L. D., Hope, M. J. & Cullis, P. R. (1986). Vesicles of variable sizes produced by a rapid extrusion procedure. *Biochim Biophys Acta - Biomembr* **858**, 161–168.

McMahon, H. T. & Boucrot, E. (2015). Membrane curvature at a glance. *J Cell Sci* **128**, 1065–1070.

McMahon, H. T. & Gallop, J. L. (2005). Membrane curvature and mechanisms of dynamic cell membrane remodelling. *Nature* **438**, 590–596.

van Meer, G. (2005). Cellular lipidomics. *EMBO J* **24**, 3159–65. EMBO Press.

van Meer, G., Voelker, D. R. & Feigenson, G. W. (2008). Membrane lipids: where they are and how they behave. *Nat Rev Mol Cell Biol* **9**, 112–124.

Menzies, F. M., Fleming, A. & Rubinsztein, D. C. (2015). Compromised autophagy and neurodegenerative diseases. *Nat Rev Neurosci* **16**, 345–357. Nature Publishing Group, a division of Macmillan Publishers Limited. All Rights Reserved.

Mesmin, B., Drin, G., Levi, S., Rawet, M., Cassel, D., Bigay, J. & Antonny, B. (2007). Two lipid-packing sensor motifs contribute to the sensitivity of ArfGAP1 to membrane curvature. *Biochemistry* **46**, 1779–90.

Metlagel, Z., Otomo, C., Takaesu, G. & Otomo, T. (2013). Structural basis of ATG3 recognition by the autophagic ubiquitin-like protein ATG12. *Proc Natl Acad Sci U S A* **110**, 18844–9.

Miller, L. K., Trimarchi, R. E., Browne, D. & Pennock, G. D. (1983). A temperature-sensitive mutant of the baculovirus Autographa californica nuclear polyhedrosis virus defective in an early function required for further gene expression. *Virology* **126**, 376–80.

Mishra, V. K., Palgunachari, M. N., Segrest, J. P. & Anantharamaiah, G. M. (1994). Interactions of synthetic peptide analogs of the class A amphipathic helix with lipids. Evidence for the snorkel hypothesis. *J Biol Chem* **269**, 7185–91.

Mizushima, N. & Komatsu, M. (2011). Autophagy: Renovation of Cells and Tissues. *Cell* **47**, 728–741.

Mizushima, N., Yoshimori, T. & Ohsumi, Y. (2003). Role of the Apg12 conjugation

system in mammalian autophagy. *Int J Biochem Cell Biol* **35**, 553–61.

Mizushima, N., Yoshimori, T. & Ohsumi, Y. (2011). The role of Atg proteins in autophagosome formation. *Annu Rev Cell Dev Biol* **27**, 107–32.

Montes, L.-R., Alonso, A., Goñi, F. M. & Bagatolli, L. A. (2007). Giant unilamellar vesicles electroformed from native membranes and organic lipid mixtures under physiological conditions. *Biophys J* **93**, 3548–54.

Moravcevic, K., Mendrola, J. M., Schmitz, K. R., Wang, Y.-H., Slochower, D., Janmey, P. A. & Lemmon, M. A. (2010). Kinase associated-1 domains drive MARK/PAR1 kinases to membrane targets by binding acidic phospholipids. *Cell* **143**, 966–77.

Moreau, K., Ravikumar, B., Renna, M., Puri, C. & Rubinsztein, D. C. (2011). Autophagosome precursor maturation requires homotypic fusion. *Cell* **146**, 303–17.

Moreau, K., Renna, M. & Rubinsztein, D. C. (2013). Connections between SNAREs and autophagy. *Trends Biochem Sci* **38**, 57–63.

Morero, R. D., Viñals, A. L., Bloj, B. & Farías, R. N. (1985). Fusion of phospholipid vesicles induced by muscle glyceraldehyde-3-phosphate dehydrogenase in the absence of calcium. *Biochemistry* **24**, 1904–1909.

Murhammer, D. W. (Ed.). **(2007).** *Baculovirus and Insect Cell Expression Protocols*. Methods in Molecular Biology™. Totowa, NJ: Humana Press.

Nair, U., Jotwani, A., Geng, J., Gammoh, N., Richerson, D., Yen, W.-L., Griffith, J., Nag, S., Wang, K. & other authors. **(2011).** SNARE proteins are required for macroautophagy. *Cell* **146**, 290–302.

Nakatogawa, H. & Ohsumi, Y. (2012). SDS-PAGE techniques to study ubiquitin-like conjugation systems in yeast autophagy. *Methods Mol Biol* **832**, 519–29.

Nakatogawa, H., Ichimura, Y. & Ohsumi, Y. (2007). Atg8, a ubiquitin-like protein required for autophagosome formation, mediates membrane tethering and hemifusion. *Cell* **130**, 165–78.

Nath, S., Dancourt, J., Shteyn, V., Puente, G., Fong, W. M., Nag, S., Bewersdorf, J., Yamamoto, A., Antonny, B. & Melia, T. J. (2014). Lipidation of the LC3/GABARAP family of autophagy proteins relies on a membrane-curvature-sensing domain in Atg3. *Nat Cell Biol* **16**, 415–24.

Nieva, J. L., Goñi, F. M. & Alonso, A. (1989). Liposome fusion catalytically induced by phospholipase C. *Biochemistry* **28**, 7364–7.

Nixon, R. A., Wegiel, J., Kumar, A., Yu, W. H., Peterhoff, C., Cataldo, A. & Cuervo, A. M. (2005). Extensive involvement of autophagy in Alzheimer disease: an immuno-electron microscopy study. *J Neuropathol Exp Neurol* **64**, 113–22.

Noble, G. T., Stefanick, J. F., Ashley, J. D., Kiziltepe, T. & Bilgicer, B. (2014). Ligand-targeted liposome design: challenges and fundamental considerations. *Trends Biotechnol* **32**, 32–45.

Noda, N. N. & Fujioka, Y. (2015). Atg1 family kinases in autophagy initiation. *Cell Mol Life Sci* **72**, 3083–96.

Noda, N. N., Ohsumi, Y. & Inagaki, F. (2010a). Atg8-family interacting motif crucial for selective autophagy. *FEBS Lett* **584**, 1379–85.

Noda, N. N., Satoo, K., Fujioka, Y., Kumeta, H., Ogura, K., Nakatogawa, H., Ohsumi, Y. & Inagaki, F. (2011). Structural basis of Atg8 activation by a homodimeric E1, Atg7. *Mol Cell* **44**, 462–75. Elsevier Inc.

Noda, N. N. & Inagaki, F. (2015). Mechanisms of Autophagy. *Annu Rev Biophys* **44**, 101–122.

Noda, T., Kim, J., Huang, W. P., Baba, M., Tokunaga, C., Ohsumi, Y. & Klionsky, D. J. (2000). Apg9p/Cvt7p is an integral membrane protein required for transport vesicle formation in the Cvt and autophagy pathways. *J Cell Biol* **148**, 465–80.

Noda, T., Matsunaga, K., Taguchi-Atarashi, N. & Yoshimori, T. (2010b). Regulation of membrane biogenesis in autophagy via PI3P dynamics. *Semin Cell Dev Biol* **21**, 671–6.

Ohashi, K. & Otomo, T. (2015). Identification and characterization of the linear region of ATG3 that interacts with ATG7 in higher eukaryotes. *Biochem Biophys Res Commun* **463**, 447–52.

Oh-oka, K., Nakatogawa, H. & Ohsumi, Y. (2008). Physiological pH and Acidic Phospholipids Contribute to Substrate Specificity in Lipidation of Atg8. *J Biol Chem* **283**, 21847–21852.

Okamoto, K. (2014). Organellophagy: eliminating cellular building blocks via selective autophagy. *J Cell Biol* **205**, 435–45.

Orsi, a, Razi, M., Dooley, H. C., Robinson, D., Weston, a E., Collinson, L. M. & Tooze, S. a. (2012). Dynamic and transient interactions of Atg9 with autophagosomes, but not membrane integration, are required for autophagy. *Mol Biol Cell* **23**, 1860–73.

Pennock, G. D., Shoemaker, C. & Miller, L. K. (1984). Strong and regulated expression of Escherichia coli beta-galactosidase in insect cells with a baculovirus vector. *Mol Cell Biol* **4**, 399–406.

Polson, H. E. J., de Lartigue, J., Rigden, D. J., Reedijk, M., Urbé, S., Clague, M. J. & Tooze, S. a. (2010). Mammalian Atg18 (WIPI2) localizes to omegasome-anchored phagophores and positively regulates LC3 lipidation. *Autophagy* **6**, 506–522.

Pomorski, T. & Menon, a. K. (2006). Lipid flippases and their biological functions. *Cell Mol Life Sci* **63**, 2908–2921.

Popelka, H., Uversky, V. N. & Klionsky, D. J. (2014). Identification of Atg3 as an intrinsically disordered polypeptide yields insights into the molecular dynamics of autophagy-related proteins in yeast. *Autophagy* **10**, 1093–104.

Radoshevich, L., Murrow, L., Chen, N., Fernandez, E., Roy, S., Fung, C. & Debnath, J. (2010). ATG12 Conjugation to ATG3 Regulates Mitochondrial Homeostasis and Cell Death. *Cell* **142**, 590–600.

Ragusa, M. J., Stanley, R. E. & Hurley, J. H. (2012). Architecture of the Atg17 Complex as a Scaffold for Autophagosome Biogenesis. *Cell* **151**, 1501–1512.

Reeves, J. P. & Dowben, R. M. (1969). Formation and properties of thin-walled phospholipid vesicles. *J Cell Physiol* **73**, 49–60.

Reggiori, F., Tucker, K. a, Stromhaug, P. E. & Klionsky, D. J. (2004). The Atg1-Atg13 complex regulates Atg9 and Atg23 retrieval transport from the pre-autophagosomal structure. *Dev Cell* **6**, 79–90.

Reggiori, F., Shintani, T., Nair, U. & Klionsky, D. J. (2005). Atg9 cycles between mitochondria and the pre-autophagosomal structure in yeasts. *Autophagy* **1**, 101–9.

Risselada, H. J., Bubnis, G. & Grubmüller, H. (2014). Expansion of the fusion stalk and its implication for biological membrane fusion. *Proc Natl Acad Sci U S A* **111**, 11043–8.

Romanov, J., Walczak, M., Ibiricu, I., Schüchner, S., Ogris, E., Kraft, C. & Martens, S. (2012). Mechanism and functions of membrane binding by the Atg5–Atg12/Atg16 complex during autophagosome formation. *EMBO J* **31**, 4304–4317.

Rubinsztein, D. C., Mariño, G. & Kroemer, G. (2011). Autophagy and aging. *Cell* **146**, 682–95.

Rubinsztein, D. C., Shpilka, T. & Elazar, Z. (2012). Mechanisms of autophagosome biogenesis. *Curr Biol* **22**, R29–34.

Sakoh-Nakatogawa, M., Matoba, K., Asai, E., Kirisako, H., Ishii, J., Noda, N. N., Inagaki, F., Nakatogawa, H. & Ohsumi, Y. (2013). Atg12–Atg5 conjugate enhances E2 activity of Atg3 by rearranging its catalytic site. *Nat Struct Mol Biol* **20**, 433–439.

Sakoh-Nakatogawa, M., Kirisako, H., Nakatogawa, H. & Ohsumi, Y. (2015). Localization of Atg3 to autophagy-related membranes and its enhancement by the Atg8-family interacting motif to promote expansion of the membranes. *FEBS Lett* **589**, 744–9.

Sambrook, J. & MacCallum, P. (2001). *Molecular Cloning: A Laboratory Manual.*,

Third Edit. Cold Spring Harbor Laboratory Press.

Sekito, T., Kawamata, T., Ichikawa, R., Suzuki, K. & Ohsumi, Y. (2009). Atg17 recruits Atg9 to organize the pre-autophagosomal structure. *Genes Cells* **14**, 525–38.

Sentelle, R. D., Senkal, C. E., Jiang, W., Ponnusamy, S., Gencer, S., Selvam, S. P., Ramshesh, V. K., Peterson, Y. K., Lemasters, J. J. & other authors. **(2012).** Ceramide targets autophagosomes to mitochondria and induces lethal mitophagy. *Nat Chem Biol* **8**, 831–8.

Shahnazari, S., Yen, W.-L., Birmingham, C. L., Shiu, J., Namolovan, A., Zheng, Y. T., Nakayama, K., Klionsky, D. J. & Brumell, J. H. (2010). A Diacylglycerol-Dependent Signaling Pathway Contributes to Regulation of Antibacterial Autophagy. *Cell Host Microbe* **8**, 137–146.

Shahnazari, S., Namolovan, A., Klionsky, D. J. & Brumell, J. H. (2011). A role for diacylglycerol in antibacterial autophagy. *Autophagy* **7**, 331–333.

Shibutani, S. T. & Yoshimori, T. (2014). A current perspective of autophagosome biogenesis. *Cell Res* **24**, 58–68.

Shintani, T. & Klionsky, D. J. (2004). Autophagy in health and disease: a double-edged sword. *Science* **306**, 990–5.

Shpilka, T., Weidberg, H., Pietrokovski, S. & Elazar, Z. (2011). Atg8: an autophagy-related ubiquitin-like protein family. *Genome Biol* **12**, 226.

Siegel, D. P., Green, W. J. & Talmon, Y. (1994). The mechanism of lamellar-to-inverted hexagonal phase transitions: a study using temperature-jump cryo-electron microscopy. *Biophys J* **66**, 402–14.

Siegel, D. P. (1986). Inverted micellar intermediates and the transitions between lamellar, cubic, and inverted hexagonal lipid phases. I. Mechanism of the L alpha-----HII phase transitions. *Biophys J* **49**, 1155–1170.

Siegel, D. P. (1999). The Modified Stalk Mechanism of Lamellar/Inverted Phase Transitions and Its Implications for Membrane Fusion. *Biophys J* **76**, 291–313.

Singer, S. J. & Nicolson, G. L. (1972). The fluid mosaic model of the structure of cell membranes. *Science* **175**, 720–31.

Smith, G. E., Fraser, M. J. & Summers, M. D. (1983a). Molecular Engineering of the Autographa californica Nuclear Polyhedrosis Virus Genome: Deletion Mutations Within the Polyhedrin Gene. *J Virol* **46**, 584–93.

Smith, G. E., Summers, M. D. & Fraser, M. J. (1983b). Production of human beta interferon in insect cells infected with a baculovirus expression vector. *Mol Cell Biol* **3**, 2156–65.

Sou, Y. -s., Tanida, I., Komatsu, M., Ueno, T. & Kominami, E. (2006).

Phosphatidylserine in Addition to Phosphatidylethanolamine Is an in Vitro Target of the Mammalian Atg8 Modifiers, LC3, GABARAP, and GATE-16. *J Biol Chem* **281**, 3017–3024.

Sou, Y., Waguri, S., Iwata, J., Ueno, T., Fujimura, T., Hara, T., Sawada, N., Yamada, A., Mizushima, N. & other authors. **(2008).** The Atg8 conjugation system is indispensable for proper development of autophagic isolation membranes in mice. *Mol Biol Cell* **19**, 4762–75.

Stanley, R. E., Ragusa, M. J. & Hurley, J. H. (2014). The beginning of the end: how scaffolds nucleate autophagosome biogenesis. *Trends Cell Biol* **24**, 73–81.

Struck, D. K., Hoekstra, D. & Pagano, R. E. (1981). Use of resonance energy transfer to monitor membrane fusion. *Biochemistry* **20**, 4093–9.

Suetsugu, S., Kurisu, S. & Takenawa, T. (2014). Dynamic shaping of cellular membranes by phospholipids and membrane-deforming proteins. *Physiol Rev* **94**, 1219–48.

Suzuki, K., Kirisako, T., Kamada, Y., Mizushima, N., Noda, T. & Ohsumi, Y. (2001). The pre-autophagosomal structure organized by concerted functions of APG genes is essential for autophagosome formation. *EMBO J* **20**, 5971–5981.

Suzuki, S. W., Yamamoto, H., Oikawa, Y., Kondo-Kakuta, C., Kimura, Y., Hirano, H. & Ohsumi, Y. (2015). Atg13 HORMA domain recruits Atg9 vesicles during autophagosome formation. *Proc Natl Acad Sci U S A* **112**, 3350–5.

Swartz, J. R. (2001). Advances in Escherichia coli production of therapeutic proteins. *Curr Opin Biotechnol* **12**, 195–201.

Szoka, F. & Papahadjopoulos, D. (1980). Comparative properties and methods of preparation of lipid vesicles (liposomes). *Annu Rev Biophys Bioeng* **9**, 467–508.

Taherbhoy, A. M., Tait, S. W., Kaiser, S. E., Williams, A. H., Deng, A., Nourse, A., Hammel, M., Kurinov, I., Rock, C. O. & other authors. **(2011).** Atg8 transfer from Atg7 to Atg3: a distinctive E1-E2 architecture and mechanism in the autophagy pathway. *Mol Cell* **44**, 451–61. Elsevier Inc.

Tanida, I., Tanida-Miyake, E., Komatsu, M., Ueno, T. & Kominami, E. (2002a). Human Apg3p/Aut1p Homologue Is an Authentic E2 Enzyme for Multiple Substrates, GATE-16, GABARAP, and MAP-LC3, and Facilitates the Conjugation of hApg12p to hApg5p. *J Biol Chem* **277**, 13739–13744.

Tanida, I., Nishitani, T., Nemoto, T., Ueno, T. & Kominami, E. (2002b). Mammalian Apg12p, but not the Apg12p.Apg5p conjugate, facilitates LC3 processing. *Biochem Biophys Res Commun* **296**, 1164–70.

Tanida, I., Ueno, T. & Kominami, E. (2004). LC3 conjugation system in mammalian autophagy. *Int J Biochem Cell Biol* **36**, 2503–18.

Tooze, S. a, Jefferies, H. B. J., Kalie, E., Longatti, A., McAlpine, F. E., McKnight, N. C., Orsi, A., Polson, H. E. J., Razi, M. & other authors. **(2010).** Trafficking and signaling in mammalian autophagy. *IUBMB Life* **62**, 503–8.

Tooze, S. A. (2010). The role of membrane proteins in mammalian autophagy. *Semin Cell Dev Biol* **21**, 677–682.

Tooze, S. A. & Yoshimori, T. (2010). The origin of the autophagosomal membrane. *Nat Cell Biol* **12**, 831–835.

Veatch, S. L. & Keller, S. L. (2003). Separation of liquid phases in giant vesicles of ternary mixtures of phospholipids and cholesterol. *Biophys J* **85**, 3074–83.

Vicinanza, M., Korolchuk, V. I., Ashkenazi, A., Puri, C., Menzies, F. M., Clarke, J. H. & Rubinsztein, D. C. (2015). PI(5)P regulates autophagosome biogenesis. *Mol Cell* **57**, 219–34.

Villar, A. V, Goñi, F. M. & Alonso, A. (2001). Diacylglycerol effects on phosphatidylinositol-specific phospholipase C activity and vesicle fusion. *FEBS Lett* **494**, 117–20.

Walczak, M. & Martens, S. (2013). Dissecting the role of the Atg12-Atg5-Atg16 complex during autophagosome formation. *Autophagy* **9**, 424–425.

Webber, J. L., Young, A. R. J. & Tooze, S. a. **(2007).** Atg9 trafficking in Mammalian cells. *Autophagy* **3**, 54–6.

Weidberg, H., Shvets, E., Shpilka, T., Shimron, F., Shinder, V. & Elazar, Z. (2010). LC3 and GATE-16/GABARAP subfamilies are both essential yet act differently in autophagosome biogenesis. *EMBO J* **29**, 1792–1802.

Weidberg, H., Shpilka, T., Shvets, E., Abada, A., Shimron, F. & Elazar, Z. (2011). LC3 and GATE-16 N Termini Mediate Membrane Fusion Processes Required for Autophagosome Biogenesis. *Dev Cell* **20**, 444–454.

Wilhelmy, L. (1863). Ueber die Abhängigkeit der Capillaritäts-Constanten des Alkohols von Substanz und Gestalt des benetzten festen Körpers. *Ann der Phys und Chemie* **195**, 177–217.

Wilz, L., Fan, W. & Zhong, Q. (2011). Membrane curvature response in autophagy. *Autophagy* **7**, 1249–50.

Wirawan, E., Vanden Berghe, T., Lippens, S., Agostinis, P. & Vandenabeele, P. (2012). Autophagy: for better or for worse. *Cell Res* **22**, 43–61.

Wong, E. & Cuervo, A. M. (2010). Autophagy gone awry in neurodegenerative diseases. *Nat Neurosci* **13**, 805–11.

Wong, Y. C. & Holzbaur, E. L. F. (2015). Autophagosome dynamics in neurodegeneration at a glance. *J Cell Sci* **128**, 1259–67.

Xie, Z. & Klionsky, D. J. (2007). Autophagosome formation: core machinery and

adaptations. *Nat Cell Biol* **9**, 1102–9.

Xie, Z., Nair, U. & Klionsky, D. J. (2008). Atg8 controls phagophore expansion during autophagosome formation. *Mol Biol Cell* **19**, 3290–8.

Xiong, Q., Ünal, C., Matthias, J., Steinert, M. & Eichinger, L. (2015). The phenotypes of ATG9, ATG16 and ATG9/16 knock-out mutants imply autophagy-dependent and -independent functions. *Open Biol* **5**, 150008.

Xu, H., Zick, M., Wickner, W. T. & Jun, Y. (2011). A lipid-anchored SNARE supports membrane fusion. *Proc Natl Acad Sci U S A* **108**, 17325–30.

Xu, Y., Zhang, F., Su, Z., McNew, J. A. & Shin, Y.-K. (2005). Hemifusion in SNARE-mediated membrane fusion. *Nat Struct Mol Biol* **12**, 417–22.

Yamada, Y., Suzuki, N. N., Hanada, T., Ichimura, Y., Kumeta, H., Fujioka, Y., Ohsumi, Y. & Inagaki, F. (2007). The Crystal Structure of Atg3, an Autophagy-related Ubiquitin Carrier Protein (E2) Enzyme that Mediates Atg8 Lipidation. *J Biol Chem* **282**, 8036–8043.

Yamamoto, H., Kakuta, S., Watanabe, T. M., Kitamura, a., Sekito, T., Kondo-Kakuta, C., Ichikawa, R., Kinjo, M. & Ohsumi, Y. (2012). Atg9 vesicles are an important membrane source during early steps of autophagosome formation. *J Cell Biol* **198**, 219–233.

Yang, Z. & Klionsky, D. J. (2010). Mammalian autophagy: core molecular machinery and signaling regulation. *Curr Opin Cell Biol* **22**, 124–131.

Yen, W.-L., Legakis, J. E., Nair, U. & Klionsky, D. J. (2007). Atg27 is required for autophagy-dependent cycling of Atg9. *Mol Biol Cell* **18**, 581–93.

Young, A. R. J., Chan, E. Y. W., Hu, X. W., Köchl, R., Crawshaw, S. G., High, S., Hailey, D. W., Lippincott-Schwartz, J. & Tooze, S. a. (2006). Starvation and ULK1-dependent cycling of mammalian Atg9 between the TGN and endosomes. *J Cell Sci* **119**, 3888–900.

Zens, B., Sawa-Makarska, J. & Martens, S. (2015). In vitro systems for Atg8 lipidation. *Methods* **75**, 37–43.

Zimmerberg, J. & Kozlov, M. M. (2006). How proteins produce cellular membrane curvature. *Nat Rev Mol Cell Biol* **7**, 9–19.

Publications

Publications

Landajuela, A*., Hervás, J. H*., Antón, Z., Montes, L.-R., Gil, D., Valle, M., Rodriguez, J. F., Goñi, F. M. & Alonso, A. (2016). Lipid geometry and bilayer curvature modultae LC3/GABARAP-mediated model autophagosome elongation. *Biophys J* 110, 411-22.

* These two authors contributed equally to this work.

In preparation

Hervás, J. H., Landajuela, A., Antón, Z., Montes, L. R., Goñi, F. M. & Alonso, A. Human Atg3 membrane association induces tethering of negatively-charged membranes.

Other Publications

Posada, I. M. D., Sánchez-Magraner, L., Hervás, J. H., Alonso, A., Monaco, H. L. & Goñi, F. M. (2014). Membrane binding of human phospholipid scramblase 1 cytoplasmic domain. *Biochim Biophys Acta - Biomembr* **1838**, 1785–1792.

Antón, Z*., Landajuela, A*., Hervás, J. H., Montes, L. R., Velasco, G., Hernández-Tiedra, S., Goñi, F. M. & Alonso. Human ATG8-Cardiolipin Interactions in Mitophagy: Specific Properties of LC3, GATE-16 and GABARAP (*Submitted*)

Acknowledgements

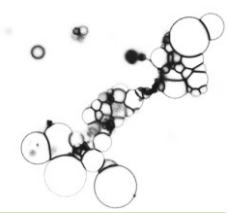

Acknowledgements

The present thesis has been performed at the “Unidad de Biofísica” (CSIC, UPV/EHU) under the supervision of Prof. Alicia Alonso Izquierdo and Dr. Lidia Ruth Montes Burgos. The work has been supported by the Spanish Ministry of Economy (BFU 2011-28566) co-financed by the European Union (FEDER), and the Basque Government (IT838-13). JHH received a research fellowship from the University of the Basque Country (February 2012 - January 2016).

The author is grateful to Prof. Félix Mª Goñi for their valuable assistance throughout the thesis, and to Dr. J. Francisco Rodriguez and colleagues [National Center of Biotechnology (CNB-CSIC), Madrid] for their training in molecular biology techniques and Baculovirus expression system. The author is also grateful to Dr. Sharon Tooze (Cancer Research UK, London Research Institute, London, UK) for giving the opportunity to collaborate in one of her projects through a three months stay, Dr. Banafshe Larijani for the mass spectrometry analysis and discussion, and Dr. Ane Landajuela, Dr. Jesús Sot, Zuriñe Antón and Araceli Marcos for their valuable opinions and discussion throughout the thesis.